ABSTRACT

Title of Dissertation:	OBSERVATIONS AND EMISSIONS OF ENERGY-ASSOCIATED OZONE PRECURSORS IN THE MID-ATLANTIC UNITED STATES
	Timothy P. Vinciguerra, Doctor of Philosophy, 2016
Dissertation directed by:	Professor Sheryl Ehrman, Department of Chemical and Biomolecular Engineering

Surface ozone is formed in the presence of NO_x ($NO + NO_2$) and volatile organic compounds (VOCs) and is hazardous to human health. A better understanding of these precursors is needed for developing effective policies to improve air quality.

To evaluate the year-to-year changes in source contributions to total VOCs, Positive Matrix Factorization (PMF) was used to perform source apportionment using available hourly observations from June through August at a Photochemical Assessment Monitoring Station (PAMS) in Essex, MD for each year from 2007-2015. Results suggest that while gasoline and vehicle exhaust emissions have fallen, the contribution of natural gas sources to total VOCs has risen.

To investigate this increasing natural gas influence, ethane measurements from PAMS sites in Essex, MD and Washington, D.C. were examined. Following a period of decline, daytime ethane concentrations have increased significantly after

2009. This trend appears to be linked with the rapid shale gas production in upwind, neighboring states, especially Pennsylvania and West Virginia. Back-trajectory analyses similarly show that ethane concentrations at these monitors were significantly greater if air parcels had passed through counties containing a high density of unconventional natural gas wells.

In addition to VOC emissions, the compressors and engines involved with hydraulic fracturing operations also emit NO_x and particulate matter (PM). The Community Multi-scale Air Quality (CMAQ) Model was used to simulate air quality for the Eastern U.S. in 2020, including emissions from shale gas operations in the Appalachian Basin. Predicted concentrations of ozone and PM show the largest decreases when these natural gas resources are hypothetically used to convert coal-fired power plants, despite the increased emissions from hydraulic fracturing operations expanded into all possible shale regions in the Appalachian Basin.

While not as clean as burning natural gas, emissions of NO_x from coal-fired power plants can be reduced by utilizing post-combustion controls. However, even though capital investment has already been made, these controls are not always operated at optimal rates. CMAQ simulations for the Eastern U.S. in 2018 show ozone concentrations decrease by ~5 ppb when controls on coal-fired power plants limit NOx emissions to historically best rates.

OBSERVATIONS AND EMISSIONS OF ENERGY-ASSOCIATED OZONE PRECURSORS IN THE MID-ATLANTIC UNITED STATES

by

Timothy P. Vinciguerra

Dissertation submitted to the Faculty of the Graduate School of the
University of Maryland, College Park, in partial fulfillment
of the requirements for the degree of
Doctor of Philosophy
2016

Advisory Committee:
Professor Sheryl Ehrman, Chair
Professor Richard Calabrese
Doctor Timothy Canty
Professor Russell Dickerson
Professor Michael Zachariah
Professor Ross Salawitch, Dean's Representative

Dedication

To my parents, Ruth and Mark Vinciguerra, and my wife, Dr. Brittany Vinciguerra.

Acknowledgements

I would like to first and foremost thank my advisor, Sheryl Ehrman, for her patience, guidance, and insight. I would never have found an interest in air quality modeling on my own.

I would also like to thank the various other mentors I have had, especially Russ Dickerson, Tim Canty, and Ross Salawitch.

I also greatly appreciate all the assistance I have received from the undergraduates I have had a chance to work with over the past years: Simon Yao, Joseph Dadzie, Alexa Chittams, Rahma Zakaria, Thomas Deskins, Brian Constantine, Vitor Goncalves, Cyndi M'Bagui Matsanga, and Sheena Liu.

Thank you for the support from graduate and former graduate students Dan Goldberg, Linda Hembeck, Hao He, Dan Anderson, Julie Nicely, and Allison Ring.

For teaching me how to run the SMOKE model, I would like to thank Chinmay Satam. For helping me troubleshoot the countless SMOKE errors I have encountered, I would like to thank Eric Zalewsky for his years of support.

Thank you to the Maryland Department of the Environment for financial support, and especially Tad Aburn and Mike Woodman for the opportunity to contribute to policy-relevant work.

Finally, I would like to thank my family and friends for their continued love and support.

Table of Contents

List of Tables

List of Figures

List of Abbreviations

BEIS	Biogenic Emission Inventory System
BenMAP	Environmental Benefits Mapping and Analysis Program
CAMD	Clean Air Markets Division
CAMx	Comprehensive Air Quality Model with Extensions
CB05	Carbon Bond Mechanism, Version 5
CENSARA	Central States Air Resource Agencies
CMAQ	Community Multiscale Air Quality Model
CMB	Chemical Mass Balance
CSAPR	Cross-State Air Pollution Rule
EKMA	Empirical Kinetic Modeling Approach
ERTAC	Eastern Regional Technical Advisory Committee
eGRID	Emissions & Generation Resource Integrated Database
EGU	Electrical Generating Units
EIA	U.S. Energy Information Agency
EPA	U.S. Environmental Protection Agency
HYSPLIT	Hybrid Single Particle Lagrangian Integrated Trajectory Model
ICI	Industrial, Commercial, and Institutional
LADCO	Lake Michigan Air Directors Consortium
MANEVU	Mid-Atlantic/Northeast Visibility Union
MAR	Marine, Aircraft, and Railway
MARAMA	Mid-Atlantic Regional Air Management Association
MCIP	Meteorology-Chemistry Interface Processor
MDE	Maryland Department of the Environment
MDL	Minimum Detection Limit
MEGAN	Model of Emissions of Gases and Aerosols from Nature
MIR	Maximum Incremental Relativity
MOVES	Motor Vehicles Emissions Simulator
NAAQS	National Ambient Air Quality Standards
NAM	North American Mesoscale
NEI	National Emissions Inventory
NOAA	National Oceanic and Atmospheric Administration
OTC	Ozone Transport Commission
PAMS	Photochemical Assessment Monitoring Station
PAR	Photosynthetically Active Radiation
PM	Particulate Matter
$PM_{2.5}$	Particulate Matter measuring less than 2.5μm in diameter
PMF	Positive Matrix Factorization
SCR	Selective Catalytic Reduction
SIP	State Implementation Plan
SESARM	Southeastern States Air Resource Managers
SMOKE	Sparse Matrix Operator Kernel Emissions
SNCR	Selective Non-Catalytic Reduction

TNMOC	Total Non-Methane Organic Compounds
TSV	Total Spatial Variance
VMT	Vehicle Miles Traveled
VOC	Volatile Organic Compound
WRF	Weather Research and Forecasting Model

Chapter 1 Introduction

1.1 Ozone, Particulate Matter, and Human Health

Air quality in the US remains a primary concern for human health, even as concentrations of pollutants continue to decrease (EPA, 2016a, 2016b). The U.S. Environmental Protection Agency (EPA) has outlined six criteria pollutants hazardous to human health and public welfare: carbon monoxide (CO), lead (Pb), nitrogen dioxide (NO_2), ozone (O_3), particulate matter (PM), and sulfur dioxide (SO_2) (EPA, 2015a).

In particular, ozone and PM still exist at hazardous levels. Ground level ozone is a colorless, odorless gas which can cause several health problems related to the respiratory system such as lung and throat irritation, coughing and wheezing, aggravation of asthma, and inflammation and damage to the lining of lungs (EPA, 2015a). Children and persons with respiratory disease are most at risk on high ozone days, and plants and animals are also negatively affected by ozone. PM can originate from a variety of sources such as dust, ash, mist, smoke, or fumes. $PM_{2.5}$ refers to fine PM measuring less than 2.5μm in diameter, and particles less than 10μm in diameter, are referred to as PM_{10} or coarse. Particulate matter of any size can be harmful, but fine particles are able to penetrate deep into the lungs, causing serious damage. PM has been known to cause both pulmonary and cardiovascular problems and can even culminate in lung cancer or early death. Similar to ozone, children are most at risk from exposure, in addition to those with heart and lung diseases. PM can also deter plant growth and impair visibility (EPA, 2015a).

As part of the Clean Air Act, the EPA is mandated to set National Ambient Air Quality Standards (NAAQS) for these criteria pollutants. For ozone, the current NAAQS established in

2015 is a daily maximum 8-hour average of 70 ppb, and the NAAQS established for $PM_{2.5}$ in 2012 is a 24-hour average of 35 $\mu g/m^3$ and an annual average of 12 $\mu g/m^3$ (EPA, 2016c). Nonattainment areas unable to meet these standards must provide a State Implementation Plan (SIP) to outline which air quality and emissions controls programs are planned or in effect to demonstrate attainment of the NAAQS (EPA, 2016d). **Figures 1.1 and 1.2** show how Northeastern states (from Maryland northward along the East Coast) have succeeded in lowering concentrations of ozone and $PM_{2.5}$. The NOx SIP Call from 2003-2008 created a cap and trade program to limit NOx ($NO + NO_2$) emissions (EPA, 2009), and its effect on reducing ozone is visible in **Figure 1.1**.

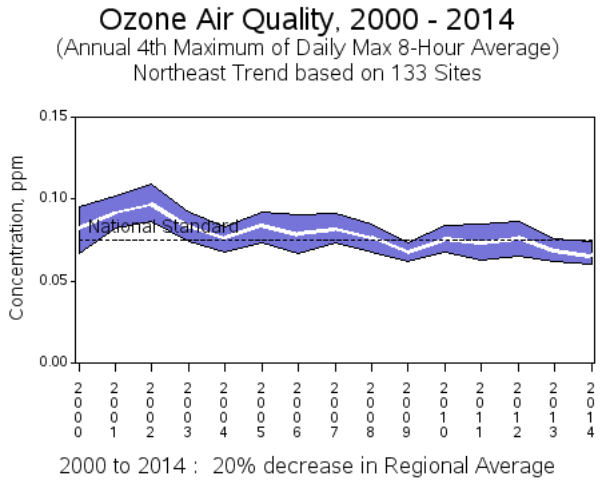

Figure 1.1 Ozone recorded in Northeastern states. The purple region delimits the 10th through 90th percentiles, and the white line provides the average value (EPA, 2016a).

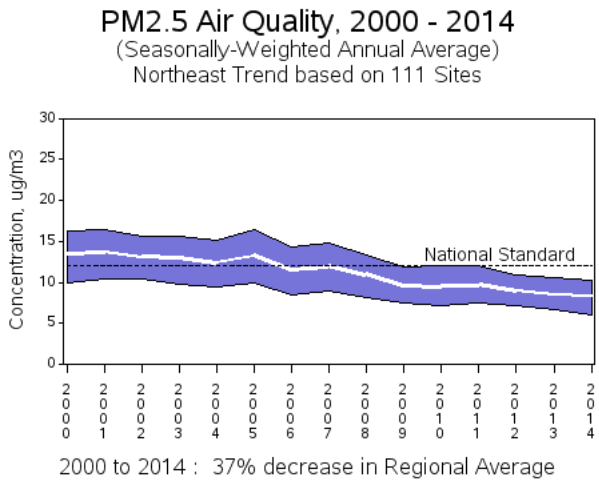

Figure 1.2 $PM_{2.5}$ recorded in Northeastern states. The purple region delimits the 10th through 90th percentiles, and the white line provides the average value (EPA, 2016b).

1.2 Surface Ozone

The primary ozone precursors NO_x ($NO + NO_2$) and volatile organic compounds (VOCs), have been investigated to understand how to best limit concentrations of surface ozone. VOCs can come from a multitude of anthropogenic sources, but on a global scale, a significant majority of VOC emissions are biogenic in origin. The majority of NO_x emissions are the result of fossil fuel combustion, although biomass burning, soils, and lightning have notable contributions (Seinfeld and Pandis, 2006; Sillman, 1999).

1.2.1 Tropospheric Ozone Formation Mechanism

The presence of VOCs and NO_x will allow for the formation of ozone in the troposphere. Hydrocarbons (represented as RH in the reaction) will react with OH radicals to form alkyl peroxy radicals (RO_2) (**Equation 1-1**). These formed peroxy radicals will next react quickly with NO to form NO_2 and regenerate reactive radicals OH or HO_2 (**Equations 1-2**, **1-3**). The photolysis of NO_2 by ultraviolet light leads to the formation of $O(^3P)$ radical (**Equation 1-4**), which quickly attaches to oxygen to produce ozone (**Equation 1-5**).

$$RH + OH + O_2 \rightarrow RO_2 + H_2O \quad \textbf{(1-1)}$$

$$RH + OH \rightarrow R + H_2O \quad \textbf{(1-1a)}$$

$$R + O_2 + M \rightarrow RO_2 + M \quad [\text{fast}] \quad \textbf{(1-1b)}$$

$$RO_2 + NO + O_2 \rightarrow NO_2 + R'CHO + HO_2 \quad \textbf{(1-2)}$$

$$RO_2 + NO \rightarrow RO + NO_2 \quad \textbf{(1-2a)}$$

$$RO + O_2 \rightarrow R'CHO + HO_2 \quad [\text{fast}] \quad \textbf{(1-2b)}$$

$$HO_2 + NO \rightarrow NO_2 + OH \quad \textbf{(1-3)}$$

$$NO_2 + h\upsilon \rightarrow NO + O(^3P) \quad \textbf{(1-4)}$$

$$O(^3P) + O_2 + M \rightarrow O_3 + M \quad \textbf{(1-5)}$$

The rate of reaction between hydrocarbon species and OH (**Equation 1-1a**) varies depending on the properties of a given hydrocarbon molecule such as number of carbon atoms and types of bonds (**Figure 1.3**). Many aromatics and alkenes will react quickly, lasting less than a day; isoprene has a lifetime of only 1.5 hours. Shorter-chain alkanes, on the other hand, can last several days, or even multiple weeks in the case of ethane (Parrish et al., 2007; Blake and Blake, 2003).

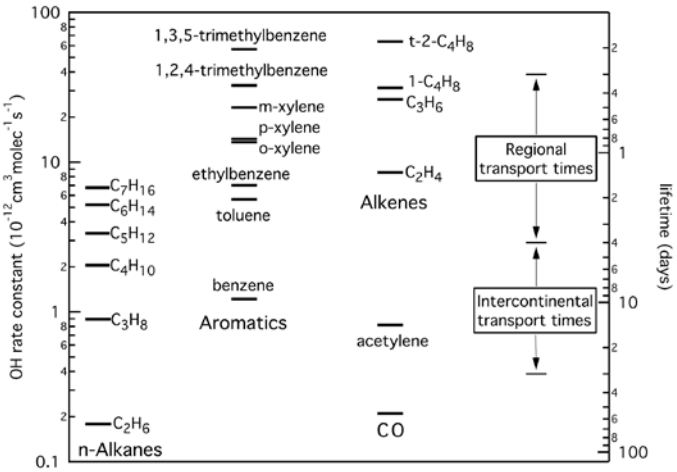

Figure 1.3 Rate constants (left y-axis) and lifetimes (right y-axis) for select hydrocarbon species (Parrish et al., 2007).

Radicals are ultimately terminated through the formation of nitric acid (**Equation 1-6**) or peroxides (**Equations 1-7, 1-8**). Ozone is also able to react with NO to regenerate NO_2 and oxygen (**Equations 1-9**). However, peroxides and NO_2 will undergo daytime photolysis to recreate radicals and ozone.

$$OH + NO_2 + M \rightarrow HNO_3 + M \quad (\mathbf{1\text{-}6})$$
$$HO_2 + HO_2 \rightarrow H_2O_2 + O_2 \quad (\mathbf{1\text{-}7})$$
$$RO_2 + HO_2 \rightarrow ROOH + O_2 \quad (\mathbf{1\text{-}8})$$
$$O_3 + NO \rightarrow NO_2 + O_2 \quad (\mathbf{1\text{-}9})$$

CO also serves as an ozone precursor, and acting similarly to hydrocarbons, yields HO_2 by reacting with OH (Seinfeld and Pandis, 2006).

$$CO + OH + O_2 \rightarrow CO_2 + HO_2 \quad (\mathbf{1\text{-}10})$$

1.2.2 Ozone Isopleths and Nonlinearity

One useful tool for understanding ozone formation has been the ozone empirical kinetic modeling approach (EKMA) isopleth diagram (EPA, 1989), which helps to effectively visualize the sensitivity and nonlinear response of ozone production due to NO_x and VOCs. **Figure 1.4** demonstrates that reducing both VOC and NO_x emissions results in less ozone, but it can also be seen that if only NO_x emissions are lowered from 1995, then ozone production would increase. This is an example of a VOC-limited region. On the other hand, the left part of **Figure 1.5** indicates that focusing only on reducing VOC emissions can yield no net change in ozone production. This is an example of a NO_x-limited region.

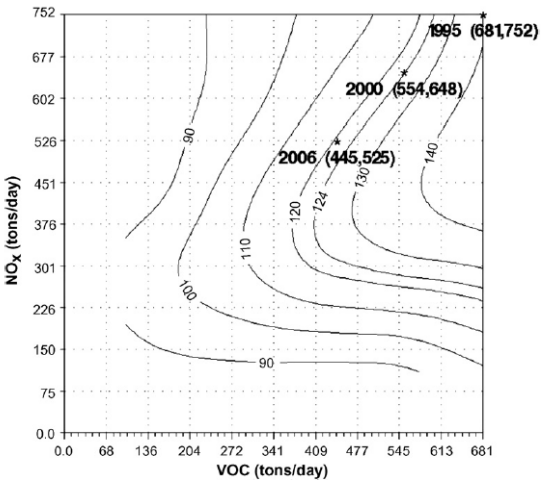

Figure 1.4 Isopleth displaying San Francisco Bay Area Ozone attainment strategy. Ozone is shown in ppb (Kear et al., 2008).

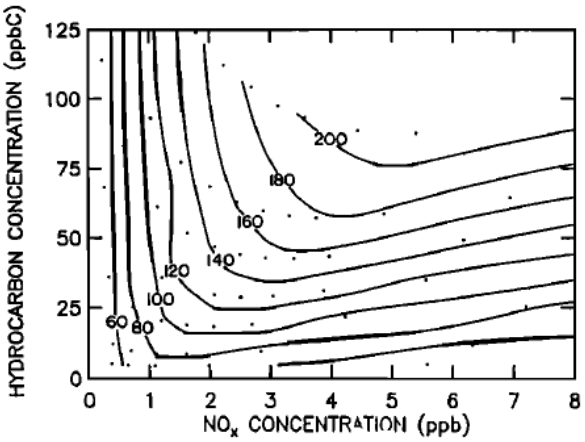

Figure 1.5 Ozone contours at 4pm simulating a rural eastern U.S. environment with NOx limited conditions using a two-layer box model. Ozone is shown in ppb (Sillman et al., 1990).

It can also be seen in **Figures 1.4 and 1.5** that a straight line can be drawn through the ozone maximums of each contour; this "knee region" separates the VOC-limited region from the NO_x-limited region. As a result, shifting the ratio significantly can alter the modeled isopleth. In addition to uncertainties with modeled data, daily emissions of NO_x and VOC can be highly variable, and locations can change from being NO_x-sensitive one day to being VOC-sensitive the next (and even within the same day), making it extremely difficult to prioritize emission regulations in policy making (Kear et al., 2008; Sandoval et al., 2001; Seinfeld and Pandis, 2006; Sillman, 1999; Thielmann et al., 2001).

In addition to the difficulties previously mentioned, the chemical properties and NO_x or VOC limitations can also vary depending upon climate and geography of a given city. Variables such as humidity, biogenic sources, and types of industrial facilities play a further role in complicating the NO_x, VOC, and ozone relationship. A study of ozone and its precursors was performed by Kleinman et al. (2005) to investigate the differences in ozone production events in five metropolitan areas in the United States from 1995-2000. Events were found to be vastly different, ranging from highly NO_x-limited to highly VOC-limited. In Nashville, an extreme event developed as a result of stagnation where a large air mass concentrated with high biogenic

isoprene combined with NO_x. In the coastal city of Houston, petrochemical plants emit both NO_x and light olefins to produce the highest levels of ozone for the cities studied. The arid environment of Phoenix has low OH and a low VOC/NO_x ratio that leads to no high ozone production values. It was also found that Nashville and New York City were NO_x-limited (although measurements were made outside of the population centers containing high NO_x), but ozone production in Phoenix, Houston, and Philadelphia was VOC-limited.

Over time, total emissions of NOx have been significantly reduced as major sources such as motor vehicles and power plants have been made cleaner, and ozone production sensitivities have shifted. A study of 2005-2007 OMI NO_x observations by Duncan et al. (2010) showed most of the ozone produced in the United States is now sensitive to NO_x. A CAMx simulation by Goldberg et al. (2016) similarly indicated the state of Maryland was almost exclusively NO_x-limited in July 2011. As widespread NO_x reductions continue with cleaner combustion products, it would be expected that more areas will become NO_x-limited.

1.3 Air Quality Monitoring

The U.S. Environmental Protection Agency has established numerous sites for monitoring a variety of pollutants. Following the 1990 Clean Air Act Amendments, Photochemical Assessment Monitoring Stations (PAMS) were created to monitor ozone, its precursors of NO_x and VOCs, and surface meteorology in regions of ozone nonattainment (EPA, 2014a). During the summer months of June, July, and August when ozone levels can often be hazardous to human health, concentrations are recorded every hour, providing rich datasets for analysis. These measurements provide control agencies and policy makers with a way to monitor and adjust air quality strategies for reaching attainment of the ozone NAAQS.

In the Baltimore-Washington area, there are three monitors that collect VOC measurements. The monitor at Essex, MD was set up to track emissions for the Baltimore ozone nonattainment area (**Figure 1.6**). Similarly, a station at McMillan Reservoir monitors VOC concentrations for the Washington, D.C. area. The third site in Beltsville, MD has a significantly smaller sample size, only obtaining VOC measurements on every third hour of every third day.

Figure 1.6 The PAMS monitor at Essex, MD (a) noted by the yellow pin marker on the map to the east of Baltimore. The monitor is located in the corner of a parking lot in a residential neighborhood. (b) noted by the yellow star in an aerial view of Essex.

1.4 Emissions and Air Quality Modeling

Air quality models can be beneficial tools for both researchers and policymakers. These models can provide insight for the interactions between emissions, meteorology, and pollutant chemistry and dynamics (The Institute for the Environment, 2012). One such use is adjusting existing emissions inventories to demonstrate the effects of policies to control criteria pollutants or greenhouse gases, and model results can help users understand the efficiency or attainment feasibility from proposed regulatory programs.

A basic schematic for air quality modeling is shown in **Figure 1.7**. Meteorological models serve as inputs to emissions models for temperature and wind-sensitive calculations. An air quality model will finally perform photochemical reactions as determined by inputted emission rates of various pollutants and current meteorological conditions to predict concentrations of criteria air pollutant species.

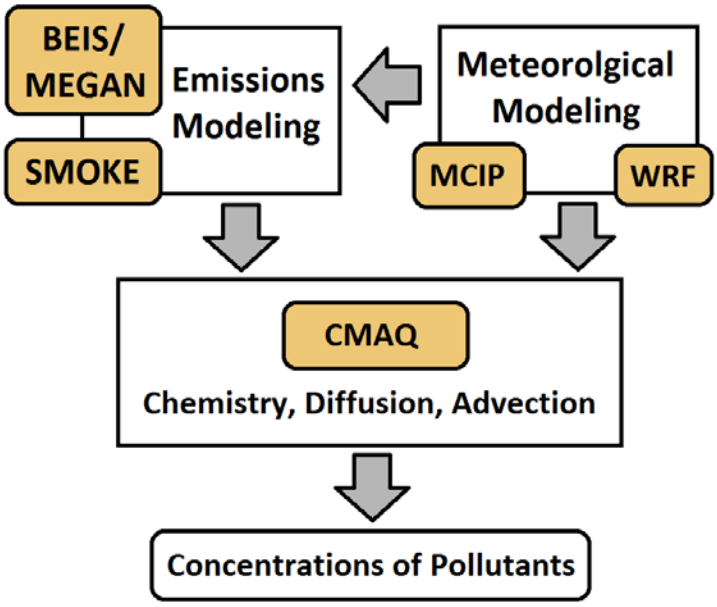

Figure 1.7 A simplified flowchart outlining the major components of air quality modeling

1.4.1 SMOKE Model

The Sparse Matrix Operator Kernel Emissions (SMOKE) modeling system allows users to convert emissions inventories to a gridded format with hourly temporal resolution that can be used as input into a photochemical air quality model. SMOKE is primarily used to process the pollutants CO, NOx, VOCs, NH_3, SO_2, and $PM_{2.5}$ and PM_{10}, but can also include other various toxic species and has no limitation on the number of pollutants that can be processed.

Emissions estimates are available from the National Emissions Inventory (NEI) or regional associations such as the Mid-Atlantic Regional Air Management Association (MARAMA). Regional air pollution control organizations such as Mid-Atlantic/Northeast Visibility Union (MANEVU), Lake Michigan Air Directors Consortium (LADCO), Southeastern States Air Resource Managers (SESARM), and Central States Air Resource Agencies (CENSARA) work to verify these emission values for use in air quality modeling. Emissions from these four regions combine to form the Ozone Transport Commission (OTC) modeling domain for the Eastern United States (**Figure 1.8**).

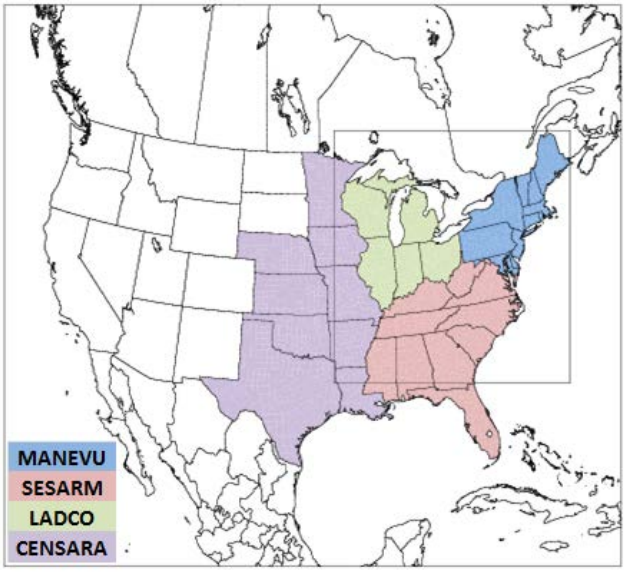

Figure 1.8 The OTC modeling domain is outlined by the interior box nested in the domain for the continental United States. The states composing the MANEVU, SESARM, LADCO, and CENSARA regions are colored (OTC, 2013).

Emissions come from biogenic and various anthropogenic sources such as point, area, nonroad, and mobile sources. Point sources come from heavy industrial sites and can be emitted from the surface or elevated stacks. These sources include electricity generating units (EGU), industrial, commercial, and institutional (ICI) boilers, and various production and manufacturing facilities such as metals, solvents, plastic, food, and printing. Area emissions are emitted at the surface over a large region and because they cannot be pinpointed, they are averaged. These sources include residential heating and building surface coatings and can also include smaller industrial sources such as dry cleaning not included in point source emissions. Nonroad emissions cover vehicles that do not travel on roads. These emissions include vehicles and tools used for construction and lawn and garden in addition to marine, aircraft, and railway (MAR) sources which are sometimes counted as area sources. Mobile emissions are not processed directly with emissions inventories, but instead use vehicle miles traveled (VMT) and speed activity data cross-referenced with lookup tables from the Motor Vehicles Emissions Simulator (MOVES) model. These emissions include on-road vehicles such as light-duty gasoline cars and heavy-duty diesel trucks. Off-road mobile emissions also account for emissions from idling and refueling. Other sources such as wildfire emissions and offshore emissions are needed for the OTC domain.

Biogenic emissions are created outside of the SMOKE model, using either the Model of Emissions of Gases and Aerosols from Nature (MEGAN), or the Biogenic Emission Inventory System (BEIS), but must be combined with anthropogenic emissions from SMOKE before use in an air quality model like CMAQ. Emissions are calculated based on leaf area index, plant functional type, plant specific species composition data, and emission factors such as meteorology and photosynthetically active radiation (PAR). The emission differences between

these models can strongly affect the formation of ozone and PM. MEGAN v2.10 was found to offer the most up-to-date algorithms, technical improvements, and most reasonable emissions distributions (Sakulyanontvittaya et al., 2012; Canty et al., 2015) when performing air quality modeling based on 2007 meteorology. BEIS v3.61 uses improved land use and canopy representation and best match observations for air quality modeling with 2011 meteorology (Bash et al., 2015; Goldberg et al., 2016).

SMOKE processes emissions inventories and transforms them through temporal allocation, spatial allocation, and chemical speciation. While EGUs have hourly emissions data, most inventories are presented with units of tons/year, and temporal allocation provides a means to represent these emissions on an hourly basis. Emissions vary based on seasons, hour of day, as well as weekdays versus weekends and holidays, and these profiles are used to allocate the annual emissions. Emissions are also often provided by county and can be spatially allocated by comparing county lines to grid cells. The fraction of each county contained in a given grid cell is used to calculate emission rates for that cell. Finally, the pollutants provided in emissions inventories need to be speciated for use in a reaction mechanism. For example, VOCs encompass several carbon species which can have greatly differing lifetimes; ethane lasts for several weeks, whereas isoprene reacts in about an hour (Blake and Blake, 2003). To overcome this obstacle, speciation profiles are used to separate VOCs into groups with similar reactivities.

Work shown here used SMOKE v3.1 to create emissions with hourly temporal resolution, 12km x 12km spatial resolution, and speciated for the CB05 chemical mechanism. More information about this version of the SMOKE model can be obtained from: https://www.cmascenter.org/smoke/documentation/3.1/manual_smokev31.pdf.

1.4.2 CMAQ Model

In addition to the emissions rates provided by SMOKE, the Community Multiscale Air Quality (CMAQ) model incorporates meteorological data such as wind and temperature, and chemical reaction kinetics to calculate expected pollutant concentrations for various species. Because emissions are as much a regional issue as they are local, an air quality model is needed to simulate the formation and transport of air pollution, and CMAQ is designed to be transparent for users for both operation and optimization.

To initiate the first time step of a modeling run, CMAQ uses initial conditions to estimate the existing chemical conditions at this time. Similarly, boundary conditions are used to account for horizontal emission fluxes at the edges of the modeling domain. CMAQ uses total column ozone above the surface to model photolysis frequencies assuming clear-sky conditions. Because of the approximations involved in these start-up processes, "spin-up time" is often factored into modeling runs, and the first several modeled days of modeling results are often discarded.

CMAQ v5.0 and v5.0.2 with the CB05 chemical mechanism (Yarwood et al., 2005) were used for modeling shown later, with two weeks allotted for spin-up time. This version of CMAQ includes notable upgrades over earlier versions such as incorporation of NO_x emissions from lightning (Allen et al., 2012) and in-line photolysis calculations. The in-line photolysis module uses updated absorption cross sections and quantum yields and allows CMAQ to make use of the PM and ozone levels that have been predicted during a modeling run instead of relying solely on look-up tables. More information about CMAQ v5.0 and version updates can be obtained from: http://www.airqualitymodeling.org/cmaqwiki/index.php?title=CMAQ_version_5.0_(February_2010_release)_OGD.

1.5 Greenhouse Gases

Air quality models are typically used with a primary interest in criteria air pollutants, but pollutants that contribute to climate change are also of concern. Unlike photons in the ultraviolet (UV) range of the spectrum, photons from the infrared (IR) region generally lack the energy to break bonds. However, if the energy of a photon matches a vibrational mode of a molecule, it can be absorbed, which causes the molecule to vibrate. These vibrations cause the bonds to either bend (lower energy) or stretch (higher energy) (Eubanks et al., 2006).

These vibrational modes can be seen using CO_2, the earth's most abundant greenhouse gas, as an example. In **Figure 1.9a**, the symmetric stretching of CO_2 can be seen, and asymmetric stretching is shown in **Figure 1.9b**. **Figures 1.9c and 1.9d** show the bending vibrations in the vertical and horizontal planes. The oxygen atoms have partial negative charges due to the electrons surrounding them. When the molecule undergoes symmetric stretching, the shifts in charge distribution negate each other and IR absorption does not occur. However, when CO_2 bends or stretches asymmetrically, the charges are no longer symmetrically distributed, creating a change in the dipole moment which allows the molecule to absorb corresponding IR radiation. After the molecules absorb and vibrate, they reemit IR radiation as they return to their ground state. This ability to absorb and return IR radiation from the earth's surface makes molecules such as CO_2 greenhouse gases (Eubanks et al., 2006).

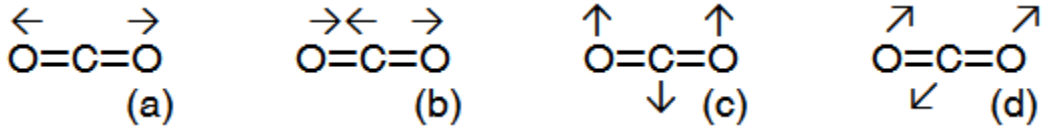

Figure 1.9 Symmetric (a) and asymmetric (b) stretching of CO_2 and bending (c,d) of CO_2. Adapted from Eubanks et al. (2006).

1.5.1 Methane

Following CO_2, methane is the next most prevalent greenhouse gas, accounting for about 9% of total anthropogenic U.S. greenhouse gas emissions in 2012. Approximately 60% of methane emissions are caused by humans, and these sources include natural gas and petroleum usage, enteric fermentation and manure from domestic livestock, rice production, biomass burning, and landfills and waste. Methane is also naturally emitted from anaerobic bacteria in wetlands, the single largest source of methane. To a lesser degree methane can also come from termites, oceans, volcanoes, wildfires, and sediment (Eubanks et al., 2006; IPCC, 2007). The primary sink for methane is reaction with the OH radical in the troposphere, but it can also be removed by biological oxidation in dry soil, loss to the stratosphere, and oxidation by marine chlorine (IPCC, 2007).

Compared to CO_2, methane has a much shorter lifetime (12 years as opposed to 50-100 years) (Eubanks et al., 2006), but methane has a warming potential that is 30 times greater than CO_2 (IPCC, 2013). In **Figure 1.10** it can be seen that the abundance of CO_2 in the atmosphere (~400 ppm) has created a broadened absorption band. As a result, adding small amounts of CO_2 will have a relatively small effect as the band is already saturated and the IR radiation emitted at that wavelength is already absorbed. However, no such saturation effect is present in the methane absorption band. Because the concentration of methane is much lower (~1.9 ppm), smaller increases can greatly increase the amount of IR absorbed by methane, making it a much more effective greenhouse gas (Archer, 2011; NOAA, 2016). The radiative forcing from CO_2 can be described by a logarithmic expression, whereas methane has a square-root dependence shared with N_2O because of overlapped absorption bands (IPCC, 2001).

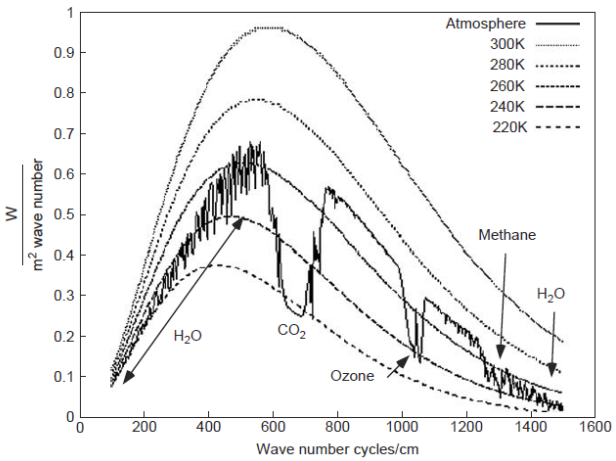

Figure 1.10 The solid line shows model-generated spectrum of IR escaping the top of the atmosphere. The dashed and dotted lines represent blackbody spectrum for a range of temperatures (Archer, 2011).

Although the research shown in the following chapters does not directly address the effect of methane on climate, it is important to keep in mind that methane is the primary component of natural gas. If more than about 3.2% of methane is lost to the atmosphere between production and delivery of natural gas, the climate benefits over coal combustion are lost (Alvarez et al., 2012). Results from several studies display a wide range of estimates for methane loss from shale oil and gas operations, ranging between 0.18% and 17.3%; these findings are summarized in **Table 1.1** (Allen et al., 2013; Caulton et al., 2014; Howarth et al., 2011; Karion et al., 2013; Kirchgessner et al., 1997; Peischl et al., 2013, 2015; Petron et al., 2012; Schneising et al., 2014). Increases in ethane concentrations from natural gas would not only suggest consequences for air quality, but are also indicative of increased concentrations of methane and climate change.

Table 1.1 A survey of estimates of methane leakage from natural gas production operations.

Leakage	Region	Method	Reference
2.8% - 17.3%	Southwestern PA	Aircraft sampling compared to PA, WV, and OH production data	Caulton et al., 2014
12%	Los Angeles Basin, CA	Aircraft CalNex field measurements, emissions inventory estimates	Peischl et al., 2013
6.2% - 11.7%	Uintah, UT	Aircraft sampling-based mass balance	Karion et al., 2013
10.1 ± 7.3%	Bakken (ND, SK)		
~10%	Marcellus (PA, WV)	SCIAMACHY retrieval of CH_4	Schneising et al., 2014
9.1 ± 6.2%	Eagle Ford (TX)		
3.6% - 7.9%	US national	Estimates based on emission estimates from EPA and GAO reports	Howarth et al., 2011
2.3% - 7.7%	Northeastern Colorado	Ground level ambient tall tower and mobile sampling	Pétron et al., 2011
1.42%	US national	Source sampling	Kirchgessner et al., 1997
1.0 - 2.8%	Fayetteville (AR)	Aircraft sampling compared to natural gas production data	Peischl et al., 2015
1.0 - 2.1%	Haynesville (LA, TX)		
0.18 - 0.41%	Northeastern PA		
0.42%	US national	Source sampling and national emission inventory estimates	Allen et al., 2013

Chapter 2 Source Apportionment and Changes from a Decade of VOC Measurements at Essex, MD

2.1 Introduction

Volatile organic compounds (VOCs) are important pollutants as they are precursors for ozone (Crutzen, 1974; Haagensmit et al., 1953) and secondary organic aerosols (SOA), which are a major component of particulate matter (Hallquist et al., 2009; Schuetzle et al., 1975). These resulting pollutants can have adverse human health effects, as pulmonary and cardiovascular complications can arise in the presence of high concentrations of these criteria pollutants (EPA, 2016e; EPA, 2016f; Liao et al., 2004; Pope and Dockery, 2006; WHO, 2005). Some VOCs, especially aromatics such as benzene, are also classified as toxic, hazardous air pollutants having direct negative impacts on human health (EPA, 2016g). As a result, it is of critical importance to limit the emissions of VOCs, especially the most toxic and reactive species, and understand the sources of such species.

In a typical urban environment, there can be a variety of anthropogenic VOC emission sources: vehicle exhaust, gasoline, natural gas, other fossil fuel usage, surface coatings, solvents, petroleum refineries, and other industrial and manufacturing processes. Additionally in areas such as Baltimore, Maryland which also feature an appreciable amount of vegetation, biogenic sources become a significant source of VOCs, especially the highly-reactive isoprene compound. Because the concentrations and reactivity rates of individual species are significantly varied, it is important to quantify and qualify the sources which compose the observed VOCs.

To better quantify the precursor species and conditions leading to surface ozone formation, the EPA established the Photochemical Assessment Monitoring Station (PAMS)

network to collect measurements of ozone and its precursors. During the summer months of June through August, when surface ozone concentrations are expected to be most dangerous for human health, these measurements are made on an hourly basis. One such monitor was established in 1994 at Essex, MD, representing the Baltimore metropolitan ozone non-attainment area. In addition to meteorological parameters and other pollutants, measurements of 55 individual hydrocarbon species plus a measurement for total non-methane organic compounds (TNMOC) are available from this site.

Positive Matrix Factorization (PMF), the most commonly used (Hopke, 2016) and recently updated (Norris et al., 2014) source apportionment model, was used to find the sources of VOCs at the Essex monitor for recent years. The analysis in this chapter draws from the procedures and findings from a previous source apportionment study which used the Unmix model (Henry, 2003) with hourly measurements of 23 individual VOC species obtained from the Essex monitor during the summers of 1996-1999 (Choi and Ehrman, 2004). Six source factors were identified: liquid gasoline, gasoline vapor, vehicle exhaust, surface coatings, natural gas, and biogenic. Combined, the three gasoline-related factors represented nearly two-thirds of the total VOCs observed at the monitor. The other three sources made up mostly equal parts of the remaining total VOC concentrations.

2.2 Methods

The VOC measurements collected at PAMS monitors can be used in a technique called source apportionment, which is also often used for PM species. This method takes a matrix of ambient species concentrations recorded over several time intervals and separates it into a number of sources. These sources can be determined by identifying tracer species that make up a significant portion of the total source mass or mostly only appear in a certain source. Source

apportionment studies have been performed for cities all across the globe (Brown et al., 2007; Buzcu-Guven et al., 2008; Chen et al., 2002; Choi and Ehrman, 2004; Fujita, 2001; Leuchner and Rappenglück, 2010; Morino et al., 2011; Watson et al., 2001; Yuan et al., 2012), and can be very useful tool for understanding the magnitudes for sources of emissions and how these source contributions change over time.

The EPA Positive Matrix Factorization (PMF) model is one available tool developed for source apportionment (Hopke, 2000; Norris et al., 2014). As a multivariate factor analysis tool, PMF takes a matrix of speciated data and decomposes it into two matrices: factor profiles and factor contributions, and these factors can then be identified by using tracer species. This process is described by **Equation 2-1**:

$$x_{ij} = \sum_{k=1}^{p} g_{ik} f_{kj} + e_{ij} \quad \textbf{(2-1)}$$

Given matrix *x* of speciated data with *i* samples and *j* chemical species, PMF uses user-determined *p* factors to identify *g*, the mass contributed by each factor to each sample, and *f*, the species profile of each source, with residuals e_{ij}.

Like any model used for source apportionment, the PMF modeling system must also obey certain physical constraints to ensure realistic solutions are presented. The model must reproduce the original observations, predict non-negative source compositions and contributions, and, for each source, predict a mass contribution whose sum is less than or equal to the measured total mass (Hopke, 2003).

PMF also allows users to apply uncertainty estimates to individual data points, as a similarly-formatted but separate input file must be provided to accompany the measurements used as data input. This is especially advantageous for measurements that are made below a detection limit, where the value of the measurement is low and possibly not recorded accurately.

Uncertainty weighting allows users to keep these lower value data points but also make them less influential on the solution than measurements recorded with more certainty above a detection limit. As shown in **Equation 2-2**, given uncertainties *u*, the PMF solution seeks to minimize the objective function *Q*, a goodness-of-fit parameter for assessing how well the model fits its inputs.

$$Q = \sum_{i=1}^{n} \sum_{j=1}^{m} [(x_{ij} - \sum_{k=1}^{p} g_{ik} f_{ik})/u_{ij}]^2 \quad \textbf{(2-2)}$$

Source apportionment can also be performed by the chemical mass balance (CMB) (Miller et al., 1972) and Unmix (Henry, 2003) models. In general, resolved factors from PMF are in good agreement with results from the other models (Norris et al., 2014; Song et al., 2008), although PMF does offer some advantages. Unlike PMF, data points cannot be individually weighted for uncertainty in Unmix (as an equal weight criterion is part of the Unmix approach), making measurements below the detection limit more difficult to work with. CMB requires the user to provide source profiles prior to apportioning mass (*f* would be a matrix of known values in **Equation 2-1**), so the model has knowledge of a solution to work toward, whereas PMF converges to a solution without fixed expectations (Norris et al., 2014).

For this study, EPA PMF v5.0.14, was used to perform source apportionment of hourly VOC measurements obtained by Gas Chromatography – Flame Ionization Detector (GC-FID) with weekly calibration to standards from the Essex, MD PAMS monitor from the summers of 2007 through 2015. These measurements were obtained from the EPA via the downloadable interface at: https://aqs.epa.gov/api. Similar to the Unmix source apportionment of VOCs from 1996-1999 at this location (Choi and Ehrman, 2004; Choi, 2004), along with total non-methane organic compounds (TNMOC) measurements, 23 critical, individual VOC species were determined for this study: ethane, ethylene, propane, propylene, acetylene, n-butane, isobutane, n-pentane, isopentane, 3-methylpentane, n-hexane, isoprene, 3-methylhexane, 2,2,4-

trimethylpentane, 2,3,4-trimethylpentane, 2-methylhexane, 2,3-dimethylbutane, 2-methylpentane, m/p-xylene, benzene, toluene, o-xylene, and 1,2,4-trimethylbenzene. The other 32 measured species were excluded from modeling because a significant percentage (20% or more) of measurements were consistently below the minimum detection limit (MDL) over at least four years.

Uncertainties for these measurements were calculated based on the methodology outlined by Brown et al. (2007). If a measurement was missing at a given hour, the median value for the species was used and provided an uncertainty of four times the median value. Measurements below the detection limit were given the value of half the MDL and had an uncertainty of 1.5*MDL. Measurements above the detection limit were given an uncertainty that followed the formula of (analytical uncertainty)*(concentration) plus MDL/3, where analytical uncertainty was set to 0.05 based on weekly calibrations to standards (Acefaw Belay, personal communication). Additional model uncertainty was set to 10% and applied to all values to help minimize and normally distribute residuals and account for modeling errors that could arise from atmospheric chemical transformations and source profile variations.

In addition to applying uncertainties for specific measurements, the PMF model also provides users with the ability to apply additional uncertainty to a species. Species are by default categorized as ‘strong’ but can be changed to ‘weak’ or ‘bad’ if a user-defined threshold is exceeded for categories such as low measurements, low signal-to-noise ratios, or large, non-normalized residuals. When a species is designated as ‘strong,’ no additional uncertainty is included. If a species is categorized as ‘weak,’ the uncertainties associated with all measurements are tripled, and setting a species as ‘bad’ will exclude its use by the model. TNMOC was used for the total variable, which is set to ‘weak’ by default. These species

exhibited a lower quartile of measurements below the MDL during a given year and were categorized as 'weak': 2- and 3-methylpentane in 2007, 1,2,4-trimethlybenzene in 2013, and 2-methlyhexane in 2014. All other species were 'strong.'

For each year, 100 base model runs were performed, and the run returning the lowest Q(robust) value (goodness-of-fit excluding uncertainty-scaled residuals greater than 4) was selected for reporting results. All base runs successfully converged to a solution, and exhibited stable Q(robust) values. Furthermore, Q(robust) values were at most 5% of the Q(true) value (goodness-of-fit considering all data points).

Additionally, 100 bootstrap runs along with a displacement run were performed for the best run for each year to ensure no significant errors existed in the factor solutions found. Displacement error estimates accounts for rotational ambiguity, as having only one constraint (non-negative source contributions) will likely not provide a unique solution despite finding a minimum for *Q*. Bootstrap error estimates also account for rotational ambiguity to a lesser degree, but are most useful for determining random error effects and discerning if a subset of observations are strongly influencing the solution (Paatero et al., 2014; Brown et al., 2015).

2.3 Results and Discussion

2.3.1 Identification of Source Factors

Figure 2.1a shows the five factor profiles returned for analysis of 2015 hourly measurements, and results from the other years displayed similar profiles (**Figure 2.1b**). Tracer species identified from previous studies were used to determine the factor solutions (Choi and Ehrman, 2004; Fujita, 2001; Sonoma Technology, 2011). The biogenic factor was determined by the large percentage of isoprene, and low percentages of other species. The natural gas factor was indicated by ethane and propane, gasoline sources by n-pentane, vehicle exhaust by

ethylene, propylene, and acetylene, and industrial sources by aromatics such as m/o/p-xylenes and 1,2,4-trimethylbenzene.

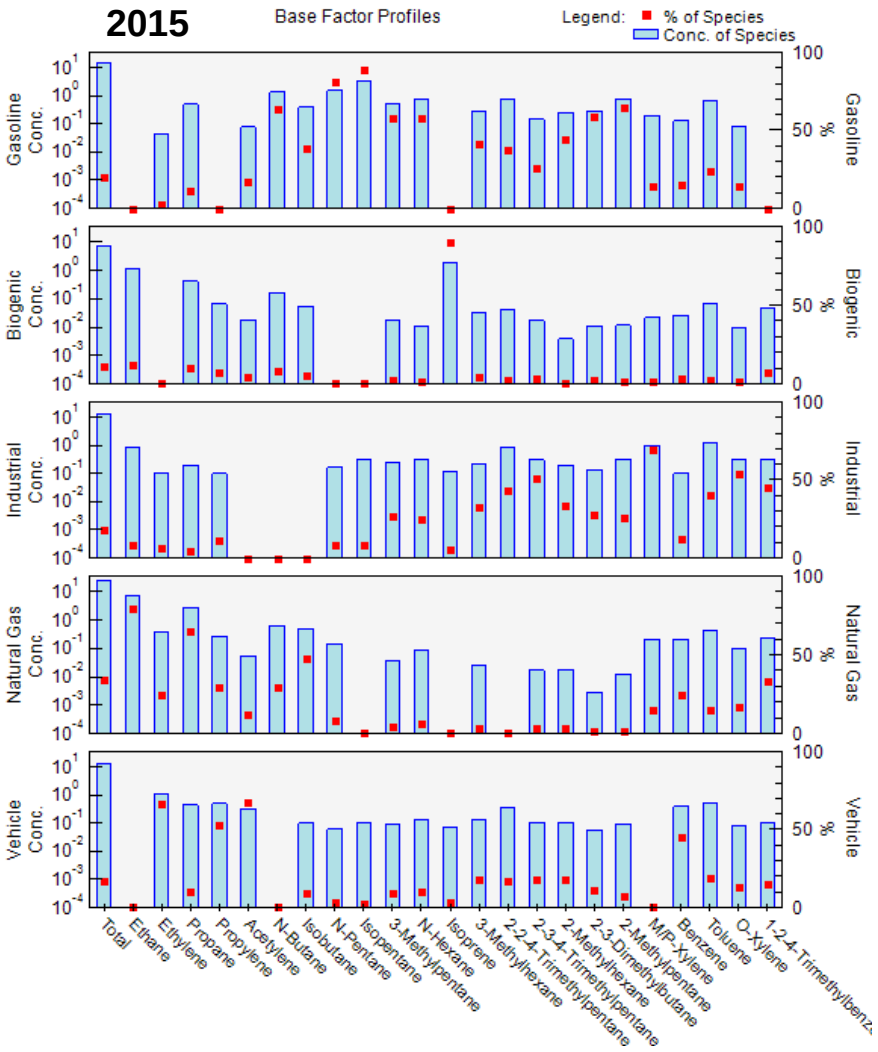

Figure 2.1 (a) Base factor profiles for 2015 VOC measurements at Essex, MD. Species concentrations are shown in the blue bars, and species percentages are marked by the red dots. Note the left-side y-axis for concentration is log-scaled.

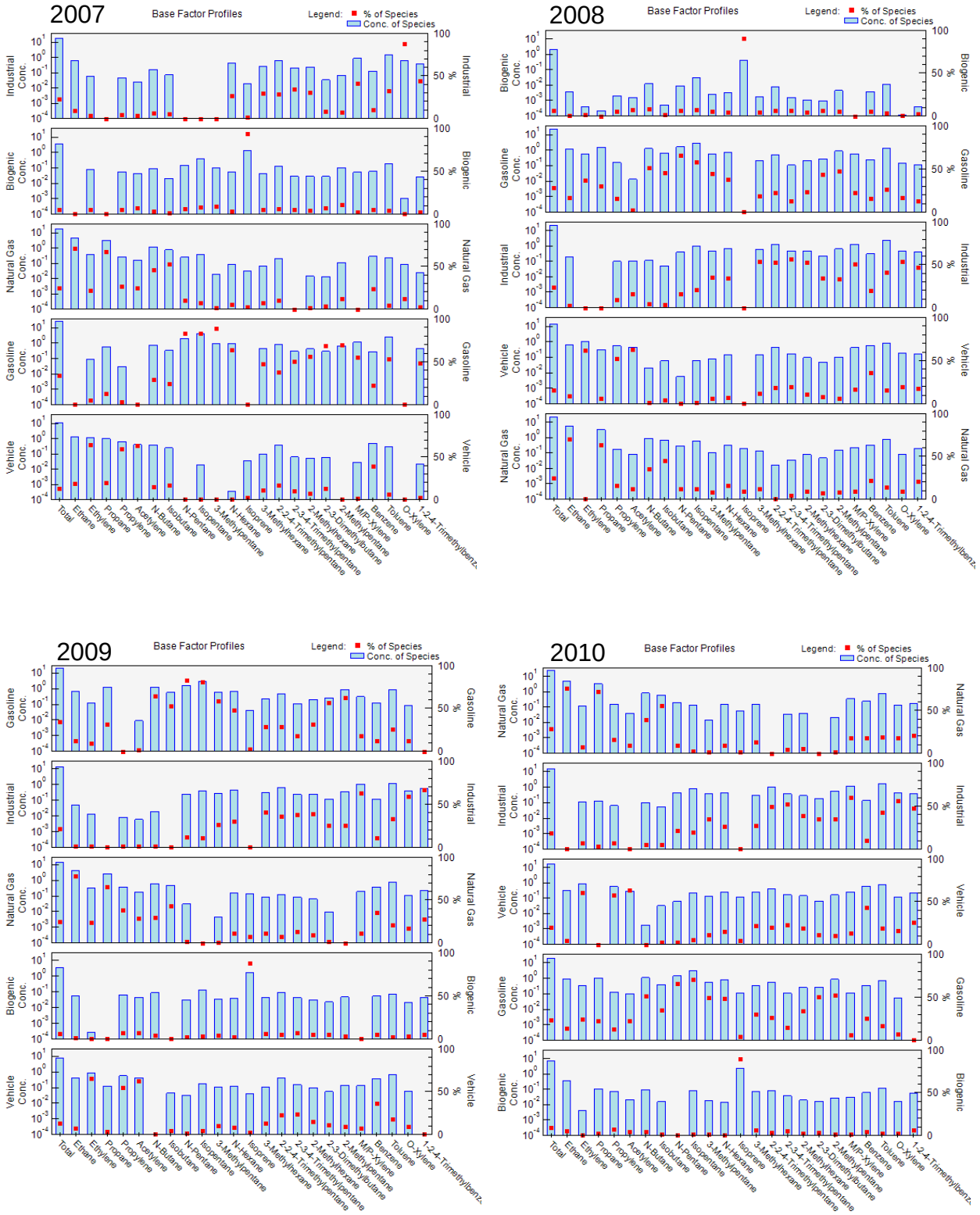

Figure 2.1 (b) 2007-2014 base factor profiles for VOC measurements at Essex, MD. Species concentrations are shown in the blue bars, and species percentages are marked by the red dots. Note the left-side y-axis for concentration is log-scaled.

Figure 2.1 (b) (continued) 2007-2014 base factor profiles for VOC measurements at Essex, MD. Species concentrations are shown in the blue bars, and species percentages are marked by the red dots. Note the left-side y-axis for concentration is log-scaled.

After initially attempting the six source solution presented by Choi and Ehrman (2004), a five factor solution was finally determined to make the most mathematical and physical sense. Whereas the aforementioned study saw gasoline in separate liquid and vapor source categories, PMF results for the later years showed a singular gasoline factor. One explanation could be that liquid gasoline was the smallest overall source, and a third of the gasoline vapor source. As VOC emissions have decreased over the past two decades, determination of this small source could become more difficult, and would be more likely to combine with the larger gasoline vapor factor which shares similar emission sources and diurnal variations.

With a six factor solution in PMF, results were not as consistent between base model runs, and the compositions of factors did not all make physical sense. While five of the six factors seemed similar to source patterns from previous studies, the sixth factor offered a small contribution (<5%) and contained only notable amounts of species such as 2- and 3-methylhexane that are usually spread between factors representative of gasoline, vehicle exhaust, and industrial sources, suggesting fewer factors should be used for determining a solution. When a four factor solution was attempted, the solution suffered as the gasoline factor was split between the natural gas and industrial factors.

In addition to looking at composition and tracer species to determine the resulting factors resolved by the model, diurnal profiles for each of the sources were also investigated to see if reasonable temporal trends existed (**Figure 2.2a**). Vehicle exhaust is seen to peak early in the morning as commuters head to work and again in the late afternoon and early evening as people head home. The biogenic source is seen to rise around sunrise, as photosynthesis begins, and trails off as the sun begins to set. The biogenic source exhibits a local minimum in the late morning where the emission rate is slower than the reaction rates consuming species such as

isoprene. Furthermore, these profiles matched the patterns observed in the Choi and Ehrman (2004) study. Diurnal profiles for the other years are shown in **Figure 2.2b.**

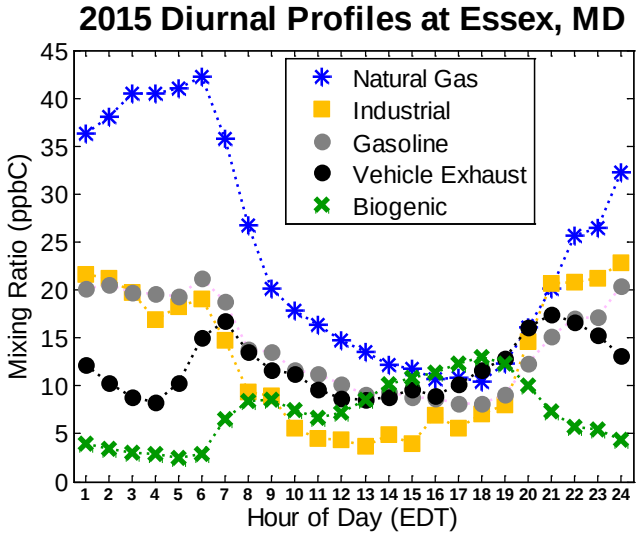

Figure 2.2 (a) Diurnal profiles for median concentrations from each of the five different factor solutions for 2015 VOCs.

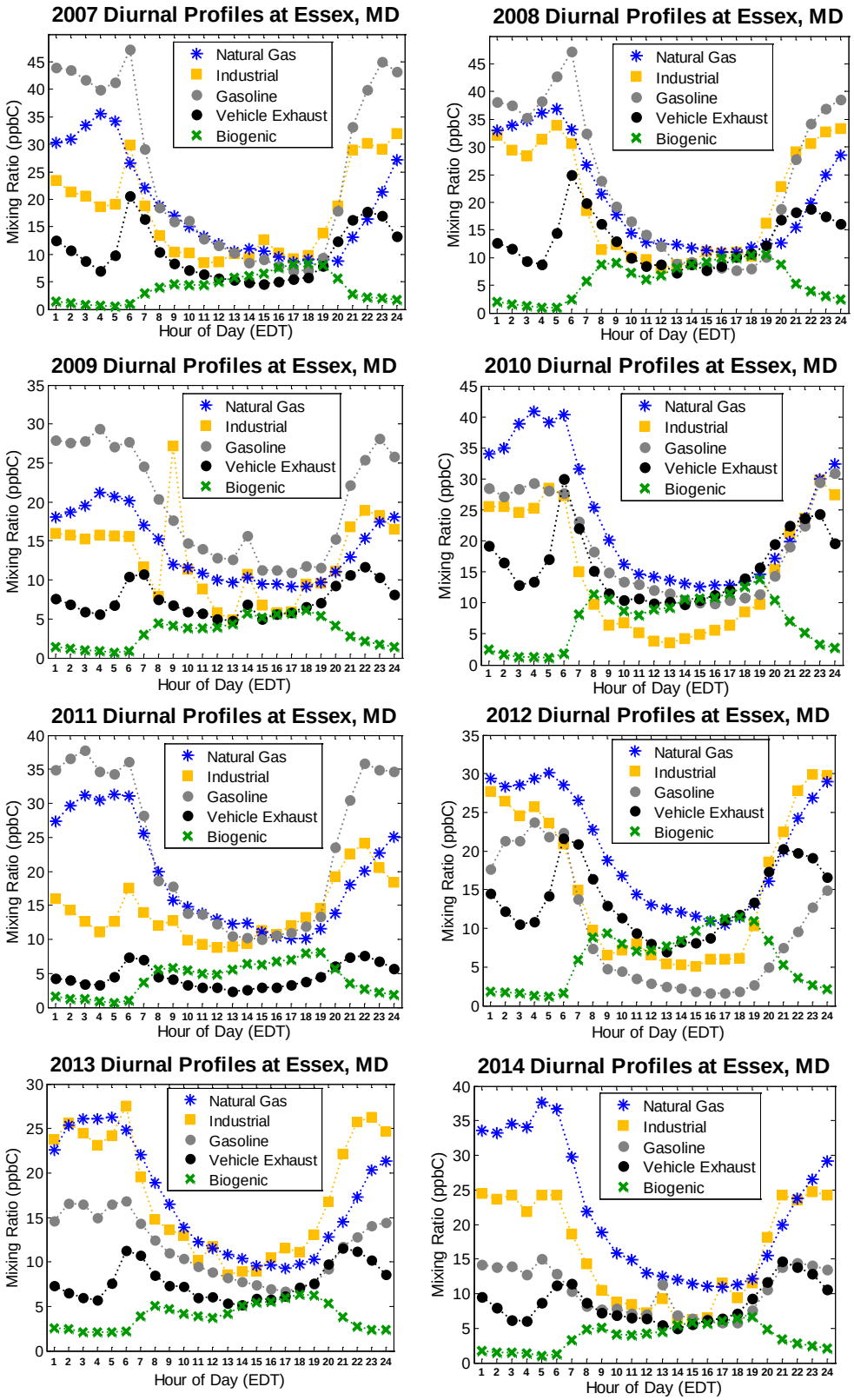

Figure 2.2 (b) Diurnal profiles for median concentrations from each of the five different factor solutions for VOCs, for each of the years 2007-2014.

2.3.2 Annual Results and Overall Trends

The results from the base model runs for each of the years are presented by percentage in **Figure 2.3** (along with the median and interquartile ranges found from each of the corresponding bootstrap error estimation runs, shown in **Figure 2.4**) and by total NMOC concentration in stacked bar plots (**Figure 2.5**). The gasoline and vehicle exhaust factors are closely related to mobile emission sources and are presented together as the sum of their contributions. On average, error estimations show an interquartile range of roughly 10% or less for each factor (or 20% for the combined gasoline and exhaust factors). Additionally, the resulting trends presented in **Figure 2.3** are also visible in **Figure 2.4**, indicating the solutions can be viewed with a reasonable degree of certainty.

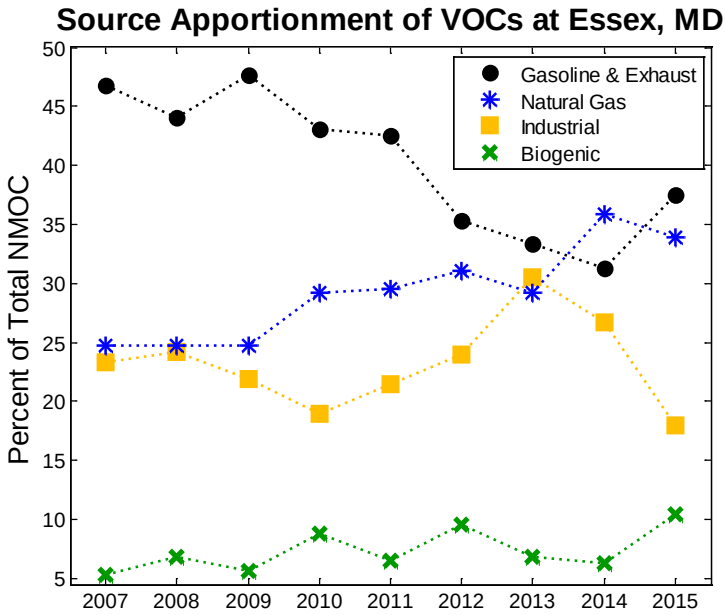

Figure 2.3 Percent of TNMOC mass provided by each factor for each year at Essex, MD.

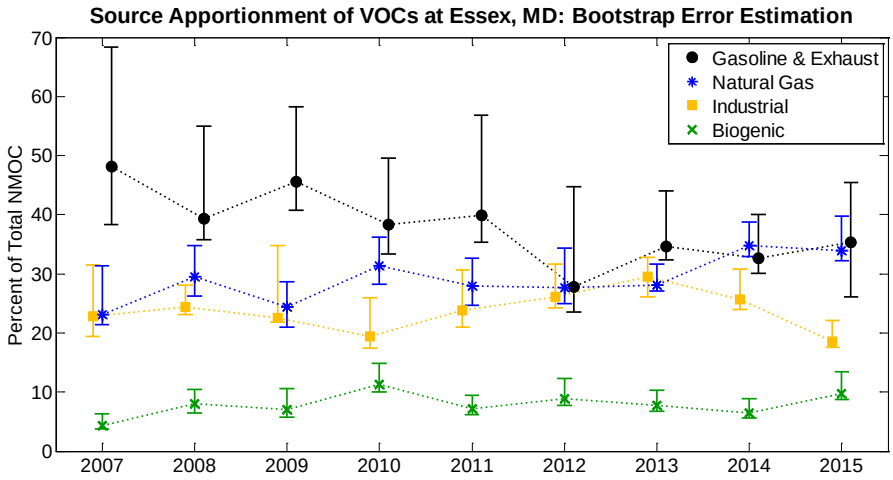

Figure 2.4 Bootstrap error estimation results for percent of TNMOC mass provided by each factor for each year at Essex, MD. Markers show the median for each factor, with the error bars representing the 25th and 75th percentiles.

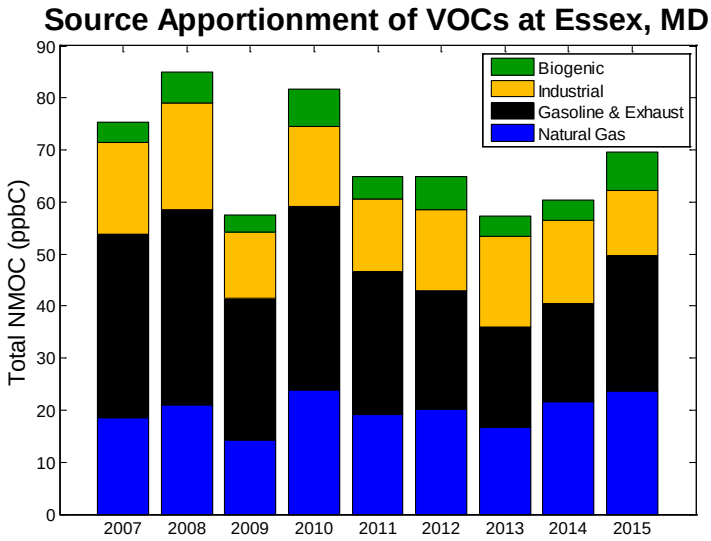

Figure 2.5 Concentration of TNMOC mass contributed by each factor at Essex, MD.

From 2007-2009, the gasoline and exhaust factors represented nearly half of all VOCs measured at the monitor. This percentage declined over the years, and was only responsible for roughly a third of TNMOC in later years. Lower concentrations of gasoline and exhaust can be seen to contribute to the decrease of TNMOC as the years have progressed. Several improvements and regulations have likely led to the decrease of these factors. The average age of

an automobile in 2014 was 11.4 years (USDOT, 2015), and almost an entire generation of the vehicle fleet had turned over during the years of this study. As a result of better technology and regulations, car emissions have become much cleaner over the years and would be expected to be lower in 2015 than in 2007. In 2007, the Maryland Clean Cars Program began enforcing strict rules for low emission vehicles (LEV) to lower ozone precursors (MDE, 2012). Additionally, during the time period of this study multiple federal regulations came into effect that would have decreased the impact of the gasoline factor. In 2007, the U.S. EPA issued final regulations to limit the content of benzene in gasoline and the evaporation of gasoline from portable fuel containers (EPA, 2016h), and in 2008, regulations began to limit evaporative losses from bulk gasoline plants, terminals, and pipeline facilities (EPA, 2008a).

Natural gas initially made up about 25% of the modeled VOC concentrations for 2007-2009, but began to increase in 2010. This increasing percentage for natural gas is similar to the increasing concentrations of ethane reported by Vinciguerra et al. (2015), and could be attributable to the rapid increase of upwind natural gas operations in the Marcellus Shale regions that began around that time. Further analysis and discussion of measurements of ethane concentrations at the Essex, MD monitor and natural gas is presented in Chapters 3 and 4.

The biogenic source is relatively constant by mass, contributing around 5-10% of the total NMOC. Isoprene emissions have a positive correlation with increasing temperatures up to ~40°C (Rasulov et al., 2010). Thus, the impact of summers such as 2010 which are extremely warm, would result in larger concentrations and percentages from the biogenic factor. On the other hand, a much cooler summer such as 2009 would make up a lower percentage of total NMOC. A slight positive correlation (r^2=0.21) was observed between daytime median biogenic factor concentration and median temperature (**Figure 2.6)**. Although the trends for the biogenic

factor do not correlate as well as expected with temperature, it does generally explain the year-to-year variability (**Figures 2.6 and 2.7**).

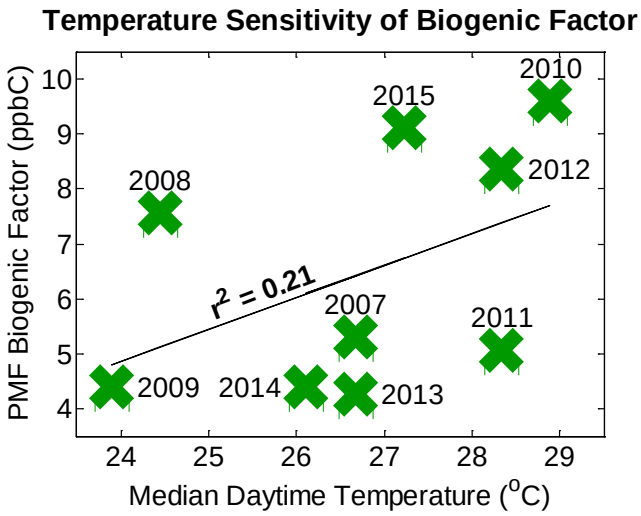

Figure 2.6 A positive, albeit weak correlation between median daytime summer temperatures and PMF biogenic factor solutions for years 2007-2015.

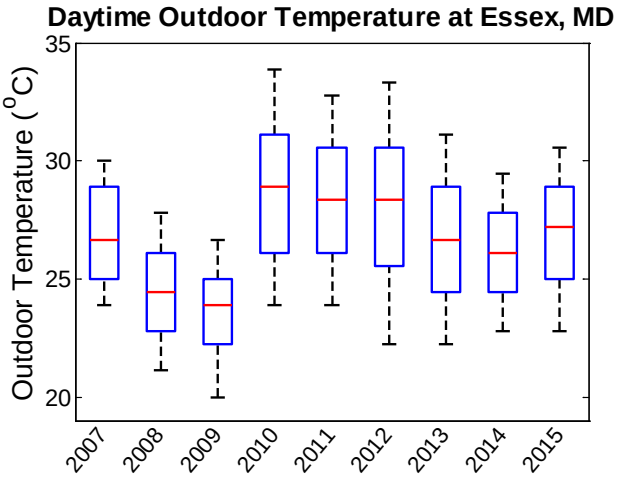

Figure 2.7 Daytime temperatures recorded at the Essex monitor. The median temperature is shown by red bars, the 25th and 75th percentiles marked by the blue boxes, and the 10th and 90th percentiles are represented by the whiskers.

The industrial factor, which includes sources such as surface coatings, printing, solvents, and other manufacturing processes, exhibited a maximum contribution (~30%) in 2013 but

decreased significantly over the next two years. Similarly, the 2013 value added was at its highest since the 2009 recession for the basic chemical and paint, coating, and adhesive manufacturing companies in Maryland reporting to the Annual Survey of Manufacturers (**Figure 2.8**), and in 2014 the value decreased (2015 data is unavailable at the current time). Concentrations of industrial factor VOCs exhibited a positive correlation to value added (measure of manufacturing activity derived from value of shipments less cost of materials, contract work, etc.) by these manufacturers from 2009 to 2014 (**Figure 2.9**). Several chemical plants are located 10-15km upwind from the monitor around Curtis Bay (**Figure 2.10**) where a variety of chemical products are manufactured. There are also several auto body shops within 2-3 km of the monitor, with one only two blocks away, whose surface coating services could make up a significant part of the industrial factor (**Figure 2.11**). The industrial factor varies over the years with increasing and decreasing contributions to total VOC, but it consistently trends with economic values.

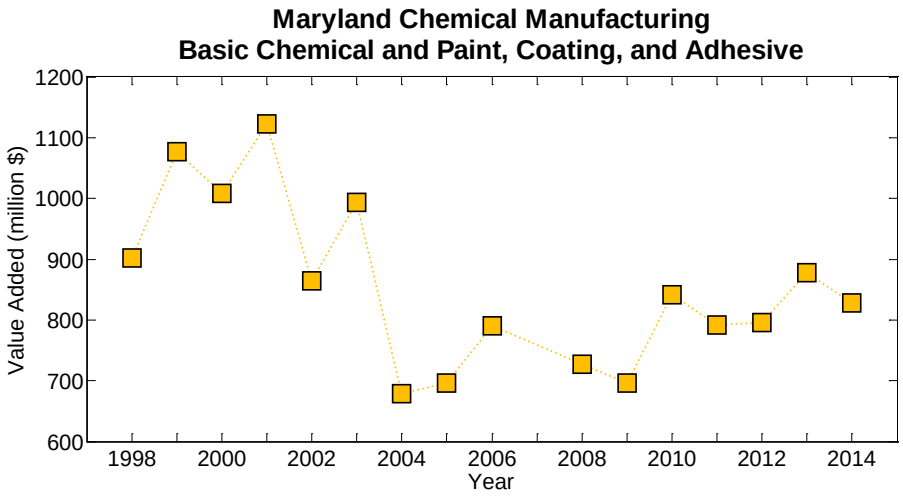

Figure 2.8 Value added for basic chemical and paint, coating, and adhesive manufacturers in the state of Maryland (Annual Survey of Manufacturers, 2016).

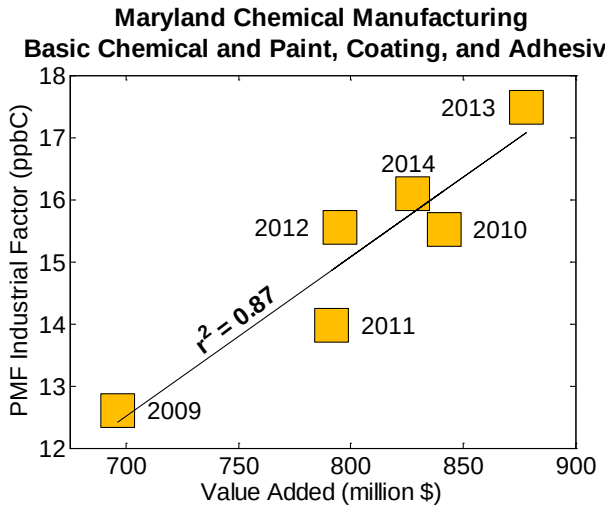

Figure 2.9 Strong, positive correlation between basic chemical and paint, coating, and adhesive manufacturing value added and the industrial factor solution for years 2009-2014.

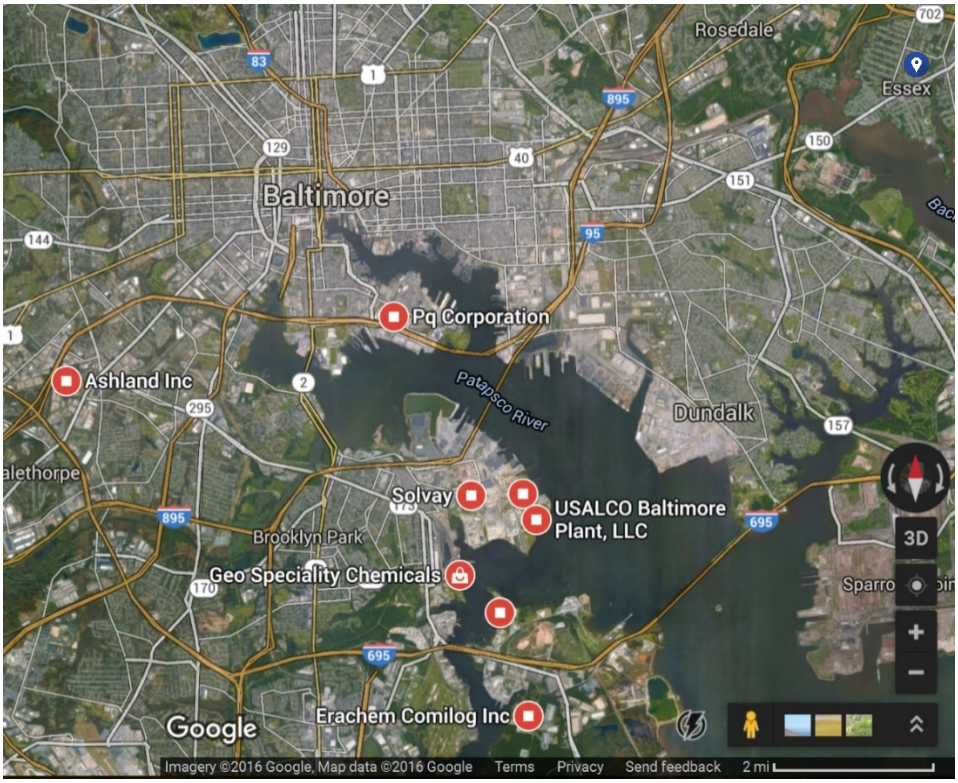

Figure 2.10 Google Maps results for Baltimore chemical plants (red markers) upwind of the Essex, MD monitor (blue marker).

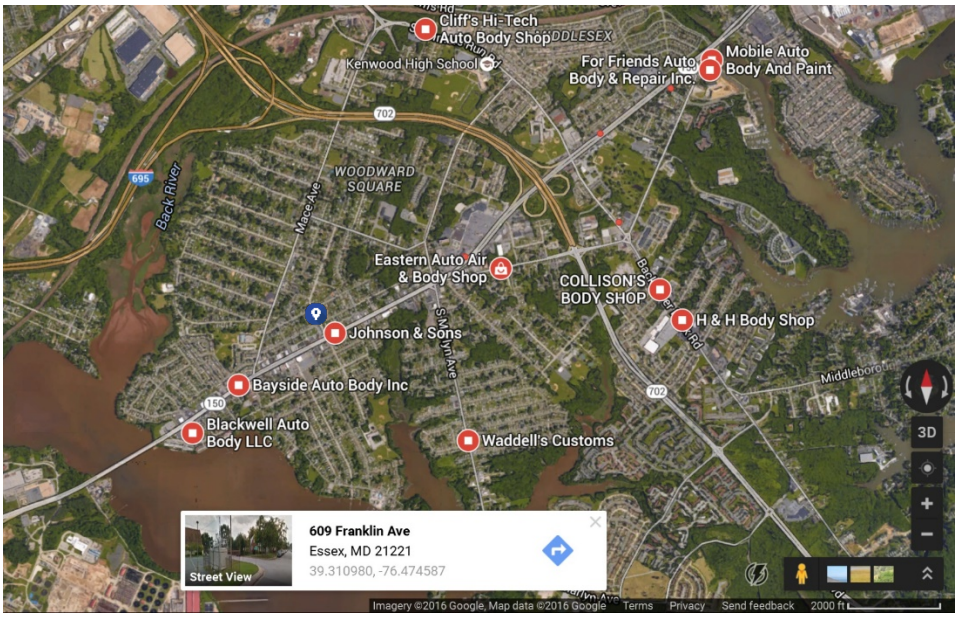

Figure 2.11 Google Maps results for auto body shops (red markers) surrounding the Essex, MD monitor (blue marker). Johnson & Sons is only two blocks away from the monitor. Approximated street address for the monitor is shown in the inset.

2.3.3 Reactivity-Weighted VOCs

The analysis thus far has considered VOC mass, but ozone formation depends on concentration and reactivity, and could vary as the composition of total VOCs has evolved through the years. Similar to the analysis done by Choi and Ehrman (2004), reactivity-weighted concentrations for the source categories from the Essex site were calculated. Each measured VOC species concentration is multiplied by its corresponding calculated ozone impact value from the maximum incremental relativity (MIR) scale (g O_3 formed/g C) listed in **Table 2.1**, to achieve this reweighting. Developed initially by Carter (1994), the MIR scale is derived from one-day box model simulations where the emissions of a given VOC species are gradually increased to quantify its capacity for ozone production. The MIR values for all species were recently updated by employing the SAPRC-07 chemical mechanism (Carter, 2010), and aromatic

species were further updated with the SAPRC-11 mechanism (Carter, 2012), with non-aromatic species showing no significant changes with the newest mechanism.

Table 2.1 Species and their respective MIR multipliers.

Species	MIR (g O_3/g VOC)[a]	Species	MIR (g O_3/g VOC)[a]
Ethane	0.28	Isoprene	10.61
Ethylene	9	3-Methylhexane	1.61
Propane	0.49	2,2,4-Trimethylpentane	1.26
Propylene	11.66	2,3,4-Trimethylpentane	1.03
Acetylene	0.95	2-Methylhexane	1.19
n-Butane	1.15	2-3-Dimethylbutane	0.97
Isobutane	1.23	2-Methylpentane	1.5
n-Pentane	1.31	M&P-Xylene	8.79
Isopentane	1.45	Benzene	1.43
3-Methylpentane	1.8	Toluene	5.3
n-Hexane	1.24	O-Xylene	8.73
		1,2,4-Trimethylbenzene	9.35

[a] Based on results from the SAPRC-07 mechanism with updated values for aromatics from SAPRC-11 (Carter, 2010; Carter, 2013)

This reactivity reweighting was applied to the factor solutions found for each year. The emphasis of this study is focused on the impacts of the VOC factors on ozone formation, so the profiles were estimated for the daytime hours (9am – 7pm EDT) when ozone is most efficiently formed. For each factor, the median factor concentration during this time interval was calculated and multiplied by each reweighted species contribution to determine the reweighted concentration. This process was repeated for each of the years, and the factor comparisons are presented by concentration in **Figure 2.12** and percentage in **Figure 2.13**.

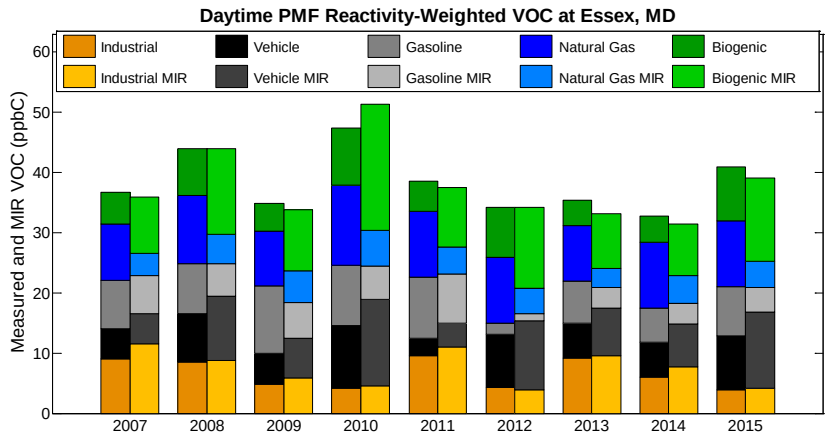

Figure 2.12 Daytime VOC mass presented based by measured concentration (left bar) and reweighted for reactivity (right bar) for each modeled year.

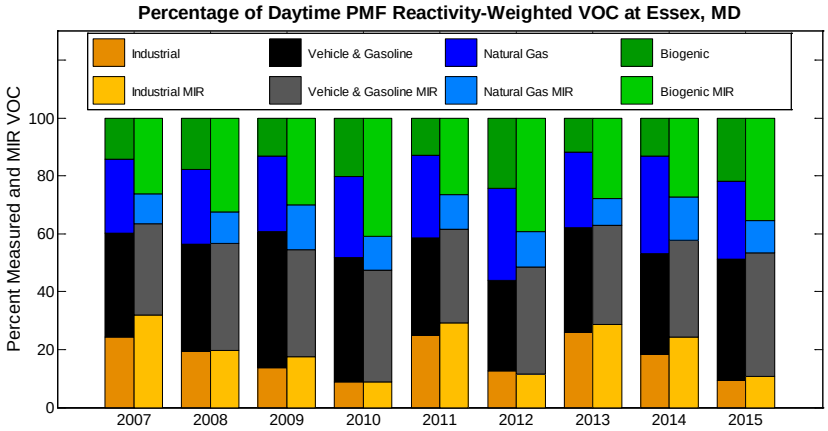

Figure 2.13 Daytime VOC percentage by measured concentration (left bar) and reweighted for reactivity (right bar) for each modeled year.

One of the largest changes observed is for the biogenic factor, which was seen to double in concentration and percent of TNMOC because of the highly reactive nature of isoprene. By measured concentration, biogenic VOCs were originally shown to be a minor fraction of the total mix, but reactivity reveals they constitute one of the most important VOC emission sources for the area. Because isoprene is so reactive, it is likely underestimated as it may have been emitted and reacted before being measured (Choi and Ehrman, 2004; Fujita, 2001). Thus, the biogenic

factor would be underrepresented in these results, and be an even greater component of reactive VOC sources.

The other large change occurs in the natural gas factor, which alternatively is cut in about half. Dominant species in natural gas such as ethane and propane are relatively unreactive, having MIR values under 0.5, causing this dramatic decrease. Natural gas was one of the largest VOC factors based on measurements, but with respect to reactivity, it contributes one of the smallest impacts on ozone formation. An increasing percentage of natural gas was observed over the later years in the previous analysis, but adjusting for reactivity removes any such trend, as the overall effect on ozone formation is minimal.

The industrial factor is marginally larger but mostly unchanged when considering reactivity. While it does contain many reactive aromatic species, it is also composed of larger alkane species which have MIR values close to unity. In years where the industrial factor concentration was more abundant with aromatics, the MIR increase would be expected to be larger.

Gasoline and exhaust factors are still grouped together in **Figure 2.12**, but presented in different shades because the individual factors respond differently to MIR adjustments. However, when taken together the gasoline decreases (less reactive alkanes) are offset by the vehicle exhaust increases (more reactive alkenes), leaving the overall combined factor unchanged by the process. When all factors are reweighted using MIR, gasoline and vehicle exhaust are seen to be the most significant anthropogenic source of VOCs. It is worth noting that the monitoring station is situated at the corner of a residential intersection, in the corner of a parking lot (**Figure 1.6**), so one might expect the influence of vehicular emissions, as well as gasoline sources to a lesser extent, to be potentially overrepresented for this location. However,

there are four-lane highways ~1.5 km away encompassing the monitor (with MD 150 passing through Essex two black away), and three gas stations with ~0.5 km, which would also make such emissions fairly ubiquitous for the area.

While this methodology provides insight for appreciating the effects of VOC emissions on ozone formation, an uncertainty analysis is necessary. Due to low concentrations, the modeling process utilized less than half of the available measured species. In addition to the measured species, there are thousands of unmeasured VOC species exhibiting a wide range of reactivities that are not measured or available for this study. For example, in addition to isoprene, biogenic sources emit other unmeasured species (such as α- and β-pinene and other monoterpenes) that are also reactive (MIR ~4) (Carter, 2010), but unaccounted for in this analysis. Unmeasured isoprene oxidation products such as formaldehyde and methyl vinyl ketone (MVK) would also be expected to significantly impact results. Similarly, larger alkanes (heptane, octane, nonane, decane) exhibited low measurements that excluded them from PMF modeling. These species would be expected to appear in the industrial, gasoline, and vehicle factors, and their low MIR values (1.07, 0.90, 0.78, 0.68, respectively) could lower the impacts of these sources. Using only 23 VOC species to assess the reactivity of VOC factor solutions will contain inherent errors, however the species not included were a result of measurements below the detections limit, and would be unlikely to significantly impact these results.

2.4 Conclusions

Ambient hourly measurements of VOC species from 2007-2015 at the Essex, MD monitor were separated into source factors using the PMF model. The industrial and biogenic factors varied through the years, but have provided relatively consistent percentages of the total NMOC. The percentage of VOCs coming from the gasoline and vehicle exhaust factors has

shown a declining trend as vehicle and fuel standards have improved, but the percentage from the natural gas factor has increased. Results for 2015 may suggest a potential reversal of trends as a sharp increase was observed for the gasoline and exhaust factors, but it remains to be seen if this is a trend reversal or just part of year-to-year fluctuations.

These PMF solutions were reweighted for reactivity using MIR, which provided a method for understanding the reduction of VOCs with respect to ozone formation. Biogenic sources, which make up a low percentage of total concentration, were shown to be one of the major contributors of VOCs forming ozone. Gasoline and vehicle exhaust appear to be the major source of anthropogenic VOCs contributing to ozone formation, despite the decreasing trend observed from modeled measurements. As these emissions continue to decline as expected over the following years, biogenic emissions could become the single most important source of ozone-forming VOCs. Although natural gas concentrations were seen to increase, the MIR weighting suggests the trend exhibits no significant, direct impact on ozone formation. However, if this increase is a result of upwind natural gas operations, other combustion-related emissions associated with obtaining shale gas such as NO_x and more reactive VOCs could lead to increased ozone production.

Chapter 3 Regional Air Quality Impacts of Hydraulic Fracturing and Shale Natural Gas Activity: Evidence from Ambient VOC Observations

The majority of this chapter appears as published in Vinciguerra et al. (2015). Content has been modified for clarity.

3.1 Introduction

As global energy demands continue to grow, new and alternative energy sources have been sought out. One emerging energy source, natural gas, is gaining favor over coal because of lower emissions of CO_2 and significantly lower nitrogen oxides (NO_x) and sulfur oxides (SO_x) (de Gouw et al., 2014; EPA, 2014b). In the United States, natural gas production has quickly increased and its cost has dropped, making it an economically viable energy source (EIA, 2014a). Because of these advantages, natural gas usage is expected to grow rapidly and displace coal as the second largest source of energy by 2025 (ExxonMobil, 2014).

An increasingly popular method of obtaining natural gas resources is through the combination of horizontal drilling to allow access a large amount of the shale, followed by hydraulic fracturing, where a mixture of water, sand, and chemical additives is pumped at high pressure to free and extract natural gas trapped within shale layers (USGS, 2014). According to the U.S. Energy Information Agency (EIA) the amount of natural gas obtained from shale gas wells in the United States has tripled between 2009 and 2012 (EIA, 2014b), providing more than a third of total U.S. natural gas production by 2012 (EIA, 2014c). The major shale plays which account for more than 60% of total U.S. shale gas production since 2010 are the Barnett in Texas, the Haynesville in Texas and Louisiana, and the Marcellus, centered in Pennsylvania and

West Virginia where about a third of natural gas production since 2013 has occurred (EIA, 2014d).

Although its composition can vary due to geographical location, shale gas is predominately, and sometimes almost entirely, methane, a greenhouse gas with climate implications (Bullin and Krouskop, 2009). Compared to coal, combustion of natural gas for generating electricity produces only about half the CO_2 and reduces climate forcing, but only if less than about 3% of the methane escapes into the atmosphere (Howarth et al., 2011; Alvarez et al., 2012). Several studies have been conducted to determine the total leakage-based emissions from natural gas operations; estimates range from as low as 0.42% up to 17.3% (Allen et al., 2013; Caulton et al., 2014; Howarth et al., 2011; Karion et al., 2013; Kirchgessner et al., 1997; Pétron et al., 2012; Pieschl et al., 2013; Schneising et al., 2014). In 2013 the Intergovernmental Panel on Climate Change increased the 100 year global warming potential of methane to be 28 to 34 times greater than that of CO_2 (IPCC, 2013). Thus, it is vital to quantify the leakage rate, and apply necessary control technologies to curtail emissions.

In addition to climate impacts from methane emissions, air quality can also be affected by natural gas operations and the numerous emission sources associated with the drilling, hydraulic fracturing, and production processes and associated equipment. In the Mid-Atlantic States, the Marcellus shale in the Appalachian basin is estimated to contain $4x10^{12}$ m^3 of unproved technically recoverable shale gas (EIA, 2012). A modeling effort for this shale play by Roy et al. (2014) considered numerous emission sources such as completion venting, a process in which fluid and debris are cleared from the well, and the natural gas and diesel engines powering various trucks, compressors, drilling rigs, and pumps. This study predicted that for the year 2020, Marcellus shale activities would, on average, account for 12% of the total NO_x and volatile

organic compound (VOC) emissions and 14% of the total particulate matter (PM) in the region, and these emissions could complicate attainment of PM and ozone standards.

Along with these standard emissions associated with drilling and fracturing a well, there are other sources related to hydraulic fracturing to consider. When liquid unloadings are performed to clear a well bore of accumulated liquids for increased production, methane can be released to the atmosphere, and most of the methane emitted in these instances comes from a small fraction of wells which are frequently unloaded (Allen et al., 2014). Large emissions of VOCs have been observed on oil and gas well pads because of leaks from dehydrators, storage tanks, compressor stations, and pneumatic devices and pumps, as well as evaporation and flow back pond water (Warneke et al., 2014). Another non-negligible source of methane emissions are abandoned wells - those no longer active in the natural gas production process. There are an estimated 300,000 – 500,000 abandoned wells in Pennsylvania, and it has been suggested that they could account for up to 7% of Pennsylvania's 2010 anthropogenic methane emissions (Kang et al., 2014).

While the consequences for localized pollution from emissions associated with hydraulic fracturing processes are certainly of significance, the transport of these emissions to downwind regions is also a major issue, especially for major metropolitan areas already struggling to attain current standards (Kemball-Cook et al., 2010). Although the State of Maryland does not currently have extensive shale natural gas operations within its borders (MDE, 2015), the neighboring states including Pennsylvania and West Virginia house thousands of wells responsible for a tenfold increase in natural gas production volumes from 2009 to 2013 (PADEP, 2014). **Figure 3.1** shows counties in neighboring states where new unconventional natural gas wells were drilled from 2005 through 2012, the most recent year for which well production

information is available for all four states, and is also indicative of regions where hydraulic fracturing occurs.

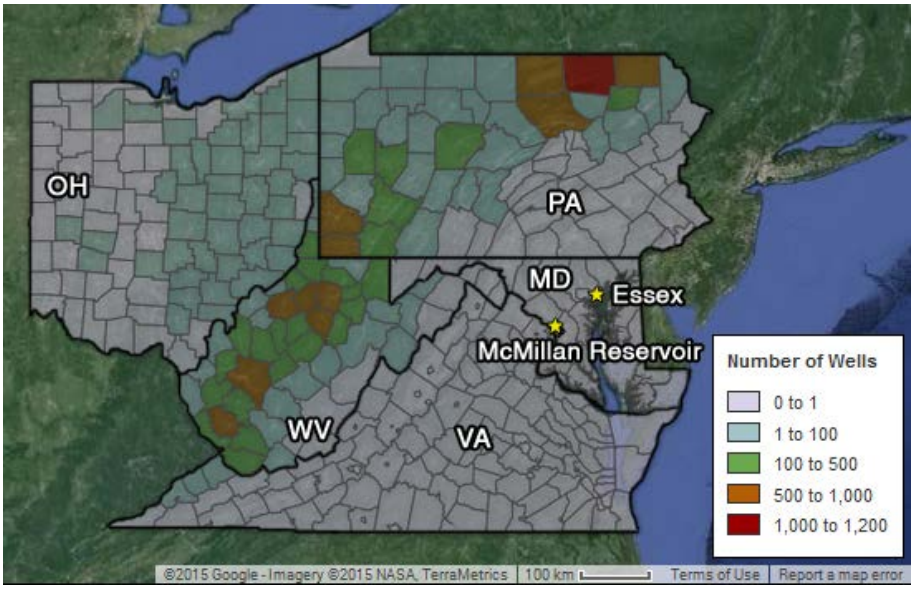

Figure 3.1 Number of total unconventional natural gas wells drilled by county in the Marcellus shale region from 2005 through 2012. The northern and southeast counties of Pennsylvania contain the most newly-drilled wells. Essex, MD and McMillan Reservoir (DC) monitor locations are also shown.

Ethane emissions in the Northern Hemisphere are mainly anthropogenic with about 70% originating from fossil fuels (mostly evaporative), and biomass burning and biofuel use making up the remainder of emission sources (Simpson et al., 2014). In northwestern Pennsylvania with nearby areas of oil and gas production, Pekney et al. (2014) observed average ethane concentrations of 9.2, 10.3, and 15.9 ppb. These concentrations are well above the ~1 ppb Northern Hemisphere background concentration of ethane (Rinsland et al., 1987; Rudolph et al., 1996) and indicate the local impact of emissions from oil and gas wells. The transport of emissions by prevailing winds is a well-documented occurrence affecting Maryland and other East coast states (Hains et al., 2008; He et al., 2013a, 2013b, 2014; Ryan et al., 1998; Taubman et al., 2004, 2006). A back-trajectory investigation by Taubman et al. (2006) found that the majority of wind trajectories arriving in the Mid-Atlantic U.S. passed through the regions where

hydraulic fracturing now occurs. Wind data collected at the wind profiler in Beltsville, MD also show a high frequency of winds arriving from the northwest and west (**Figure 3.2**). Additional wind roses are available in the supporting information (**Figures A1.1-A1.3**). In this chapter, I quantify how observed concentrations of ethane monitored in Baltimore, MD and Washington, DC, have risen as a likely result of the development of the Marcellus Shale Play.

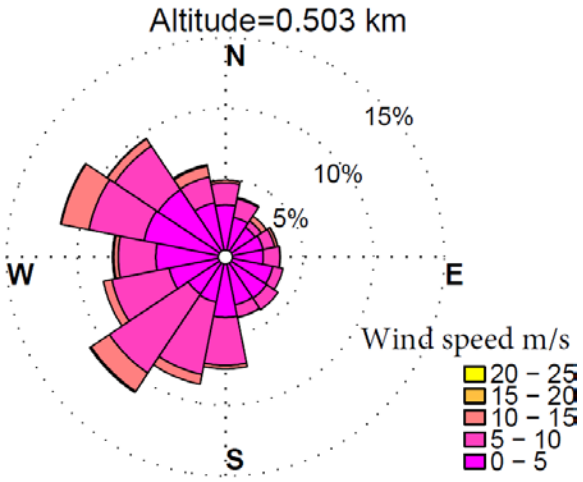

Figure 3.2 Wind rose showing wind velocity frequencies and direction at 503 m AGL provided by the wind profiler at Beltsville, MD. Wind velocities are taken from daytime hours (10am – 7pm) during the month of July in years 2012-2014. Winds are predominantly from the west where natural gas operations have increased in recent years. [Wind rose provided by Kostya Vinnikov].

3.2 Methods

The U.S. Environmental Protection Agency (EPA) has established numerous sites for monitoring pollutants. Following the 1990 Clean Air Act Amendments, Photochemical Assessment Monitoring Stations (PAMS) were created to monitor ozone, its precursors of NO_x and VOCs, and surface meteorology in regions of ozone nonattainment (EPA, 2014a). The monitor at Essex, MD was set up to track emissions for the Baltimore ozone nonattainment area. This is the monitor closest to the Marcellus shale which provides a historical record of VOC

measurements with hourly resolution. During the summer months of June, July, and August when ozone levels can often be hazardous to human health, concentrations are recorded every hour, providing a rich dataset for analysis. A suite of 56 VOCs are measured by GC-FID and calibrated weekly to maintain analytical precision to within +/-5% (Acefaw Belay, MDE, personal communication). Although methane is not included, ethane is measured and can be used as a tracer for fugitive natural gas production emissions, as the ethane recovered from natural gas production is separated from the methane ultimately distributed commercially. The composition varies geographically, but ethane makes up a significant portion (3-16%) of the Marcellus shale gas (Bullin and Krouskop, 2009). Methane, with an atmospheric photochemical lifetime of about a decade, is relatively well mixed in the troposphere. Ethane, with a photochemical lifetime of several weeks (Blake and Blake, 2003), is essentially inert with respect to photochemical loss on time scales of transport from the sources to the monitors (1-2 days), but still shows strong spatial and temporal gradients, making it a useful tracer.

In addition to the Essex, MD location, another Mid-Atlantic PAMS location with similar surroundings and conditions was considered: McMillan Reservoir in Washington, DC. Like Maryland, Washington, DC does not currently have hydraulic fracturing operations within its borders, but could easily be affected by transported emissions from neighboring states. Measurements from 1996-2013 are shown for these locations. A site outside the city of Atlanta, Georgia in Rockdale County was selected to serve as a control environment, as its air quality is influenced by urban emissions from heavy motor vehicle traffic and natural gas delivery, as well as biogenic emissions, similar to the Baltimore/Washington region, but Georgia and nearby states do not have extensive natural gas production. At this location, measurements from 1996-2013 are also shown.

As the boundary layer collapses following sunset, the concentrations of ethane increase due to the change in mixing volume. Because of this strong dependency on boundary layer height, only the concentrations during local daytime hours from 10am to 7pm were considered since the boundary layer depth should show little long-term trend. For each site, each year analyzed in this study contains at least 200 concentration observations from at least two different months, with the exception of June only for 2010 and August only for 2013 at Rockdale County.

3.3 Results and Discussion

3.3.1 Trend Analysis

The historical decline of total non-methane organic compounds (TNMOC) at Essex, MD (**Figure 3.3**) shows that strategies to curtail VOC emissions from sources such as solvent usage, gasoline storage and distribution, and other industrial processes have been successful (MDE, 2011; EPA, 2015b). In **Figure 3.4a,** Essex, MD ethane concentrations followed this same general downward trend continuing for about a decade beginning in 1996. However, around the same time that hydraulic fracturing operations began in surrounding states (circa 2009), ethane concentrations stopped decreasing, and were unmistakably increasing by 2012 and 2013 (**Figure 3.4**).

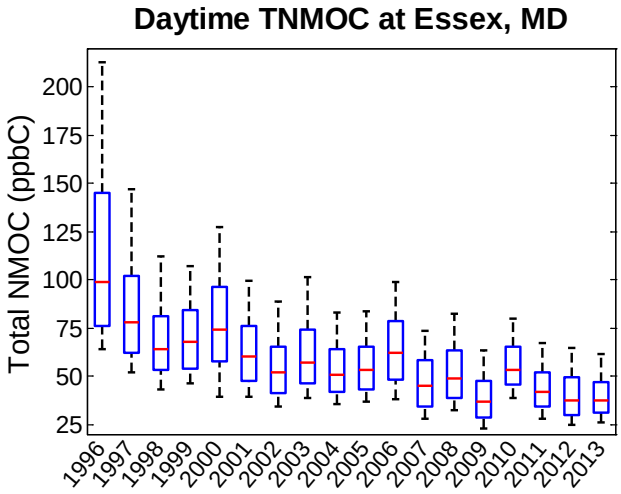

Figure 3.3 Daytime TNMOC concentrations at Essex, MD from 1996 to 2013 are shown by box and whisker plots. The box provides the 25th and 75th percentiles, with the median represented by the red bar, and the whiskers extend to the 10th and 90th percentiles.

To test for the possibility that ethane is increasing at Essex, MD because of a local source, the site at McMillan Reservoir in Washington, DC was also considered. **Figure 3.4b** shows an increase in ethane concentrations at McMillan Reservoir during the most recent years, despite several years exhibiting a decreasing trend. This new trend of increased ethane concentrations at more than one location suggests that several downwind areas could be affected by the transport of fugitive emissions and other pollutants associated with natural gas operations.

In contrast (**Figure 3.4c**), ethane concentrations have continued to trend slightly downward since 1996, and no discernible increasing trend is evident in the Atlanta region in the more recent years. If increased ethane concentrations were attributable to sources other than natural gas production and associated operations, then this site should show similar increases, but the State of Georgia has no major hydraulic fracturing activity within its borders or in neighboring states. TNMOC plots for the McMillan and Rockdale sites are available in the supporting information (**Figures A1.4 and A1.6**).

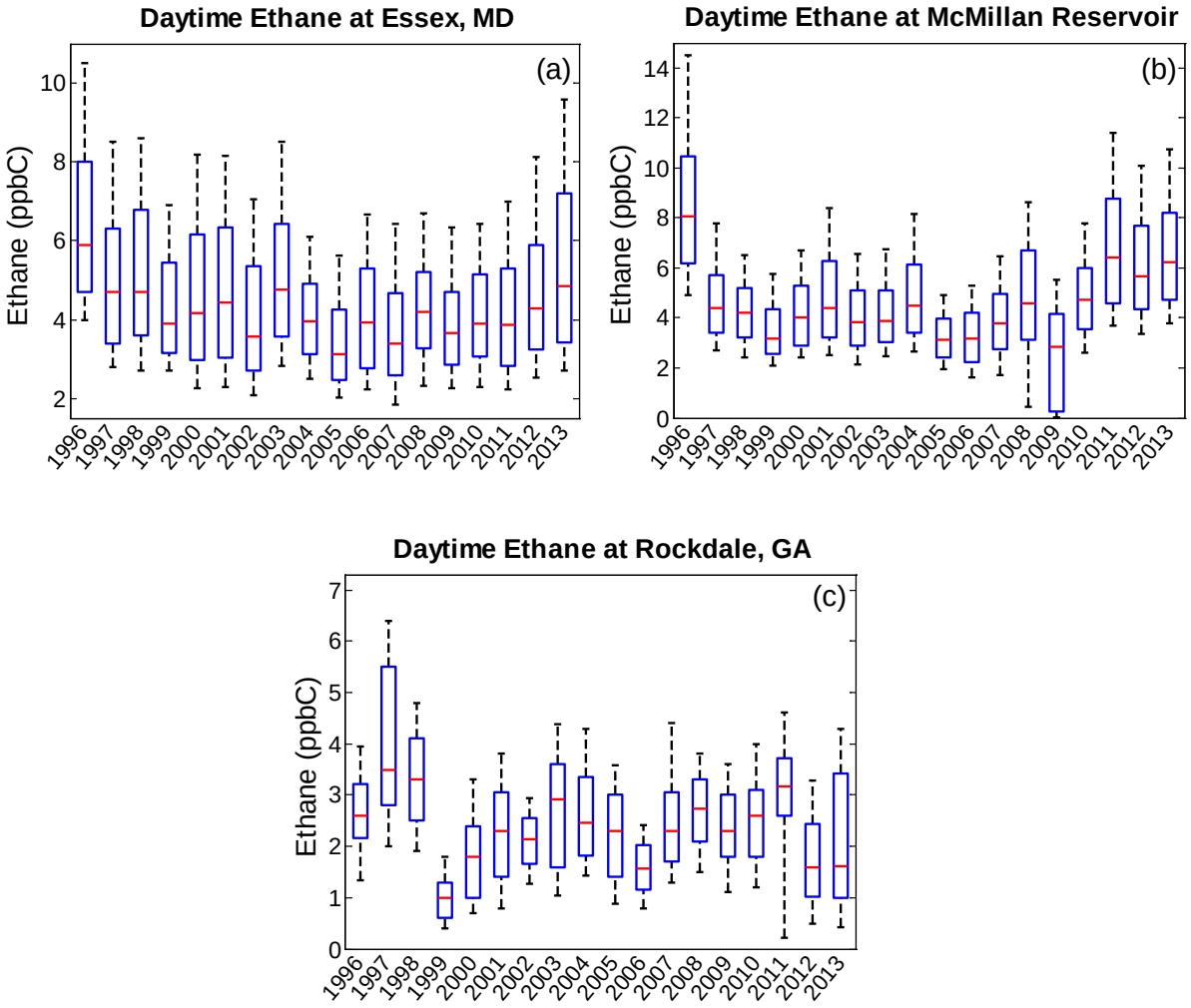

Figure 3.4 From 1996 to 2013, hourly daytime ethane concentrations from (a) Essex, MD, (b) McMillan Reservoir (DC), and (c) Rockdale County, GA are presented by box and whisker plots with the same statistical parameters as **Figure 3.3**.

Another approach taken was considering how the diurnal cycle of ethane has shifted at the Essex, MD site. **Figure 3.5** demonstrates the departure of concentrations of ethane from a previously established baseline over the most recent years. While there are year-to-year differences in ethane concentrations from 2004-2010 shown in **Figure 3.4a**, the overall trend is nearly flat for the time period. As a result the concentrations from these years were averaged together to establish the lowest placed diurnal cycle seen as the blue squares in **Figure 3.5**. The overall concentrations of ethane have increased annually– in the past three years the baseline has

increased by 1.1 ppbC. This sudden rise, especially given that TNMOC is decreasing, is indicative of a rapidly growing emission source such as natural gas operations.

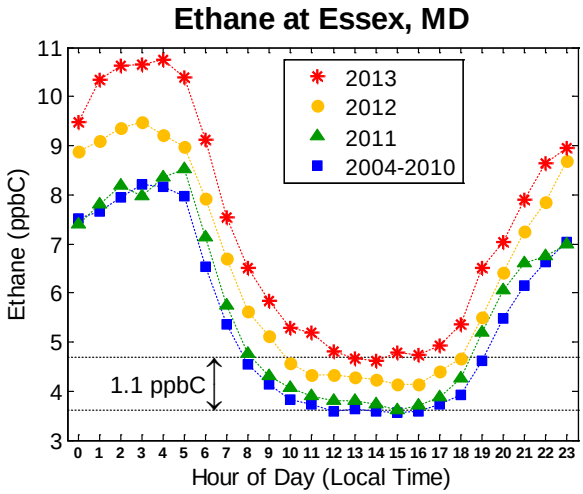

Figure 3.5 The diurnal cycle of ethane at Essex, MD showing the geometric mean concentration at each hour. Concentrations of ethane from 2004 to 2010 were averaged to establish a period unaffected by natural gas operations, and subsequent years show a continuing departure from this baseline.

Finally, the ratio of ethane to TNMOC at Essex, MD was examined and compared to natural gas production in the Marcellus shale (**Figure 3.6**). From 2000 to 2007, the median amount of ethane remained around 7-8% of the total NMOC, but rose quickly after 2010 to nearly 15% by 2013. The upwind production rates exhibit a similar rapid increase. For each year, the median production rate from June through August was compared to the median observation at Essex, MD during the same months. With r^2=0.82, a strong correlation was found between the Essex, MD ethane to total ratio and natural gas production in the Marcellus shale. Likewise, a positive correlation of r^2=0.59 was found when daytime ethane concentrations at Essex, MD from June, July, and August of 2010-2013 were compared to production rates from the Marcellus shale (**Figure 3.7**). Additional ratio (**Figures A1.5 and A1.7**) and correlation (**Figures A1.8-A1.10**) plots are available in the supporting information.

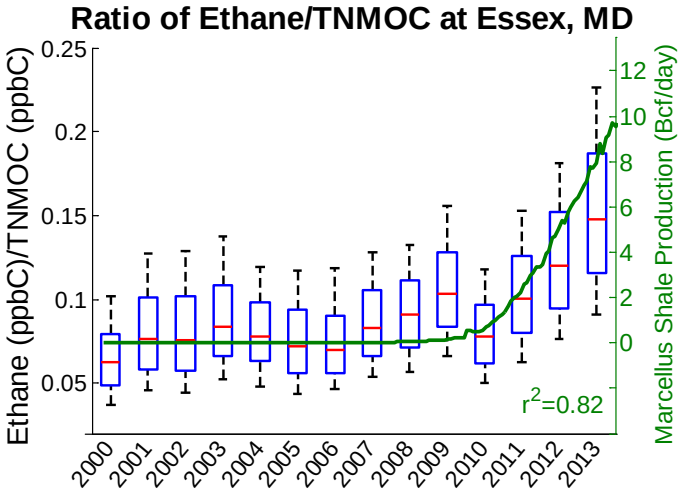

Figure 3.6 The ratio of ethane to TNMOC observed at Essex, MD is shown by box and whisker plots with the same statistical parameters as **Figure 3.3**. In addition, the production rates from the Marcellus shale in Pennsylvania and West Virginia are shown in green. A strong correlation was observed with an r^2 value of 0.82.

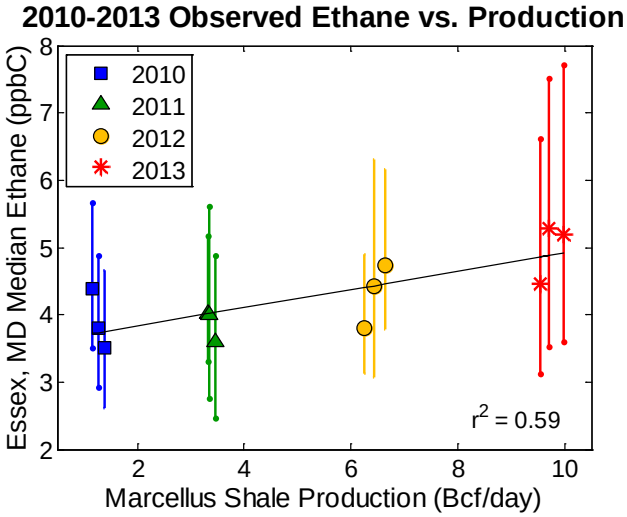

Figure 3.7 Monthly summer values from 2010 through 2013 of observed daytime ethane concentrations at Essex, MD vs. Marcellus Shale production. The uncertainty bars provide the 25th and 75th percentiles of measured ethane during each month.

3.3.2 Other Measured VOCs at Essex, MD

In both Essex, MD and Washington, DC, the sum of observed VOC (TNMOC) has generally decreased over the past decades, leveling off since about 2009 (**Figures 3.3 and A1.4**).

Rockdale County, GA, has shown no discernable trend (**Figure A1.6**). Propane has shown no increase in Essex, but has increased in Washington, DC (**Figures A1.11 & A1.12**). The diversified uses of propane such as cooking, heating, and equipment and vehicular use (EIA, 2015a) might hide slight increases from upwind natural gas operations. From the limited measurements of well gas composition available in the public domain, propane is estimated to make up about 5% of wet Marcellus shale gas (Conder and Lawlor, 2014; Foster, 2013; Pace Global, 2010); the driest reported regional composition was 1% propane (Bullin and Krouskop, 2009). Only 30% of the shale gas produced in Pennsylvania since 2010 is wet gas (down from 35% in 2009) (PADEP, 2014), indicating shale gas propane is much less abundant as ethane. At the Atlanta site, the ethane to propane ratio is near unity, much lower than that found in natural gas, reflecting the use of propane fuel in urban areas (**Figures A1.13 and A1.14**). The ratio of ethane to propane in Essex is rising to approach the natural gas emissions ratio (**Figure A1.21**). Total production of propane and propylene in the East Coast region slightly increased in 2013 (EIA, 2015b), but a production increase at natural gas plants (EIA, 2015c) has been offset by an overall decline from refineries (EIA, 2015d), and thus, industrial emissions are expected to have remained relatively constant. The Sasol refinery in Baltimore was taken out of service in July 2007, and this removed source of VOCs might also hide slight recent increases from upwind sources (Christopher Wheeling, MDE, personal communication).

Concentrations of n-butane have decreased significantly from initial values in 1996, but slight increases in 2012 and 2013 were observed (**Figure A1.15**). Concentrations of n-pentane, isopentane, ethylene, and benzene have continued to decrease from 1996 (**Figure A1.16- A1.19**). Isoprene, a dominant VOC from biogenic sources, shows no trend (**Figure A1.20**).

The ratios of ethane to n-butane, n-pentane, and ethylene were also investigated (**Figures A1.22- A1.24**) and demonstrated an increasing trend from around 2011, similar to what is seen in **Figure 3.4**. Finally, the ratio of isopentane to n-pentane was evaluated (**Figure A1.25**). Gilman et al. (2013) showed this ratio to be lower in regions with natural gas production and greater in urban environments. Essex, MD had a median ratio of 2.7 from 2000-2003, but the median ratio has since decreased to about 2, indicating an influence of natural gas production.

3.3.3 Statistical Analysis

It is necessary to apply statistical tests for significance. Because of the lognormal distribution of ethane concentrations, nonparametric tests were performed using the JMP Pro 10.0.2 statistical software. The Essex, MD PAMS hourly daytime ethane concentrations from 2004-2013 were collected and grouped by year for comparisons. To test for differences between years, the Kruskal-Wallis test (McBean and Rovers, 1998) was used to determine if daytime ethane concentrations during at least one year were different from the concentrations during other years. The result returned a p-value less than 0.0001, indicating at least one of the years contained significantly different concentrations.

To determine which year(s) had significantly different daytime ethane concentrations when compared to other years, the Steel-Dwass post-hoc test (SAS Institute Inc., 2013) was used, assuming a 95% confidence interval. The results (**Table A1.2**) suggest that, in general, the years of 2005, 2007, 2012, and 2013 had ethane concentrations significantly different from each of the other years. Looking at **Figure 3.4a**, it can be inferred that the years of 2005 and 2007 had significantly lower ethane concentrations, while 2012 and 2013 have significantly higher concentrations. It is also significant that a p-value less than 0.0001 was returned when comparing

2013 to 2012, indicating that ethane concentrations in 2013 were already significantly greater than they were a year prior.

This procedure was repeated for daytime ethane concentrations from 2004-2013 at the other two sites. At McMillan Reservoir, ethane concentrations in 2005, 2006, 2007 and 2009 were significantly lower than in the other years, and in 2011, 2012, and 2013 ethane concentrations were significantly greater (**Table A1.4**). McMillan Reservoir observed significant ethane concentration increases in recent years, but unlike Essex, these ethane concentrations have not significantly increased over each passing year. At the Rockdale County site, ethane concentrations were significantly lower in 2005, 2006, and 2012 and significantly greater in 2008 and 2011 (**Table A1.6**). The shift from significantly greater in 2011 to lower in 2012 suggests long-term effects are not causing increases in ethane concentrations at this location. Descriptive statistics for daytime ethane concentrations from all three sites are also available in the supporting information (**Tables A1.1, A1.3, and A1.5**).

3.3.4 Local Natural Gas Sources

The recent increase in ethane concentrations at Essex, MD has been demonstrated and coincides with the spread of wells promoting increased natural gas production, but it is also important to rule out other possible local natural gas sources. Landfills and waste water treatment plants are known sources of methane, but do not emit ethane (Aydin et al., 2011). Natural gas storage fields exist in Garrett County, MD (~250km west of Essex, MD) but there is no evident recent change in usage (EIA, 2014e), and it is unlikely that these storage fields have started to degrade so quickly since 2009 (Cleveland, 2004).

The use of compressed natural gas in the transportation sector was also considered. Only ~0.5% of total Maryland natural gas consumption is used for vehicles, whose usage peaked in

2006 and 2008, only to decline rapidly thereafter (EIA, 2014f). Additionally, while other metropolitan areas chose to convert public transportation vehicles to use natural gas, the Maryland Transit Authority instead switched diesel buses to diesel-electric hybrid buses (MDOT, 2013). The state of Maryland has ten compressed natural gas fueling stations: seven have been operational prior to 2006, two recently added stations are located more than 60 km away, and one was opened in 2012 over 10 km away from the Essex, MD receptor (DOE, 2014). Although nearby leaks from these stations could be significant, none of them are in the immediate vicinity of the monitor.

Finally, fugitive emissions from pipeline leaks were evaluated as a source responsible for the observed increase in atmospheric ethane concentration. Information on methane loss for local utility companies was ambiguous, but Maryland's total natural gas consumption has remained nearly constant from 1997 to 2013 (EIA, 2014e). If fugitive loss rates were constant, fugitive emissions would also be expected to remain constant during this time period.

3.4 Conclusions

Recently, ethane concentrations have significantly increased at Essex, Maryland, and the emissions associated with hydraulic fracturing operations appear to be the only plausible source for this trend. This indicates that a substantial fraction of natural gas is escaping uncombusted, and the signal is detectable hundreds of kilometers downwind. This effect was also noticed in nearby Washington, DC, but not outside Atlanta, GA, a city without upwind hydraulic fracturing. As shale natural gas production continues to expand, this increasing trend will continue in downwind regions until more efficient control technologies are applied. Although ethane is not a criteria pollutant, additional pollutants are likely transported at increasing rates; these could cause ozone and PM to rise and complicate attainment of air quality standards for major urban

centers downwind. The observed increase in ethane (1.1 ppbC) corresponds to an expected regional increase in methane of ~5 ppb. In future analyses, concentrations of shorter-lived (e.g., NO_x) monitored closer to natural gas operations will be evaluated, and back-trajectory analysis will be incorporated to further evaluate the influence of natural gas operations on climate and regional air quality.

Chapter 4 Updates to "Regional Air Quality Impacts of Hydraulic Fracturing and Shale Natural Gas Activity: Evidence from Ambient VOC Observations"

4.1 Introduction

At the time of publication of Vinciguerra et al. (2015), VOC measurements were only available through 2013. For the Essex, MD and McMillan Reservoir, DC monitoring locations, hourly measurements are now available for the summers of 2014 and 2015. No additional hourly VOC measurements are currently available from the Rockdale County, GA monitor. Key figures and tables from Chapter 3 have been updated to include these newly available measurements.

4.2 Daytime Essex Ethane and TNMOC Observations Through 2015

At Essex, daytime (10am – 7pm) concentrations of total non-methane organic compounds (TNMOC) have generally continued to decrease over the past two decades, although 2015 concentrations were at their highest since 2010 (**Figure 4.1**). Daytime ethane concentrations at Essex continued to increase from 2011. Ethane concentrations decreased slightly from 2013 to 2014, before again increasing in 2015 to the highest observed concentrations since 1996. Ethane concentrations for McMillan Reservoir also remained elevated from pre-2010 concentrations, although the 90^{th} and 75^{th} percentiles appear to have decreased in 2014 and 2015 (**Figure 4.2a**).

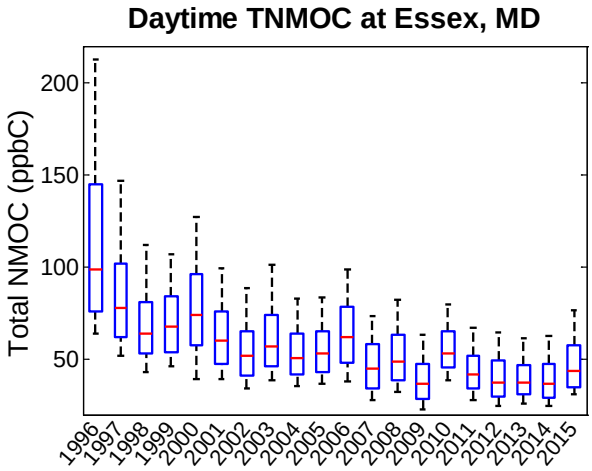

Figure 4.1 Daytime TNMOC concentrations at Essex, MD from 1996 to 2015 are shown by box and whisker plots. The box provides the 25th and 75th percentiles, with the median represented by the red bar, and the whiskers extend to the 10th and 90th percentiles.

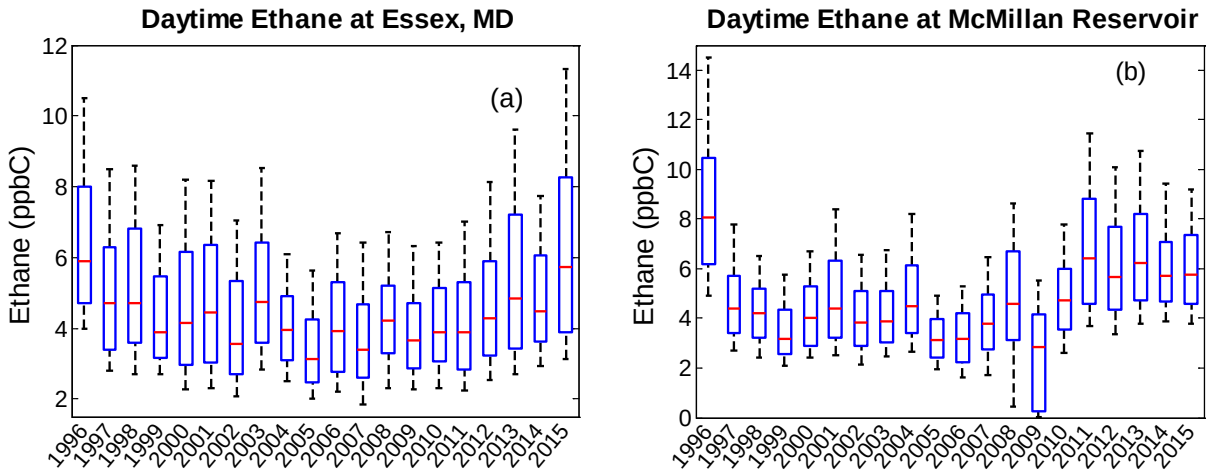

Figure 4.2 From 1996 to 2015, hourly daytime ethane concentrations from (a) Essex, MD and (b) McMillan Reservoir (DC) are presented by box and whisker plots with the same statistical parameters as **Figure 4.1**.

The Steel-Dwass post-hoc test (SAS Institute Inc., 2013) was run again for Essex and McMillan using the JMP Pro 11.0.0 statistical software to compare daytime ethane measurements from 2004-2015. At Essex, ethane concentrations from the years 2005 and 2007 remained significantly lower than other years, while measurements from 2012 and 2013 remained significantly greater (**Table 4.1**). Ethane measurements in 2014 were significantly

greater than almost all previous years, except for 2013; no significant difference was found between these two years. 2015 ethane concentrations were found to be significantly greater than all previous years, returning a p-value less than 0.0001 for each comparison.

At the McMillan Reservoir monitor, ethane concentrations in 2005, 2006, 2007 and 2009 remained significantly lower than in the other years, and in 2011, 2012, and 2013 ethane concentrations were still significantly greater (**Table 4.2**). Ethane concentrations in 2014 and 2015 were also found to be significantly greater than other years. Measurements of ethane in 2012, 2014, and 2015 were not statistically different from each other, but were greater than other years (except 2011 and 2013). The ethane concentrations in 2011 and 2013 were not significantly different from each other, but were greater than all other years.

Table 4.1. P-Values from Steel-Dwass All Pairs Comparisons of Ethane at Essex, MD[a]

Year	2004	2005	2006	2007	2008	2009	2010	2011	2012	2013	2014	2015
2004	*	*	*	*	*	*	*	*	*	*	*	*
2005	**<0.0001**	*	*	*	*	*	*	*	*	*	*	*
2006	1	**<0.0001**	*	*	*	*	*	*	*	*	*	*
2007	**0.0002**	0.366	**0.001**	*	*	*	*	*	*	*	*	*
2008	0.2113	**<0.0001**	0.1945	**<0.0001**	*	*	*	*	*	*	*	*
2009	0.2014	**<0.0001**	0.659	0.2002	**<0.0001**	*	*	*	*	*	*	*
2010	1	**<0.0001**	0.9998	**<0.0001**	0.4005	**0.0454**	*	*	*	*	*	*
2011	1	**<0.0001**	1	**<0.0001**	0.2262	0.3049	1	*	*	*	*	*
2012	**<0.0001**	**<0.0001**	**<0.0001**	**<0.0001**	0.2836	**<0.0001**	**<0.0001**	**<0.0001**	*	*	*	*
2013	**<0.0001**	**<0.0001**	**<0.0001**	**<0.0001**	**<0.0001**	**<0.0001**	**<0.0001**	**<0.0001**	**<0.0002**	*	*	*
2014	**<0.0001**	**<0.0001**	**<0.0001**	**<0.0001**	**<0.0001**	**<0.0001**	**<0.0001**	**<0.0001**	**0.0394**	0.2686	*	*
2015	**<0.0001**	**<0.0001**	**<0.0001**	**<0.0001**	**<0.0001**	**<0.0001**	**<0.0001**	**<0.0001**	**<0.0001**	**<0.0001**	**<0.0001**	*

[a]Bolded values highlight significant p-values that fall below the assumed α=0.05 criteria

Table 4.2. P-Values from Steel-Dwass All Pairs Comparisons of Ethane at McMillan Reservoir[a]

Year	2004	2005	2006	2007	2008	2009	2010	2011	2012	2013	2014	2015
2004	*	*	*	*	*	*	*	*	*	*	*	*
2005	**<0.0001**	*	*	*	*	*	*	*	*	*	*	*
2006	**<0.0001**	1	*	*	*	*	*	*	*	*	*	*
2007	**<0.0001**	**<0.0001**	**<0.0001**	*	*	*	*	*	*	*	*	*
2008	1	**<0.0001**	**<0.0001**	**<0.0001**	*	*	*	*	*	*	*	*
2009	**<0.0001**	**<0.0001**	**<0.0001**	**<0.0001**	**<0.0001**	*	*	*	*	*	*	*
2010	0.978	**<0.0001**	**<0.0001**	**<0.0001**	0.9984	**<0.0001**	*	*	*	*	*	*
2011	**<0.0001**	**<0.0001**	**<0.0001**	**<0.0001**	**<0.0001**	**<0.0001**	**<0.0001**	*	*	*	*	*
2012	**<0.0001**	**<0.0001**	**<0.0001**	**<0.0001**	**<0.0001**	**<0.0001**	**<0.0001**	**<0.0001**	*	*	*	*
2013	**<0.0001**	**<0.0001**	**<0.0001**	**<0.0001**	**<0.0001**	**<0.0001**	**<0.0001**	0.9986	**0.0001**	*	*	*
2014	**<0.0001**	**<0.0001**	**<0.0001**	**<0.0001**	**<0.0001**	**<0.0001**	**<0.0001**	**<0.0001**	0.9976	**0.0002**	*	*
2015	**<0.0001**	**<0.0001**	**<0.0001**	**<0.0001**	**<0.0001**	**<0.0001**	**<0.0001**	**<0.0001**	0.9989	**0.0014**	1	*

[a]Bolded values highlight significant p-values that fall below the assumed α=0.05 criteria

Table 4.3. Descriptive Statistics for Daytime Ethane Concentrations at Essex, MD

Year	Count	Minimum	10%	25%	Median	75%	90%	Maximum
2004	478	1.01	2.478	3.11	3.95	4.91	6.202	8.68
2005	403	0.64	2.014	2.47	3.13	4.25	5.62	41.67
2006	659	1.65	2.22	2.77	3.93	5.29	6.69	16
2007	603	0.05	1.84	2.59	3.4	4.66	6.436	12.33
2008	799	1.36	2.29	3.28	4.2	5.21	6.72	12.25
2009	781	0.05	2.27	2.86	3.65	4.71	6.338	24.23
2010	740	1.63	2.282	3.07	3.89	5.1475	6.43	16.89
2011	850	0.05	2.23	2.84	3.88	5.2925	7.018	23.87
2012	899	1.66	2.53	3.23	4.28	5.9	8.16	18.81
2013	879	0.05	2.7	3.42	4.85	7.2	9.63	189.41
2014	815	0.05	2.94	3.62	4.49	6.08	7.758	16.36
2015	828	0.05	3.13	3.8925	5.73	8.27	11.322	24.03

Table 4.4. Descriptive Statistics for Daytime Ethane Concentrations at McMillan Reservoir

Year	Count	Minimum	10%	25%	Median	75%	90%	Maximum
2004	789	0.005	2.62	3.43	4.5	6.12	8.2	31.16
2005	555	0.005	1.96	2.4	3.11	3.97	4.95	14.76
2006	705	0.005	1.606	2.22	3.16	4.21	5.27	10.59
2007	807	0.005	1.69	2.76	3.79	4.96	6.492	13.56
2008	847	0.15903	0.45416	3.1429	4.5959	6.7192	8.62606	19.1417
2009	902	0.005	0.005	0.27	2.825	4.1725	5.527	18.15
2010	746	0.005	2.614	3.55	4.73	5.9825	7.833	31.55
2011	725	0.005	3.68	4.59	6.41	8.79	11.436	19.54
2012	863	0.005	3.374	4.37	5.66	7.67	10.086	33.86
2013	897	0.005	3.786	4.73	6.24	8.19	10.796	19.69
2014	860	0.23	3.89	4.66	5.71	7.0675	9.474	22.73
2015	826	0.47	3.751	4.58	5.74	7.375	9.233	29.04

4.3 Essex Ethane Diurnal Profile Through 2015

By 2013, daytime ethane concentrations were found to have increased by about 1.1 ppbC from the average concentrations observed between 2004 and 2010 (**Figure 4.3**). In 2015, this departure from 2004-2010 values continued and had roughly doubled to a 2 ppbC increase. The diurnal profile for ethane concentrations in 2014 showed a slight decrease, residing between the values found in 2012 and 2013.

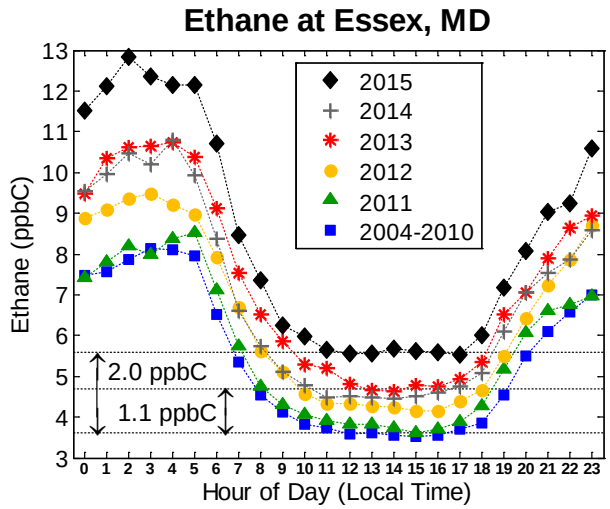

Figure 4.3 The diurnal cycle of ethane at Essex, MD showing the geometric mean concentration at each hour. Concentrations of ethane from 2004 to 2010 were averaged to establish a period unaffected by natural gas operations, and subsequent years show a continuing departure from this baseline.

4.4 Essex Ethane and Marcellus Production Through 2015

Ethane made up roughly 7% of total NMOC from 2000-2010, and was seen to increase to ~15% in 2013. For 2014 and 2015, this percentage did not continue to increase along with natural gas production, but instead leveled off at around 14% of total NMOC. In 2014 ethane concentrations were not significantly different from 2013, so the percentage of the total would not have been expected to increase. For 2015, ethane concentrations increased significantly, but TNMOC was also much higher than in previous years. As a result the ratio would not be expected to change significantly.

The r^2 value, comparing the median Marcellus production rate to the median observed ratio at Essex from June through August of each year, was recalculated and found to maintain the same value (0.82). The green production line was originally overlaid to visually match with observations through 2013, so it appears to not match the later years as well (**Figure 4.4a**). If the

range of the right y-axis were adjusted to shift the production curve downward, it would still fit all values from 2010 onward well, and thus maintaining r^2=0.82 seems reasonable (**Figure 4.4b**).

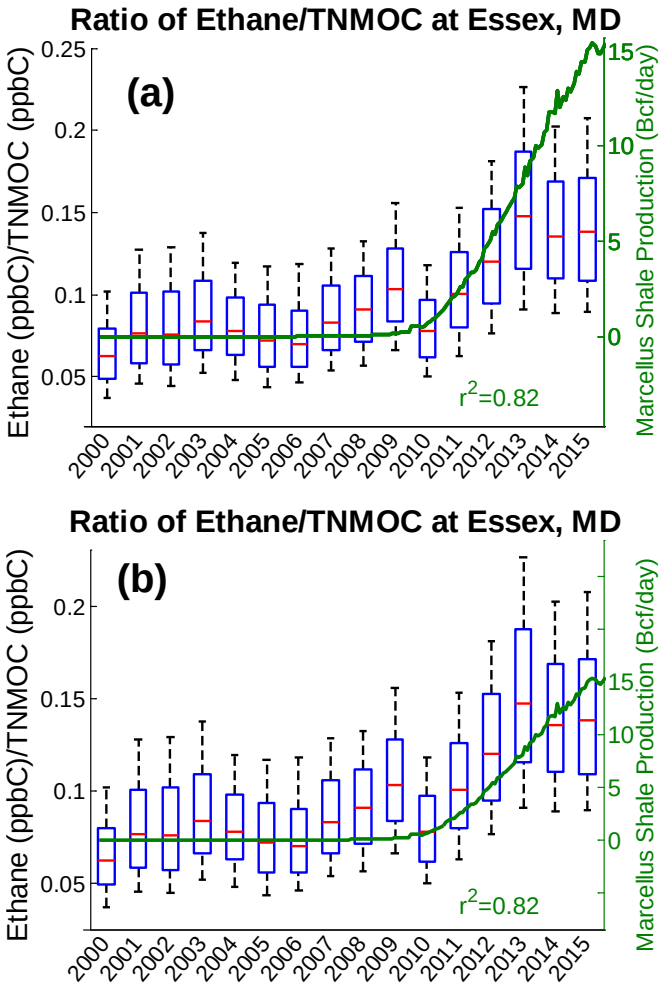

Figure 4.4 (a) The ratio of ethane to TNMOC observed at Essex, MD is shown by box and whisker plots with the same statistical parameters as **Figure 4.1**. In addition, the production rates from the Marcellus shale are shown in green. A strong correlation was observed with an r^2 value of 0.82. (b) Production curve overlay rescaled to better fit visually among 2014 and 2015 data.

There were also newer regulations affecting onshore oil and gas production (EPA, 2012; Healey and Pergande, 2014) that might have contributed to the leveled-off ratios observed in 2014 and 2015. In October 2013, continuous bleed pneumatic devices at production facilities needed to limit gas venting to 6 standard cubic feet per hour (~0.17 m^3/hour). While occurring in

the 2013 calendar year, these reductions would not have been observable at the Essex monitor until 2014 because measurements were only made during June through August. Gas production storage tanks with an expected VOC emission rate of six tons per year were required to reduce VOCs by 95% by April 2014 for vessels commissioned after April 2013 and April 2015 for older storage tanks. In January 2015, the completion venting procedure (clearing fluid and debris from a well before production) required removal of VOC emissions through reduced emissions completion (REC) processing and could no longer be flared.

June, July, and August production data were matched with median ethane concentrations for the same months for 2014 and 2015, and a positive correlation still remained (**Figure 4.5**). The r^2 value decreased from 0.59 to 0.48, as observed ethane values in 2014 did not increase, but the inclusion of newer measurements still shows a positive correlation between upwind Marcellus shale production and observations at the Essex monitor.

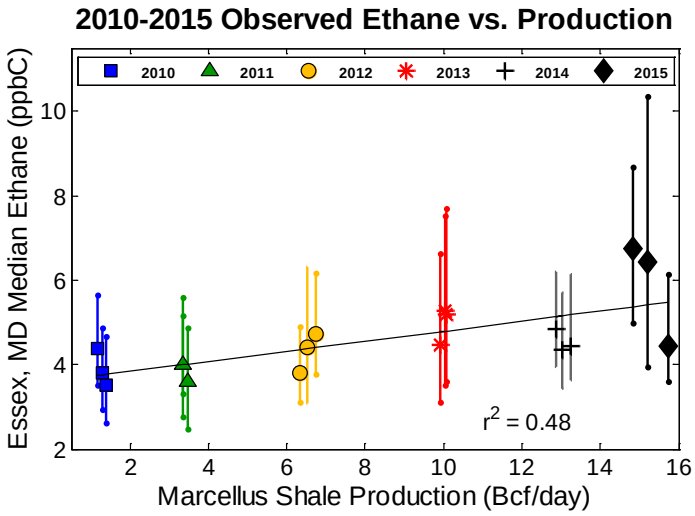

Figure 4.5 Monthly summer values from 2010 through 2015 of observed daytime ethane concentrations at Essex, MD vs. Marcellus Shale production. The uncertainty bars provide the 25th and 75th percentiles of measured ethane during each month.

4.5 Summary

The additions of 2014 and 2015 ethane measurements did not seem to significantly change most of the conclusions presented in Vinciguerra et al. (2015). Ethane concentrations still remained greater after 2010 than in earlier years at both the Essex and McMillan monitors, and ethane measurements at Essex still continue to correlate with upwind Marcellus shale production rates. Notably, the ethane/TNMOC was found to hold relatively constant at ~15% from 2013 to 2015, instead of continuing to increase. Based on these newly available measurements, if upwind shale gas operations continue to increase or maintain current production rates, observations at the Essex and McMillan monitors would be expected to maintain ethane concentrations elevated from levels before 2010.

Chapter 5 Regional Influences of Marcellus Shale Natural Gas Activity: Trajectory Analysis of Baltimore/Washington Ethane Concentrations

This study was made possible with assistance from several undergraduate researchers. Rahma Zakaria reran HYSPLIT to create new outputs that included mixing depth estimates. Alexa Chittams calculated county well densities, Thomas Deskins developed the Matlab program used for determining a back-trajectory's grouping, and Brian Constantine performed the Mann-Whitney tests. Mr. Constantine and Mr. Deskins performed 5-hour clustering.

5.1 Introduction

Over the past decade, natural gas production has rapidly increased with the combined practices of high volume hydraulic fracturing and horizontal drilling to extract the natural gas trapped in shale formations. In the Appalachian Basin, an abundance of natural gas continues to be obtained (over 500 million m^3 per day at the beginning of 2016) from the Marcellus and Utica shale formations (EIA, 2016a). A 2013 assessment of U.S. shale gas resources estimated 14.2 trillion m^3 of remaining reserves and undeveloped shale gas resources in the Marcellus and Utica shale formations (ARI, 2013), suggesting current production rates could potentially continue for well over half a century.

These large quantities of available natural gas have also driven down dependency on coal for electricity generation. In 2015, the amount of electricity generated in the U.S. by natural gas was equivalent to coal (EIA, 2016b), and the burning natural gas instead of coal reduces the atmospheric burden of CO_2 and climate impacts (de Gouw et al., 2014). However, methane is a greenhouse gas with a 100 year global warming potential of methane about 30 times greater than CO_2 (IPCC, 2013), and if more than about 3% of methane is lost to the atmosphere between the

production and combustion stages, the benefits of natural gas over coal are lost with respect to climate (Howarth et al., 2011; Alvarez et al., 2012). Several studies, with varying sampling methods, display a wide range of methane loss estimates from shale oil and gas operations, ranging from as low as 0.18% upwards to 17.3% (Allen et al., 2013; Caulton et al., 2014; Howarth et al., 2011; Karion et al., 2013; Kirchgessner et al., 1997; Peischl et al., 2013, 2015; Petron et al., 2012; Schneising et al., 2014).

Similarly, while natural gas combustion also provides cleaner emissions of particulate matter, hydrocarbons, and nitrogen oxides (as well as SO_2 and Hg) compared to coal (Roy and Choi, 2015), there are concerns about air quality impacts regarding the additional emissions involved with shale gas operations to obtain the natural gas. A shale gas well has numerous emission sources and processes such as completion venting, a process in which fluid and debris are cleared from the well, storage tanks, pneumatic devices, and the natural gas and diesel engines powering various trucks, compressors, drilling rigs, and pumps (Roy et al., 2014). In addition to affecting local air quality, these emissions could also impact attainment of air quality standards in downwind metropolitan areas (Kemball-Cook et al., 2010).

Shale gas operations are widespread in the states of Pennsylvania and West Virginia, but are not permitted in the neighboring states of New York and Maryland (MGA, 2015; NYSDEC, 2015). Emissions, however, do not remain confined to state borders, and occurrences of prevailing winds transporting emissions that affect Maryland and other East coast states are well-documented (Hains et al., 2008; He et al., 2013a, 2013b, 2014; Ryan et al., 1998; Taubman et al., 2004, 2006). Taubman et al. (2006) showed that the majority of wind trajectories arriving in the Mid-Atlantic U.S. passed through regions where shale gas operations now occur. Wind profiler

data collected in Beltsville, MD during the summers of 2010-2015 similarly show a high frequency of winds that arrived from the northwestern and western directions (**Figure 5.1**).

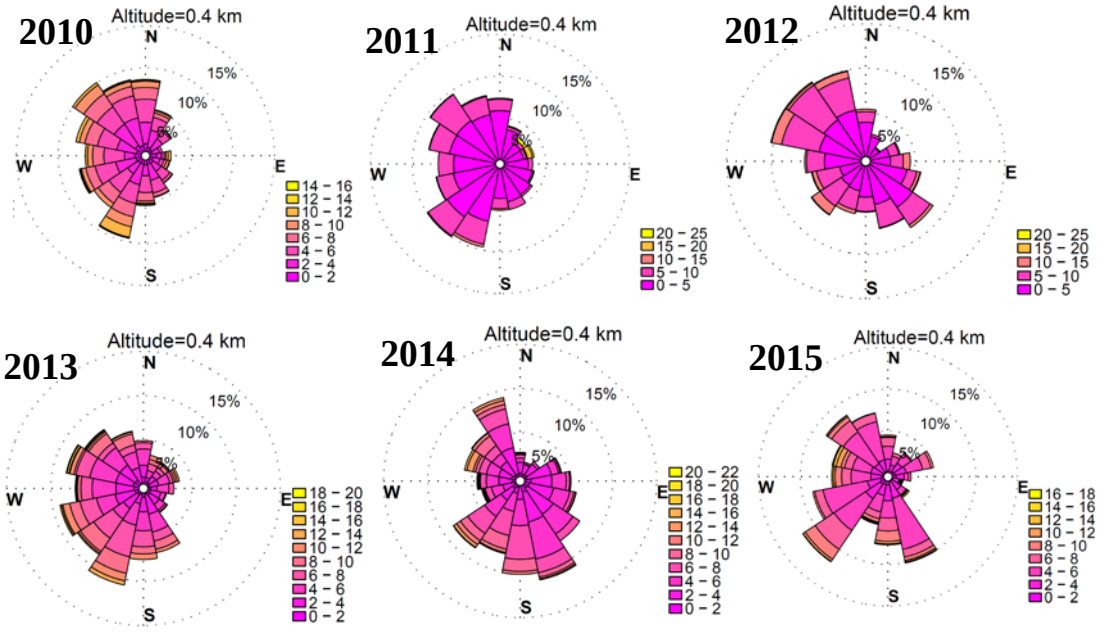

Figure 5.1 Wind roses showing wind velocity frequencies and direction at 400 m AGL provided by the wind profiler at Beltsville, MD. Wind velocities are taken from daytime hours (10am - 7pm) during the months of June-August for each of the years 2010-2015. Winds often arrived from the west where natural gas operations have increased in recent years. [Wind roses provided by Kostya Vinnikov].

In Chapter 3, measurements of ethane, the second-largest component in natural gas, were found to increase after 2009, following years of declining ethane and total VOC concentrations at Photochemical Assessment Monitoring Stations (PAMS) in the Baltimore and DC areas. These increased ethane concentrations were also found to correlate with the rapid growth of shale gas production in the upwind states such as Pennsylvania and West Virginia. This chapter continues the investigation of ethane concentrations from these monitors and utilizes back-trajectories to further inspect the influence of upwind shale gas production.

5.2 Methods

The Hybrid Single Particle Lagrangian Integrated Trajectory Model (HYSPLIT) was used to create back-trajectories for air parcels arriving at the PAMS monitors in Essex, MD and McMillan Reservoir in D.C. Using meteorological inputs, HYSPLIT follows an air parcel from a fixed location backward (as well as forward) through time and space (Drexler, 1999; Stein, 2015).

The 12 km grid-resolution North American Mesoscale (NAM) archived meteorological data were used for this analysis, as this dataset provides the highest horizontal resolution available from the HYSPLIT meteorological archives for the period of investigation and is often used in HYSPLIT studies across the United States (e.g., Crippa and Pryor, 2013; Hahnenberger and Nicoll, 2012; He et al., 2014).

Back-trajectories were generated from the Essex and McMillan PAMS sites for each local daytime (10am – 7pm) hour during the months of June, July, and August of 2008 through 2015. Concentrations of ethane exhibited a strong dependency on mixing volume, especially as the boundary layer collapses following sunset, and only measurements during local daytime hours were considered as the boundary layer depth should show little long-term trend. Trajectories were run backward in time for 48 hours, and air parcels were given an arrival height of 100 m, similar to other ambient receptor-based studies (e.g., Atwood et al., 2013; Burley et al., 2014; Jaars et al., 2014; Riuttanen et al., 2013). Although an arrival height at a higher altitude could be used, Essex's close proximity to the Chesapeake Bay creates lower daytime boundary heights than what would be observed more inland (Goldberg et al., 2014).

5.2.1 Assignments of Back-Trajectories to Groups

The number of active unconventional natural gas wells were obtained for counties in the upwind states of Ohio, Pennsylvania, Virginia, and West Virginia from 2008-2015 (OOGA, 2016; PADEP, 2016a; VDMME, 2016; WVDEP, 2016). Well densities were calculated for each county by dividing the number of active unconventional wells by the area of each county. After comparing histograms of well densities for numerous counties, a value of 0.05 wells/km^2 was empirically selected to represent the threshold for determining if a county had a high density of wells or a low density of wells.

For each of the analyzed years, maps were generated to delimit the counties exhibiting a high density of active unconventional wells. These counties are generalized by **Figure 5.2**. In 2008, high well density counties were mostly confined to West Virginia and southwestern Pennsylvania. In 2009, counties in northeastern Pennsylvania began to cross the threshold to high density. Both high density areas continued to expand in subsequent years, but fewer counties crossed the threshold to high well density after 2011, with 2015 having no new high density counties.

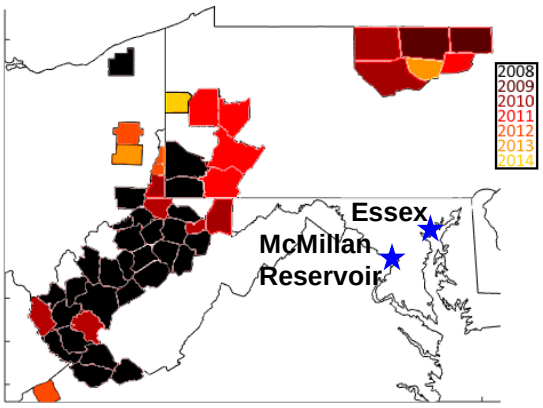

Figure 5.2 Counties containing a high density (>0.05 wells/km^2) of active unconventional wells. Colors progress from black to red to yellow to delimit counties passing the threshold in subsequent years. The monitor locations are indicated by blue stars.

A Matlab program was created for comparing the coordinates of the back-trajectories to the maps of high well density counties. For each year from 2008 to 2015, each 48-hour hourly back-trajectory was plotted, and the program logged any high density county that it passed through (**Figure 5.3**). If a trajectory failed to pass through a county with a high density of wells, it was assigned to the low well density grouping.

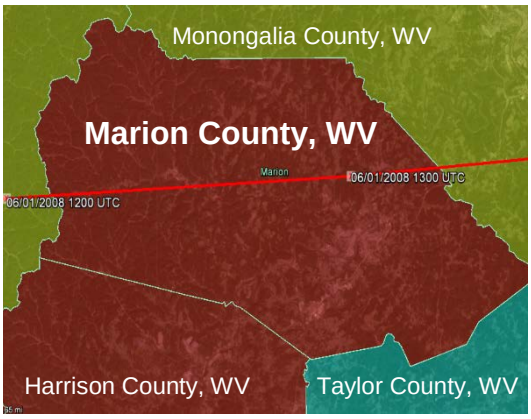

Figure 5.3 Example of a back-trajectory (red line) passing through a county containing a high density of wells. County shapes are seen in yellow if below the 0.05 wells/km^2 threshold, and blue if there are no reported unconventional wells.

High well density trajectories were further screened by comparing the mixing height, estimated from the NAM meteorological input, to the height of the trajectory when it passed over the high density county. If a back-trajectory's height was between the surface and 10% above the mixing height, the trajectory was assigned to the high well density grouping. Trajectories which failed to meet this height criterion were excluded from further analysis, as it would be unlikely for the air parcel to be affected by surface emissions from natural gas production.

5.2.2 Sensitivity Testing

5.2.2.1 Sensitivity to Arrival Height of 100 m

Back-trajectories were tested using an arrival height of half of the mixing layer over Essex. An arrival height higher than 100 m did not affect the number of days when a trajectory passed over a county with a high density of unconventional wells, but roughly half of these days would be excluded because trajectories were greater than 10% above the mixing height while over a high density county. Because of this limitation, the arrival height of half the boundary layer was not used.

Ensemble trajectories, which initiate concurrent back-trajectories from surrounding horizontal and vertical grid cells, were run to investigate wind shearing for the test hours of 1800 UTC during the month of July 2011 (31 total ensembles). Overall, these trajectory ensembles demonstrated similar paths, with only four instances where individual trajectories in an ensemble differed depending on starting location. Ensembles were similarly initiated from McMillan Reservoir for the test hours of 1800 UTC during the month of July 2013 (31 total ensembles), and only two ensembles containing individual trajectories traveling in different directions. With limited wind shear evident from the sample ensembles performed, the 100m arrival height appears sufficient for this study.

5.2.2.2 Sensitivity to 48-hour Back-Trajectory Run-length

Since ethane has a lifetime of several weeks, 168 hour (7 day) back-trajectories were run for 1800 UTC for each day of July 2011 (31 total trajectories) to investigate the possibility of winds shifting back toward high density counties following the initial 48 hours. Only four 168 hour back-trajectories returned to high density well counties; two of these trajectories passed at a

height greater than 10% above the mixing height and would be excluded. As a result, 48 hours appears to be an adequate duration for classifying a trajectory as high or low well density.

5.2.2.3 Sensitivity to Meteorological Inputs: NAM 12 km vs NAM 4 km

At the beginning of 2016, 4 km NAM meteorology became available, but are only archived for a week before being removed. The file sizes for the 4 km NAM are significantly larger (8 GB vs 0.4 GB), and only two days (June 21-22, 2016) were used to briefly compare 48-hour back-trajectories calculated with 4 km and 12 km resolutions. The overall paths from both meteorological inputs are generally the same, but differences do exist. In **Figure 5.4**, both back trajectories from Essex on June 21, 2016 arrived from Kentucky and Tennessee, roughly following along the Ohio River. However, the trajectory from the 12km NAM reaches Essex by passing through West Virginia, whereas the 4 km trajectory arrives from Pennsylvania. Although the final 24-hour approaches to Essex differ geographically, both of these areas would contain high well density counties, and the trajectory's designation would be unlikely to change.

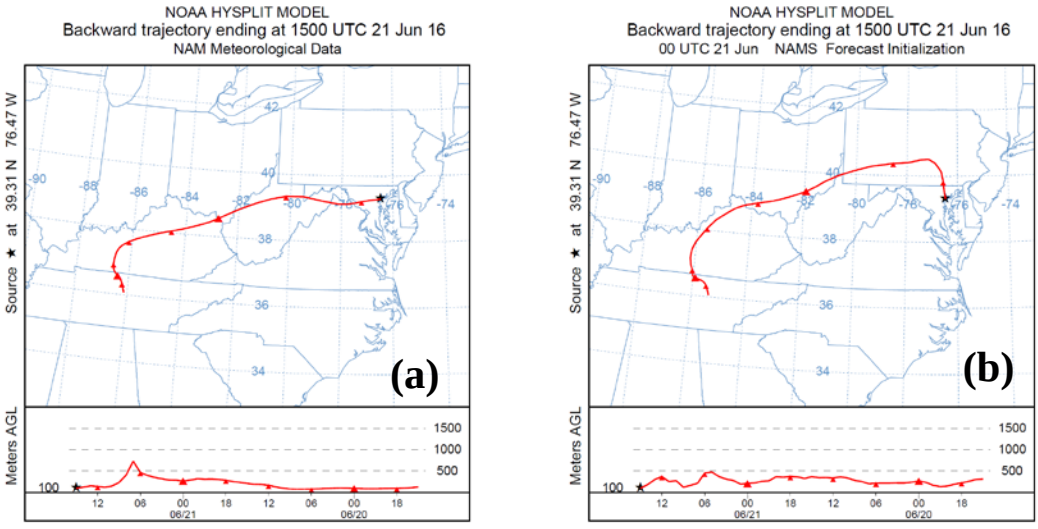

Figure 5.4 Back-trajectories from Essex, MD at 1500 UTC on June 21, 2016 using (a) 12 km NAM meteorology and (b) 4 km NAM meteorology inputs.

Winds from the northeast arrived at Essex on June 22, 2016 (**Figure 5.5)**, showing similar paths from both meteorological inputs. The final 24-hour approaches to Essex are comparable, originating from around the Michigan/Canada border. Beyond that time, some vertical differences do arise. The 12 km trajectory passes over land from Minnesota, starting from a higher altitude, whereas the 4 km trajectory spends significant time slightly north, but over the Great Lakes with lower altitudes.

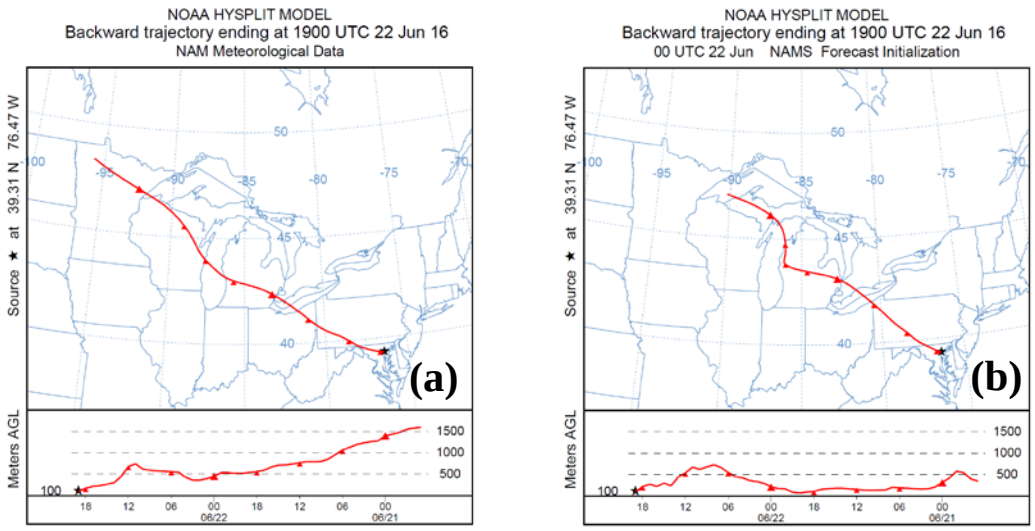

Figure 5.5 Back-trajectories from Essex, MD at 1900 UTC on June 22, 2016 using (a) 12 km NAM meteorology and (b) 4 km NAM meteorology inputs.

The resulting trajectories from 12 km and 4 km meteorological input can have differences, but overall the trajectories appear similar enough to suggest the 12 km meteorology represents general wind patterns such that conclusions for this study should not be drastically affected.

5.2.2.4 Sensitivity to Well-Density Threshold of 0.05 wells/km^2

The well density threshold was empirically selected at 0.05 wells/km^2 after comparing histograms of well densities for numerous counties. To investigate the possible sensitivity of

results based on this threshold, the process was repeated using values of 0.01, 0.04, and 0.1 wells/km^2 for classifying high-density counties in 2014. With the currently-used threshold of 0.05 wells/km^2, 45 counties were classified as high-density. When the density threshold was reset to values of 0.01, 0.04, and 0.1 wells/km^2, the number of high-density counties was 72, 49, and 37, respectively. However, even though there were different numbers of counties determined from varying thresholds, identical results were found for all four of the different thresholds that showed no statistical difference in ethane observations between high density trajectory days and low density days in 2014. This is likely a result of trajectories passing through multiple high-density counties en route to Essex, and additional counties would not change a trajectory's classification. These results indicate the well density threshold is not a sensitive parameter and should not affect results.

5.2.3 Dispersion Modeling

The HYSPLIT dispersion model was also utilized to provide a proof-of-concept validation for upwind counties causing noticeable increases of ethane concentrations. After identifying several sequential hourly trajectories that passed through a county containing a high density of wells, the dispersion of ethane gas was modeled as emitting from the center of this county. To estimate the emissions of ethane, annual methane emissions estimates from unconventional natural gas operations were obtained from the Pennsylvania Department of Environmental Protection (PADEP, 2016b). Using this annual estimate for methane emissions, hourly ethane emissions were calculated assuming that the shale gas composition was 90% methane and 10% ethane (Bullin and Krouskop, 2009; Conder and Lawlor, 2014) and that the emission rates were constant throughout the entire year.

5.2.4 Trajectory Clustering and 5-Hour Local Source Analysis

Individual hour back-trajectories can be grouped by similar paths through a process called clustering. When the clustering process is initialized, each trajectory is defined as a unique cluster (N trajectories and N clusters), and the total spatial variance is zero. In the first iteration, the cluster spatial variance (sum of squared distances between the endpoints of trajectories in a given cluster and the mean of the cluster's trajectories) is calculated for each combination of trajectory pairs. Next, the total spatial variance (TSV), the sum of every cluster spatial variance is calculated, and the pair of clusters resulting in the lowest increase in TSV are combined. The second iteration thus contains N-1 clusters, and paired clusters will remain together. For each following iteration, variances are recalculated and clusters are paired by the same process until N trajectories are in a single cluster (ARL, 2013).

The number of clusters to use can be selected by viewing a plot like one shown in **Figure 5.6** that displays the percent change in TSV as more and more clusters are combined. The number of clusters can be selected by locating the number of clusters before a large increase (~5%) in TSV occurs. For example, in **Figure 5.6**, at least four clusters should be used, as using three or fewer results in a substantial increase in TSV. It can also be seen that using up to 11 clusters would also help to minimize TSV, but no significant TSV reductions occur when selecting additional clusters.

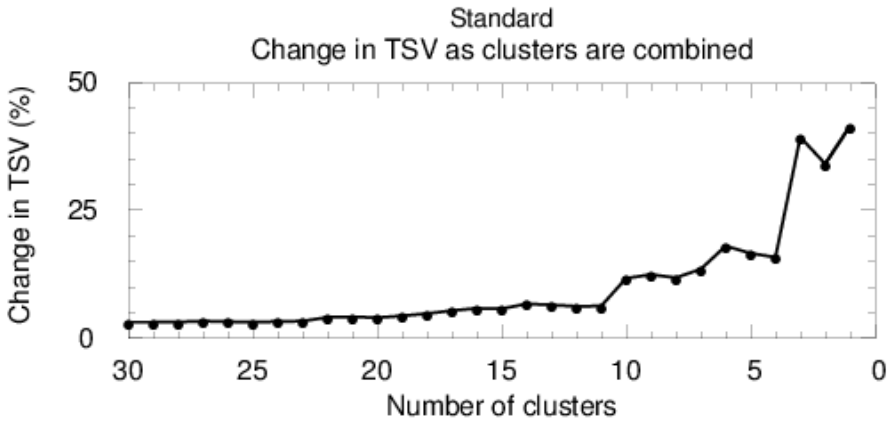

Figure 5.6 Percent change in total spatial variance. Large increases, such as the one seen between 3 and 4 clusters, should be avoided when selecting the number of clusters to use.

Although there are numerous upwind counties containing a high density of unconventional wells, there are also more local natural gas storage and transmission sources that could be influencing the concentrations of ethane (**Figure 5.7**). The analysis in Chapter 3 found no increases from other sources, but trajectory clustering can be used for further examination. To investigate possible effects from local sources, the first five hours were used from each of the previously generated 48-hour back-trajectories and clustered together. For both high well density trajectories and low well density trajectories, five clusters were generated, providing two different maps for each year.

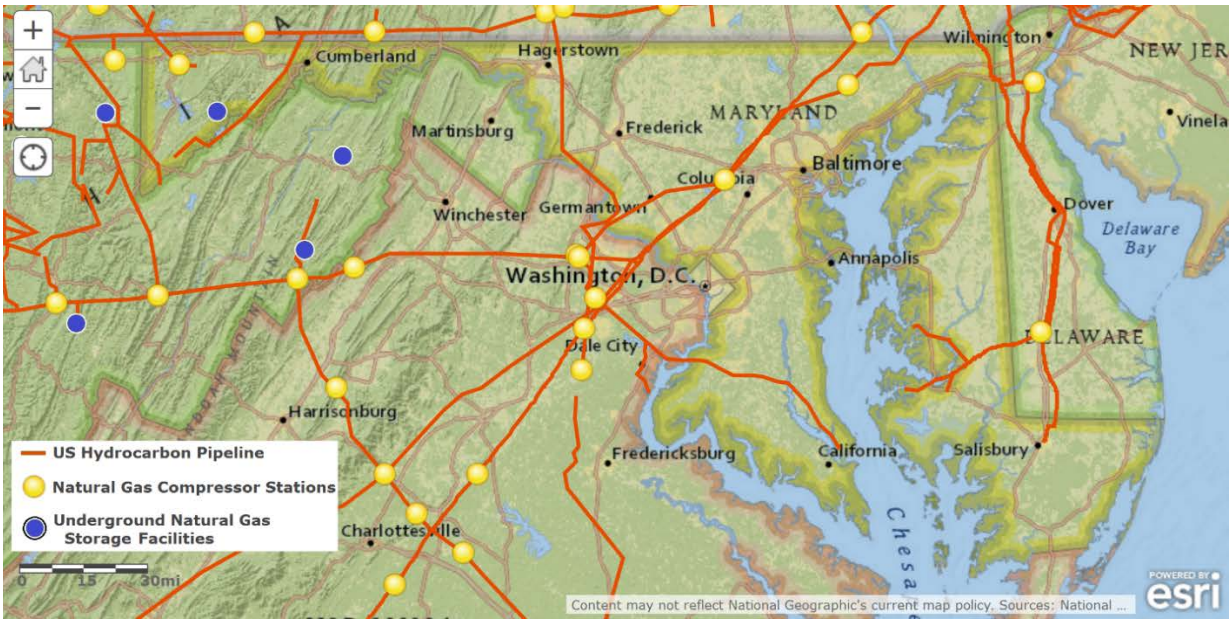

Figure 5.7 Natural gas pipelines (red-orange line), compressor stations (yellow dots), and underground storage facilities (blue dots) within and around Maryland and Washington, D.C. Modified from Auch (2014).

5.3 Results

5.3.1 Comparison of Daytime Ethane Concentrations by Trajectory Grouping

Although hourly observations are available and hourly back-trajectories can be calculated, wind patterns are often similar enough that consecutive observations are not truly independent. To test for autocorrelation, two different approaches were employed, using observations and trajectories from 2015 as a basis for all years. In the first approach, ethane concentrations were correlated with observations one hour apart, two hours apart, etc. The lowest correlation was found between observations at 10am and those at 7pm. HYSPLIT's clustering feature was also utilized to determine the duration of episodic wind patterns. On average, winds shifted from belonging to one cluster grouping to another every ten hours. As a result, one day consisting of ten daytime hours of measurements was used as an independent observation in this study.

For each day, the ten-hour daytime average ethane concentration was obtained. If the majority of hours in a day contained high density back-trajectories, the day was categorized as being high density and assigned the daily average ethane concentration. Alternatively, a day consisting of a majority of hours with low density back trajectories was classified as low density. Days that contained an equal number of hours of high density trajectories and low density trajectories were excluded from further analysis. Additionally, some days were dominated by trajectories that passed through high density counties but at altitudes above the mixing height; observations from such days were excluded.

For each year, ten-hour daytime average concentrations at Essex, MD were found to be greater for days associated with high well density back-trajectories (**Figure 5.8**). The Mann-Whitney U-test was performed using the Minitab 17 statistical software to find if days where trajectories passed through high well density counties were associated with significantly greater ethane concentrations than those observed when trajectories arrived from low well density counties. The results are summarized in **Table 5.1**. With 80% confidence, each of the years except 2014 were found to have ethane concentrations significantly greater when air parcels passed through high well density counties than if they had not.

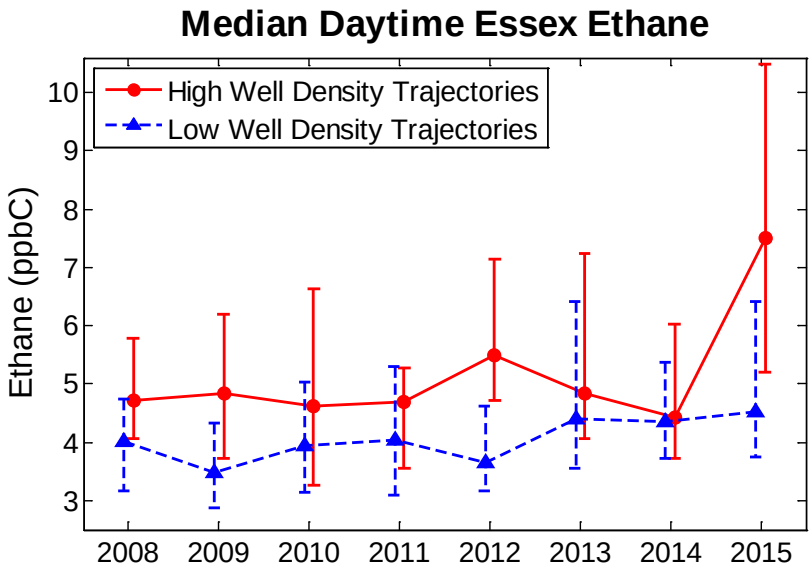

Figure 5.8 Comparison of ten-hour daytime average ethane concentrations at Essex, MD by trajectory path groupings. Median concentrations for each group are shown by the markers, with the whiskers denoting the 25th and 75th percentiles.

Table 5.1 Descriptive statistics for daytime ethane concentrations at Essex, MD and p-values returned from testing for $\text{median}_{\text{high well density}} > \text{median}_{\text{low well density}}$.[a]

Year	High Well Density		Low Well Density		Mann-Whitney
	N	Median	N	Median	p-value
2008	12	4.7	68	4.0	**0.0131**
2009	18	4.8	49	3.5	**0.0015**
2010	11	4.6	42	3.9	**0.1118**
2011	14	4.7	48	4.0	**0.1930**
2012	21	5.5	55	3.6	**0.0001**
2013	12	4.8	57	4.4	**0.1632**
2014	13	4.4	58	4.4	0.3578
2015	28	7.5	50	4.5	**0.0001**

[a]A bolded p-value less than α=0.2 signifies significantly greater ethane concentrations for days with high well density trajectories.

Unlike other years, winds in 2014 were more frequent from the southeast, which would result in fewer trajectories arriving from high well density counties. This overall lower impact on ethane concentrations observed at the Essex monitor in 2014 could explain the lack of dissimilarity between the well density grouping measurements. Additionally, 2014 featured over half of the high well density trajectories passing through northeastern Pennsylvania counties (more than any other year). 2013 featured a similar number of high and low well trajectories, but

only had 20% of high well density trajectories passing through northeastern Pennsylvania. Wells in these counties would be expected to contain natural gas composed of less ethane than the gas found in southwestern Pennsylvania and West Virginia (Bullin and Krouskop, 2009), and would increase ethane concentrations at slower rate.

Well density processing was repeated for back-trajectories from McMillan Reservoir, and corresponding ethane measurements yielded similar results to the Essex monitor (**Figure 5.9, Table 5.2**). For each of the years analyzed, with the exception of 2012 and 2014, days with high well density ethane concentrations were significantly higher than those with low density concentrations. Observing similar results at both these monitors continues to affirm that the cause of elevated ethane concentrations is more regional in nature, and less localized.

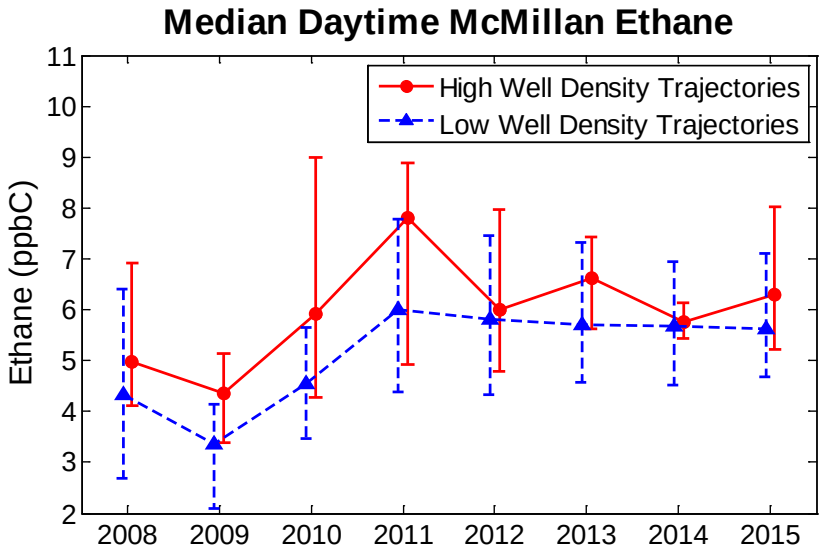

Figure 5.9 Comparison of ten-hour daytime average ethane concentrations at McMillan Reservoir by trajectory path groupings. Median concentrations for each group are shown by the markers, with the whiskers denoting the 25th and 75th percentile.

Table 5.2 Descriptive statistics for daytime ethane concentrations at McMillan Reservoir; p-values returned from testing for $median_{high\ well\ density} > median_{low\ well\ density}$.[a]

Year	High Well Density		Low Well Density		Mann-Whitney
	N	Median	N	Median	p-value
2008	11	5.0	65	4.3	**0.0660**
2009	19	4.4	39	3.4	**0.0102**
2010	11	5.9	45	4.5	**0.0227**
2011	15	7.8	38	6.0	**0.0517**
2012	21	6.0	54	5.8	0.2163
2013	16	6.6	56	5.7	**0.0708**
2014	12	5.8	63	5.7	0.3271
2015	34	6.3	50	5.6	**0.0658**

[a] A bolded p-value less than $\alpha=0.2$ signifies significantly greater ethane concentrations for days with high well density trajectories.

5.3.2 Dispersion Modeling

Using detailed information obtained from hourly back-trajectory paths, forward plume dispersion simulations were performed to validate the potential impact on ethane observations at the Essex monitor following a release in an upwind county. High ethane concentrations were observed at Essex on June 20, 2012, which contained several back trajectories which had passed through Armstrong County, PA. Ethane gas was modeled to continuously emit and disperse from a 10 meter height at the center of the county from June 19 at 7pm local time until June 20 at 7pm.

Over the first 10 hours of the dispersion simulation, the modeled plume moved to the southwest, in the direction of Maryland (**Figure 5.10a**). The plume continued in this direction and arrived over Essex, remaining throughout the duration of daytime observations from the monitor; the mid-afternoon plume, 19 hours after the start of the simulation, is shown in **Figure 5.10b**. As the modeled plume persisted over Essex, MD throughout June 20, observed ethane concentrations were greater than they were during the previous day, when winds had arrived from low well density regions (**Figure 5.11**).

Although the plume was over Essex, a large modeled concentration was not seen to correspond with the highest observations in the last two daytime hours of June 20. This is likely a limitation of modeling only a single county, as wells in surrounding counties are realistically always emitting as well and would also contribute to observations.

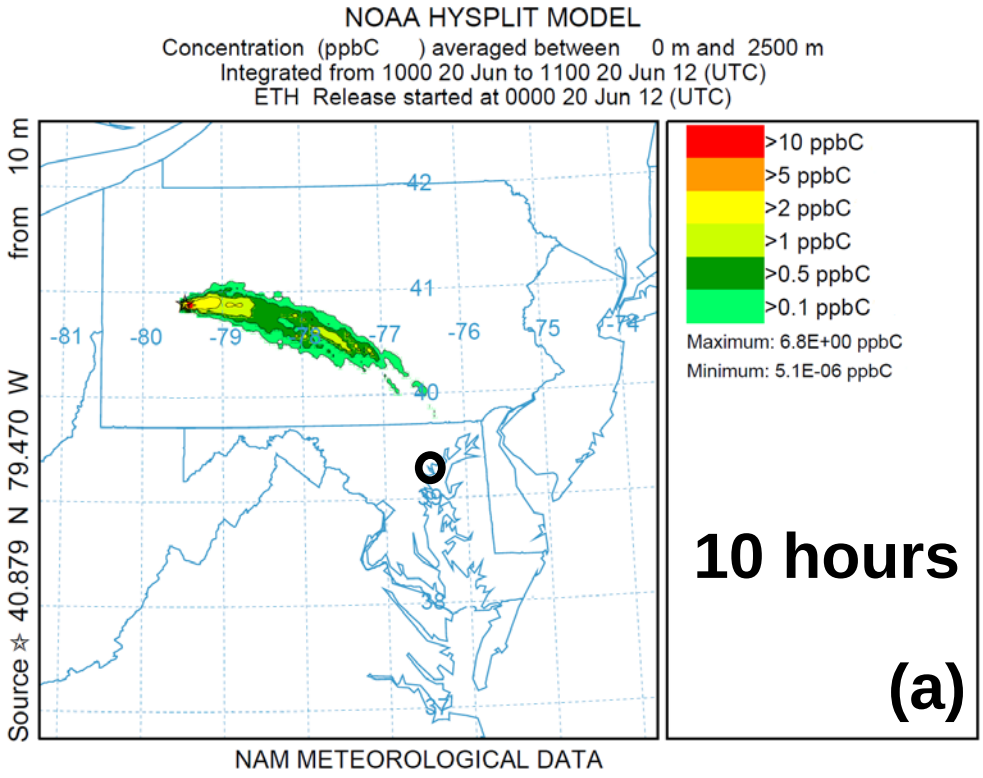

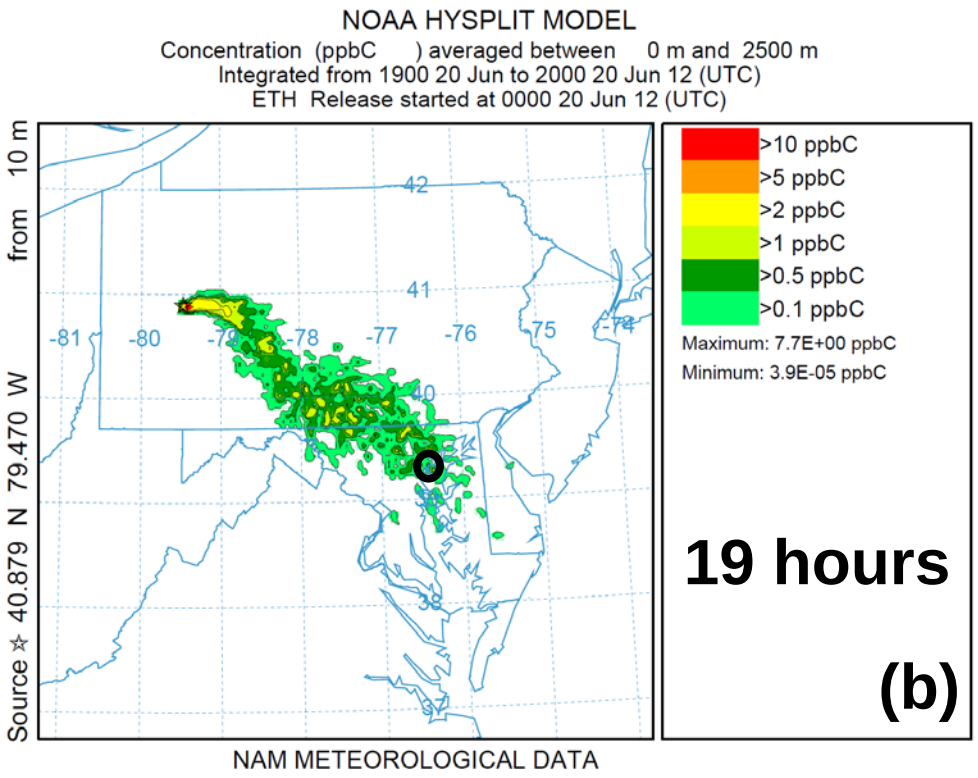

Figure 5.10 Snapshots of ethane dispersion plume from Armstrong County, PA (a) 10 hours after release and (b) 19 hours after release, as the plume persists over Essex, MD. The black disc approximates the location of Essex.

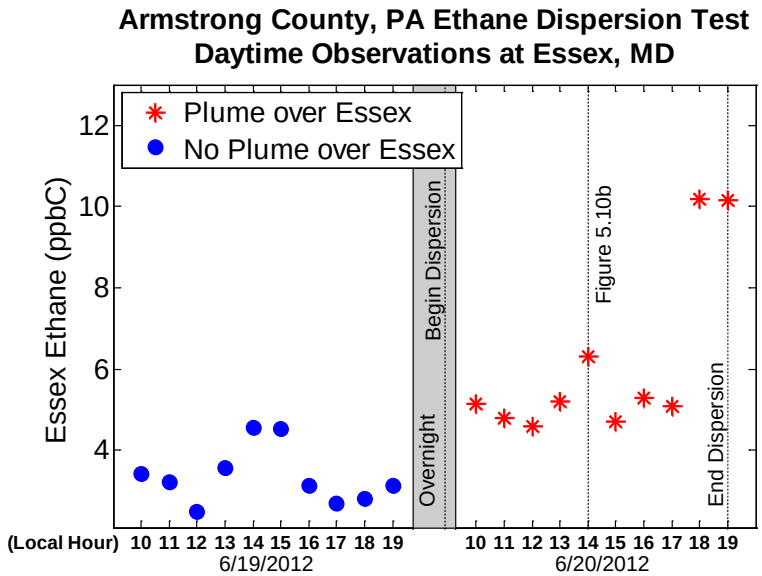

Figure 5.11 Daytime measurements of ethane at the Essex, MD monitor during the Armstrong County, PA dispersion simulation. Markers change from blue dots to red stars when the plume passed over Essex, MD. The measurement corresponding with the event shown in **Figure 5.10b** is also noted.

This process was also repeated for July 1, 2012, when ethane concentrations had continued to increase, following three consecutive days dominated by winds arriving from high density counties. Many trajectories arriving on this day passed through Fayette County, PA. The dispersion began at 7pm (local time) on June 30, 2012, and the resulting plume pushed eastward toward Essex over the following hours (**Figure 5.12a**). The plume arrived at Essex as daytime observations began (**Figure 5.12b**), with a corresponding modeled and observed maximum around 3pm (**Figure 5.12c, Figure 5.13**). Winds later pushed this plume southward (**Figure 5.12d**), and by the next day, observed concentrations, no longer influenced by high density wells, were drastically lower (**Figure 5.13**).

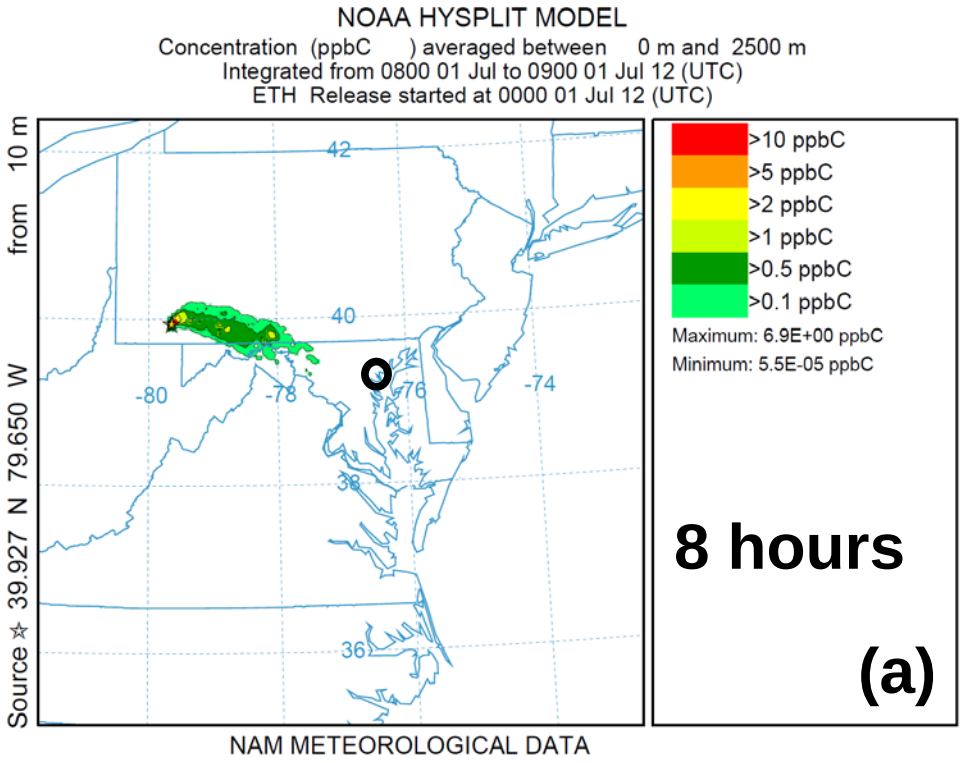

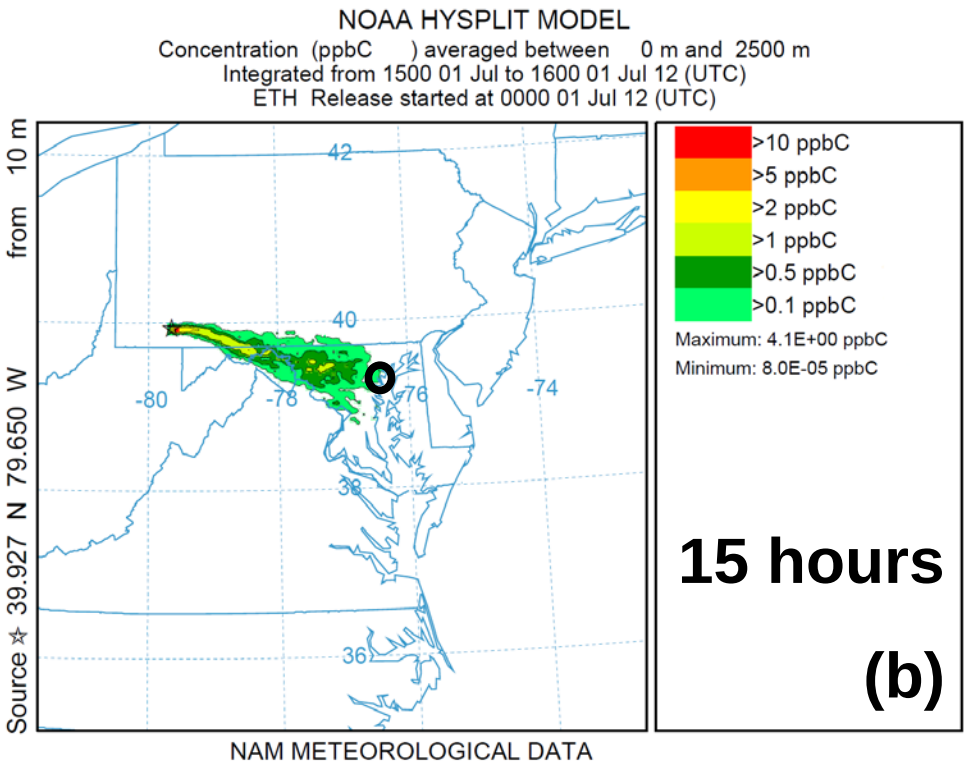
NOAA HYSPLIT MODEL
Concentration (ppbC) averaged between 0 m and 2500 m
Integrated from 1500 01 Jul to 1600 01 Jul 12 (UTC)
ETH Release started at 0000 01 Jul 12 (UTC)
from 10 m
Source ☆ 39.927 N 79.650 W
42
40
-80
-78
-76
-74
38
36
>10 ppbC
>5 ppbC
>2 ppbC
>1 ppbC
>0.5 ppbC
>0.1 ppbC
Maximum: 4.1E+00 ppbC
Minimum: 8.0E-05 ppbC
15 hours
(b)
NAM METEOROLOGICAL DATA

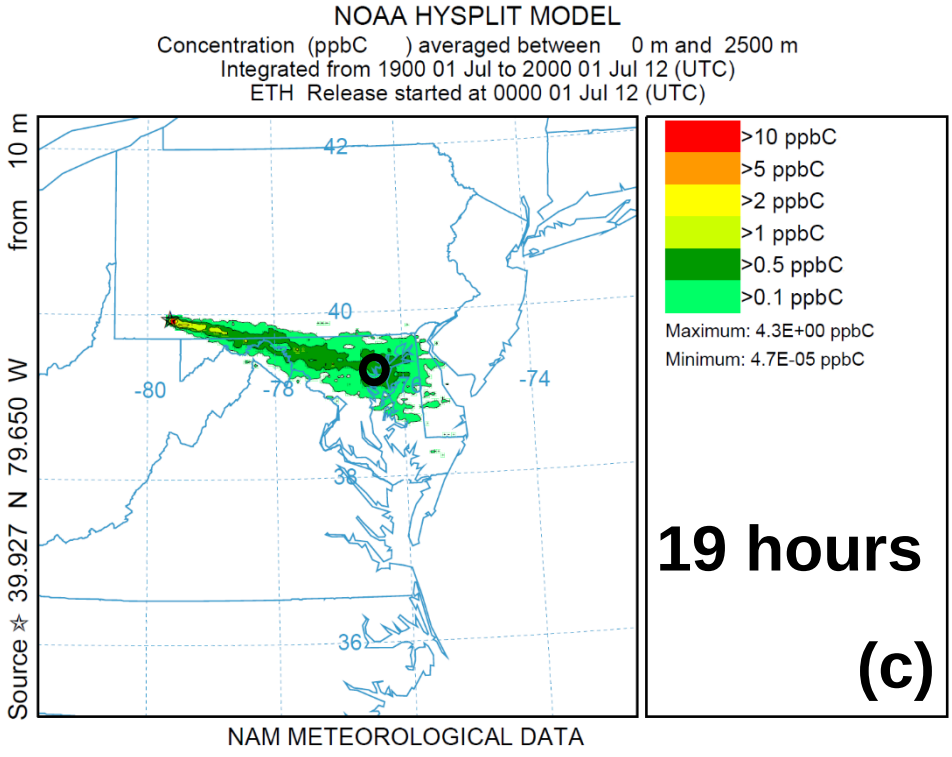
NOAA HYSPLIT MODEL
Concentration (ppbC) averaged between 0 m and 2500 m
Integrated from 1900 01 Jul to 2000 01 Jul 12 (UTC)
ETH Release started at 0000 01 Jul 12 (UTC)
from 10 m
Source ☆ 39.927 N 79.650 W
42
40
-80
-78
-74
38
36
>10 ppbC
>5 ppbC
>2 ppbC
>1 ppbC
>0.5 ppbC
>0.1 ppbC
Maximum: 4.3E+00 ppbC
Minimum: 4.7E-05 ppbC
19 hours
(c)
NAM METEOROLOGICAL DATA

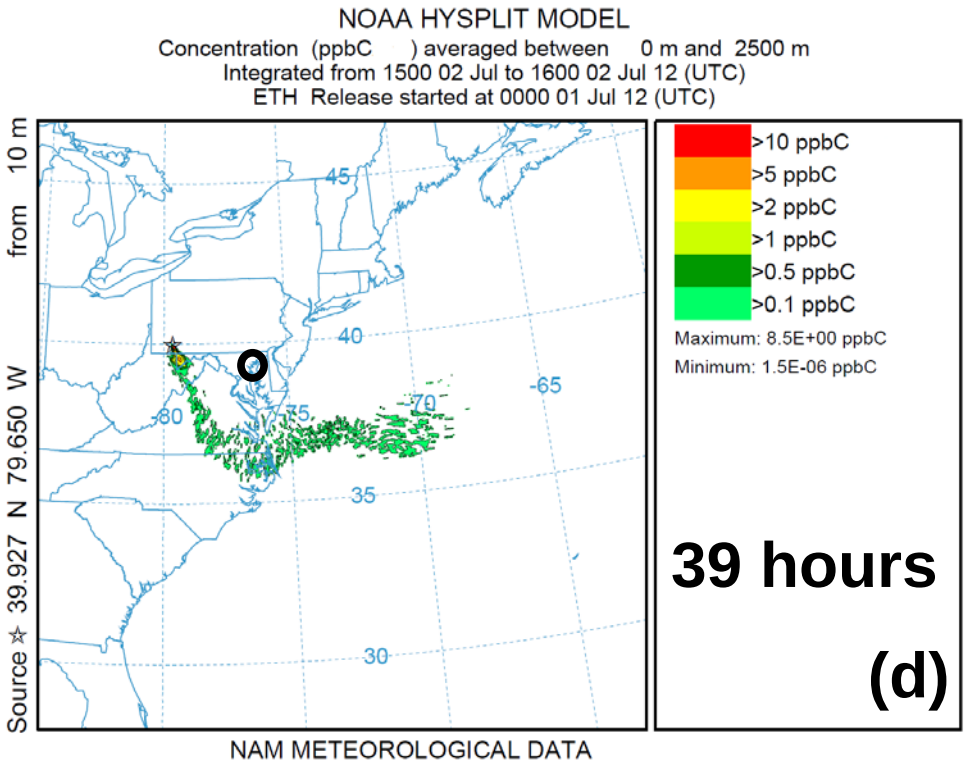

Figure 5.12 Snapshots of ethane dispersion plume from Westmoreland County, PA (a) 5 hours after release, (b) as the plume first appears over Essex, MD during daytime hours.

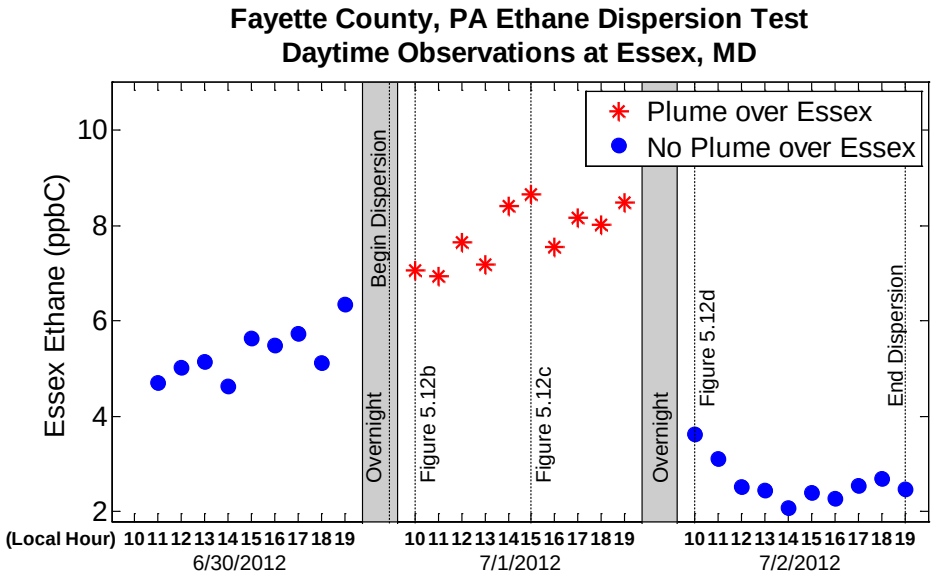

Figure 5.13 Daytime measurements of ethane at the Essex, MD monitor during the Fayette County, PA dispersion simulation. Markers change from blue dots to red stars when the plume passed over Essex, MD. No measurement was available for hour 10 on June 30. The measurement corresponding with the events shown in **Figures 5.12b, c, and d** are also noted.

5.3.3 Isopentane to n-Pentane Ratio

In addition to methane and ethane, the ratio of isopentane/n-pentane has been reported as another indicator of natural gas (Gilman et al., 2013). A natural gas signal will show an isopentane/n-pentane ratio around 0.9, whereas an urban environment rich in gasoline-related emissions will have exhibit a ratio two to three times greater (**Figure 5.12**). This study in Colorado did not feature areas as densely populated with gasoline vehicles as in the Baltimore area, but still provides an additional approach for analyzing measurements trends at the Essex monitor.

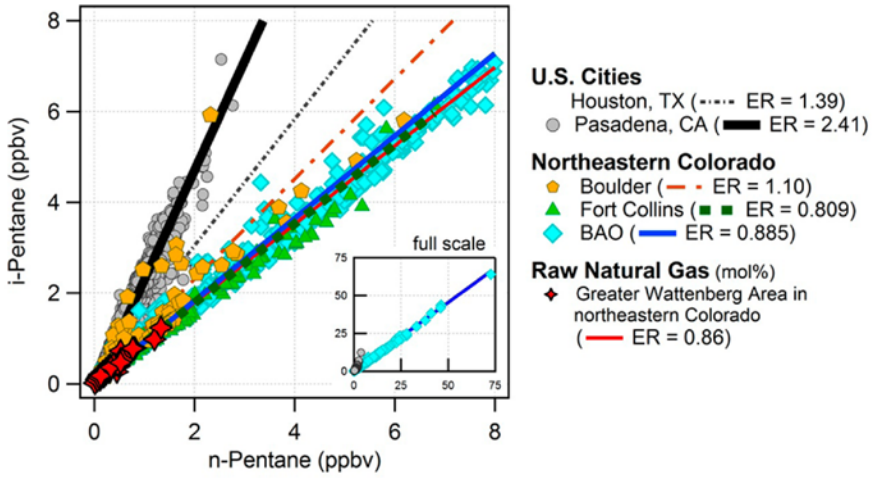

Figure 5.14 Ratio of isopentane to n-pentane in various environments (Gilman et al., 2013)

Using the same well density trajectory groupings, the isopentane/n-pentane concentration ratios were analyzed, similar to the ethane concentrations shown earlier. From 2008 through 2012, the pentane ratios for high well trajectories were not consistently lower than their low well trajectory counterparts, and were sometimes greater. However, from 2013 through 2015, pentane ratios for the two groups diverged. While the pentane ratios for low well trajectories remained at roughly 2 over the three years, the ratios associated with high well trajectories were significantly

lower and continued to decrease as natural gas production increased, reaching around 1.9 in 2015 (**Figure 5.15, Table 5.3**). While the significant differences took longer to appear than when considering ethane concentrations, both analyses demonstrate a significant impact of natural gas operations on downwind VOC observations.

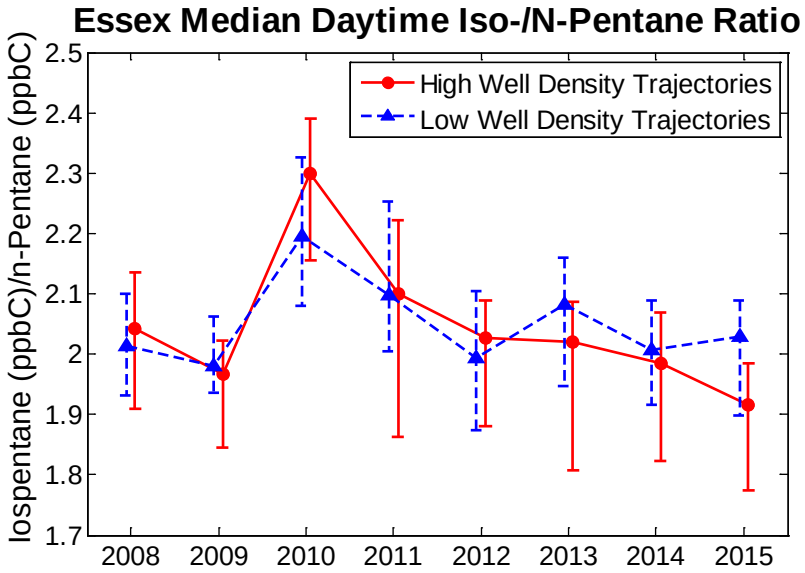

Figure 5.15 Comparison of isopentane/n-pentane concentration ratios at Essex, MD by trajectory path groupings. Median concentrations for each group are shown by the marker, with the whiskers denoting the 25th and 75th percentiles.

Table 5.3 Descriptive statistics for daytime isopentane to n-pentane concentration ratios at Essex, MD and p-values returned from testing for $median_{high\ well\ density} < median_{low\ well\ density}$.[a]

Year	High Well Density		Low Well Density		Mann-Whitney
	N	Median	N	Median	p-value
2008	10	2.04	67	2.01	>0.9999[b]
2009	19	1.97	50	1.98	**0.1718**
2010	12	2.30	42	2.20	>0.9999[b]
2011	15	2.10	51	2.10	0.4033
2012	22	2.03	56	1.99	>0.9999[b]
2013	14	2.02	55	2.08	**0.0398**
2014	15	1.98	57	2.01	**0.1337**
2015	30	1.92	53	2.03	**0.0003**

[a]A bolded p-value less than α=0.2 signifies significantly lower ratios for days with high well density trajectories.
[b]$Median_{high\ well\ density}$ was greater or roughly equal to $median_{low\ well\ density}$, p-values of >0.9999 were assigned.

5.3.4 Consideration of Possible Local Emission Sources

Trajectories that passed through counties with a high density of wells were shown to have an association with high ethane observations. However, these trajectories that pass through counties with a high density of wells could also pass through natural gas transmission sources that lay to the northwest and west of the monitors (**Figure 5.7**), which could also impact observed ethane concentrations. For each year from 2008 to 2015, trajectories for the first five hours of the 48-hour back-trajectories were clustered to investigate possible influences from other natural gas sources such as leakage from transmission pipelines or compressor stations that are closer the monitoring stations. Back-trajectories from the high well density groupings were clustered separately from the low well density trajectories; this was done for both the Essex and McMillan monitors, creating four different cluster maps for each year (**Figures 5.16-5.23**). Median cluster concentrations are reported next to each mean cluster trajectory.

First, the high well density trajectory clusters were investigated (**Figures 5.16-5.23a,b**). Clusters with higher median ethane concentrations often came from the west, and mean trajectories paths from the west often traveled far (on average ~75 km) in five hours from the West Virginia border suggesting influences from farther away. Clusters associated with lower concentrations of ethane often came from the east or north. Average trajectory paths for clusters arriving from the east did not tend to travel nearly as far (only ~20 km) as those from the west. In general, shorter trajectories did not have higher ethane concentrations, indicating high concentrations are not likely a result of leakage from local natural gas transmission infrastructure.

There are pipelines and compressor stations to the north of Baltimore and Washington D.C. (**Figure 5.7**), yet several trajectory clusters arriving from the north cross these natural gas sources and are associated with low ethane concentrations, suggesting these locations would not be expected to be sources of large ethane concentrations. Clusters arriving at Essex from the west could be associated with upwind shale gas production, but there are also natural gas pipelines, compressor stations, and underground storage sites in this direction. However, clusters arriving from north or northwest of the McMillan monitor would pass through some of these same potential sources, yet did not contain higher concentrations (and often had lower ethane concentrations); **Figure 5.19a and b** provide an example of this. Thus, it seems that the natural gas pipeline transmission infrastructure is an unlikely consistent contributor to higher ethane concentrations.

Low well density trajectory clusters were similarly investigated (**Figures 5.16-5.23c,d**). The results were mostly consistent with what was found for the high well density clusters. Higher concentrations of ethane were typically associated with trajectories from the west, while lower concentrations tended to arrive from the east. McMillan had some higher ethane concentrations in 2010-2012 coming from the south, but were later lower from 2013 to 2015. As with the high well density trajectory clusters, there was no discernible local source that could serve as a consistent source of increased ethane concentrations.

While pipelines and compressor stations in Maryland appear unlikely to be significant contributors to higher ethane concentrations at the Essex monitor, several compressor stations are west of D.C. and the McMillan monitor that cannot be distinguished from upwind natural gas wells in the Marcellus Shale region. Similarly, several underground facilities exist in West Virginia as well as one in western Maryland that are co-located with natural gas operations.

However, over the past decade, the amounts of injections and withdrawls from these underground storage facilities have shown no trends (EIA, 2016c), and it is doubtful that the structural integrity of a majority of these storage facilities would have rapidly deteriorated over the past years. Thus, while natural gas distribution infrastructure might contribute to ethane observations, upwind shale gas production remains the most reasonable, significant contributor to higher ethane observations.

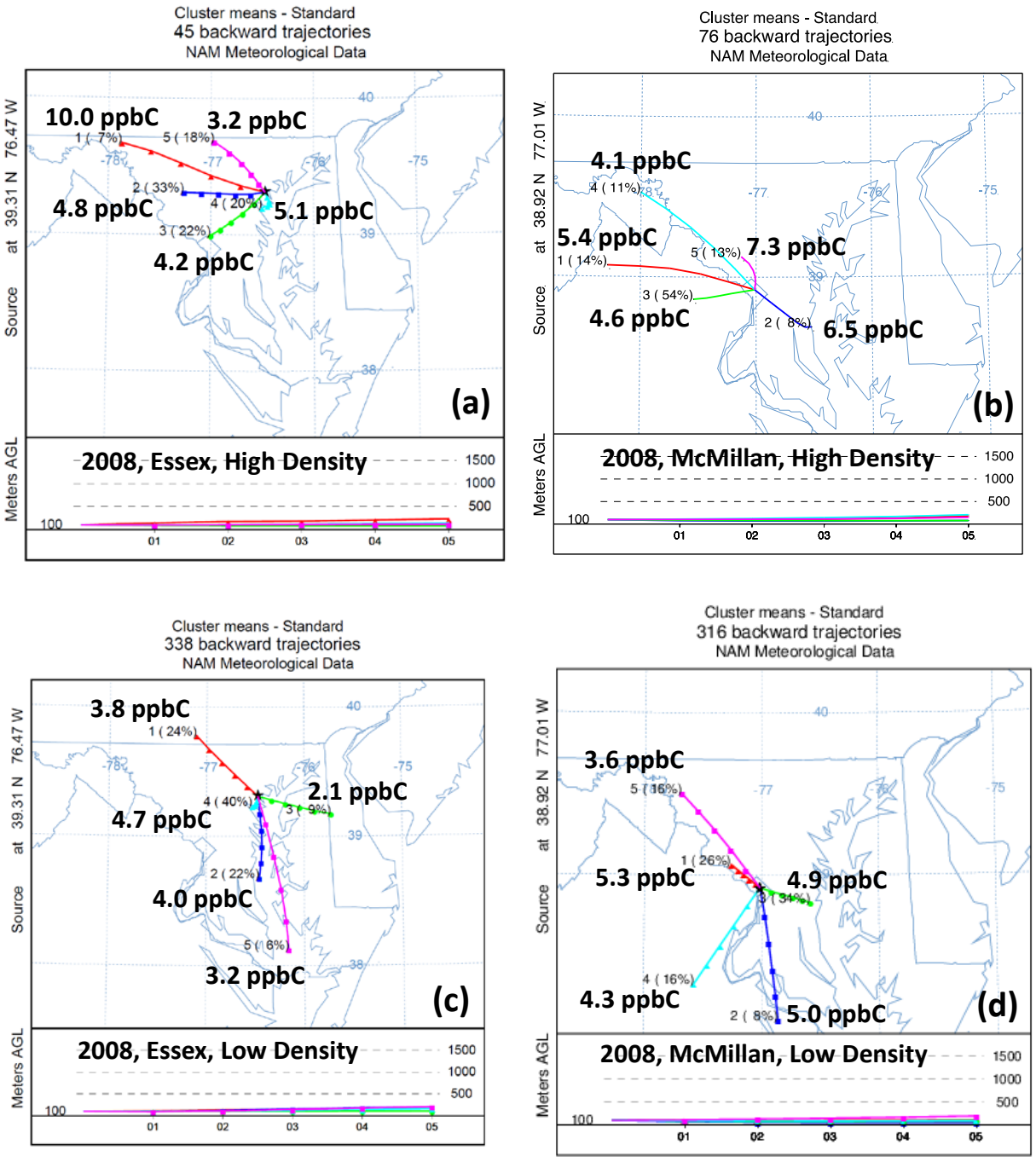

Figure 5.16 2008 clusters from high well density back-trajectories from the (a) Essex and (b) McMillan monitors, and low well density back-trajectories from (c) Essex and (d) McMillan monitors. The median ethane concentration for the cluster is printed next to each cluster's mean trajectory.

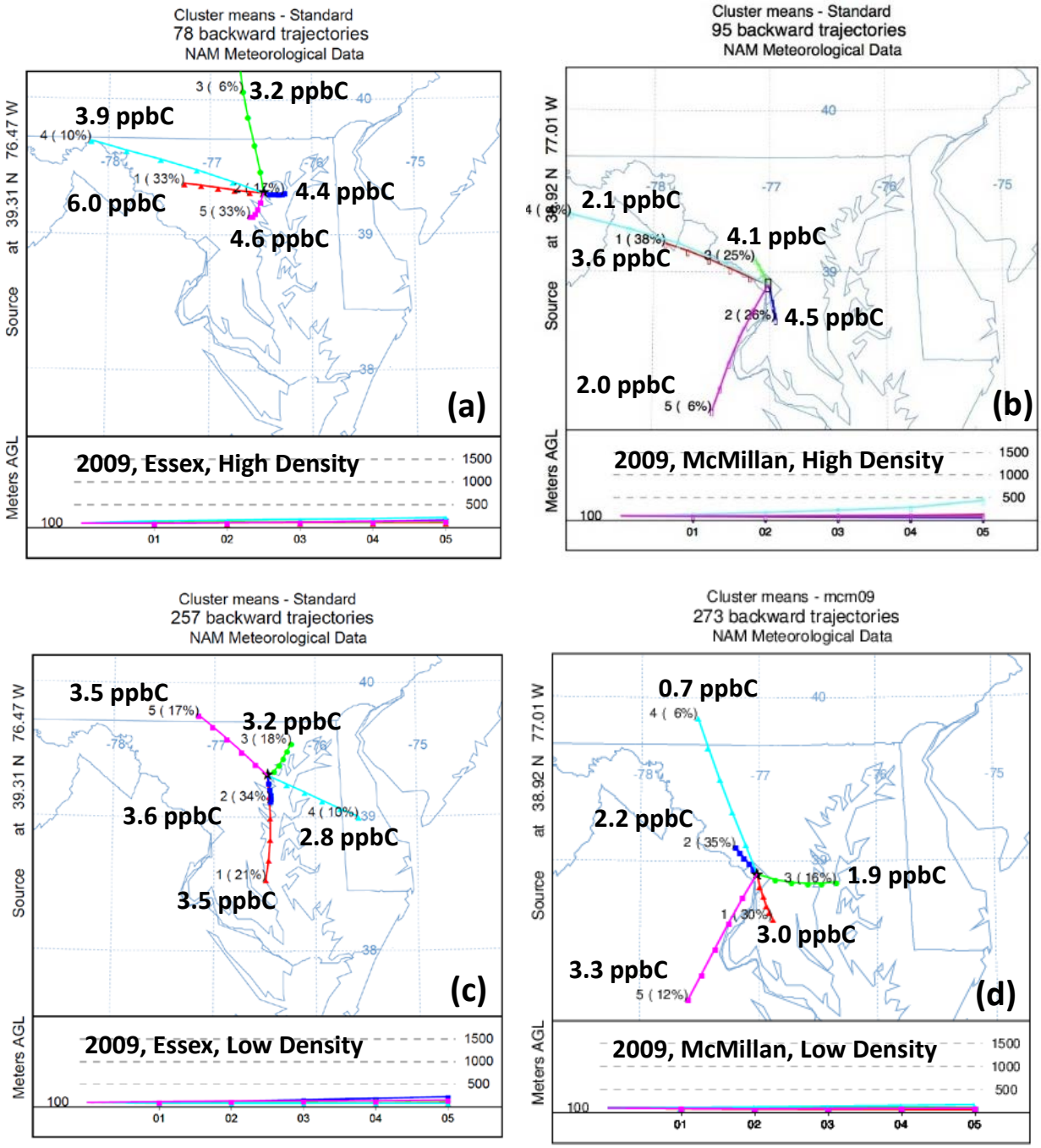

Figure 5.17 2009 clusters from high well density back-trajectories from the (a) Essex and (b) McMillan monitors, and low well density back-trajectories from (c) Essex and (d) McMillan monitors. The median ethane concentration for the cluster is printed next to each cluster's mean trajectory.

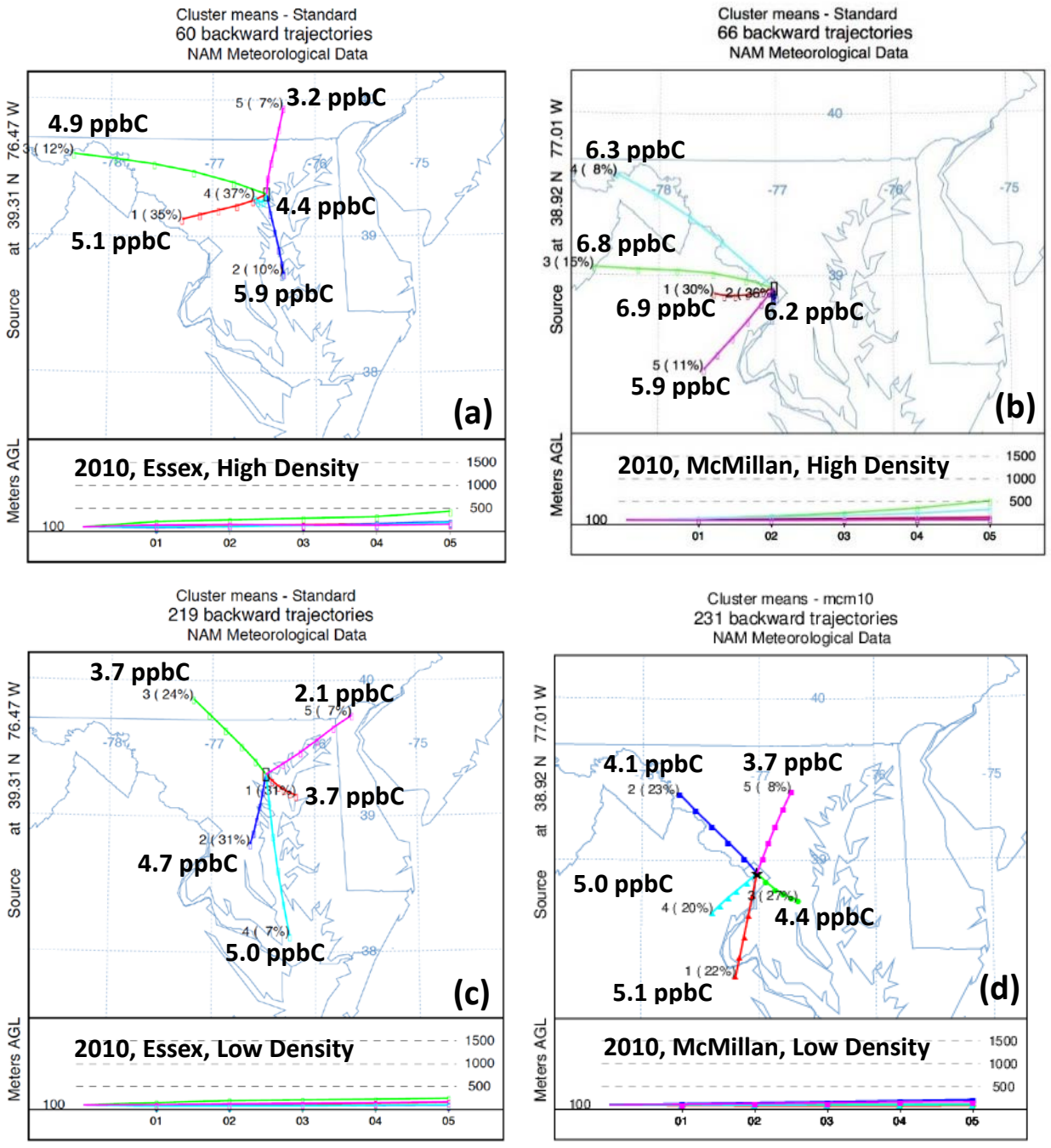

Figure 5.18 2010 clusters from high well density back-trajectories from the (a) Essex and (b) McMillan monitors, and low well density back-trajectories from (c) Essex and (d) McMillan monitors. The median ethane concentration for the cluster is printed next to each cluster's mean trajectory.

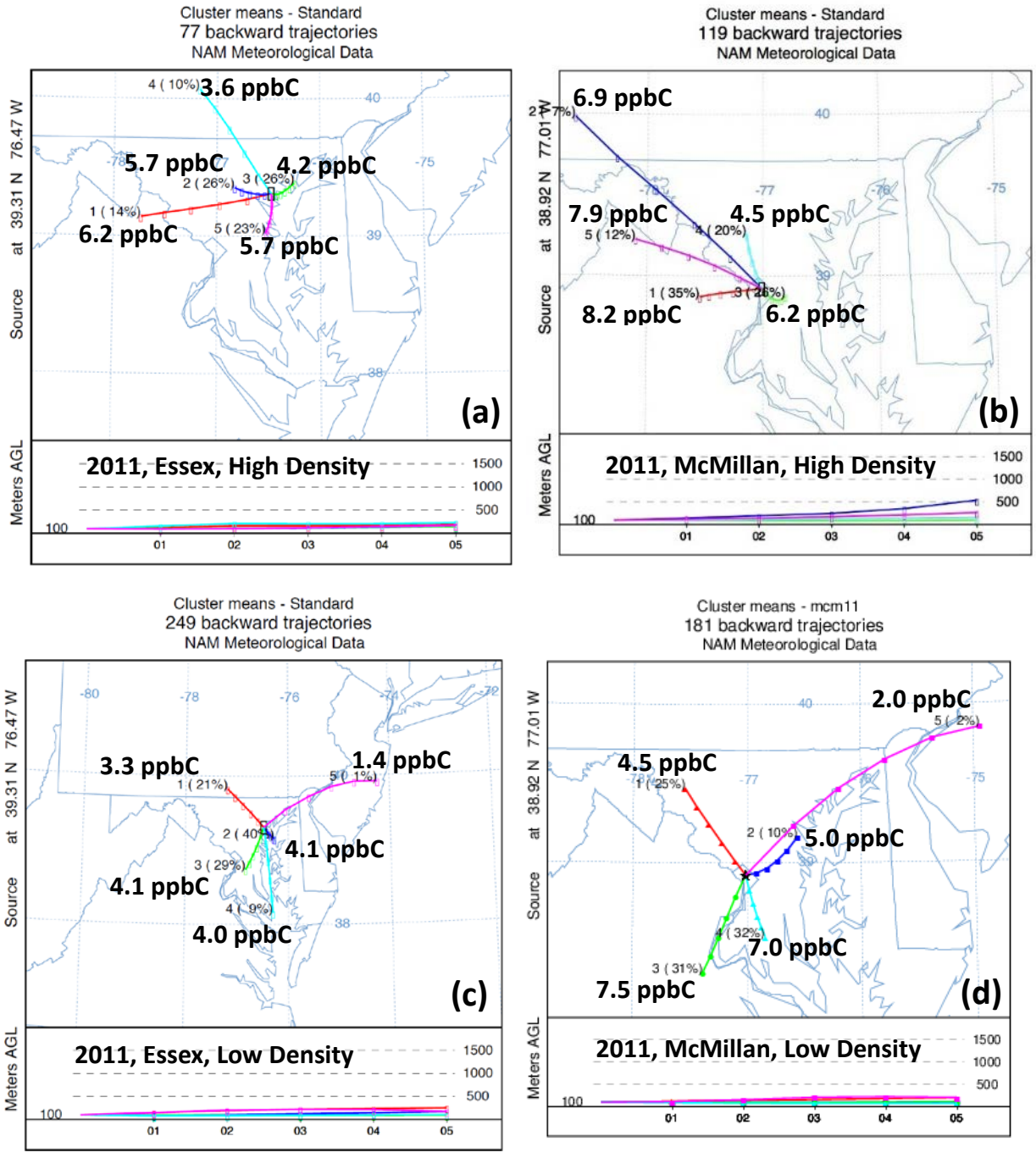

Figure 5.19 2011 clusters from high well density back-trajectories from the (a) Essex and (b) McMillan monitors, and low well density back-trajectories from (c) Essex and (d) McMillan monitors. The median ethane concentration for the cluster is printed next to each cluster's mean trajectory.

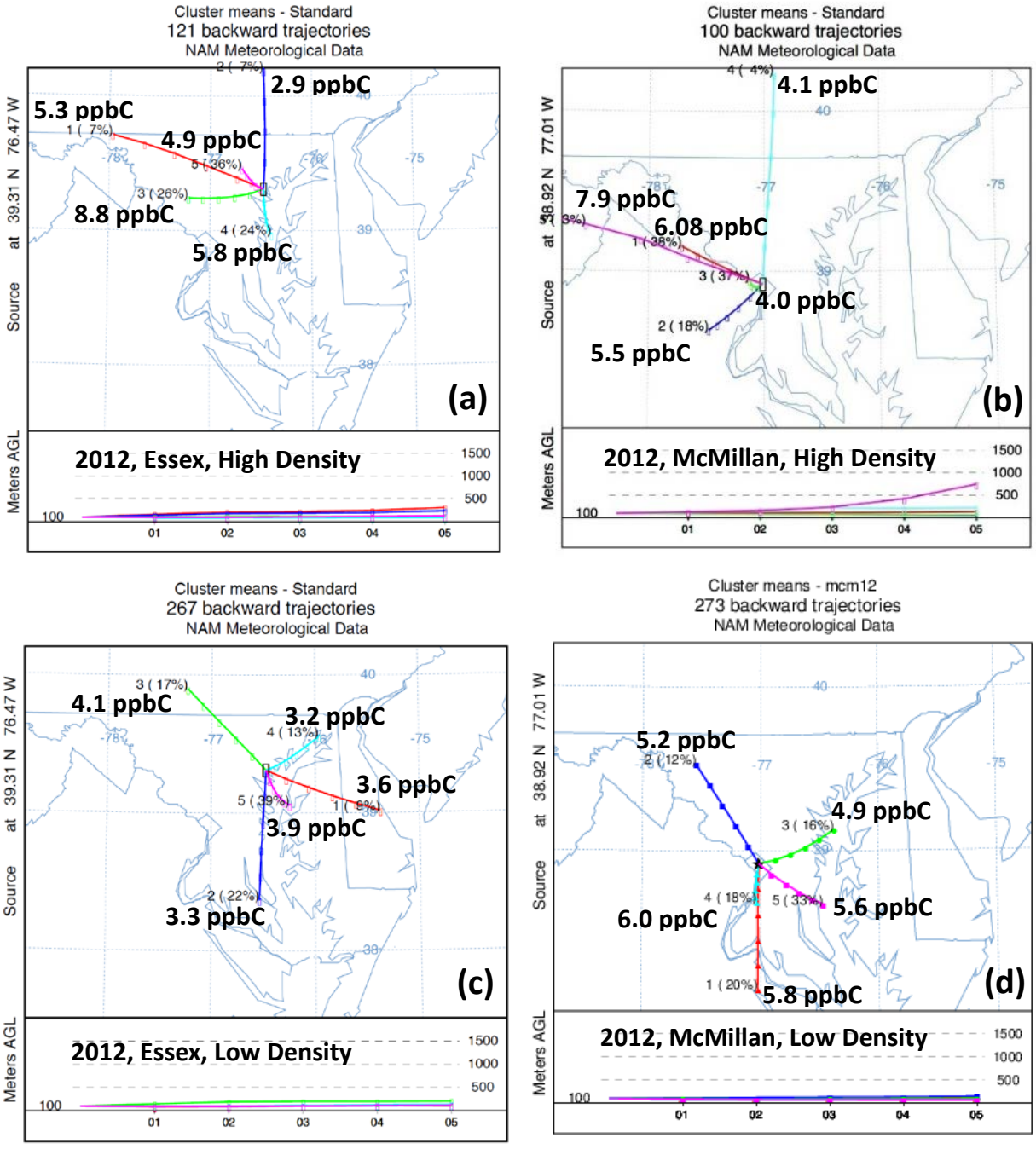

Figure 5.20 2012 clusters from high well density back-trajectories from the (a) Essex and (b) McMillan monitors, and low well density back-trajectories from (c) Essex and (d) McMillan monitors. The median ethane concentration for the cluster is printed next to each cluster's mean trajectory.

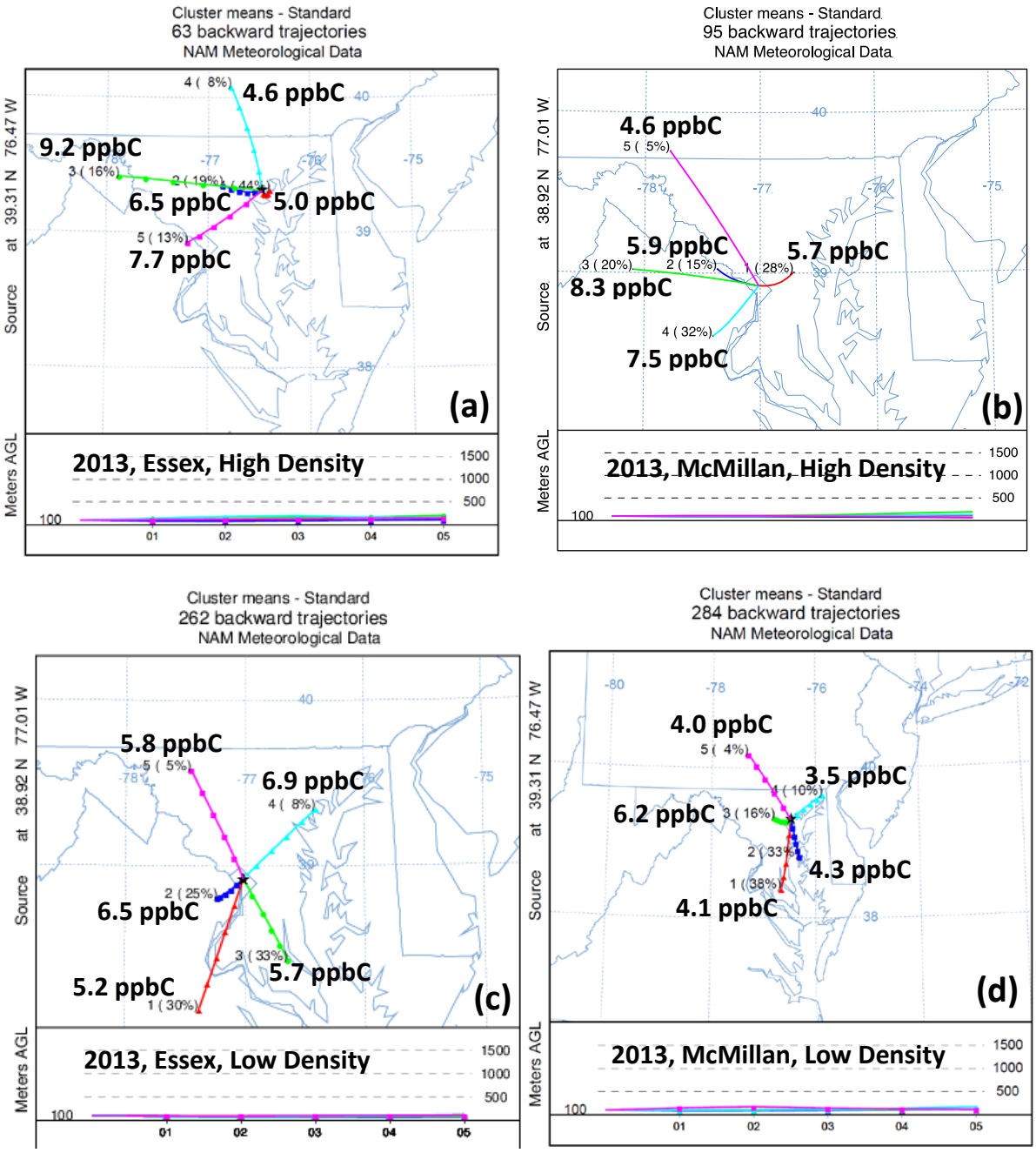

Figure 5.21 2013 clusters from high well density back-trajectories from the (a) Essex and (b) McMillan monitors, and low well density back-trajectories from (c) Essex and (d) McMillan monitors. The median ethane concentration for the cluster is printed next to each cluster's mean trajectory.

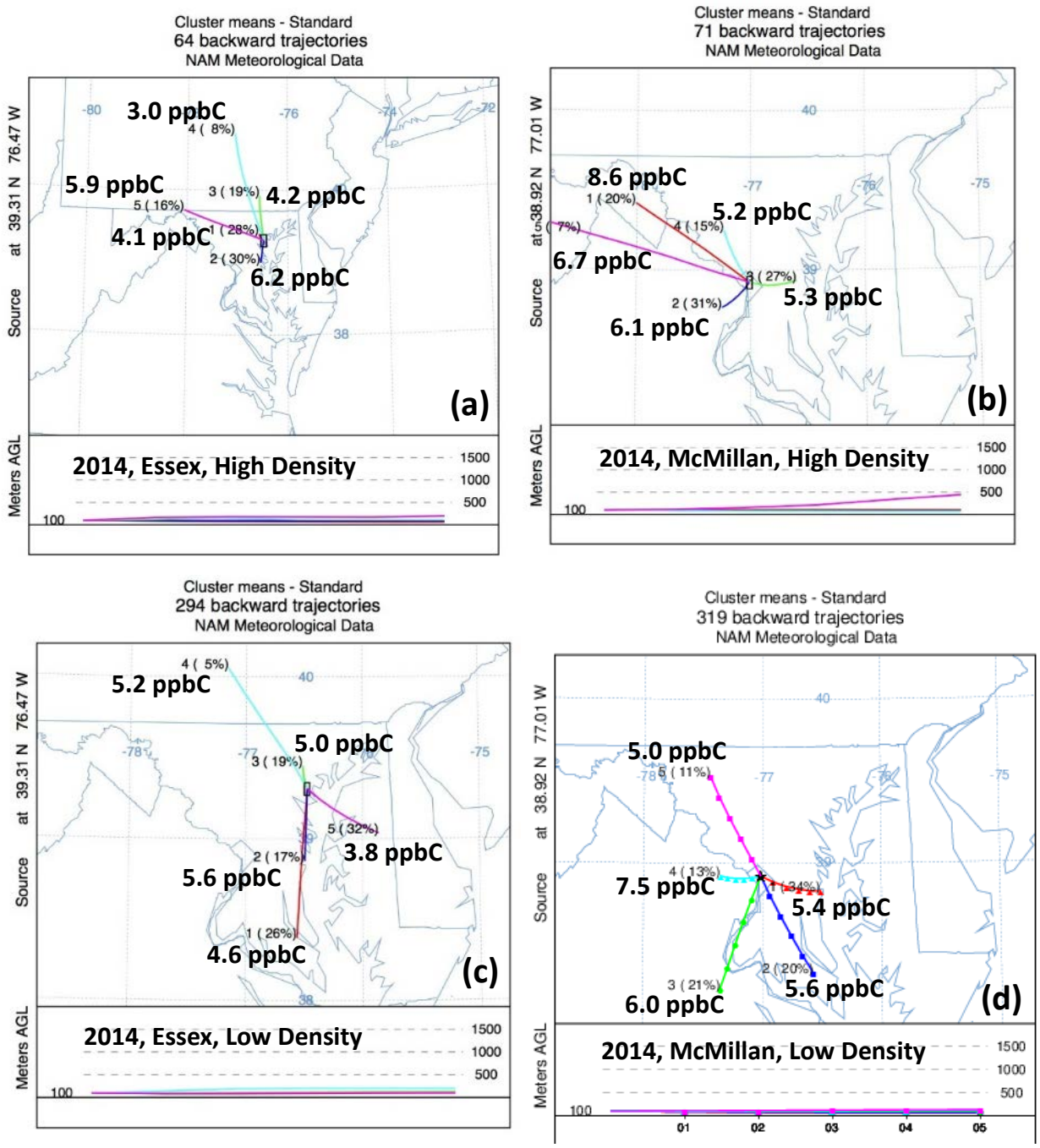

Figure 5.22 2014 clusters from high well density back-trajectories from the (a) Essex and (b) McMillan monitors, and low well density back-trajectories from (c) Essex and (d) McMillan monitors. The median ethane concentration for the cluster is printed next to each cluster's mean trajectory.

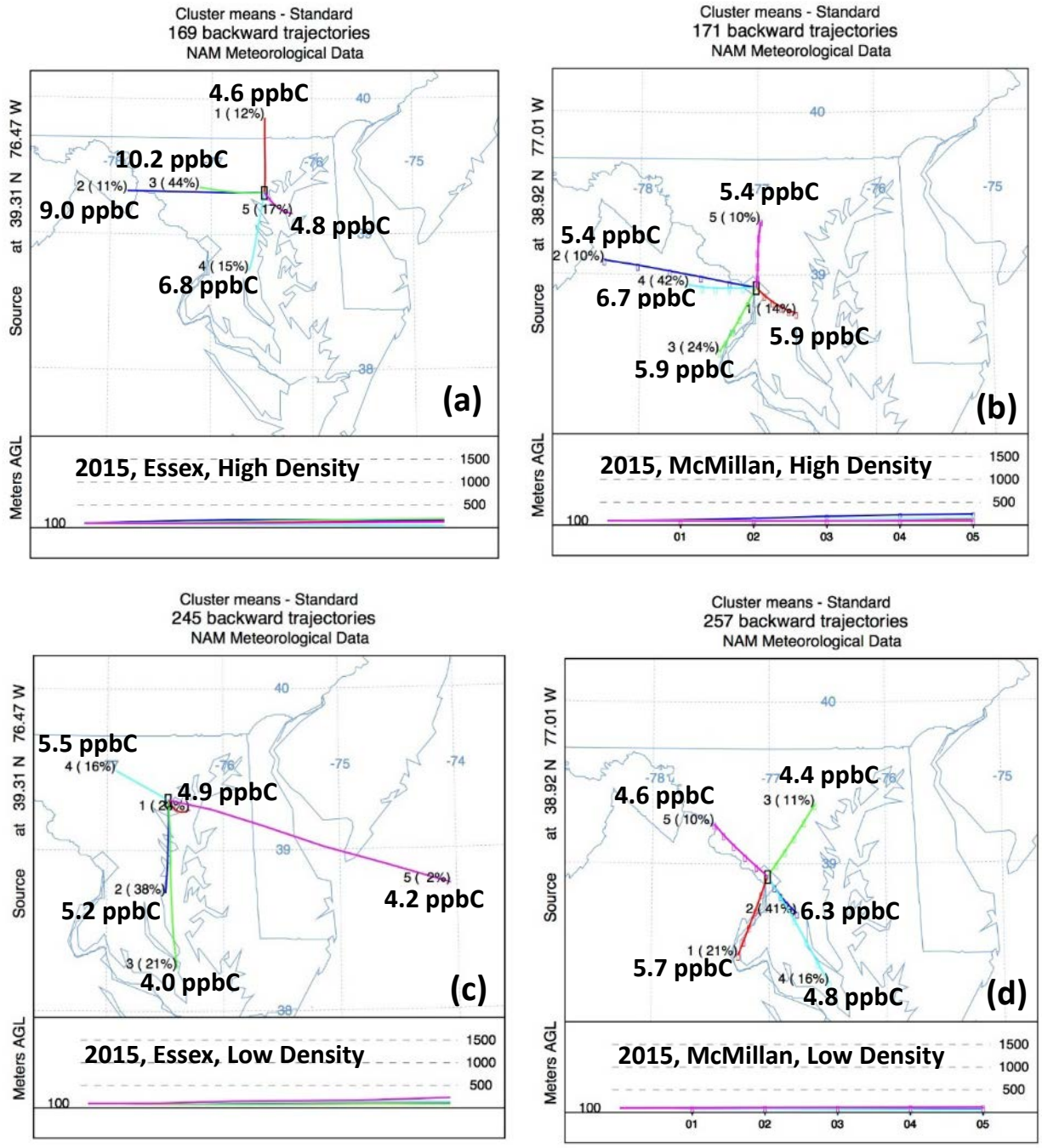

Figure 5.23 2015 clusters from high well density back-trajectories from the (a) Essex and (b) McMillan monitors, and low well density back-trajectories from (c) Essex and (d) McMillan monitors. The median ethane concentration for the cluster is printed next to each cluster's mean trajectory.

5.4 Conclusions

When examining measurements based on back-trajectories, ethane concentrations from the monitors at Essex, MD and McMillan Reservoir in D.C. were significantly greater when trajectories passed through counties containing a high density of unconventional natural gas wells. The ratio of isopentane/n-pentane at Essex was significantly lower from 2013 onward, further indicating an influence of natural gas on observations. Analysis of five-hour back-trajectories failed to reveal a consistent local source of natural gas emissions, and did not indicate an influence from local natural gas storage, compressors, and transmission pipelines. This wind trajectory analysis further supports the assertion from Chapter 3 that increasing ethane concentrations are attributable to upwind natural gas production operations.

Chapter 6 Impacts of Increased Hydraulic Fracturing Activity and Natural Gas Usage

This study was performed with Atmospheric and Oceanic Science graduate student Linda Hembeck and funded by the University of Maryland Council on the Environment's Green Fellowship. I processed and prepared the emissions, and Ms. Hembeck modified the emissions of VOC, NO_x and $PM_{2.5}$ in grid cells containing unconventional natural gas wells and ran the photochemical model.

6.1 Introduction

Air quality pollutants, including oxides of nitrogen and sulfur (NO_x and SO_x), volatile organic compounds (VOCs), ozone, and particulate matter of diameter 2.5 μm or smaller ($PM_{2.5}$), can be harmful to the health and welfare of humans and the environment (EPA, 2015a). Changing the fuel sources which power engines, electronic devices, heat and cool homes, etc. can significantly reduce one pollutant but sometimes increase another, resulting in different environmental effects. Not only is it important to consider the different mixture of pollutants in this analysis but also the change in their origin.

Over the past several years, the combined techniques of horizontal drilling and hydraulic fracturing have rapidly increased unconventional natural gas production in the United States, especially in the Appalachian Basin (**Figure 6.1**). Throughout the different stages of a well, various pollutants are emitted, notably VOCs, NO_x, and $PM_{2.5}$. Sources of these emissions include the diesel compressors and trucks needed for drilling and fracturing, and condensate tanks, wellhead compressors, and compressor stations needed for gas recovery. A large amount of VOC emissions can

also occur during the flowback process, where the well is vented to remove liquids and debris prior to the recovery process. A study by Roy et al. (2014) predicted that in the year 2020, activities related to unconventional natural gas production will account for 12% of the total NO_x and VOC emissions and 14% of the total $PM_{2.5}$ in the Marcellus Shale region (within the Appalachian Basin).

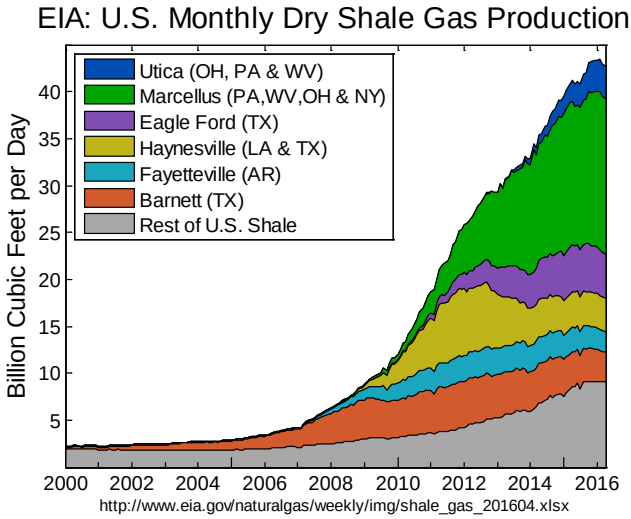

Figure 6.1 Dry shale gas production rates for the largest shale regions in the U.S through April 2016. The Utica and Marcellus shale residing in the Appalachian Basin are shown in blue and green, respectively. Adapted from EIA (2016a).

Natural gas is projected to displace coal as the 2nd largest overall energy source by 2025 (ExxonMobil, 2014). By the end of 2015, equivalent amounts of electricity were generated from natural gas and coal (EIA, 2016b), making power plant emissions much cleaner. While natural gas extraction operations emit many pollutants even with recent regulations (EPA, 2012), burning natural gas in power plants releases significantly less NO_x and SO_x compared to traditional coal combustion (Roy and Choi, 2015). Reductions in power plant NO_x would be expected to decrease levels of surface ozone, which would have an enormous benefit on human

health and agriculture, but increases in pollutants due to installation and operation of hydraulic fracturing well pads could negate those potential benefits.

In response to the redistribution of pollutant emissions, two possible scenarios were considered for the year 2020: A) Unconventional wells are assumed in areas of current operation, but no future policies are enacted, leaving power plant emission rates unchanged, and B) All coal-fired power plants are converted to burn natural gas instead, but hydraulic fracturing operations are expanded into all states that lie within the Appalachian Basin to provide this energy resource. These two 2020 scenarios were compared to each other as well as to a 2007 base case.

6.2 Methods

6.2.1 Preparation of Emissions

Emissions were created for the summer months of June, July, and August using the Sparse Matrix Operator Kernel Emissions (SMOKE) version 3.1 emissions inventory modeling system, assuming 2007 meteorology for the base case and both 2020 scenarios. More information about this model version is available at: https://www.cmascenter.org/smoke/documentation/3.1/html/.

6.2.1.1 2007 Base Case

Existing hourly Level 3 2007 emissions inventory estimates developed by the Mid-Atlantic Regional Air Management Association (MARAMA) and the New York State Department of Environmental Conservation (NYSDEC) as part of the Ozone Transport Commission (OTC) were used for the 2007 base case (MARAMA, 2016a). For the base case and following scenarios, the anthropogenic emissions generated

with SMOKE were combined with 2007 biogenic emissions from the Model of Emissions of Gases and Aerosols from Nature (MEGAN) version 2.10 (Guenther et al., 2012).

6.2.1.2 Scenario A

Existing hourly MARAMA Level 3 2020 projections from 2007 have been used in several OTC modeling efforts and were used as a basis of both 2020 scenarios (MARAMA, 2016b). These emission estimates were further adjusted to account for newer policies and transitions not included when the 2020 inventories were initially created. U.S. mobile emissions were reduced to account for Tier 3 fuel standards finalized by the EPA in March of 2014: -9.9% NO_x, -55.9% SO_2, -2.4% VOC, -0.4% $PM_{2.5}$, and -1.6% CO (EPA, 2014c). Electric Generating Unit (EGU) emissions were updated by using inventories created by the Eastern Regional Technical Advisory Committee (ERTAC) EGU growth model. The ERTAC model implements the most up-to-date control policies through coordination between numerous eastern states as part of a technical-driven process (MARAMA, 2016c). ERTAC EGU (Version 1.7) 2020 inventories for the continental U.S. were used for this study and processed through SMOKE. Area and point sources in the U.S. were also slightly reduced following previous OTC modeling runs to account for recently planned controls on Industrial, Commercial, and Institutional (ICI) boilers (**Table 6.1**).

Table 6.1 Adjustments made to 2020 sectors containing ICI boilers, by region and pollutant.

Emission Sector	Region	NO_x	PM	SO_2
Non-EGU Point Sources	MANEVU	-8.6%	-12.6%	-35.2%
	LADCO	-6.4%	-3.6%	-28.3%
	SESARM	-1.6%	-2.7%	-9.7%
	CENSARA	-10.7%	-0.9%	-23.5%
Area Sources	MANEVU	-6.4%	-2.2%	-51.1%
	LADCO	-3.0%	-0.7%	-61.5%
	SESARM	-7.4%	-1.5%	-77.9%
	CENSARA	-1.0%	-0.1%	-70.1%

For Scenario A, emissions were grown in grid cells that contained at least one unconventional gas well as of February 2014 (FracTracker Alliance, 2014), with the assumption that wells would populate in similar areas in the near future. Following the 2020 estimates presented by Roy et al. (2014), emissions of NO_x and VOCs were increased by 13.6% and $PM_{2.5}$ by 16.3% in these regions to account for the air quality effects of natural gas operations. The affected grid cells are shown in red in **Figure 6.2a**. The states of Maryland and New York do not currently allow hydraulic fracturing operations (MGA, 2015; NYSDEC, 2015), and were assumed to likewise not permit such activities in 2020. Visible areas of red in **Figure 6.2a** within the borders of these states are a result of grid cells shared with neighboring states that do allow these practices.

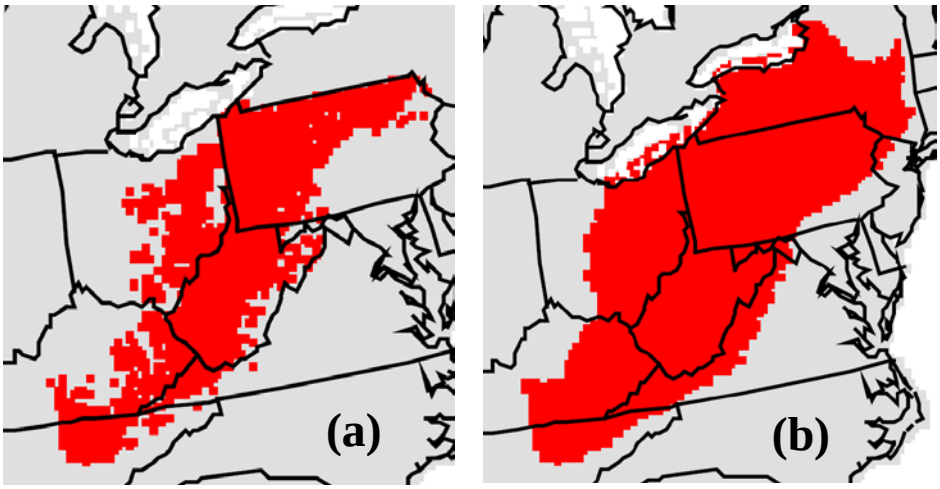

Figure 6.2 (a) Grid cells adjusted in Scenario A based on operational unconventional wells as of February 2014, and (b) grid cells adjusted in Scenario B, spanning the full Appalachian Basin.

6.2.1.3 Scenario B

For Scenario B, 2020 emissions from sources unrelated to natural gas operations or EGUs remained unaltered from Scenario A. To convert emissions from coal-fired EGUs to natural gas equivalent rates, 2012 and 2013 coal and natural gas EGU emissions monitoring data from the U.S. EPA's Clean Air Markets Division (EPA, 2014d) were compared to compute reduction values for NO_x and SO_2. These measurements come from states participating in the Clean Air Interstate Rule, excluding states such as Texas and Florida which reside outside the modeling domain. On average, natural gas EGUs produced approximately 80% less NO_x and 99% less SO_2, and these values match well with the values found in a nation-wide review of 2013 US Emissions & Generation Resource Integrated Database (eGRID) values by Roy and Choi (2015). The study also found natural gas units emit 75% less $PM_{2.5}$ and 33% less VOCs than coal-fired units, and these estimates were also used as reduction values applied to coal-fired facilities in Scenario B.

Table 6.2 Summary of reductions applied to coal-fired EGUs in Scenario B

Pollutant	NO_x	SO_2	VOC	$PM_{2.5}$
Reduction	-80%	-99%	-33%	-75%

To obtain the large quantities of natural gas that would be required to fuel the new EGUs in this scenario, hydraulic fracturing hypothetically expands into regions that are currently void of such operations. As a result, emissions within the entire Appalachian Basin (red regions shown in **Figure 6.2b** (EIA, 2013)) were adjusted by applying the same growth factors used for regions containing wells in Scenario A.

6.2.2 CMAQ

The Community Multiscale Air Quality (CMAQ) modeling system version 5.0 is used as a regulatory tool and a platform to understand the complex interactions of atmospheric chemistry. CMAQ uses SMOKE emission fluxes as inputs, incorporating meteorological data and chemical reaction kinetics to calculate the expected formation and dispersion of various pollutant species. The CMAQ simulations have 12 km × 12 km horizontal grid resolution, 34 layer sigma-coordinate vertical levels (from surface to ~20 km), and hourly output for an Eastern United States modeling domain. CMAQ uses the Weather, Research and Forecasting (WRF) Model version 3.1.1 as the meteorological driver (Skamarock and Klemp, 2008), and the Meteorology-Chemistry Interface Processor (MCIP) to further process these meteorology fields for modeling utilization. Boundary conditions were provided from a 36 km CMAQ run derived from 2007 GEOS-Chem (Bey et al., 2001), and the chemical mechanism CB05-TU (Whitten et al., 2010) was used along with the AE6

scheme for aerosols (Carlton et al, 2010). More information about this version of the model is available at: http://www.airqualitymodeling.org/cmaqwiki/index.php?title=CMAQ_version_5.0_(February_2010_release)_OGD.

6.3 Results and Discussion

The National Ambient Air Quality Standards (NAAQS) were established as part of the Clean Air Act to limit pollutants that are harmful to human health and the environment (EPA, 2016c). For ozone, attainment of the standard is determined by the fourth-highest, daily maximum 8-hour average concentration; for $PM_{2.5}$ the 98^{th} percentile of 24-hour daily averages is used. Because of their significance in determining attainment of healthy ambient conditions, these calculated values are shown for simulated concentrations of ozone (**Figures 6.3-6.5**) and $PM_{2.5}$ (**Figures 6.6-6.7**).

For both 2020 cases, concentrations of ozone are substantially reduced from 2007 levels. In the 2007 baseline, several metropolitan areas showed fourth-highest, daily maximum 8-hour average concentrations exceeding 90 ppb (**Figure 6.3a**). By 2020, many of the metropolitan areas have decreased to around 70-75 ppb in Scenario A (**Figure 6.3b**) and even lower in Scenario B (**Figure 6.3c**). High ozone concentrations are seen as a result of low boundary layers over large water bodies such as the Great Lakes and Atlantic Ocean (e.g., Goldberg et al., 2014).

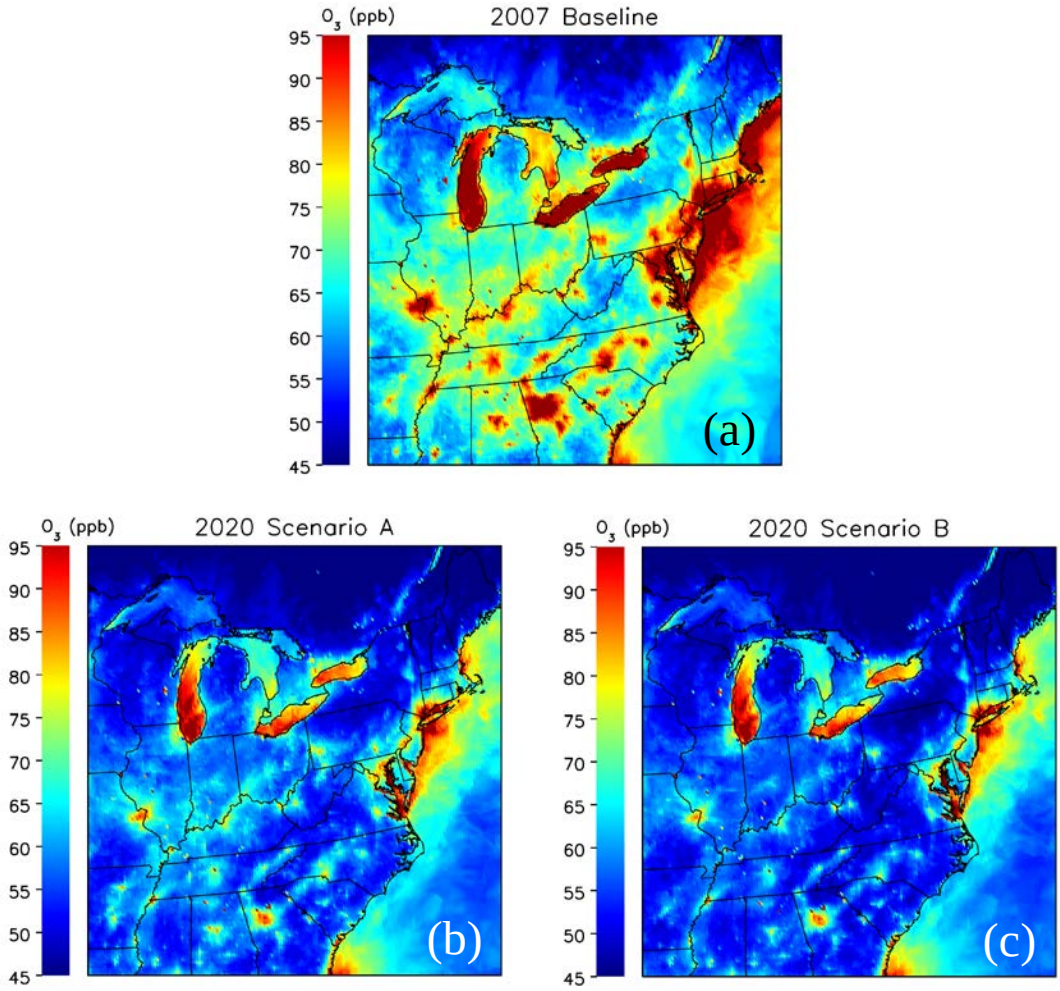

Figure 6.3 Fourth-highest, 8-hour maximum daily average ozone for (a) the 2007 baseline, (b) Scenario A, and (c) Scenario B (all coal-fired power plants replaced with natural gas).

For both Scenarios A and B, concentrations of ozone improve from 2007, and this comes primarily from the overall reduction of emissions from other sources, especially cars, over time (**Tables 6.3-6.5**). Results for Scenario A (**Figure 6.4a**) show that in regions such as West Virginia and western Pennsylvania with an

abundance of wells will not observe as great of an improvement in ozone, when compared to areas without such operations (eastern Pennsylvania). Greater improvement of ozone was observed by converting coal fired power plants to natural gas fired power plants, despite increased drilling and production activity (**Figure 6.4b**). The largest differences between Scenarios A and B occur close to and downwind of these power plants, often resulting in 10-15 ppb decreases of ozone concentrations (**Figure 6.4c**).

Table 6.3 Eastern U.S. modeling domain emissions of NO_x (tons/year) [a]

Year	Area	Marine, Aircraft, and Railroad	Nonroad	Non-EGU Point	EGU	Mobile
2007	512,092	904,378	803,268	1,066,032	2,093,155	4,452,693
2020 A	446,933	714,497	407,566	990,416	1,154,392	1,484,528
2020 B	446,933	714,497	407,566	990,416	272,543	1,484,528

[a]Emissions do not include adjustments for grid cells containing natural gas operations

Table 6.4 Eastern U.S. modeling domain emissions of VOC (tons/year) [a]

Year	Area	Marine, Aircraft, and Railroad	Nonroad	Non-EGU Point	EGU	Mobile
2007	2,731,151	63,350	1,318,108	622,167	23,348	2,131,860
2020 A	2,453,655	63,215	707,223	634,511	19,764	863,302
2020 B	2,453,655	63,215	707,223	634,511	16,049	863,302

[a]Emissions do not include adjustments for grid cells containing natural gas operations

Table 6.5 Eastern U.S. modeling domain emissions of $PM_{2.5}$ (tons/year) [a]

Year	Area	Marine, Aircraft, and Railroad	Nonroad	Non-EGU Point	EGU	Mobile
2007	715,022	41,784	78,134	231,918	245,507	181,357
2020 A	705,743	25,057	67,579	220,344	165,263	93,747
2020 B	705,743	25,057	67,579	220,344	53,305	93,747

[a]Emissions do not include adjustments for grid cells containing natural gas operations

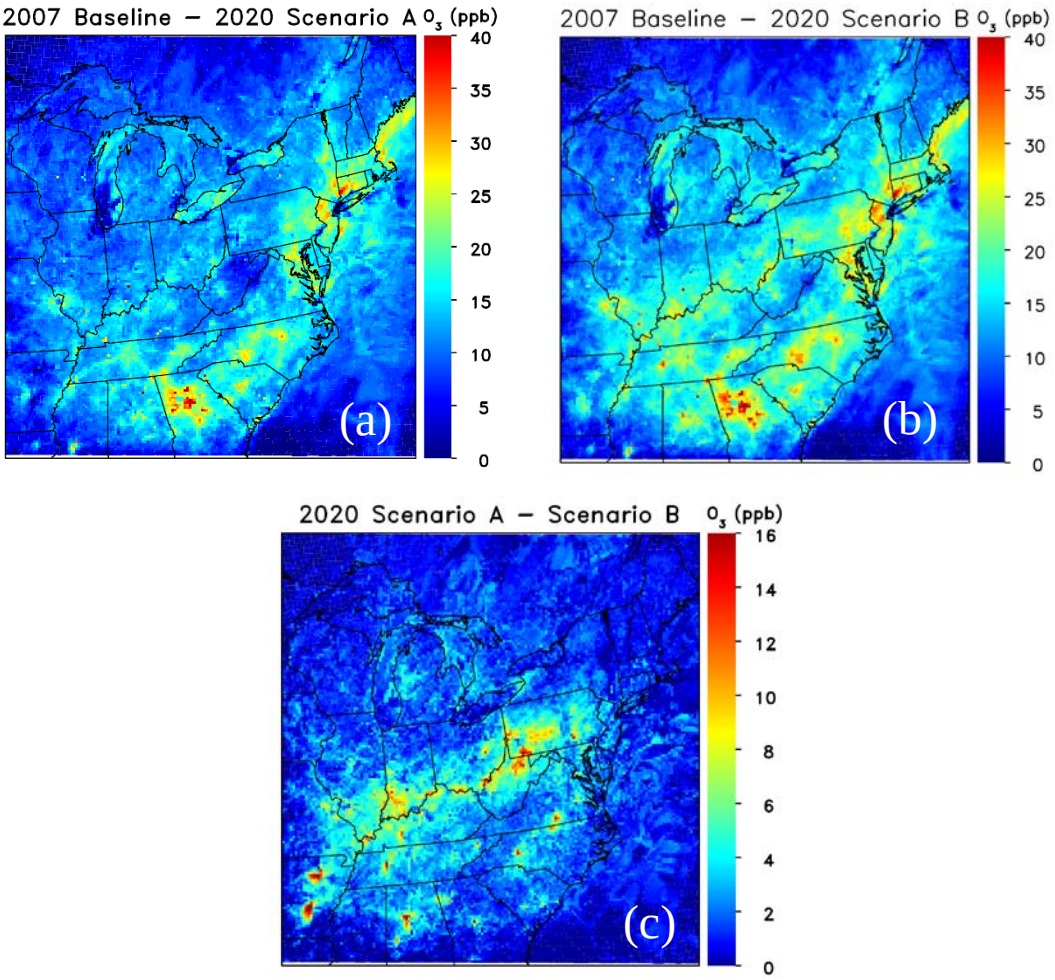

Figure 6.4 Difference of fourth-highest, 8-hour maximum daily average ozone between (a) the 2007 baseline and Scenario A, (b) the 2007 baseline and Scenario B, and (c) Scenario A and Scenario B. Color bar neglects regions where ozone increases.

There are a few notable regions where ozone concentrations increase between 2007 and 2020 (**Figure 6.5a and 6.5b**). Between these years, ozone concentrations were seen to increase around New York City and along the Lake Michigan shoreline from Chicago to Milwaukee. Some city centers such as Pittsburgh and Philadelphia show almost no change between years. These increases and non-improvements are most likely more a result of NO_x titration than natural gas operations. In 2007, NO_x emissions were so large that NO_2 was destroying ozone, but in 2020, NO_x emissions

were lower, and ozone was no longer being destroyed and instead increased. Eventually ozone will decrease in later years in these locations, as NO_x emissions continue to decrease, but in 2020 they appear to be in a transitional regime where reductions of both NO_x and VOC emissions will be needed to reduce ozone concentrations. From Scenario A to Scenario B, hydraulic fracturing operations were expanded. Because the Appalachian Basin extends under the southern parts of Lake Erie and Lake Ontario, and there is precedent for offshore hydraulic fracturing (Ross, 2013), some ozone increases were seen over these bodies of water (**Figure 6.5c**).

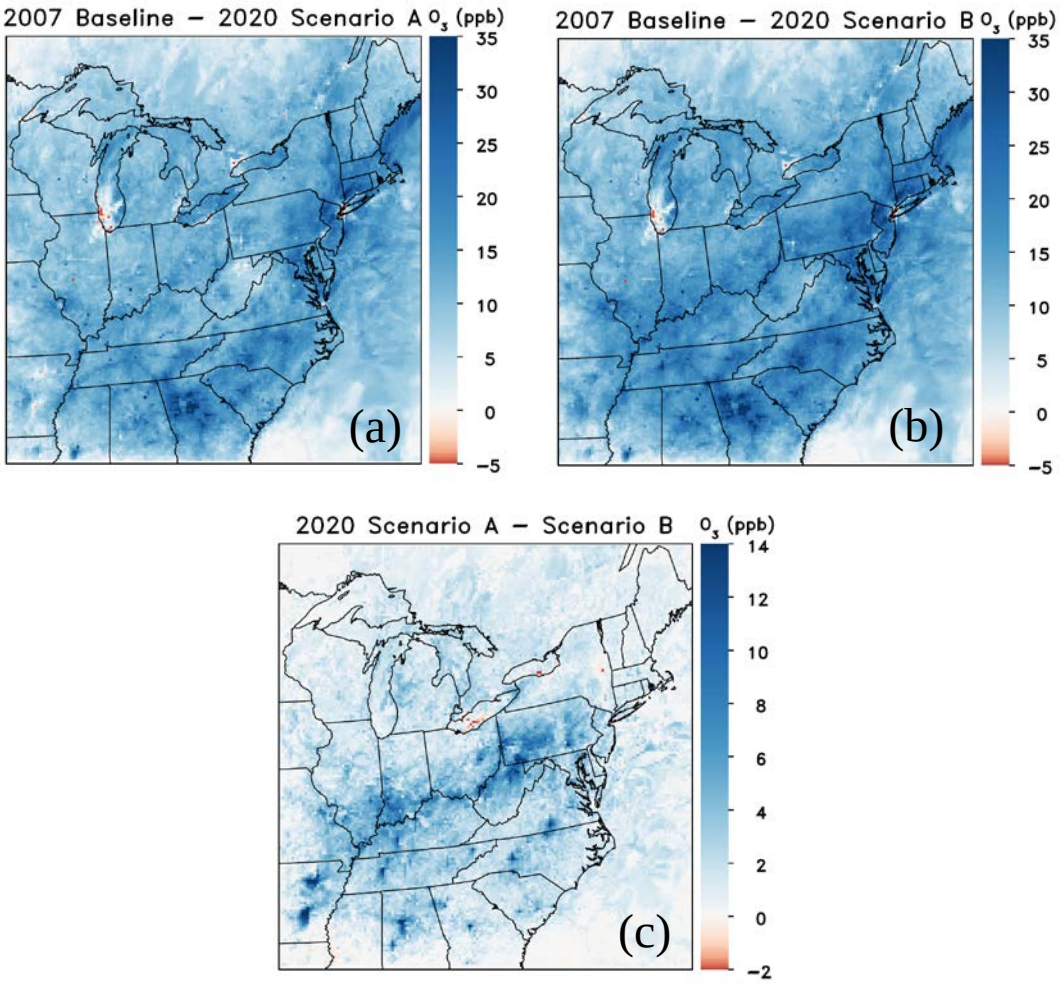

Figure 6.5 Difference of fourth-highest, 8-hour maximum daily average ozone between (a) the 2007 baseline and Scenario A, (b) the 2007 baseline and Scenario B,

and (c) Scenario A and Scenario B. Regions where ozone concentrations increase between scenarios are shown in red, whereas regions where ozone decreases are blue. Negative values reflect regions where ozone increases.

Similar to ozone, large decreases occurred between 2007 and 2020 for 98th percentile, 24-hour average $PM_{2.5}$. In 2007, several regions had high $PM_{2.5}$ concentrations of 40-45 $\mu g/m^3$ (**Figure 6.6a**). In 2020, these high concentrations were greatly reduced (**Figures 6.7a and b**) to around 20-25 $\mu g/m^3$ (**Figure 6.6b and c**), with the size of areas containing high concentrations decreasing further between Scenario A and Scenario B. Most improvements of $PM_{2.5}$ between Scenario A and Scenario B appeared mostly along the Ohio River, like ozone (**Figure 6.7c**). Unlike ozone $PM_{2.5}$ reductions between Scenario A and Scenario B were not as significant in the southeastern U.S. This could possibly be a result of the large emissions of biogenic VOCs dominating secondary organic aerosol formation in this region (Weber et al., 2007), limiting potential benefits from reduced direct emissions of $PM_{2.5}$. In both 2020 cases, Canadian concentrations of $PM_{2.5}$ remained high, especially around the Toronto and Montreal metropolitan areas, exceeding 50 $\mu g/m^3$, but adjustments were not made to Canadian EGUs. Concentrations around Chicago also remained high, but the area of high concentrations decreased in size.

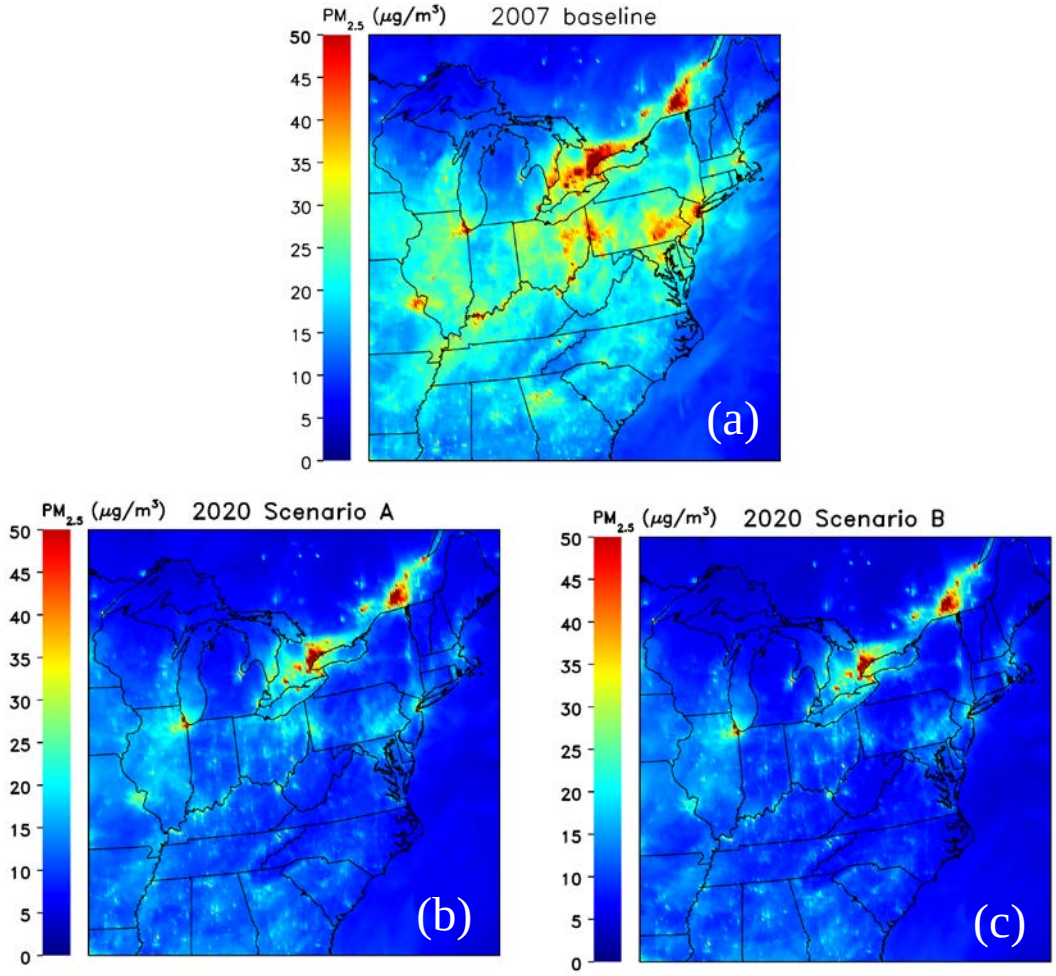

Figure 6.6 98th percentile, 24-hour average $PM_{2.5}$ for (a) the 2007 baseline, (b) Scenario A, and (c) Scenario B.

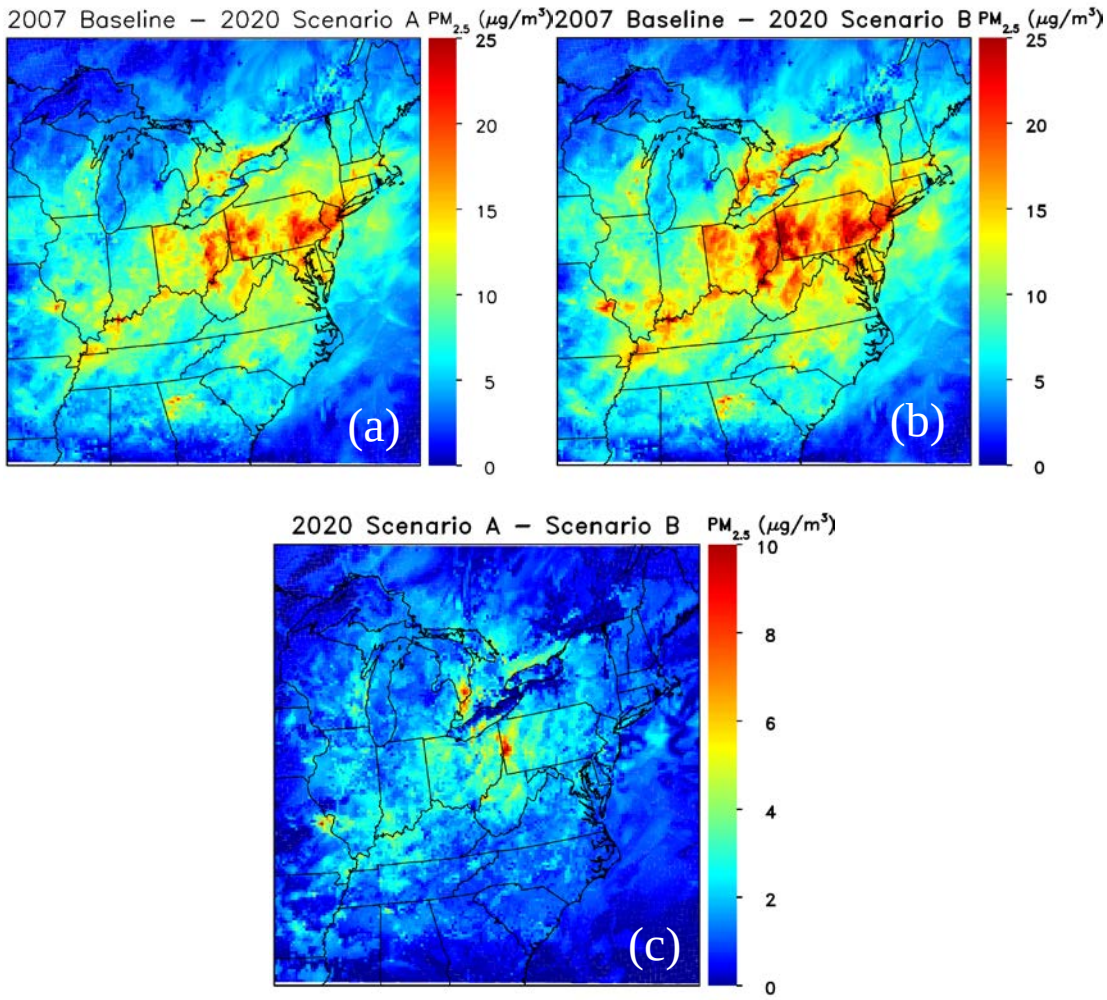

Figure 6.7 Difference of 98th percentile, 24-hour average $PM_{2.5}$ between (a) the 2007 baseline and Scenario A, (b) the 2007 baseline and Scenario B, and (c) Scenario A and Scenario B.

For both ozone and $PM_{2.5}$, emissions from widespread natural gas extraction did not become a liability, as EGU reductions had a significantly larger impact. While the overall results would not be expected to change, some approximations made in this approach could have affected the presented results from grid cell to grid cell. Estimations for natural gas operations were likely underestimated in regions with a high density of wells, and overestimated in regions with a lower density of wells as a result of this approach. Average estimates from Roy et al. (2013) were used, but if

further regulations are enacted, such as those reducing emissions from flowback and pneumatic devices (EPA, 2012), natural gas operations would make up a lower percentage of total emissions in 2020. The adjustments to coal-fired power plant units were applied using the same reduction values on every coal unit. However, some coal units may utilize several controls to minimize NO_x emissions, while others might not. As a result the reductions from switching to natural gas would be expected to be much larger for less-controlled and uncontrolled coal units than those applying full controls.

6.4 Conclusions

When compared to 2007, the overall emissions improvements gained by the year 2020 outweigh any disbenefits to concentrations of ozone or $PM_{2.5}$ from increased unconventional natural gas production emissions. In both future year scenarios benefits to human health would be expected from the lowered concentrations of these criteria pollutants, with the greatest benefits occurring as a result of converting power plants from coal to natural gas. Overall improvements for concentrations of both species were also seen in regions affected by additional emissions from unconventional natural gas wells.

It is also important to recognize that this study focused solely on impacts to air quality and did not take into consideration any other major concerns commonly associated with hydraulic fracturing, such as the effects on climate, water quality, or geological stability, which could also significantly impact human health and wellbeing. Further analyses should be performed to estimate the total combined impacts from all these other components before further encouraging such a drastic

overhaul of the energy sector which could create localized harm to health and welfare. Nonetheless, the benefits of reduced emissions from coal-fired EGUs are significant, and reductions of these emissions should be pursued, especially if shale gas operations can be conducted safely and efficiently.

Chapter 7 Expected Ozone Benefits of Reducing NOx Emissions from Coal-Fired Electricity Generating Units in the Eastern United States

This chapter has been submitted to *The Journal of the Air & Waste Management Association* and is currently in the review process. Content has been modified for clarity.

7.1 Introduction

The 2008 National Ambient Air Quality Standard (NAAQS) for surface ozone is a daily maximum 8-hour average of 75 ppb (EPA, 2008b). Regions failing to meet this standard are designated as non-attainment areas (NAAs) and required to submit a State Implementation Plan (SIP) to outline regulatory measures that would result in attainment (EPA, 2016d). In October 2015, a stricter ozone NAAQS was mandated, lowering the 8 hour standard to 70 ppb (EPA, 2015c).

Surface ozone is formed most abundantly in the presence of volatile organic compounds (VOCs) and NO_x ($NO + NO_2$) during hot, sunny summer days (Crutzen, 1974; Haagensmit et al., 1953). One significant source of NO_x comes from electricity generating units (EGUs) that often run heavily to meet demand for air conditioning on hot summer days in the U.S. EGUs also have smokestacks that emit at elevated heights and allow for long-range transport of pollutants. Various regulations such as the recent Cross-State Air Pollution Rule (EPA, 2015d) have been implemented to limit emissions in one state that could adversely affect another downwind state.

During the summer, the Bermuda high, a high pressure system that can last several consecutive days, often moves westward to a position off the Mid-Atlantic coast, and the anticyclonic flow promotes transport of emissions from sources along the Ohio River and in Pennsylvania into Mid-Atlantic and Northeastern states (Hains et al., 2008; He et al., 2013a; He et al., 2013b; He et al., 2014; Ryan et al., 1998; Smith and Tirpak, 1988; Taubman et al., 2004; Taubman et al., 2006). **Figure 7.1** shows that most of the largest coal-fired EGU NO_x emitters in the Eastern U.S. are located in these regions upwind of the East Coast, based on 2011 reported emissions (EPA, 2015e), and emissions from EGUs can have substantial impacts on downwind air quality (He, 2013a).

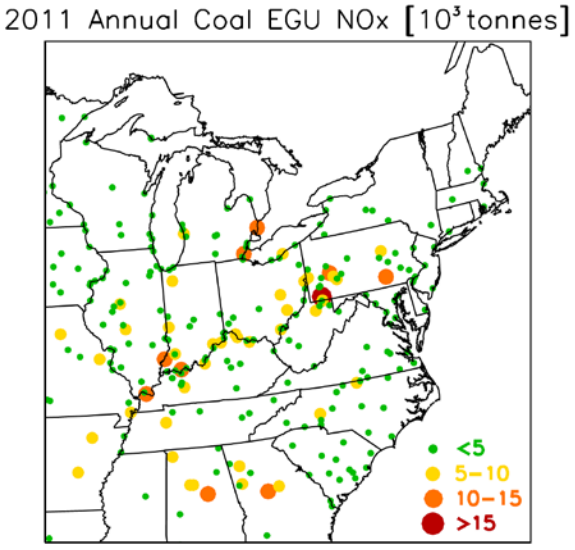

Figure 7.1 Total annual emissions of NO_x (in units of thousands of metric tons NO_2 equivalent) from coal-fired EGUs at the facility level as reported in 2011 to the Clean Air Markets Division (CAMD) (EPA, 2014d).

An analysis of 2005-2007 Ozone Monitoring Instrument (OMI) NO_x satellite observations found ozone production in most of the U.S. was sensitive to

concentrations of NO_x, and more so at higher temperatures (Duncan et al., 2010), making summertime NO_x critical to ozone formation. Similarly, CAMx modeling results for July 2011 also indicated ozone formation in and around the state of Maryland to be almost exclusively NO_x-sensitive (Goldberg et al., 2016). This has been a result of reducing local sources of NO_x, such as cleaner motor vehicles and power plants (Duncan et al., 2010). Further NO_x emission reductions will produce direct ozone decreases, but increased NO_x would have adverse effects.

Although many EGUs have recently switched to natural gas as a fuel source, coal remains an equally important source for electricity in the United States, with both fuel sources used to produce roughly a third of total generated electricity each in 2015; other non-renewable fuels contributed less than 1% (EIA, 2016b). While natural gas power plants emit NO_x, coal-fired units emit, on average, four times as much on a mass/MWh basis (Roy and Choi, 2015). One effective method of reducing NO_x emissions from coal-fired power plants is the use of devices such as selective catalytic and non-catalytic reduction (SCR and SNCR, respectively) following the combustion process that can eliminate up to 90% and 50%, respectively, of produced NO_x (EPA, 2003a; EPA, 2003b).

Under federal regulations, EGU operators are mandated to keep NO_x emissions under an allotted amount, based on a given state's emissions budget (EPA, 2016i), and installation of SCR or SNCR is often needed to meet the requirement. As long as the unit's annual and ozone season emission caps are not exceeded, current rules and regulations allow for these controls to be shut off to limit fiscal burden. Once the capital investment has been made to install such controls, the cost of

chemical reagent and efficiency reductions are the only major maintenance and operational costs (EPA, 2015f), yet emissions monitors indicate these controls are not always being utilized to their fullest potential (EPA, 2015f; EPA, 2015g; He et al., 2013b).

An investigation of average ozone season NOx emission rates from coal-fired EGUs in the Eastern U.S. revealed several units where rates increased from 2004-2014. This trend suggested unit owners and operators found it cost-effective to limit operations of SCR or SNCR systems and instead use lenient regulatory or market mechanisms to legally meet their caps (OTC, 2015). This increase in NO_x emissions from not utilizing post-combustion controls can lead to increased ozone production locally and downwind. Alternatively, operating these controls at optimal rates could decrease ozone concentrations. Using a chemical transport model, we quantify the regional impacts of EGU NOx controls on ozone formation.

7.2 Model Description

The U.S. Environmental Protection Agency (EPA) provided state agencies with air quality model-ready surface emission estimates (EPA's ed_v6_11f modeling case) for 2011 and estimated emissions for 2018, based on the 2011 National Emissions Inventory (NEI) (EPA, 2014e). The 2018 emissions estimates reflect planned "on-the-books" controls and regulations such as more efficient technologies and fuel usage for vehicles and facilities, but they do not include additional measures needed for attainment of the 2008 ozone NAAQS. We used the Sparse Matrix Operator Kernel Emissions (SMOKE) System version 3.1 (SMOKE, 2012) to process

plume rise for elevated point source inventories, such as EGUs, and combine them with the surface emissions. These emissions included the Biogenic Emission Inventory System (BEIS) version 3.14 for biogenic sources (2011 emissions were used for both 2011 and 2018), Motor Vehicle Emission Simulator (MOVES) 2010b for mobile sources, and the Integrated Planning Model (IPM) version 5.13 for the EGU sources.

These emissions processed by SMOKE were then input into to the Community Multi-scale Air Quality (CMAQ) version 5.0.2, which also incorporates meteorological data and chemical reaction kinetics to calculate expected formation and dispersion of various pollutant species (CMAQ, 2015; Foley et al., 2010). The CMAQ simulations have 12 km × 12 km horizontal grid resolution, 34 layer sigma-coordinate vertical levels (from surface to ~20 km), and hourly output for an Eastern United States modeling domain. Meteorological fields for 2011 were generated using the Weather Research and Forecasting (WRF) version 3.4 model (EPA, 2014f) and further processed through the Meteorology-Chemistry Interface Processor (MCIP) to prepare the meteorology fields for use in CMAQ. Boundary conditions were supplied by GEOS-Chem version 8-03-02 (Bey et al., 2001), and version 5 of the Chemical Bond mechanism with updates to toluene and chlorine chemistry (CB05TUCl) (Sarwar et al., 2012) was used with AE6 scheme for aerosols (Appel et al., 2013; Nolte et al., 2015). Plume-in-grid treatment was not used for the EGUs in this study, but similar results for modeled ozone would be expected, with impacts reaching even farther downwind (Karamchandani et al., 2014).

7.3 Methods

To determine and quantify the impact of NO_x emissions from coal-fired EGU sources on surface ozone concentrations, baseline runs for July 2011 and 2018, and four sensitivity scenarios for 2018 were performed by adjusting EGU NO_x emission rates based on historic records. For both 2011 and 2018, while emissions are varied, meteorology for July 2011 was held constant throughout to remove the influence of meteorological conditions on model results. The 2011 Baseline and 2018 Baseline were run using EPA-approved emissions, with the sensitivity scenarios building off of the 2018 Baseline emissions.

The Clean Air Markets Division (CAMD) of the U.S. EPA supports several regulatory programs that require continuous monitoring of large point source emissions of SO_2 and NO_x (U.S. EPA, 2015h). CAMD NO_x emission data were obtained (available for download from https://ampd.epa.gov/ampd/) for the ozone seasons during the years of 2005 through 2012 and analyzed for the states of Illinois, Indiana, Kentucky, Maryland, Michigan, North Carolina, Ohio, Pennsylvania, Tennessee, Virginia, and West Virginia. Rates can vary from unit to unit depending on multiple factors, such as installed controls, sequence of controls, gas temperature (which affects efficiency), and operational load. To capture some of these concerns, we use the average ozone season rates for each individual unit instead of simply applying only a single rate to every unit. The lowest, highest, and 2011 ozone season average NO_x emission factors [lbs./mmBtu] were found for each individual coal-fired unit equipped with SCR or SNCR controls.

The average ozone season historic CAMD NO_x emission rates for each coal-fired unit from each year from 2005 through 2012 were compared to the rates from the 2018 IPM inventory files. For each unit, the ratio between lowest historic NO_x rates and 2018 IPM NO_x rates was calculated and used as a multiplier that was applied to the hourly and annual IPM emissions inventory files and reprocessed through the SMOKE model. These new EGU emissions representing coal-fired units operating at their lowest rates were combined with the other 2018 emissions to create 2018 Scenario A.

Using a similar approach, NO_x rates for coal-fired units were instead increased to represent operation at the highest historic rates in 2018 Scenario B. In 2018 Scenario C, NO_x emissions were increased to match the observed 2011 emission rates from coal-fired units, with emission projections for 2018 in all other sectors remaining unchanged. Finally, 2018 Scenario D has units operating at lowest NO_x rates (Scenario A), and additionally includes SCR NO_x reductions for the 2018 EGUs that are expected to lack post-combustion controls. To assume SCR reductions on uncontrolled units in Scenario D, a multiplier was calculated for each unit by dividing the 2018 ozone season emission rate by the state-average SCR-controlled lowest average ozone season emission rate. The unit-specific reductions applied for each scenario are provided in **Table A2.2**, and a summary of the model scenarios is provided in **Table 7.1**.

Table 7.1 Brief descriptions of the modeling scenarios.

Scenario Name	Brief Description
2011 Baseline	2011 EPA-provided emissions were used with no modifications
2018 Baseline	2018 EPA-provided, projected emissions were used with no modifications
2018 Scenario A	2018 SCR/SNCR EGU NOx emissions are reduced to match lowest rates observed in 2005-2012 historical data.
2018 Scenario B	2018 SCR/SNCR EGU NOx emissions are reduced to match highest rates observed in 2005-2012 historical data.
2018 Scenario C	2018 SCR/SNCR EGU NOx emissions are increased to match rates observed in 2011. Emission projections for 2018 in all other sectors remain unchanged.
2018 Scenario D	2018 SCR/SNCR EGU NOx emissions are reduced to match lowest rates observed in 2005-2012 historical data. And 2018 EGUs lacking post-combustion controls modeled to include SCR NOx reductions.

A comparison of the annual NO_x emissions for all EGUs in the Eastern U.S. from each of these scenarios can be seen in **Table 7.2**. The largest reductions occur in Scenario D, followed by Scenario A. Even with NO_x emissions increased from the 2018 Baseline, Scenarios B and C still have lower emissions than what is shown for 2011. This is a result of unit shutdowns, fuel-switching, and additional controls between 2011 and 2018, and that only select coal-fired EGUs were adjusted for these scenarios (**Table A2.2**), leaving other coal-fired units, as well as units powered by other fuel sources, unchanged. Reported values for the Eastern U.S. include the western borders of Texas, Oklahoma, Kansas, Nebraska, South Dakota, and North Dakota and all states eastward.

Table 7.2 2011 and 2018 Anthropogenic Annual Eastern US EGU NO_x Emissions (in tons)

	2011 Baseline	2018 Baseline	2018 Scenario A	2018 Scenario B	2018 Scenario C	2018 Scenario D
Total annual EGU NO_x (tons)	1,695,870	1,262,505	1,117,819	1,437,663	1,302,481	1,053,253
Percent Change from 2011	---	-26%	-34%	-15%	-23%	-38%
Percent Change from 2018	+34%	---	-11%	+14%	+3%	-17%

Table 7.3 2011 and 2018 Annual Eastern U.S. Anthropogenic NO_x Emissions (in tons) by Sector

	2011 Baseline	2018 Baseline	Percent Change
Area	707,844	720,594	+2%
Nonroad	1,337,283	867,419	-35%
Onroad	4,476,491	2,031,596	-55%
EGU Point Sources	1,695,870	1,262,505	-26%
Other Point Sources	1,457,899	1,452,572	-0%
Oil and Gas Extraction	557,911	684,604	+23%
Locomotive and Marine Vessels	911,521	760,914	-17%
Residential Wood Combustion	27,349	29,839	+9%
Fire	246,027	246,027	0%
Total	11,418,195	8,056,069	-29%

Adapted from EPA, 2014g.

From 2011 to 2018, various sectors are expected to see reductions of anthropogenic NO_x emissions (**Table 7.3**), as well as anthropogenic VOC emissions (**Table A2.1**). The largest NO_x reductions come from the onroad and nonroad sources, with sizeable reduction percentages from EGUs as well as locomotives and marine vessels. Oil and gas sector emissions included in the inventory are projected to significantly increase to future year 2018. Overall for the Eastern U.S. when compared to 2011, anthropogenic emissions of NO_x are forecasted to be down 29% and VOC by 11% (EPA, 2014g).

July 2011 meteorology was chosen for these scenarios because it was an unusually hot summer for the Eastern U.S., causing several ground based ozone monitoring sites to exceed the 75 ppb standard (**Figure A2.1**) and because auxiliary data are available from NASA's DISCOVER-AQ (Crawford et al., 2014). Wind patterns also contributed to a variety of ozone events, with some influenced by local pollution during times of stagnation, whereas other ozone events were a result of transported emissions. For the Mid-Atlantic region, model design values calculated for July were similar to the design values found for the entire ozone season, with most

of the ozone exceedance days occurring in July. Observed 2011 design values for air quality monitors are calculated as the average of the fourth-highest 8-hour daily maximum ozone concentrations from the base year and the two previous years.

An analysis was performed by EPA using a similar, albeit slightly newer 2011 modeling framework (EPA's ef_v6_11g modeling case), verifying reasonable modeled ozone concentrations when using 2011 National Emissions Inventory (NEI) version 1 emissions with the CMAQ model.. Both emissions sets have 12-km resolution and are based on the 2011 NEI version 1, and the same version of CMAQ was used with the same initial and boundary conditions. There are some minor, but notable differences in the newer EPA setup: mobile emissions reflected the final Tier 3, low-sulfur gasoline rule instead of the proposed rule, oil and gas spatial surrogates were updated, agricultural and residential wood combustion temporal profiles were updated, and fugitive dust emissions were updated (EPA, 2014h). Preliminary results showed some low biases for modeled 8-hour maximum ozone in the Eastern U.S. (-10 ppb in many urban environments), but many Mid-Atlantic coastal areas appear to generally be in good agreement (+/-5 ppb) with surface ozone observations (Dolwick et al., 2014). The different boundary conditions used in the Dolwick et al. continental U.S. study and for our eastern U.S. domain may affect modeled ozone concentrations, but some of the inaccuracies of ozone precursor emissions and reaction mechanisms can make it difficult to fully validate the model (Anderson et al., 2014; Canty et al., 2015; Travis et al., 2016).

7.4 Results

7.4.1 2011 Baseline

Calculations of average 8-hour daily maximum surface ozone from the 2011 Baseline simulation show several regions across the Eastern U.S. well above 75 ppb. **Figure 7.2** shows, as minimum criteria, the average of daily maximum 8-hour average ozone for each model grid cell from at least the top six days over 60 ppb in 2011.

When evaluating results from an ozone-season length CMAQ run, the top ten days containing the highest modeled daily maximum 8-hour average ozone concentrations are typically used, based on EPA modeling guidance (Wayland, 2014). However, considering only the month of July can limit the number of total days exceeding the 60 ppb threshold in a given area. For each model grid cell, we first looked for instances of at least six, but no more than 10, days exceeding 75 ppb ozone. If six days exceeding 75 ppb were not available, the search progressed down to 74 ppb, and stepwise down until 60 ppb. For each model grid cell the 8-hour daily maximum ozone concentration for a given scenario was determined as the maximum value found from the 3 × 3 grid surrounding a given grid cell. The spatial location of the cell contributing the maximum ozone concentration, as well as the top days found, for a given grid cell are determined in the 2011 baseline and used in all future-year scenarios (Wayland, 2014).

Regulatory testing uses the ratio of a future-year scenario as a relative reduction factor and applies this ratio to base-year design values from monitoring stations to calculate its predicted future-year ozone concentrations. However,

showing concentrations only in locations with ozone monitoring stations severely limits the scope of understanding the broader impacts of the changes presented in each scenario. We wish to provide a better sense of regional change in each scenario, and thus, do not show reduction factors and future-year design values.

Low ozone concentrations in areas hat do not have six days where the daily maximum 8-hour average ozone concentration is above 60 ppb are represented as white regions seen in **Figure 7.2** and subsequent figures. High ozone concentrations are seen as a result of low boundary layers over large water bodies such as the Great Lakes and Atlantic Ocean (e.g., Goldberg et al., 2014). In July 2011, most urban regions exceed the 75 ppb standard (**Figure 7.2**).

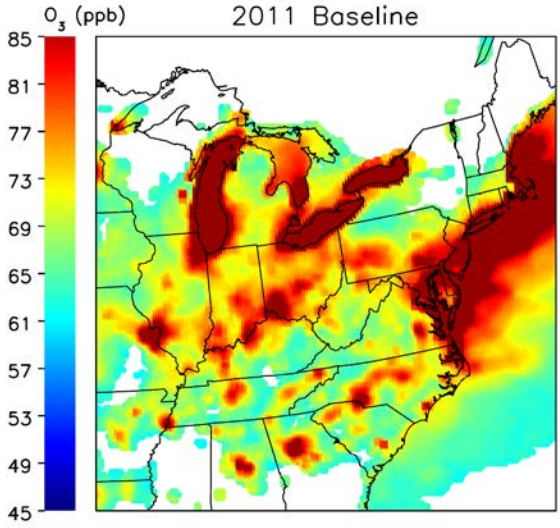

Figure 7.2 Average 8-hour daily maximum surface ozone from the top 6-10 days of the July 2011 baseline run. Regions shown in red-orange to red exceed 75 ppb.

7.4.2 2018 Baseline

Projecting forward to the future year 2018 Baseline, surface ozone concentrations are much lower than in 2011 (**Figure 7.3**) as a result of the decreased

emissions of NO_x and VOCs across various sectors. In the 2018 Baseline run, most of the modeling domain appears to show predicted ozone concentrations below the 75 ppb standard. Almost 10 ppb of modeled ozone reduction can be seen in the future year across the domain, with up to 20 ppb around many city centers, although the St. Louis, MO and Cincinnati, OH areas and a spot in southeastern Pennsylvania near a large EGU are right at 75 ppb. Despite large improvements, many regions along the east coast, notably along the Chesapeake Bay and Long Island, still show surface ozone concentrations exceeding 75 ppb.

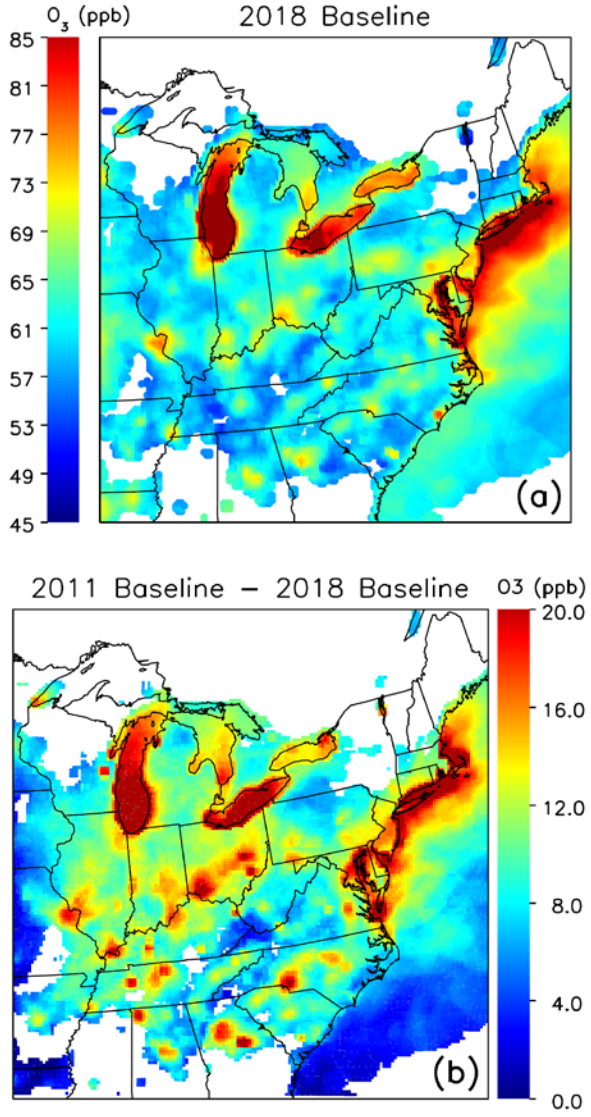

Figure 7.3 (a) Average 8-hour daily maximum surface ozone from the top 6-10 days of the July 2018 baseline run. Regions shown in red-orange to red exceed 75 ppb. (b) Difference plot (note different color bar) between surface ozone concentrations from the 2011 Baseline and 2018 Baseline runs.

7.4.3 2018 Scenario A

Scenario A explores the effects of all coal-fired EGUs in states considered for this study operating with their SCR or SNCR controls at historically lowest rates. By running EGUs with SCR and SNCR at the most effective observed rates, projected surface ozone in 2018 improves by at least 2-3 ppb along the Ohio River and into

Pennsylvania, with some areas improving up to 5 ppb (**Figure 7.4b**). Most regions are below or near 75 ppb, except for the areas along the east coast. Ozone concentrations in the areas around Cincinnati and southeastern Pennsylvania are now well below 75 ppb (**Figure 7.4a**), showing benefits from the 2018 Baseline. Roughly 10% of the total U.S. population resides in the Ohio River Basin (ORSANCO, 2016), so these widespread ozone reductions would benefit a substantial number of people. Areas along the western edge of the modeling domain, such as the St. Louis metropolitan area, remain unaffected in this scenario and do not change significantly in the other scenarios, because ozone concentrations can be significantly influenced by model boundary conditions.

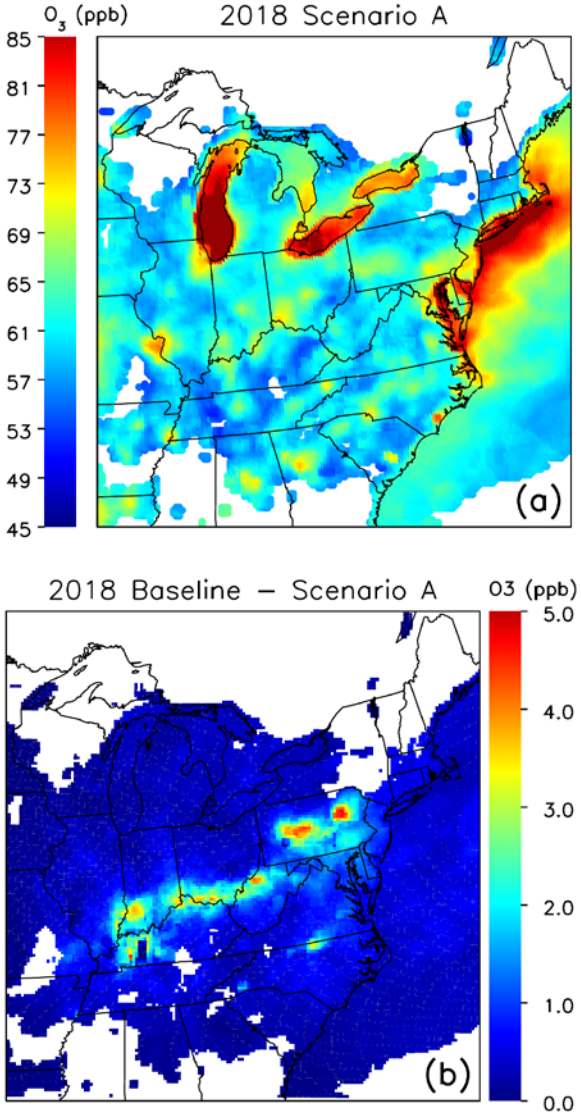

Figure 7.4 (a) Average 8-hour daily maximum surface ozone from the top 6-10 days of the July 2018 Scenario A run. Regions shown in red-orange to red exceed 75 ppb. (b) Difference plot between model surface 8-hour ozone concentrations from the 2018 Baseline and 2018 Scenario A (lowest rates) runs.

7.4.4 2018 Scenario B

Contrary to Scenario A, EGUs were adjusted to reflect historical highest rates in Scenario B. When compared to the ideal rates of Scenario A, 4-7 ppb increases in modeled ozone are seen along the Ohio River and into Pennsylvania (**Figure 7.5b**); some city regions below 75 ppb in Scenario A are now predicted to be above 75 ppb.

A few orange-colored areas reappear in **Figure 7.5a** in response to NO_x not being effectively removed from EGU sources, indicating possible risk of nonattainment. One notable area along the North Carolina and Virginia border showed an 8 ppb increase in ozone in a less populated area, where ozone concentrations approach 75 ppb. **Figure 7.1** shows a few EGUs in the vicinity of this region, likely driving this large local increase in modeled ozone concentrations. Similarly, a small area in southwestern Indiana is close to 75 ppb in Scenario B due to its proximity to several large power plants.

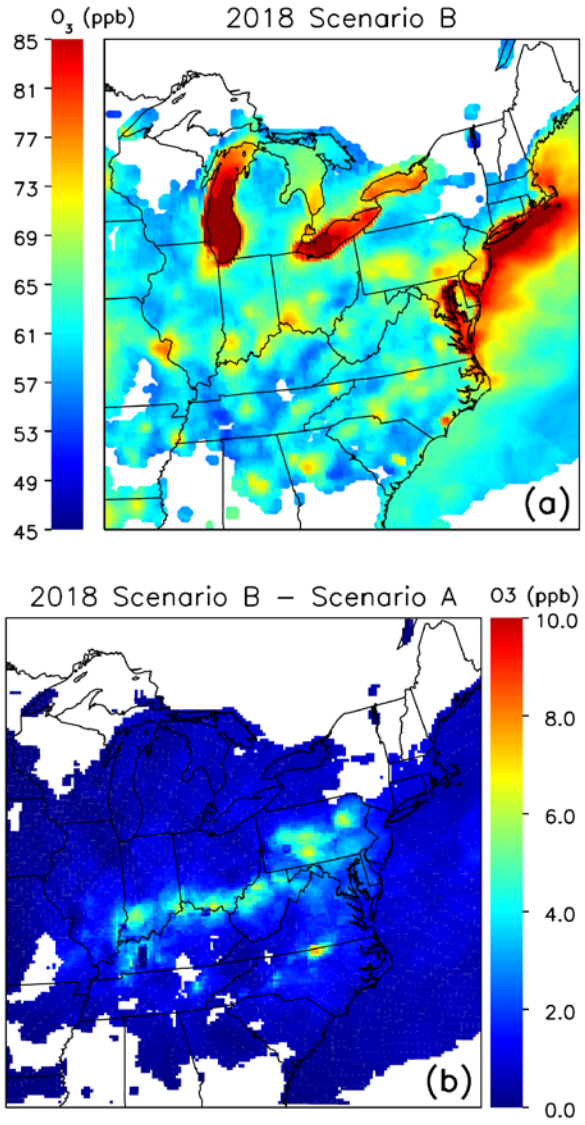

Figure 7.5 (a) Average 8-hour daily maximum surface ozone from the top 6-10 days of the July 2018 Scenario B run. Regions shown in red-orange to red exceed 75 ppb. (b) Difference plot between surface ozone concentrations from the 2018 Scenario B (highest rates) and 2018 Scenario A (lowest rates) runs.

7.4.5 2018 Scenario C

Scenario C assumed 2018 EGU emissions rates matched observed NO_x rates from 2011. While not as widespread as seen in Scenario B, **Figure 7.6a** has many of the same orange-colored areas, and only a few city regions outside the east coast appear to show modeled ozone above 75 ppb. Similarly the difference plot shows

smaller regions with a 4-5 ppb ozone increase between lowest rates and 2011 rates (**Figure 7.6b**). Areas in Indiana and Pennsylvania near the largest power plants appear to be the most affected by NO_x increases in this scenario. EGUs operating at highest rates in Scenario B would be detrimental to meeting the 75 ppb ozone standard, but Scenario C also demonstrates a significant disadvantage if the planned, future improvements to units from 2011 fail to occur.

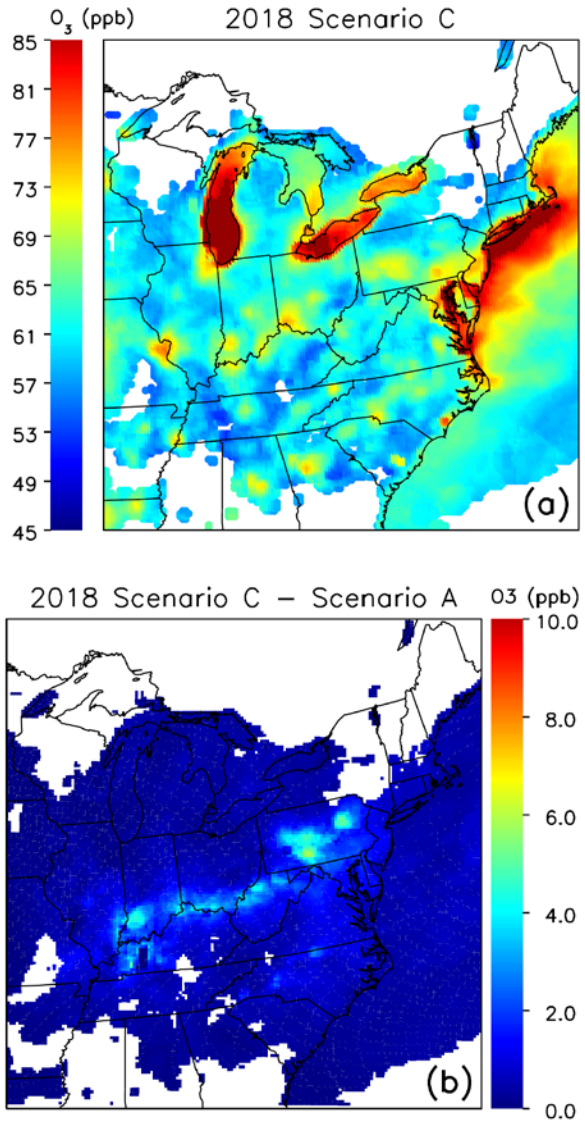

Figure 7.6 (a) Average 8-hour daily maximum surface ozone from the top 6-10 days of the July 2018 Scenario C run. Regions shown in red-orange to red exceed 75 ppb. (b) Difference plot between surface ozone concentrations from the 2011 Scenario C (2011 rates) and 2018 Scenario A (lowest rates) runs.

7.4.6 2018 Scenario D

In Scenario D, we targeted the coal-fired power plants that are not anticipated to shut down or install SCR technology by 2018. In addition to the benefits gained from running installed controls at historic lowest rates, NO_x emissions from these uncontrolled units were reduced to reflect benefits of full SCR adoption in the states

considered for this study. “Uncontrolled” refers only to the lack of post-combustion controls, as these units may utilize less efficient combustion controls such as low-NO_x burners or overfire air (U.S. EPA, 2015e; U.S. EPA, 2015f). **Figure 7.7a** shows all areas along the Ohio River and into Pennsylvania below 75 ppb in this scenario, and only a couple of urban regions outside the east coast cities appear to still show modeled ozone concentrations greater than 75 ppb. Two regions in particular seem to gain the most significant benefits from this additional reduction strategy. One area is along the Ohio River separating the states of Indiana and Kentucky, where ozone is predicted to decrease an additional 2-3 ppb, and another is around the shared Maryland, Pennsylvania, and West Virginia borders, where ozone is predicted to decrease an additional 3-4 ppb (**Figure 7.7b**).

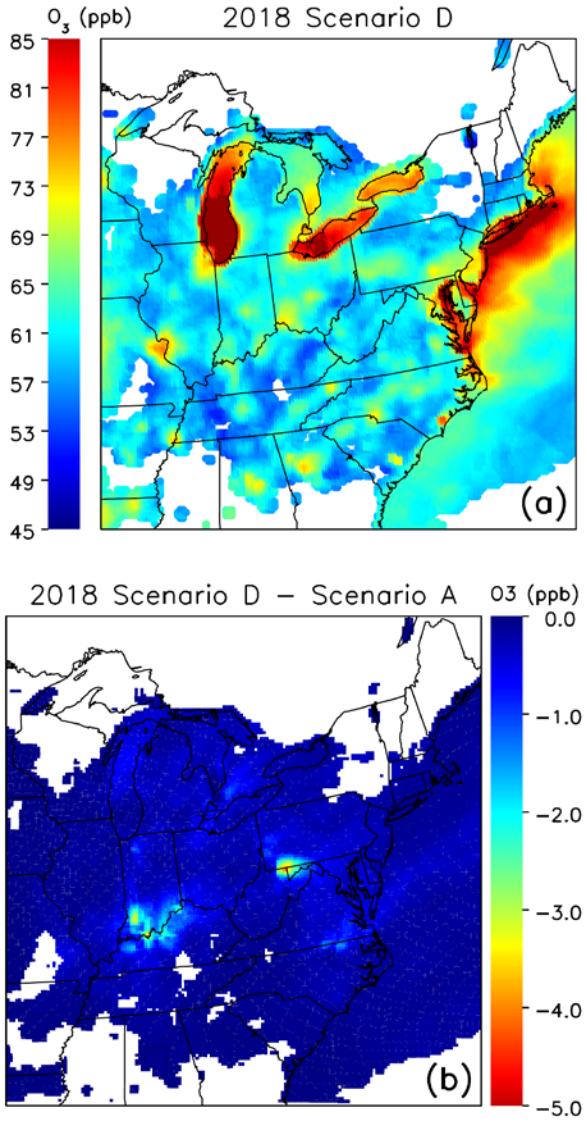

Figure 7.7 (a) Average 8-hour daily maximum surface ozone from the top 6-10 days of the July 2018 Scenario D run. Regions shown in red-orange to red exceed 75 ppb. (b) Difference plot between surface ozone concentrations from the 2018 Scenario D (lowest rates with additional SCR) and 2018 Scenario A runs (lowest rates).

7.4.7 Improvements to Mid-Atlantic East Coast

Results for Scenario A demonstrated large, noticeable modeled ozone improvements to areas along the Ohio River and into Pennsylvania when EGUs are operated at lowest rates when compared to the 2018 Baseline, but there are also important improvements to coastal states in the Mid-Atlantic region, where ozone

concentrations can be high (**Figure 7.8a**). In addition to the larger, more obvious benefits in Pennsylvania, 1.5-2 ppb of predicted reduction is seen in much of the state. A majority of Maryland and Delaware is predicted to see about a 1.5 ppb ozone reduction from Scenario A, as do parts of Virginia.

In the simulation where currently uncontrolled units now include SCRs, Scenario D, much of the Mid-Atlantic coast realizes a 1.5-2 ppb of modeled ozone reduction from the 2018 Baseline, with some downwind regions closer to affected units reaching widespread modeled reductions of 2.5-3 ppb (**Figure 7.8b**). This scenario also now brings a predicted reduction of up to 1.5 ppb to much of New Jersey as well. Although the quantity of total modeled ozone benefit along the coast from these scenarios may not seem very significant given the much larger reductions found in other upwind areas, an overall 2 ppb reduction could be monumental for areas that have been on the edge of meeting attainment.

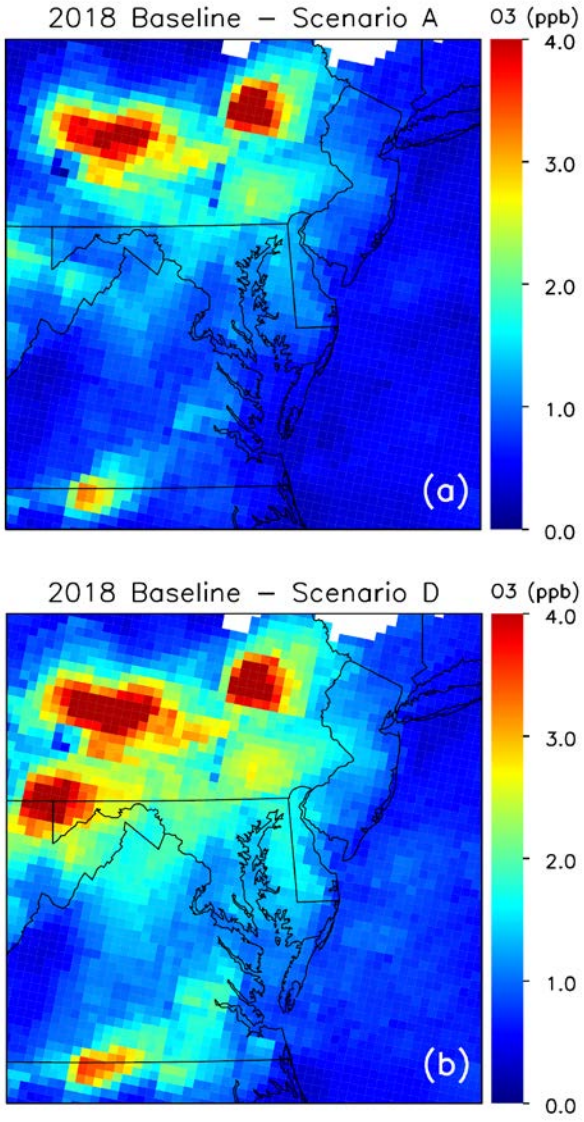

Figure 7.8 Ozone difference plots demonstrating modeled reductions from the 2018 Baseline in the coastal Mid-Atlantic states from (a) Scenario A (lowest rates) and (b) Scenario D (lowest rates with additional SCR).

7.4.8 New Ozone Standard – 70 ppb

Regions that have already struggled with meeting a 75 ppb standard will undoubtedly require further regulations to attain the new 70 ppb standard. Areas that have historically or recently been in attainment of the NAAQS may require further emissions restrictions to attain the new standard. This study may provide valuable

insight into the efficacy of EGU control strategies and a model framework to test ways for attaining the new standard.

The modeling results in **Figure 7.9** show only model grid cells where average 8-hour ozone is predicted to be 70ppb or greater. **Figure 7.9a** suggests several regions could exceed a 70 ppb standard in 2018 with expected controls in place (future case baseline), but many regions could demonstrate attainment if EGU controls are operated at their historic lowest rates (**Figure 7.9b**). Ozone decreased in Scenario A, bringing modeled ozone in all of Indiana and Kentucky below 70 ppb. The area east of Pittsburgh with modeled ozone previously over 70 ppb completely disappears, and the area west of Philadelphia decreases in size significantly. However, if EGUs operate at their highest rates (**Figure 7.9c**), most regions along the Ohio River and throughout Pennsylvania have modeled ozone exceeding 70 ppb, and while not as extreme, 2011 rates could also leave these regions with ozone concentrations above 70 ppb (**Figure 7.9d**). Adding SCRs to uncontrolled units, in addition to running other EGUs at lowest rates, further decreases the size of the areas around Cincinnati and west of Philadelphia with predicted ozone concentrations greater than 70 ppb (**Figure 7.9e**). Scenarios A and D marginally decrease the size of the widespread area exceeding 70 ppb over the East Coast, decreasing modeled ozone below 70 ppb most in the inland/western-most grid cells of Maryland and Virginia.

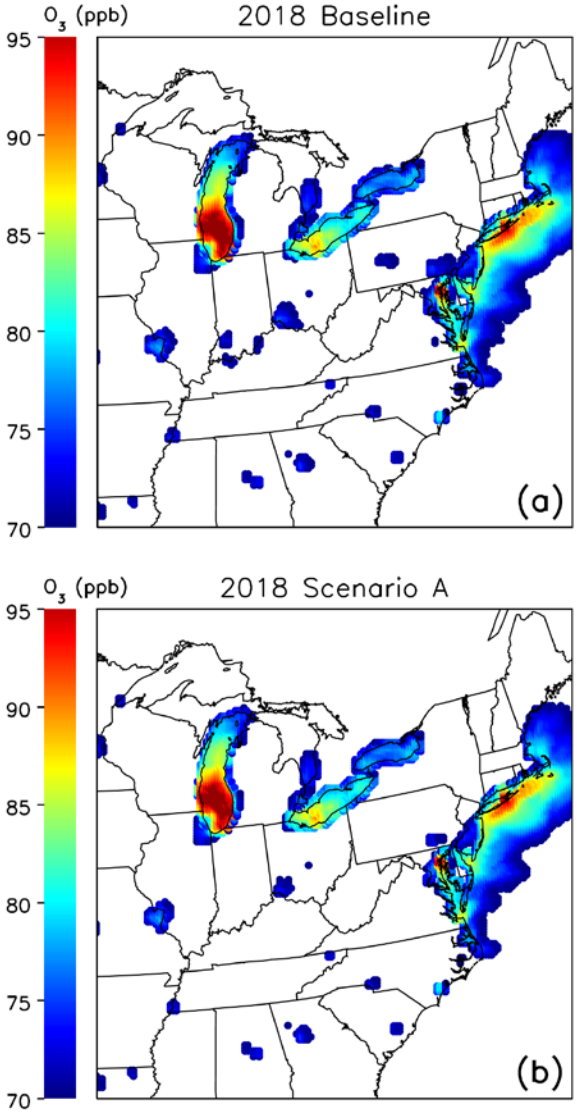
O_3 (ppb)
2018 Baseline
95
90
85
80
75
70
(a)
O_3 (ppb)
2018 Scenario A
95
90
85
80
75
70
(b)

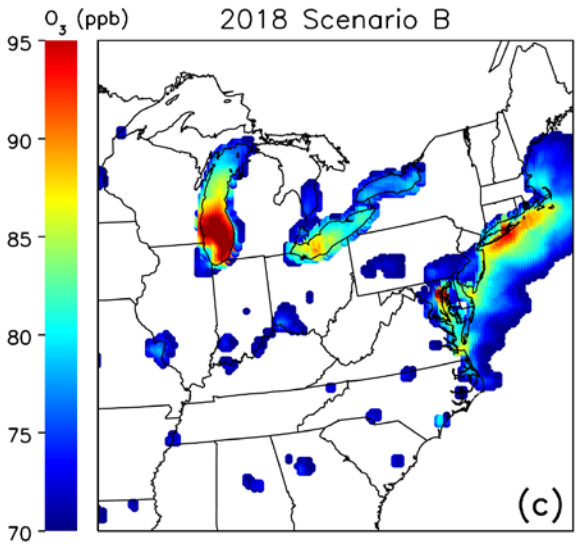
O_3 (ppb)
2018 Scenario B
95
90
85
80
75
70
(c)

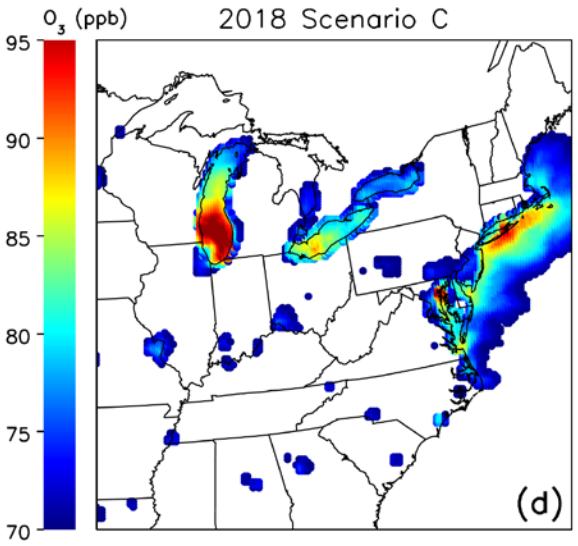
O_3 (ppb)
2018 Scenario C
95
90
85
80
75
70
(d)

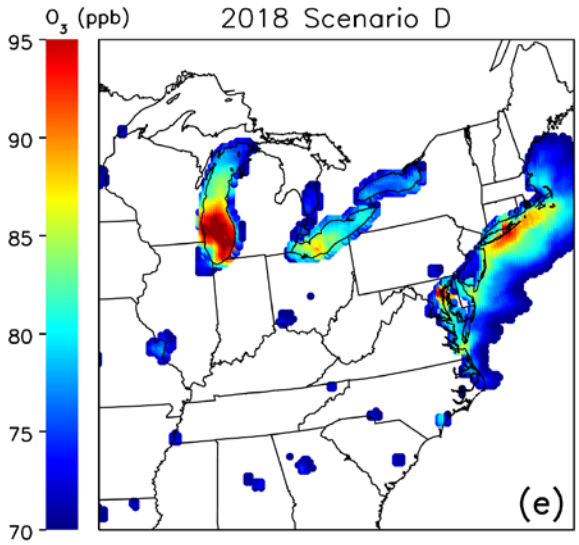

Figure 7.9 July average daily 8-hour maximum surface ozone from the top 6-10 days of (a) 2018 Baseline, (b) Scenario A (lowest rates), (c) Scenario B (highest rates), (d) Scenario C (2011 rates), and (e) Scenario D (lowest rates with additional SCR). Areas where modeled ozone exceeds the 70 ppb NAAQS are plotted, while areas below the new standard are in white.

7.5 Discussion

Table 7.4 Summary of surface ozone changes for affected areas in each modeling scenario.

2018 Scenario	EGU NOx rates	Average Surface Ozone Change	Maximum Change
Scenario A	Historic lowest	2-3 ppb decrease from 2018 baseline	5 ppb decrease in several locations
Scenario B	Historic highest	4-7 ppb increase from Scenario A	8 ppb increase at NC/VA border
Scenario C	Same as 2011	4-5 ppb increase from Scenario A	7 ppb increase in south-central PA
Scenario D	Historic lowest + SCR on uncontrolled units	2-3 ppb decrease from Scenario A	4 ppb decrease at MD/PA/WV borders

Model results show beneficial ozone reductions in coastal Mid-Atlantic States from running existing SCR and SNCR at optimal rates on upwind EGUs. Although these cost-effective reductions prove beneficial to citizens of areas along the coast, the greatest modeled benefits are seen nearby where the largest EGUs are located (**Figure 7.4b**). For many areas along the Ohio River and through Pennsylvania, the difference between EGUs running their controls and not running controls can often

result in an improvement of 5 ppb modeled ozone or greater (**Table 7.4**). Notably, 5 ppb is the difference between the 2008 and 2015 ozone standards, suggesting optimal use of EGU controls could play a critical and beneficial role in making the difference needed for attainment of the 2015 ozone standard in the coming years.

Scenario A provides the most achievable approach, as no additional capital investment is required. This scenario represented coal-fired units operating with their lowest average ozone season NO_x emission rates, which accounts for a certain level of variability (start-ups, shut-downs, variable loads, cycling the SCR/SNCR system off, etc.) throughout the ozone season, and not the absolute lowest rates that would constrain the unit with an emission factor that may not be sustainable over the long term. In the 2015 ozone season, CAMD data revealed roughly a third of units were found to have average ozone season emission rates that achieved rates even lower than what was used from the timeframe in this study. Units which did not achieve the lowest rates did not fail to do so because these low rates were unattainable, but because regulatory and market mechanisms were used to comply. Cap and trade policies were implemented with the general idea to incentivize utilization of SCR/SNCR while also allowing for flexibility. Over time, the market has evolved to a point where it can sometimes be cheaper to purchase allowances than to run existing controls (OTC, 2015). In order to achieve meaningful NO_x reductions that would allow areas to achieve attainment of the ozone NAAQS, the market system would need to be adjusted as current regulatory limits and costs of allowances appear too lenient to require widespread, optimal use of SCR/SNCR systems.

Operating EGUs at optimal rates will provide important benefits, but overall much of the East Coast will require additional pollutant reductions from other emission sources to attain the new 70 ppb standard. Although NO_x emissions from onroad and nonroad sources will decrease from 2011 to 2018, they are expected to still comprise over a third of total NO_x emissions (**Table 7.3**) and in addition to EGUs, and could be another two possible source groups targeted for significant NO_x reductions. Other point sources not belonging to the EGU or oil and gas sectors make up almost 20% of remaining NO_x emissions expected in 2018. Moving forward, NO_x reductions from sources in this category, such as cement kilns, Industrial/Commercial/Institutional (ICI) Boilers, and other industrial and manufacturing facilities may be required to drive down total NO_x emissions (**Table 7.3**).

Evaluations of the 2011 U.S. emissions inventories suggest estimates of NO_x emissions from vehicular sources are overestimated by roughly a factor of two (Anderson et al., 2014, Travis et al., 2016), and that the recycling of NO_2 is underestimated in CB05 (Canty et al., 2015); although revision 2 of version 6 of the Chemical Bond mechanism (CB6r2) appears to simulate NO_x chemistry more accurately (Goldberg et al., 2016). As a result, emissions of NO_x from EGUs would be expected to have an even broader range of influence and greater impact on ozone compared to onroad sources. Thus, the results presented here could be viewed as conservative and may represent a lower limit for significant ozone reductions achieved from running SCR and SNCR controls on EGUs at optimal rates.

7.6 Conclusions

Numerical simulations indicate that the substantial investment in SCR and SNCR units on power plants in the Eastern U.S. has provided an appreciable beneficial impact on air quality. Current regulations allow these units to be turned off for considerable periods as long as annual and ozone-season emissions caps are met. However, our model results indicate that the difference between the recorded least-effective NO_x removal rates and the rates from complete adoption and optimal utilization of NO_x removal systems on coal-fired power plants produces a calculated change in ozone that approaches 10 ppb. Even without new capital investment, predicted concentrations of ozone in 2018 could be improved by up to 5 ppb solely by running existing, operable technology at optimal rates.

Chapter 8 Conclusions and Recommendations for Future Work

8.1 Overall Conclusions

Upwind shale gas activity has significantly affected the Baltimore/Washington area. At the Essex, MD monitor, source apportionment results showed the contribution of natural gas to total VOCs increased from 2009, rising from 25% to ~35%, and the ratio of ethane/TNMOC likewise doubled from 7% to 15% during this time. Ethane concentrations were significantly greater in the years following 2009 (when rapid shale production began) at both the Essex and McMillan Reservoir monitors, as well as significantly greater when arriving winds had passed through counties with a high density of unconventional wells.

A significant increase in ethane concentrations indicates the effects of shale gas operations are detectable hundreds of kilometers downwind, and other production pollutants are also likely being transported. These associated emissions could complicate the attainment of ozone and PM air quality standards for downwind metropolitan areas in the Mid-Atlantic region. Additionally, the observed 2 ppbC increase in ethane would correspond to an expected regional increase in methane of ~10 ppb from Marcellus Shale operations (assuming shale gas content is 10% ethane).

Although the emissions from natural gas operations negatively affect air quality, the emissions from coal-fired power plants were found to have an even larger impact on regional ozone concentrations. Converting all coal units in the Eastern U.S.

to instead burn natural gas led to a significant decrease in modeled ozone concentrations. While the magnitude of reductions was not as large, modeled ozone concentrations were also appreciably decreased when running post-combustion controls on coal units at optimal rates. In both instances, a majority of the Eastern U.S. would be expected to demonstrate concentrations of ozone below the 70 ppb standard.

Marcellus Shale gas activity appears to have regional impacts and could be introducing various reactive species to major cities in the Mid-Atlantic, further burdening the difficulty of demonstrating attainment of air quality standards. However, with regulations and more efficient operations, emissions can not only be limited directly at the well pad, but the produced natural gas can additionally be used to reduce emissions by providing a cleaner fuel source for electricity generation. Coal-fired plants having already installed post-combustion controls can easily improve regional air quality by operating at optimal rates. Uncontrolled units adding SCR controls would lower ozone concentrations further, improving conditions downwind in densely-populated coastal cities; these reductions would be expected to be even larger and more impactful if utilizing natural gas instead.

8.2 Source Apportionment

PMF results suggested an increasing contribution of natural gas sources to total VOCs, while gasoline and vehicle exhaust contributions have declined. For the biogenic and industrial sectors, contributions to total VOC varied from year to year. After reweighting with respect to each VOC's predisposition toward ozone formation, motor vehicle-related emissions remained the primary anthropogenic source of

VOCs, whereas the increasing contributions from natural gas sources showed a limited direct impact with respect to reactivity. Biogenic sources contribute substantially (30-40%) to total VOC when reactivity is considered.

Assuming the Essex monitor remains active and continues making hourly measurements, new observations should be available for each forthcoming year. As these measurements become available, they can be similarly processed to see how the composition of total NMOC changes (or remains the same). Additional years could also show if contributions from the industrial factor to total NMOC will continue to decrease, or instead return to an average 20-25% contribution.

The motor vehicle fleet will continue to turnover, replacing cars with cleaner, more efficient models. In 2017, the Tier 3 Motor Vehicle and Fuel Standards will begin, and vehicular VOC emissions are expected to decrease by 3% by 2018 and by 16% by 2030 (EPA, 2014i). While vehicle and gasoline emissions would be expected to generally decrease over the years, economic factors could also be affecting the results from year to year. Trends in the price of gasoline and vehicle miles traveled (VMT) could also be investigated to further explore potential contributing factors.

In the Choi and Ehrman (2004) study, measurements from four years (1996-1999) were used together for source apportionment analysis. A similar approach could be used by grouping multiple years together, which could allow for a broader understanding of how source contributions to total NMOC have evolved over the past two decades without needing to use PMF over 20 different times.

8.3 Analysis of Ethane Concentrations

After a decade of decline, ethane measurements from PAMS sites in Essex, MD and Washington, D.C. exhibited greater concentrations after 2009, growing from ~7% of total measured NMOC to ~15% from 2013 onward. These observations correlate with the rapid shale gas production in upwind, neighboring states, as back-trajectories traveling through counties with a high density of unconventional wells were associated with significantly greater ethane observations. Ethane concentrations failed to display an increasing trend at a PAMS site outside of Atlanta, GA, a region without new widespread natural gas operations.

Similar to PMF, newer measurements could be used to see if ethane concentrations remain at elevated levels or even continue to increase. Shale gas production rates currently appear to have currently stagnated, and even decreased in some shale formations, but it remains to be seen if this will be a continuing trend, or just a periodic event as has occurred in the past. If production continues to decline, a decrease in observed ethane concentrations should be noticeable over the coming years. The addition of methane monitoring at the Essex and McMillan site would also be beneficial for tracking natural gas emissions.

New regulations might also play a role in decreasing future observations of ethane. On May 12, 2016 the EPA finalized additional rules for the oil and gas sector, to complement the 2012 standards (EPA, 2016j). Well operators will now be required to monitor for fugitive emissions, whose emissions are widely varied in the reported literature. Monitoring will be performed semiannually using optical gas (infrared) imaging, and repairs would need to be made with 30 days of discovery. Initial

monitoring surveys must take place within one year of the date of official publication in the *Federal Register*. Additionally, pneumatic pumps will route VOC emissions to existing control device/process to achieve a 95% reduction. This rule goes into effect 180 days after publication in the *Federal Register*.

Analysis of local HYSPLIT trajectory clusters showed the natural gas pipeline transmission network was not a significant contributor to the largest ethane concentrations. However, the large amounts of shale gas production are believed to have increased the ethane content in the natural gas pipelines. At the current time, I have been unable to obtain composition records from Baltimore Gas & Electric, but a colleague found natural gas from his kitchen stove to be ~8% ethane, which is much higher than expected for dry gas (Ren, personal communication). While increased ethane content in the local natural gas delivery system does not appear to be the main cause of increased ethane observations at the Essex and McMillan monitors, it could play a partial role and should be quantified.

Although the file sizes are substantially larger than 12 km NAM meteorology (8 GB vs. 0.4 GB per day), 4 km NAM files with hourly resolution are available from NOAA upon request (Ren, personal communication). Using finer resolution meteorology input would increase the accuracy of the HYSPLIT results. Using these 4 km files should prove most useful for modeling forward dispersion episodes more accurately. High ethane concentrations did not always perfectly coincide with the arrival of a plume, but this could have been a spatial and temporal limitation of the meteorological input. Even at 4 km, land/water interface issues might inhibit accurate modeling of wind vectors around Essex (Loughner et al., 2011).

8.4 Increased Shale Gas Production and Natural Gas Usage

Overall emissions reductions from 2007 to 2020 lead to improved air quality with lower concentrations of ozone and fine particulate matter. In Scenario B, hydraulic fracturing operations were expanded, and the acquired natural gas was used to convert coal-fired power plants, reducing their emissions of NO_x by 80%, SO_2 by 99%, VOC by 33%, and $PM_{2.5}$ by 75%. Burning natural gas in favor of coal causes concentrations of both ozone and $PM_{2.5}$ to further improve from Scenario A, despite widespread shale gas operations.

As a continued investigation of these results, the Environmental Benefits Mapping and Analysis Program (BenMAP) model can be used to evaluate the changes in concentrations of air pollutants to determine health and economic benefits. When comparing concentrations of fine particles and surface ozone between two scenarios, BenMAP computes the number of avoided health-related issues such as asthma attacks, lost days of school or work, non-fatal heart attacks, and premature death (**Figure 8.1**). Based on population and incorporation of "cost of illness" and "willingness to pay" metrics, an economic value can be assigned to associated benefits (EPA, 2016k). This process is summarized in **Figure 8.2**. More information about BenMAP is available from: https://www.epa.gov/benmap.

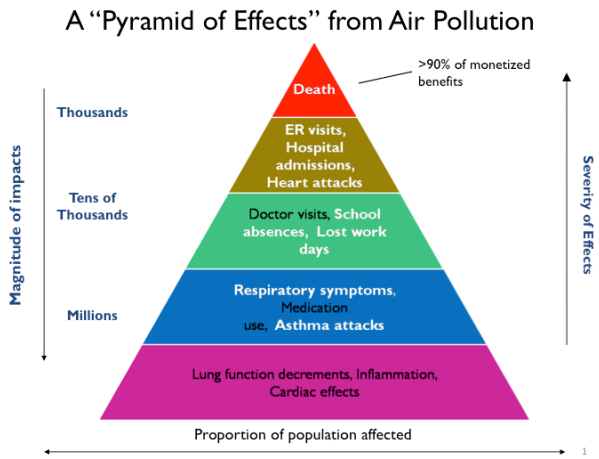

Figure 8.1 Air pollution health effects considered by BenMAP (EPA, 2016k)

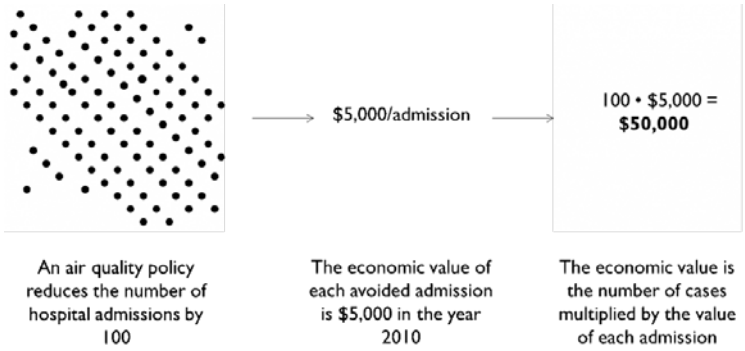

Figure 8.2 An example of applying dollar value to reduced hospital admissions (EPA, 2016k).

This study was also performed using the 2007 modeling platform, which did not contain any oil and natural gas emissions except the ones that were estimated independently as part of this study. Air quality modeling has since shifted to the 2011 modeling platform, and 2011 and future year 2018 oil and gas emissions inventories are available. This process could be repeated using these more recent inventories for 2018, which might provide better estimates for emissions when expanding these operations in Scenario B. This study worked from the assumption that emissions of

NO_x and VOC from the oil and gas sector would account for 12% of the total anthropogenic emissions in 2020. For Pennsylvania, the new 2018 inventories show agreement with this value for VOC, but the oil and gas sector is expected to account for ~20% of the state's total NO_x emissions (**Table 8.1**).

Table 8.1 2018 Annual Emissions for Pennsylvania [tons/year]

	NOx	VOC
Oil and Gas	83,900	35,430
Total Anthropogenic	424,900	315,809
O&G Percent of Total	20.2%	11.2%

Adapted from MARAMA (2016d)

Climate models should also be utilized to better evaluate these scenarios. In Scenario B, widespread methane emissions in the Appalachian Basin would have a negative climate impact, but converting coal-fired plants and consequentially decreasing ozone would be beneficial. Lower emissions of CO_2 from converted units would also be helpful, but it could be argued the almost complete removal of SO_2 would remove an aerosol cooling effect that has mitigated the warming effects of greenhouse gases.

8.5 Expected Ozone Benefits from EGU NOx Reductions

In 2018, running existing controls on coal-fired EGUs at best historic rates is predicted to decrease surface ozone by ~5 ppb or greater in areas along the Ohio River and through Pennsylvania when compared to not running controls. If further capital investment is made to add SCR to uncontrolled units, ozone decreases an additional 2-4 ppb. As the ozone standard has been tightened from 75 ppb to 70 ppb,

optimal use of post-combustion would be a key approach for demonstrating attainment of this standard.

SCR and SNCR post-combustion controls are beneficial, but still not as clean as using natural gas instead. If shale gas operations continue to produce large quantities of natural gas, power plants will continue to shift from coal to natural gas as a fuel source. In Scenario D, units having not installed any post-combustion controls were modeled to include reductions as if SCR was added. Given current trends, it may be equally likely for these units to switch to natural gas instead of investing large capital expenses toward SCR or SNCR. Updating these units to instead have natural gas-like emissions, would be expected to provide even larger decreases of ozone concentrations.

Appendix 1

Regional air quality impacts of hydraulic fracturing and shale natural gas activity: Evidence from ambient VOC observations

Supporting Information

Wind roses from the Beltsville, MD wind profiler are provided for the months of June (**Figure A1.1**), July (**Figure A1.2**), and August (**Figure A1.3**) from heights of 0.266, 0.385, 0.503, 0.681, 0.859, and 1.036 km AGL. Wind data is taken from years 2012 – 2014 during the daytime hours of 10am – 7pm. The frequency of winds from the directions of unconventional natural gas operations is substantial during these months.

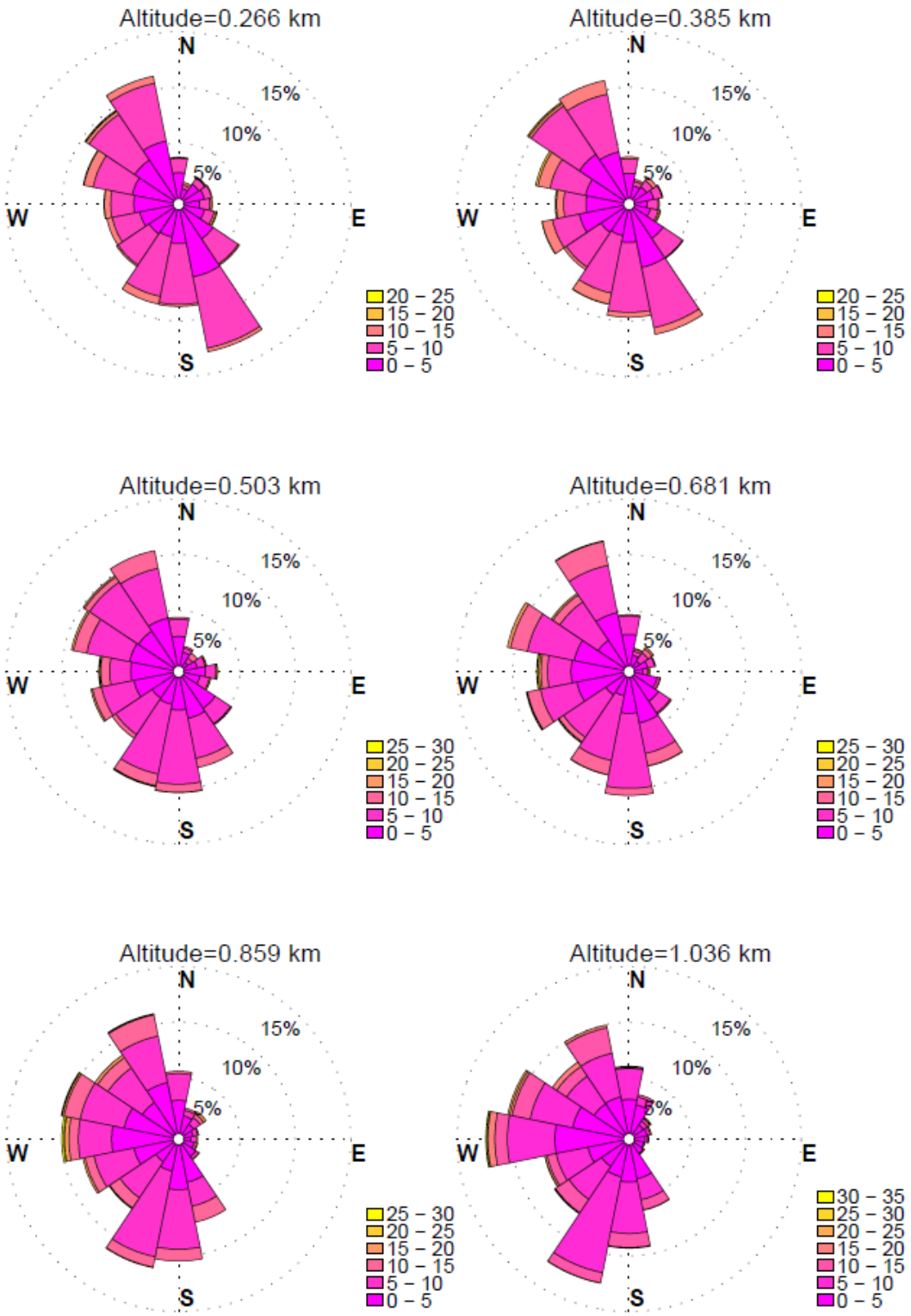

Figure A1.1. Wind roses for the month of June from the wind profiler in Beltsville, MD during daytime hours at various heights. Wind speeds have units of m/s. [Wind roses provided by Kostya Vinnikov].

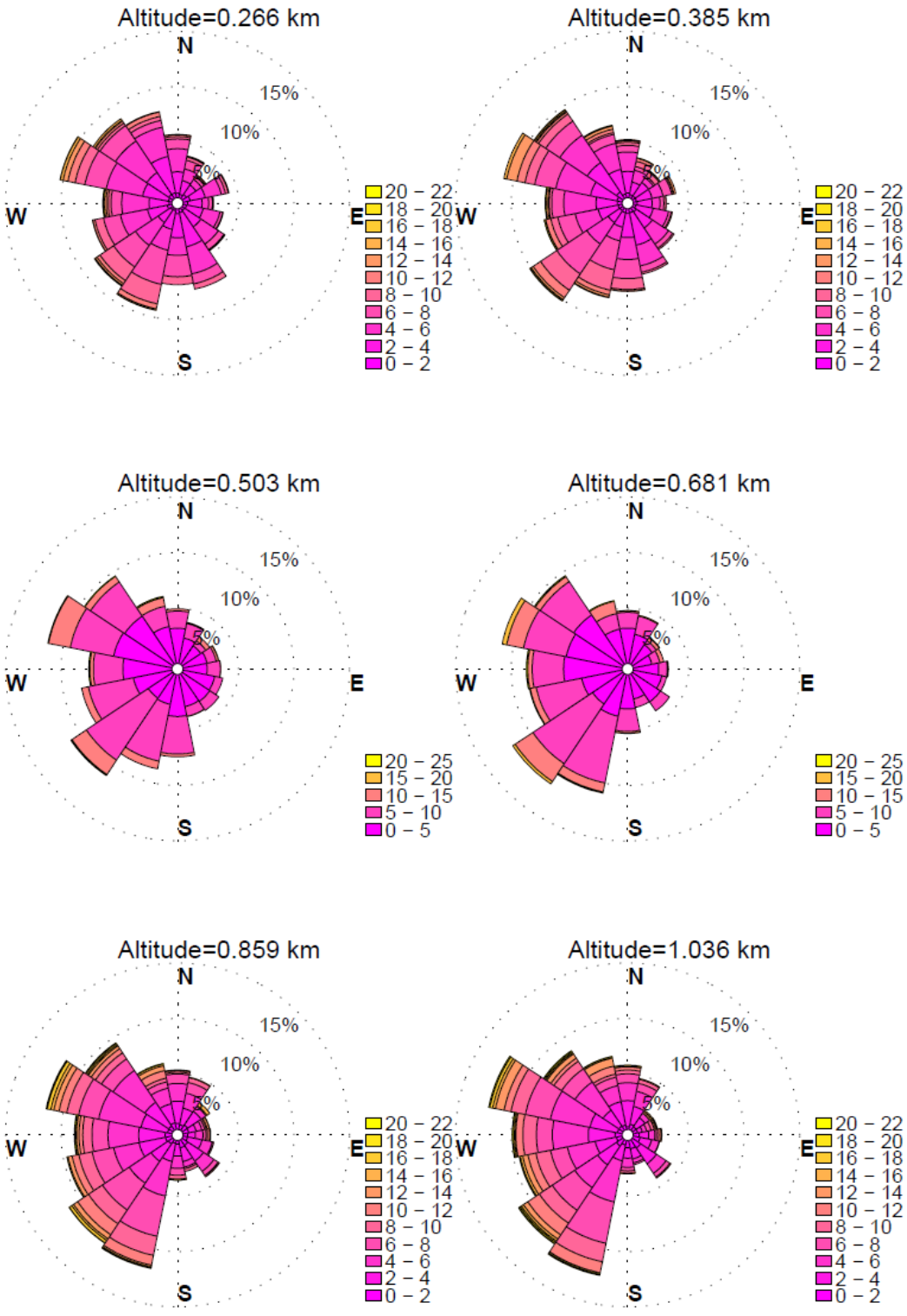

Figure A1.2. Wind roses for the month of July from the wind profiler in Beltsville, MD during the daytime hours at various heights. Wind speeds have units of m/s. [Wind roses provided by Kostya Vinnikov].

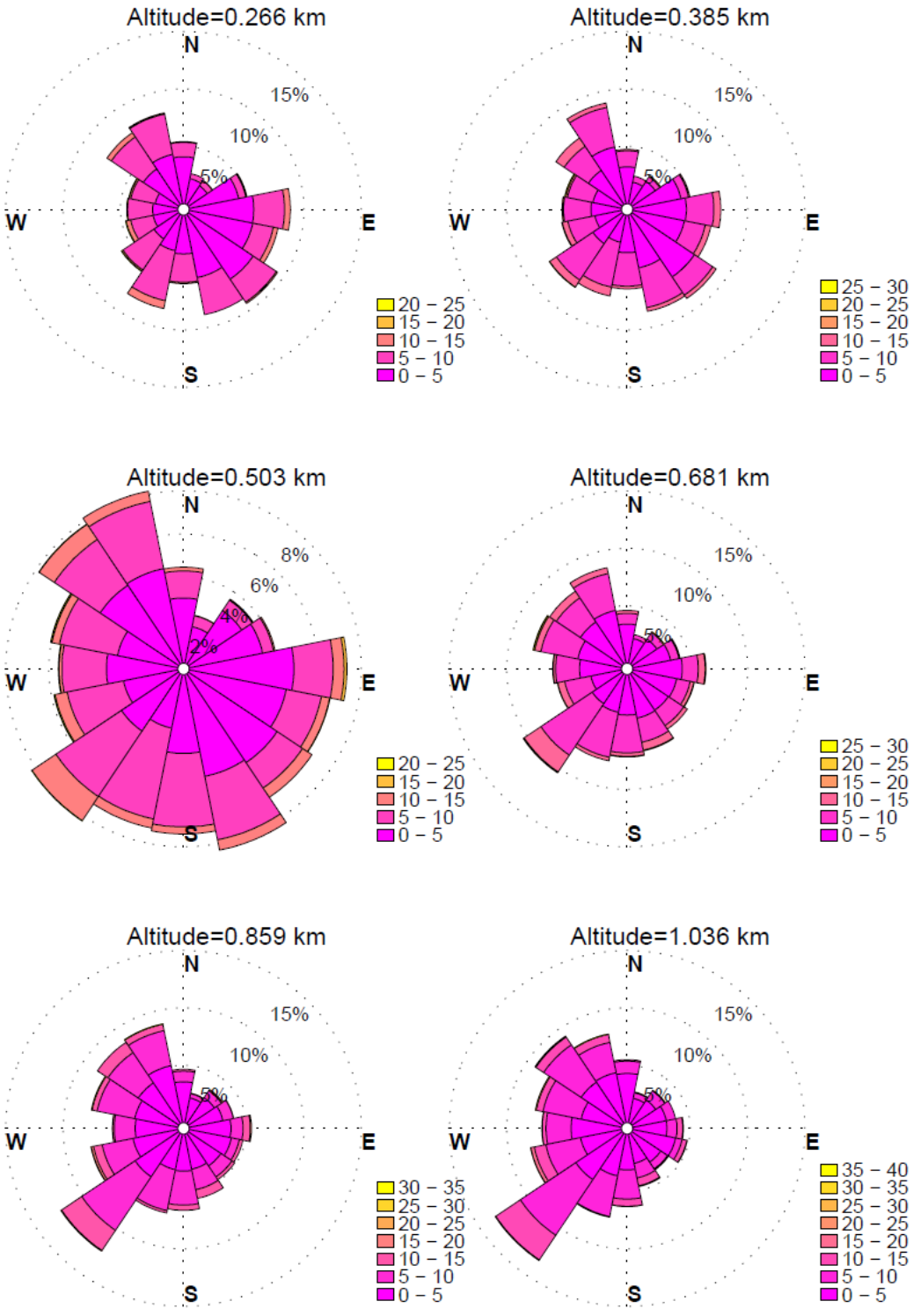

Figure A1.3. Wind roses for the month of August from the wind profiler in Beltsville, MD during the daytime hours at various heights. Wind speeds have units of m/s. [Wind roses provided by Kostya Vinnikov].

It should be noted that for some years, hourly measurements are currently unavailable for certain months. At Essex, no hourly measurements were available for the month of August in 1999, 2004, or 2005. At McMillan Reservoir, June 1996 was unavailable. At Rockdale County, Georgia, no hourly measurements are currently available from August 1999, July and August 2010, August 2012, or June and July 2013.

In **Figure A1.4**, TNMOC concentrations at McMillan declined from 1996, but increased after 2009. However, when looking at **Figure A1.5**, it can be seen that even though TNMOC increased, ethane increased even more as the ratio of ethane to TNMOC has increased over the years. Alternatively, TNMOC at Rockdale has remained relatively constant over the same time frame (**Figure A1.6**), and no increase is seen in the ratio of ethane to TNMOC (**Figure A1.7**).

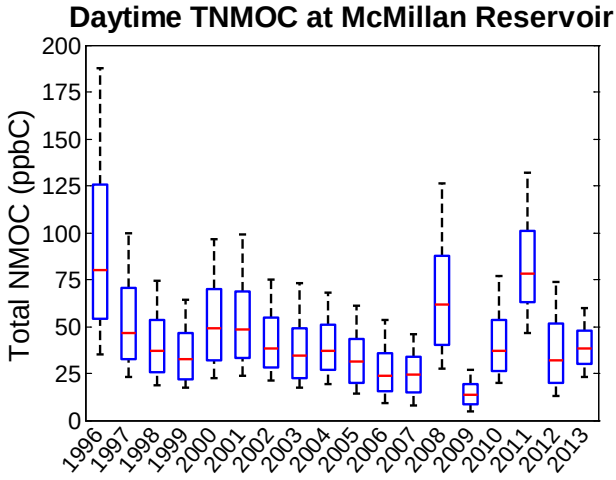

Figure A1.4. Daytime Total NMOC concentrations from 1996 to 2013 at McMillan Reservoir (DC) are presented by box and whisker plots with the same statistical parameters as **Figure 3.3**.

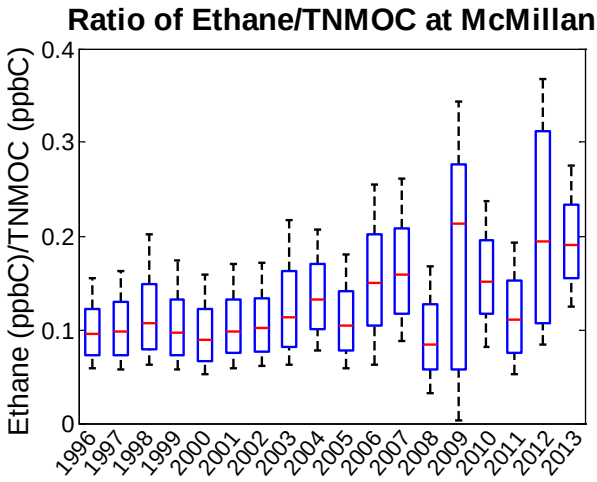

Figure A1.5. The ratio of ethane to TNMOC concentrations from 1996 to 2013 at McMillan Reservoir (DC) are presented by box and whisker plots with the same statistical parameters as **Figure 3.3**.

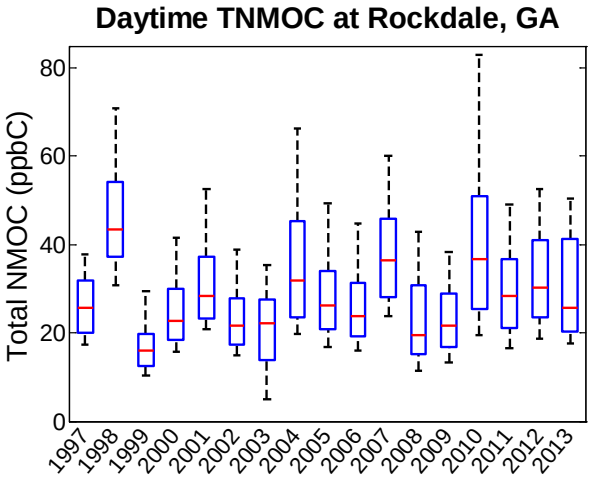

Figure A1.6. Daytime Total NMOC concentrations from 1997 to 2013 at Rockdale County, GA are presented by box and whisker plots with the same statistical parameters as **Figure 3.3**.

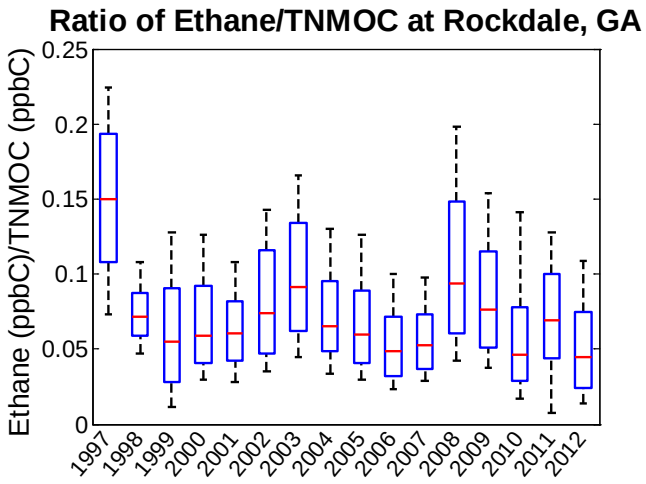

Figure A1.7. The ratio of ethane to TNMOC concentrations from 1997 to 2012 at Rockdale County, GA are presented by box and whisker plots with the same statistical parameters as **Figure 3.3**.

Similar to **Figure 3.7**, June, July, and August Essex, MD ethane measurements were compared to production rates, but values dating back to 2000 are also considered in **Figure A1.8**. This process was repeated comparing instead the ethane/TNMOC ratio to production rates from 2010-2013 (**Figure A1.9**) and 2000-2013 (**Figure A1.10**).

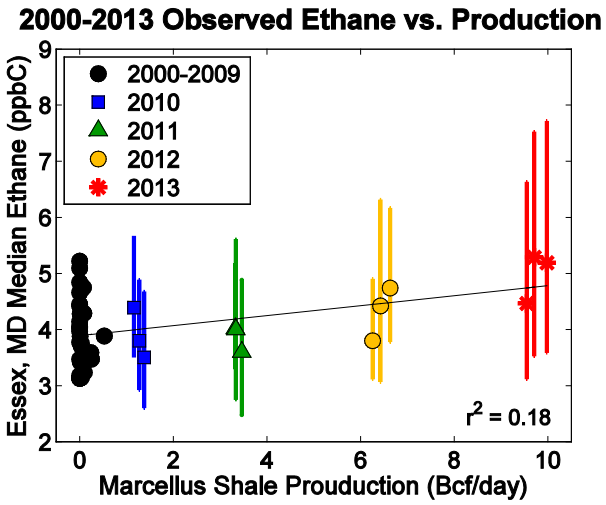

Figure A1.8. June, July, and August values from 2000 through 2013 of observed ethane concentrations at Essex, MD vs. Marcellus Shale production. The uncertainty bars provide the 25th and 75th percentiles for 2010-2013.

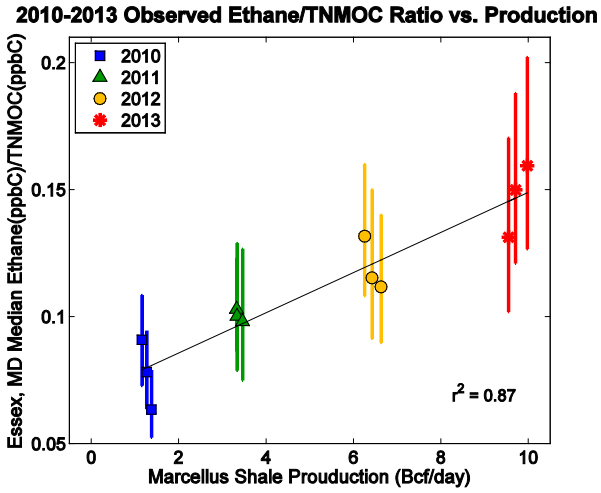

Figure A1.9. June, July, and August values from 2010 through 2013 of observed ethane to TNMOC ratio concentrations at Essex, MD vs. Marcellus Shale production. The uncertainty bars provide the 25th and 75th percentiles.

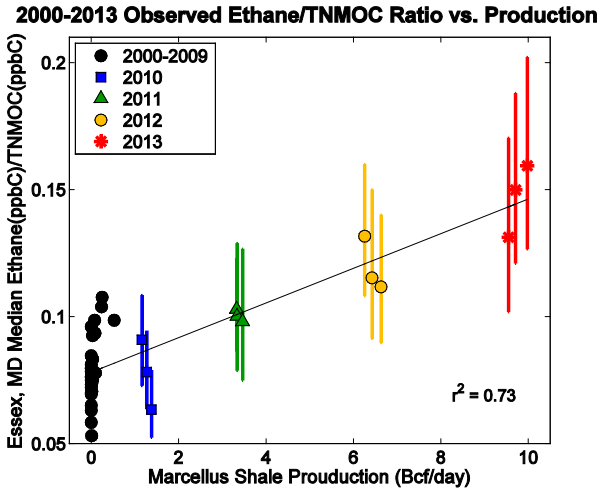

Figure A1.10. June, July, and August values from 2000 through 2013 of observed ethane to TNMOC ratio concentrations at Essex, MD vs. Marcellus Shale production. The uncertainty bars provide the 25th and 75th percentiles for 2010-2013.

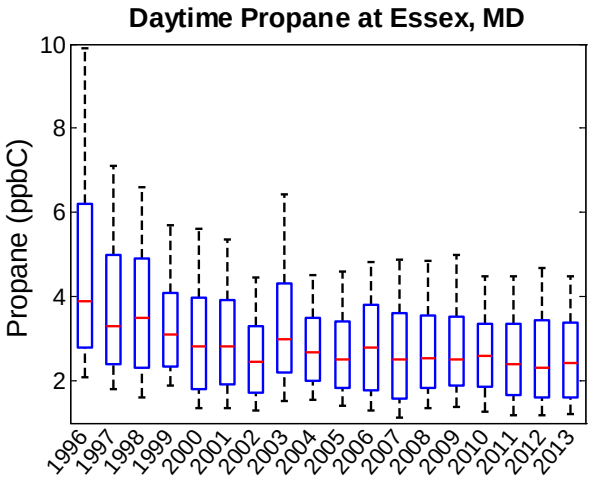

Figure A1.11. Daytime propane concentrations from 1996 to 2013 at Essex, MD are presented by box and whisker plots with the same statistical parameters as **Figure 3.3**.

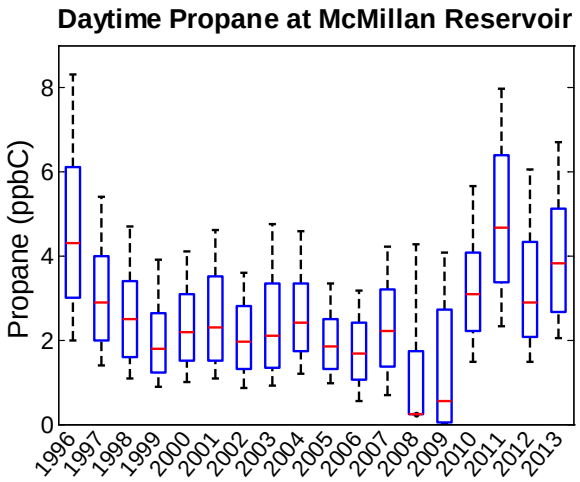

Figure A1.12. Daytime propane concentrations from 1996 to 2013 at McMillan Reservoir (DC) are presented by box and whisker plots with the same statistical parameters as **Figure 3.3**.

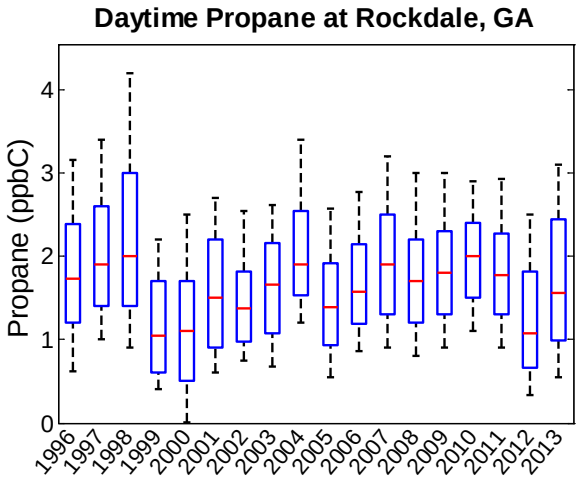

Figure A1.13. Daytime propane concentrations from 1996 to 2013 at Rockdale County, GA are presented by box and whisker plots with the same statistical parameters as **Figure 3.3**.

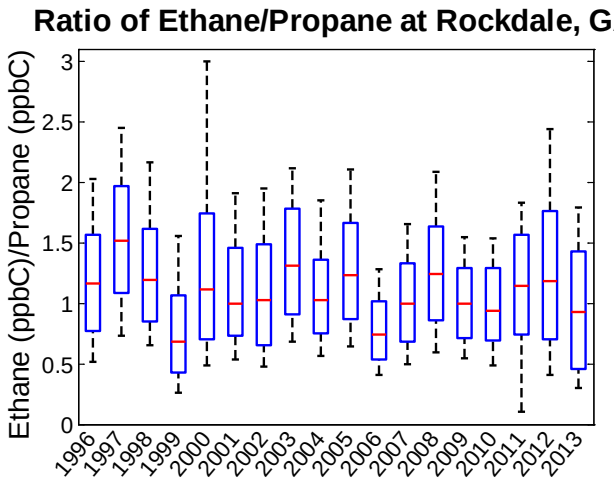

Figure A1.14. The ratio of ethane to propane concentrations from 1996 to 2013 at Rockdale County, GA are presented by box and whisker plots with the same statistical parameters as **Figure 3.3**.

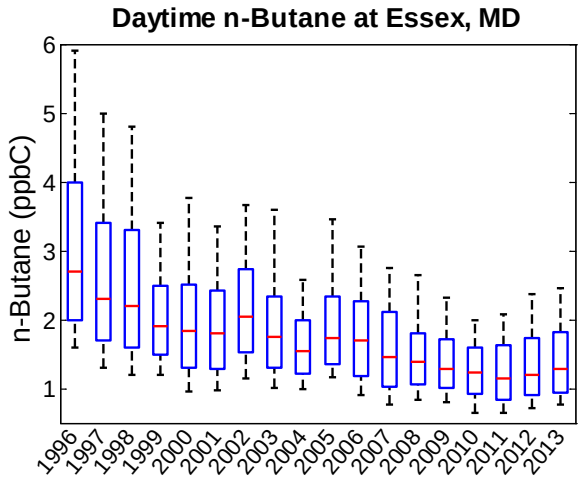

Figure A1.15. Daytime n-butane concentrations from 1996 to 2013 at Essex, MD are presented by box and whisker plots with the same statistical parameters as **Figure 3.3**.

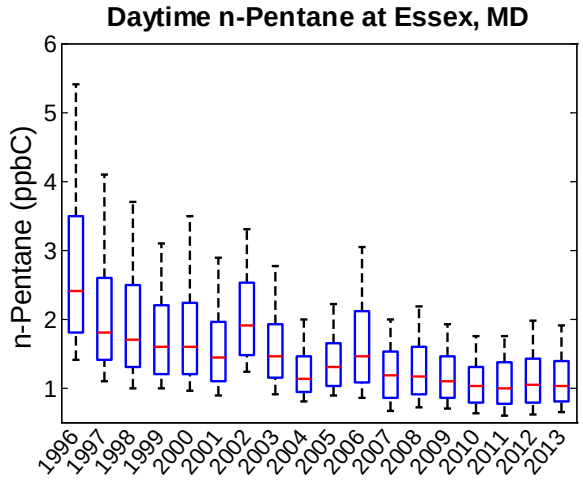

Figure A1.16. Daytime n-pentane concentrations from 1996 to 2013 at Essex, MD are presented by box and whisker plots with the same statistical parameters as **Figure 3.3**.

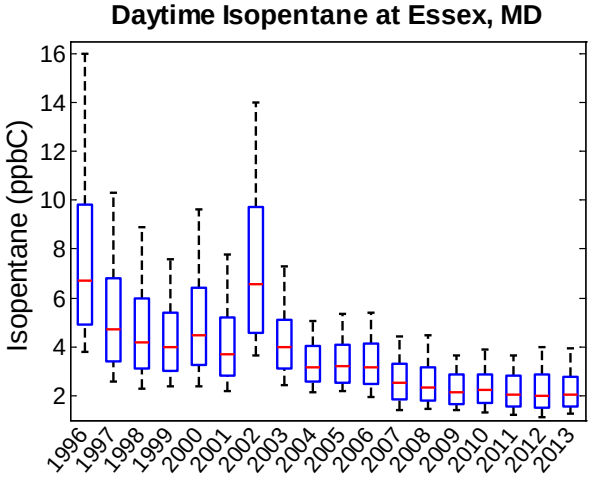

Figure A1.17. Daytime isopentane concentrations from 1996 to 2013 at Essex, MD are presented by box and whisker plots with the same statistical parameters as **Figure 3.3**.

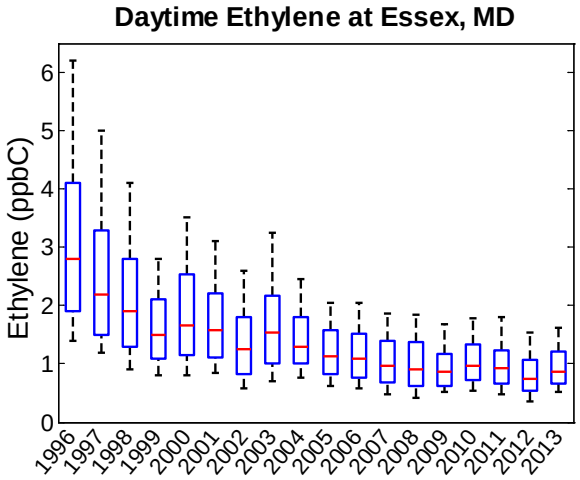

Figure A1.18. Daytime ethylene concentrations from 1996 to 2013 at Essex, MD are presented by box and whisker plots with the same statistical parameters as **Figure 3.3**.

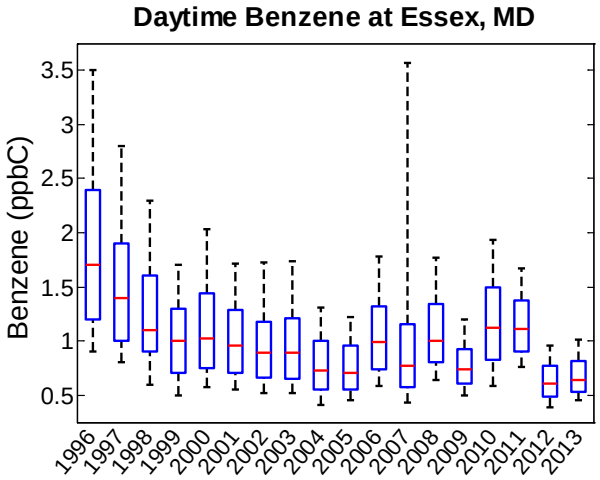

Figure A1.19. Daytime benzene concentrations from 1996 to 2013 at Essex, MD are presented by box and whisker plots with the same statistical parameters as **Figure 3.3**.

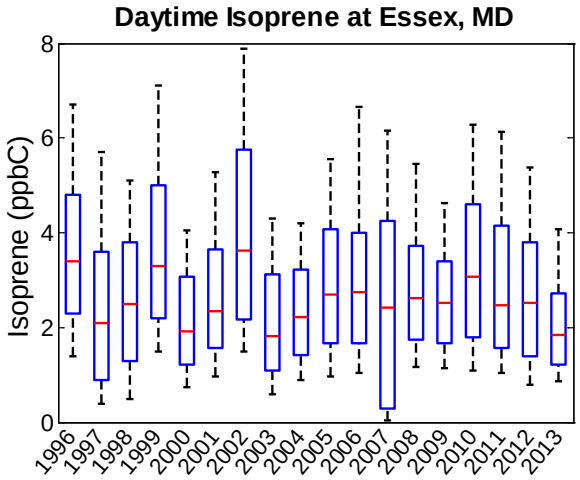

Figure A1.20. Daytime isoprene concentrations (biogenic) from 1996 to 2013 at Essex, MD are presented by box and whisker plots with the same statistical parameters as **Figure 3.3**.

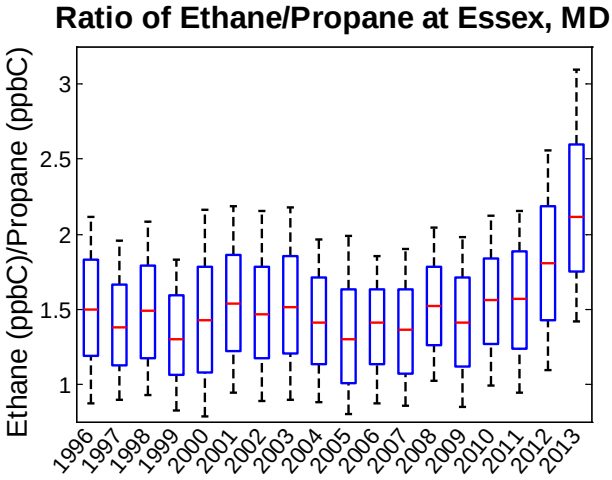

Figure A1.21. The ratio of ethane to propane concentrations from 1996 to 2013 at Essex, MD are presented by box and whisker plots with the same statistical parameters as **Figure 3.3**.

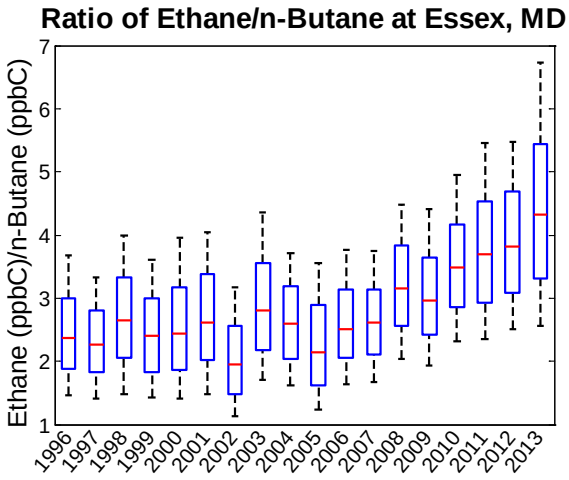

Figure A1.22. The ratio of ethane to n-butane concentrations from 1996 to 2013 at Essex, MD are presented by box and whisker plots with the same statistical parameters as **Figure 3.3**.

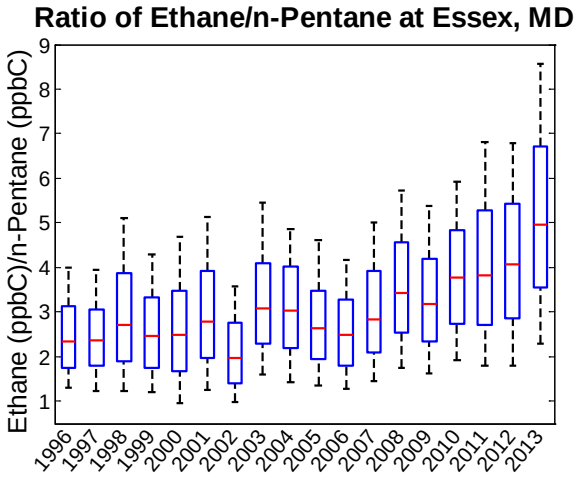

Figure A1.23. The ratio of ethane to n-pentane concentrations from 1996 to 2013 at Essex, MD are presented by box and whisker plots with the same statistical parameters as **Figure 3.3**.

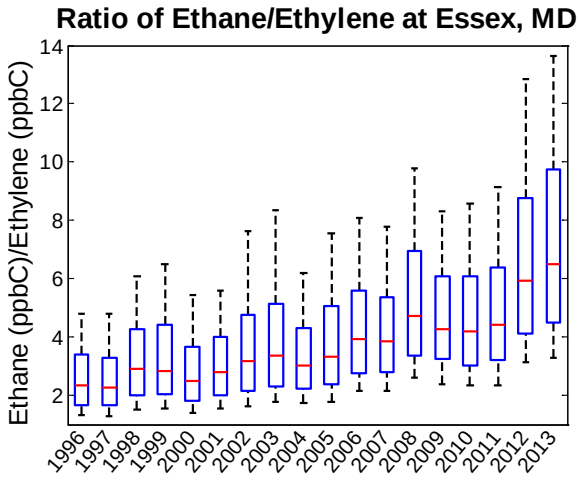

Figure A1.24. The ratio of ethane to ethylene concentrations from 1996 to 2013 at Essex, MD are presented by box and whisker plots with the same statistical parameters as **Figure 3.3**.

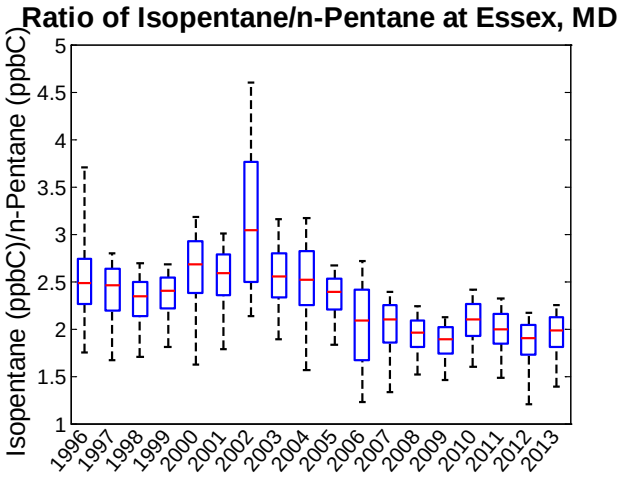

Figure A1.25. The ratio of isopentane to n-pentane concentrations from 1996 to 2013 at Essex, MD are presented by box and whisker plots with the same statistical parameters as **Figure 3.3**.

Table A1.1. Descriptive Statistics for Daytime Ethane Concentrations at Essex, MD

Year	Count	Minimum	10%	25%	Median	75%	90%	Maximum
2004	478	1.01	2.478	3.11	3.95	4.91	6.202	8.68
2005	403	0.64	2.014	2.47	3.13	4.25	5.62	41.67
2006	659	1.65	2.22	2.77	3.93	5.29	6.69	16
2007	603	0.05	1.84	2.59	3.4	4.66	6.436	12.33
2008	799	1.36	2.29	3.28	4.2	5.21	6.72	12.25
2009	781	0.05	2.27	2.86	3.65	4.71	6.338	24.23
2010	740	1.63	2.282	3.07	3.89	5.1475	6.43	16.89
2011	850	0.05	2.23	2.84	3.88	5.2925	7.018	23.87
2012	899	1.66	2.53	3.23	4.28	5.9	8.16	18.81
2013	879	0.05	2.7	3.42	4.85	7.2	9.63	189.41

Table A1.2. P-Values from Steel-Dwass All Pairs Comparisons of Ethane at Essex, MD[a]

Year	2004	2005	2006	2007	2008	2009	2010	2011	2012	2013
2004	*	*	*	*	*	*	*	*	*	*
2005	**<0.0001**	*	*	*	*	*	*	*	*	*
2006	1	**<0.0001**	*	*	*	*	*	*	*	*
2007	**0.0001**	0.2908	**0.0007**	*	*	*	*	*	*	*
2008	0.1616	**<0.0001**	0.148	**<0.0001**	*	*	*	*	*	*
2009	0.11536	**<0.0001**	0.5635	0.1526	**<0.0001**	*	*	*	*	*
2010	1	**<0.0001**	0.999	**<0.0001**	0.3209	**0.0328**	*	*	*	*
2011	1	**<0.0001**	1	**<0.0001**	0.1736	0.2387	0.9999	*	*	*
2012	**0.0001**	**<0.0001**	**<0.0001**	**<0.0001**	0.2208	**<0.0001**	**<0.0001**	**<0.0001**	*	*
2013	**<0.0001**	**<0.0001**	**<0.0001**	**<0.0001**	**<0.0001**	**<0.0001**	**<0.0001**	**<0.0001**	**<0.0001**	*

[a]Bolded values highlight significant p-values that fall below the assumed α=0.05 criteria

Table A1.3. Descriptive Statistics for Daytime Ethane Concentrations at McMillan Reservoir[a]

Year	Count	Minimum	10%	25%	Median	75%	90%	Maximum
2004	789	0.005	2.62	3.43	4.5	6.12	8.2	31.16
2005	555	0.005	1.96	2.4	3.11	3.97	4.95	14.76
2006	705	0.005	1.606	2.22	3.16	4.21	5.27	10.59
2007	807	0.005	1.69	2.76	3.79	4.96	6.492	13.56
2008	847	0.15903	0.45416	3.1429	4.5959	6.7192	8.62606	19.1417
2009	902	0.005	0.005	0.27	2.825	4.1725	5.527	18.15
2010	746	0.005	2.614	3.55	4.73	5.9825	7.833	31.55
2011	719	0.005	3.68	4.61	6.47	8.79	11.46	19.54
2012	863	0.005	3.374	4.37	5.66	7.67	10.086	33.86
2013	897	0.005	3.786	4.73	6.24	8.19	10.796	19.69

Table A1.4. P-Values from Steel-Dwass All Pairs Comparisons of Ethane at McMillan Reservoir

Year	2004	2005	2006	2007	2008	2009	2010	2011	2012	2013
2004	*	*	*	*	*	*	*	*	*	*
2005	**<0.0001**	*	*	*	*	*	*	*	*	*
2006	**<0.0001**	1	*	*	*	*	*	*	*	*
2007	**<0.0001**	**<0.0001**	**<0.0001**	*	*	*	*	*	*	*
2008	1	**<0.0001**	**<0.0001**	**<0.0001**	*	*	*	*	*	*
2009	**<0.0001**	**<0.0001**	**<0.0001**	**<0.0001**	**<0.0001**	*	*	*	*	*
2010	0.9515	**<0.0001**	**<0.0001**	**<0.0001**	0.9942	**<0.0001**	*	*	*	*
2011	**<0.0001**	**<0.0001**	**<0.0001**	**<0.0001**	**<0.0001**	**<0.0001**	**<0.0001**	*	*	*
2012	**<0.0001**	**<0.0001**	**<0.0001**	**<0.0001**	**<0.0001**	**<0.0001**	**<0.0001**	**<0.0001**	*	*
2013	**<0.0001**	**<0.0001**	**<0.0001**	**<0.0001**	**<0.0001**	**<0.0001**	**<0.0001**	0.9823	**<0.0001**	*

[a]Bolded values highlight significant p-values that fall below the assumed α=0.05 criteria

Table A1.5. Descriptive Statistics for Daytime Ethane Concentrations at Rockdale, GA

Year	Count	Minimum	10%	25%	Median	75%	90%	Maximum
2004	302	0.46	1.409	1.8075	2.465	3.37	4.325	7.15
2005	748	0.4	0.88	1.4025	2.31	3.0075	3.58	14.97
2006	877	0.38	0.798	1.15	1.57	2.035	2.444	6.93
2007	632	0.9	1.3	1.7	2.3	3.075	4.4	11.9
2008	762	0.005	1.5	2.1	2.735	3.3	3.8	6.53
2009	838	0.4	1.1	1.8	2.3	3	3.6	9.6
2010	222	0.8	1.2	1.8	2.6	3.125	4	5.1
2011	231	0.005	0.046	2.59	3.17	3.73	4.642	9.31
2012	497	0.005	0.49	1.02	1.6	2.44	3.342	6.37
2013	278	0.005	0.38	0..995	1.62	3.43	4.322	5.44

Table A1.6. P-Values from Steel-Dwass All Pairs Comparisons of Ethane at Rockdale, GA[a]

Year	2004	2005	2006	2007	2008	2009	2010	2011	2012	2013
2004	*	*	*	*	*	*	*	*	*	*
2005	**0.0003**	*	*	*	*	*	*	*	*	*
2006	**<0.0001**	**<0.0001**	*	*	*	*	*	*	*	*
2007	0.5891	**0.0493**	**<0.0001**	*	*	*	*	*	*	*
2008	0.7573	**<0.0001**	**<0.0001**	**<0.0001**	*	*	*	*	*	*
2009	0.1656	0.4944	**<0.0001**	0.9998	**<0.0001**	*	*	*	*	*
2010	0.9969	**0.0398**	**<0.0001**	0.9951	0.2235	0.7652	*	*	*	*
2011	**0.0007**	**<0.0001**	**<0.0001**	**<0.0001**	**<0.0001**	**<0.0001**	**<0.0001**	*	*	*
2012	**<0.0001**	**<0.0001**	0.9688	**<0.0001**	**<0.0001**	**<0.0001**	**<0.0001**	**<0.0001**	*	*
2013	**<0.0001**	0.1304	0.4356	**<0.0001**	**<0.0001**	**0.0004**	**0.0004**	**<0.0001**	0.687	*

[a]Bolded values highlight significant p-values that fall below the assumed α=0.05 criteria

Appendix 2

Expected ozone benefits from electricity generating unit NOx reductions in the Eastern United States

Supporting Information

Table A2.1. 2011 and 2018 Annual Eastern US Anthropogenic VOC Emissions (in tons) by Sector

	2011 Baseline	2018 Baseline	Percent Change
Area	3,129,669	2,996,415	-4%
Nonroad	1,675,927	1,115,838	-33%
Onroad	1,960,210	945,115	-52%
EGU point sources	29,654	34,003	+15%
Other Point Sources	745,140	746,513	+0%
Oil and Gas	1,755,287	2,037,590	+16%
Locomotive and Marine Vessels	38,608	27,876	-28%
Residential Wood Combustion	361,105	380,673	+5%
Fire	3,195,727	3,195,727	0%
Total	12,891,326	11,479,749	-11%

Adapted from EPA, 2014g.

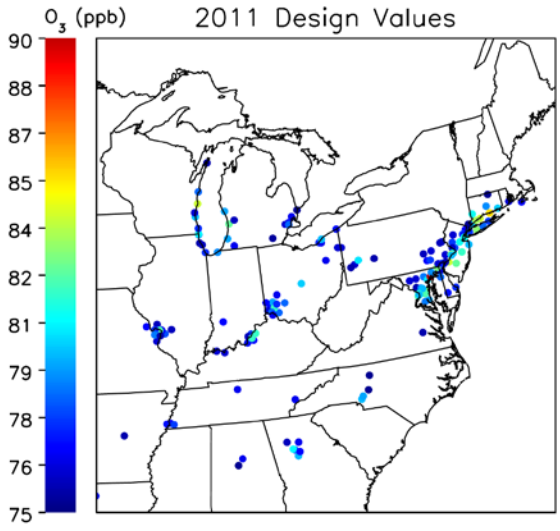

Figure A2.1. Observed design values for surface ozone monitoring sites in 2011.

Table A2.2. EGU NO_x Unit Reductions by Scenario

Plant ID	State	Facility Name	Unit ID	Scenario A	Scenario B	Scenario C	Scenario D
				Adjust IPM 2018 Down by X %	Adjust 3A Up by X %	Adjust 3A Up by X %	Adjust 3A Down by X %
889	IL	Baldwin Energy Complex	1	-10.48%	52.52%	8.04%	---
889	IL	Baldwin Energy Complex	2	-11.73%	42.24%	15.52%	---
861	IL	Coffeen	01	---	143.43%	5.05%	---
861	IL	Coffeen	02	---	134.96%	35.17%	---
963	IL	Dallman	4	---	22.30%	1.24%	---
6016	IL	Duck Creek	1	-18.79%	56.11%	29.76%	---
856	IL	E D Edwards	2	---	---	---	-72.74%
856	IL	E D Edwards	3	-4.95%	110.34%	9.66%	---
891	IL	Havana	9	-53.47%	165.17%	165.17%	---
892	IL	Hennepin Power Station	2	---	---	---	-61.05%
384	IL	Joliet 29	71	-32.88%	---	---	---
384	IL	Joliet 29	72	-33.31%	---	---	---
384	IL	Joliet 29	81	---	1.71%	---	---
384	IL	Joliet 29	82	---	1.20%	---	---
874	IL	Joliet 9	5	---	102.65%	---	---
876	IL	Kincaid Station	1	-8.80%	295.72%	248.52%	---
876	IL	Kincaid Station	2	-21.25%	258.67%	231.17%	---
976	IL	Marion	123	-33.77%	49.39%	41.16%	---
976	IL	Marion	4	-30.85%	121.99%	42.12%	---
879	IL	Powerton	51	-12.15%	---	---	---
879	IL	Powerton	52	-11.89%	---	---	---
879	IL	Powerton	61	-11.57%	---	---	---
879	IL	Powerton	62	-11.32%	---	---	---
55856	IL	Prairie State Generating Company	01	-3.14%	---	---	---

55856	IL	Prairie State Generating Company	02	---	176.71%	---	---
883	IL	Waukegan	7	---	---	---	-62.78%
883	IL	Waukegan	8	---	---	---	-58.91%
884	IL	Will County	3	-35.07%	---	---	---
884	IL	Will County	4	-27.20%	---	---	---
6137	IN	A B Brown Generating Station	1	-50.96%	120.90%	118.52%	---
6137	IN	A B Brown Generating Station	2	-27.85%	62.93%	40.04%	---
6705	IN	Alcoa Allowance Management Inc	4	-31.98%	120.57%	45.25%	---
995	IN	Bailly Generating Station	8	---	277.75%	12.33%	---
983	IN	Clifty Creek	1	-58.91%	457.41%	154.29%	---
983	IN	Clifty Creek	2	-58.83%	481.20%	152.67%	---
983	IN	Clifty Creek	3	-59.01%	459.57%	154.58%	---
983	IN	Clifty Creek	4	-34.24%	76.56%	60.66%	---
983	IN	Clifty Creek	5	-36.90%	63.47%	59.85%	---
983	IN	Clifty Creek	6	---	---	---	-74.13%
1004	IN	Edwardsport	CTG1	---	64.01%	---	---
1012	IN	F B Culley Generating Station	2	-16.79%	29.53%	7.55%	---
1012	IN	F B Culley Generating Station	3	-2.45%	74.82%	7.88%	---
6113	IN	Gibson	1	-77.74%	425.07%	425.07%	---
6113	IN	Gibson	2	-4.00%	224.70%	224.70%	---
6113	IN	Gibson	3	-61.12%	175.11%	152.35%	---
6113	IN	Gibson	4	-54.28%	134.97%	134.97%	---
6113	IN	Gibson	5	-66.14%	205.70%	205.70%	---
990	IN	Harding Street Station (EW Stout)	70	-19.78%	118.77%	15.77%	---
6213	IN	Merom	1SG1	-7.86%	68.06%	4.56%	---
6213	IN	Merom	2SG1	-24.55%	83.48%	25.72%	---

997	IN	Michigan City Generating Station	12	-7.57%	44.90%	22.62%	---
994	IN	Petersburg	1	---	---	---	-61.71%
994	IN	Petersburg	2	-67.46%	426.86%	239.61%	---
994	IN	Petersburg	3	-65.21%	235.62%	163.73%	---
994	IN	Petersburg	4	---	---	---	-60.01%
6085	IN	R M Schahfer Generating Station	14	---	232.52%	12.65%	---
6085	IN	R M Schahfer Generating Station	17	---	---	---	-46.99%
6085	IN	R M Schahfer Generating Station	18	---	---	---	-47.83%
6166	IN	Rockport	MB1	-7.40%	7.99%	---	---
6166	IN	Rockport	MB2	-10.88%	12.21%	---	---
1381	KY	Coleman	C1	---	---	---	-80.05%
1381	KY	Coleman	C2	---	---	---	-80.01%
1381	KY	Coleman	C3	---	---	---	-80.09%
6823	KY	D B Wilson	W1	-21.02%	46.96%	19.92%	---
1355	KY	E W Brown	3	-1.28%	1.29%	---	---
6018	KY	East Bend	2	-58.32%	201.16%	167.18%	---
1374	KY	Elmer Smith	1	-52.65%	184.05%	149.39%	---
1374	KY	Elmer Smith	2	-20.94%	28.68%	23.63%	---
1356	KY	Ghent	1	-41.88%	92.41%	67.19%	---
1356	KY	Ghent	2	---	---	---	-61.52%
1356	KY	Ghent	3	-83.22%	518.38%	518.38%	---
1356	KY	Ghent	4	-65.57%	767.65%	190.81%	---
6041	KY	H L Spurlock	1	-7.07%	66.47%	7.24%	---
6041	KY	H L Spurlock	2	-11.50%	41.56%	18.24%	---
6041	KY	H L Spurlock	3	-7.52%	75.53%	---	---
6041	KY	H L Spurlock	4	-6.64%	6.95%	6.79%	---
1382	KY	HMP&L Station 2	H1	-10.57%	70.79%	2.15%	---
1382	KY	HMP&L Station 2	H2	-12.17%	34.98%	25.23%	---
1364	KY	Mill Creek	1	---	---	---	-75.62%
1364	KY	Mill Creek	2	---	---	---	-76.49%
1364	KY	Mill Creek	3	-38.25%	136.67%	136.67%	---

1364	KY	Mill Creek	4	-63.58%	207.49%	182.09%	---
1378	KY	Paradise	1	-20.11%	23.12%	23.12%	---
1378	KY	Paradise	2	-23.84%	83.30%	47.57%	---
1378	KY	Paradise	3	-69.79%	286.11%	286.11%	---
6639	KY	R D Green	G1	---	---	---	-66.72%
6639	KY	R D Green	G2	---	---	---	-65.02%
1379	KY	Shawnee	10	---	---	---	-72.14%
6071	KY	Trimble County	1	-51.61%	240.13%	76.05%	---
6071	KY	Trimble County	2	---	47.02%	22.51%	---
10678	MD	AES Warrior Run	001	-67.74%	179.61%	179.61%	---
602	MD	Brandon Shores	1	-59.37%	83.19%	79.46%	---
602	MD	Brandon Shores	2	-14.20%	60.27%	29.95%	---
1571	MD	Mirant Chalk Point	1	---	24.27%	13.00%	---
1571	MD	Mirant Chalk Point (SACR)	2	-20.80%	108.30%	17.33%	---
1572	MD	Mirant Dickerson	1	-6.51%	3.83%	2.78%	---
1572	MD	Mirant Dickerson	2	-7.70%	3.09%	1.56%	---
1572	MD	Mirant Dickerson	3	-5.93%	1.48%	0.08%	---
1573	MD	Mirant Morgantown	1	-17.09%	58.62%	31.35%	---
1573	MD	Mirant Morgantown	2	-6.09%	77.67%	---	---
6034	MI	Belle River	1	---	---	---	-52.17%
6034	MI	Belle River	2	---	---	---	-52.45%
1702	MI	Dan E Karn	1	-37.70%	124.88%	82.32%	---
1702	MI	Dan E Karn	2	-25.95%	124.47%	34.10%	---
1832	MI	Erickson	1	---	---	---	-55.83%
1825	MI	J B Sims	3	---	---	---	-58.00%
1710	MI	J H Campbell	1	---	---	---	-49.29%
1710	MI	J H Campbell	3	-37.27%	71.03%	62.88%	---
1733	MI	Monroe	1	-8.25%	70.49%	4.06%	---
1733	MI	Monroe	2	-13.33%	15.38%	---	---
1733	MI	Monroe	3	-2.43%	54.45%	---	---
1733	MI	Monroe	4	-13.09%	360.20%	12.21%	---

1740	MI	River Rouge	2	---	---	---	-53.01%
1740	MI	River Rouge	3	---	---	---	-65.72%
1843	MI	Shiras	3	---	---	---	-30.68%
1743	MI	St. Clair	1	---	---	---	-63.45%
1743	MI	St. Clair	2	---	---	---	-72.31%
1743	MI	St. Clair	3	---	---	---	-74.40%
1743	MI	St. Clair	4	---	---	---	-69.16%
1743	MI	St. Clair	6	---	---	---	-37.40%
1743	MI	St. Clair	7	---	---	---	-44.98%
1745	MI	Trenton Channel	16	---	---	---	-81.32%
1745	MI	Trenton Channel	17	---	---	---	-82.20%
1745	MI	Trenton Channel	18	---	---	---	-81.99%
1745	MI	Trenton Channel	19	---	---	---	-81.32%
1745	MI	Trenton Channel	9A	---	---	---	-43.44%
1866	MI	Wyandotte	7	---	---	---	-49.88%
1866	MI	Wyandotte	8	---	---	---	-54.13%
2706	NC	Asheville	1	-41.01%	99.12%	74.73%	---
2706	NC	Asheville	2	-60.83%	132.84%	132.84%	---
8042	NC	Belews Creek	1	-51.98%	191.07%	87.14%	---
8042	NC	Belews Creek	2	-27.01%	81.41%	39.53%	---
2721	NC	Cliffside	5	-2.14%	42.50%	---	---
10380	NC	Elizabethtown Power	UNIT1	---	---	---	-91.08%
10380	NC	Elizabethtown Power	UNIT2	---	---	---	-91.69%
2727	NC	Marshall	1	---	207.80%	203.48%	---
2727	NC	Marshall	2	---	211.54%	199.45%	---
2727	NC	Marshall	3	---	105.36%	2.92%	---
2727	NC	Marshall	4	-17.63%	55.16%	16.78%	---
6250	NC	Mayo	1A	-23.14%	199.84%	21.31%	---
6250	NC	Mayo	1B	-21.67%	196.25%	16.29%	---
2712	NC	Roxboro	1	-33.47%	91.55%	86.43%	---
2712	NC	Roxboro	2	-25.29%	242.78%	---	---
2712	NC	Roxboro	3A	-44.75%	227.09%	56.47%	---
2712	NC	Roxboro	3B	-44.42%	218.12%	52.78%	---

2712	NC	Roxboro	4A	-27.88%	137.45%	26.36%	---
2712	NC	Roxboro	4B	-28.24%	139.34%	26.10%	---
54035	NC	Westmoreland -LG&E Roanoke Valley I	1	---	---	---	-82.20%
2878	OH	Bay Shore	1	---	---	---	-39.08%
2828	OH	Cardinal	1	-34.42%	95.98%	68.10%	---
2828	OH	Cardinal	2	-28.13%	45.07%	45.07%	---
2828	OH	Cardinal	3	-63.37%	933.19%	171.24%	---
8102	OH	Gen J M Gavin	1	---	29.17%	18.87%	---
8102	OH	Gen J M Gavin	2	-15.85%	57.32%	49.01%	---
2850	OH	J M Stuart	1	-6.10%	66.45%	17.15%	---
2850	OH	J M Stuart	2	---	43.70%	22.50%	---
2850	OH	J M Stuart	3	-3.90%	77.11%	20.08%	---
2850	OH	J M Stuart	4	---	96.70%	21.80%	---
6031	OH	Killen Station	2	-46.88%	297.06%	94.80%	---
2876	OH	Kyger Creek	1	-54.44%	134.64%	107.74%	---
2876	OH	Kyger Creek	2	-50.77%	128.91%	109.09%	---
2876	OH	Kyger Creek	3	-49.37%	125.67%	113.34%	---
2876	OH	Kyger Creek	4	-50.62%	119.72%	102.67%	---
2876	OH	Kyger Creek	5	-51.28%	121.40%	106.50%	---
2832	OH	Miami Fort Generating Station	7	-59.41%	180.60%	180.60%	---
2832	OH	Miami Fort Generating Station	8	-59.47%	269.26%	120.56%	---
2866	OH	W H Sammis	1	---	---	---	-70.21%
2866	OH	W H Sammis	2	---	---	---	-70.42%
2866	OH	W H Sammis	3	---	---	---	-70.35%
2866	OH	W H Sammis	4	---	---	---	-70.05%
2866	OH	W H Sammis	5	---	253.24%	104.43%	---
2866	OH	W H Sammis	6	---	248.30%	6.95%	---
2866	OH	W H Sammis	7	---	13.15%	13.15%	---
6019	OH	W H Zimmer Generating Station	1	-77.78%	341.99%	289.50%	---
10676	PA	AES Beaver Valley LLC	032	-23.87%	8.78%	3.18%	---

10676	PA	AES Beaver Valley LLC	033	-51.14%	78.21%	60.54%	---
10676	PA	AES Beaver Valley LLC	034	---	513.70%	513.70%	---
10676	PA	AES Beaver Valley LLC	035	-49.53%	52.37%	47.09%	---
6094	PA	Bruce Mansfield	1	-44.01%	63.05%	63.05%	---
6094	PA	Bruce Mansfield	2	-25.74%	59.30%	32.96%	---
6094	PA	Bruce Mansfield	3	-2.87%	158.87%	5.91%	---
3140	PA	Brunner Island	1	-23.04%	29.94%	---	---
3140	PA	Brunner Island	2	-20.42%	25.66%	---	---
3140	PA	Brunner Island	3	-33.23%	49.76%	---	---
8226	PA	Cheswick	1	-64.26%	265.70%	164.82%	---
3118	PA	Conemaugh	1	---	387.29%	387.29%	---
3118	PA	Conemaugh	2	---	355.29%	352.86%	---
10603	PA	Ebensburg Power Company	031	-10.32%	11.51%	9.41%	---
10113	PA	Gilberton Power Company	031	-49.76%	99.03%	42.05%	---
10113	PA	Gilberton Power Company	032	-50.15%	100.62%	43.53%	---
3122	PA	Homer City	1	-69.61%	186.96%	181.26%	---
3122	PA	Homer City	2	-55.95%	174.21%	171.07%	---
3122	PA	Homer City	3	-54.60%	171.56%	127.75%	---
3136	PA	Keystone	1	-88.65%	762.41%	762.41%	---
3136	PA	Keystone	2	-88.33%	738.34%	738.34%	---
3149	PA	Montour	1	-82.27%	591.57%	471.94%	---
3149	PA	Montour	2	-79.64%	616.61%	446.54%	---
50039	PA	Northeastern Power Company	031	-63.36%	172.92%	24.75%	---
50776	PA	Panther Creek Energy Facility	1	-20.65%	29.12%	23.69%	---
50776	PA	Panther Creek Energy Facility	2	-11.31%	16.65%	10.43%	---
54144	PA	Piney Creek Power Plant	031	-31.07%	90.73%	53.03%	---
50974	PA	Scrubgrass Generating Plant	1	-56.89%	135.43%	107.50%	---

50974	PA	Scrubgrass Generating Plant	2	-45.02%	90.54%	61.66%	---
3130	PA	Seward	1	-23.26%	36.84%	13.67%	---
3130	PA	Seward	2	-27.04%	43.36%	19.06%	---
54634	PA	St. Nicholas Cogeneration Project	1	-53.58%	115.41%	38.79%	---
50879	PA	Wheelabrator - Frackville	GEN1	---	---	76.81%	---
50611	PA	WPS Westwood Generation LLC	031	---	---	29.65%	---
3393	TN	Allen	1	-44.56%	69.54%	40.67%	---
3393	TN	Allen	2	-35.07%	31.79%	22.22%	---
3393	TN	Allen	3	-36.62%	47.74%	33.28%	---
3396	TN	Bull Run	1	-10.73%	57.12%	11.97%	---
3399	TN	Cumberland	1	-9.00%	56.80%	18.54%	---
3399	TN	Cumberland	2	-5.67%	67.38%	11.63%	---
3403	TN	Gallatin	1	---	---	29.58%	---
3403	TN	Gallatin	2	---	---	29.18%	---
3403	TN	Gallatin	3	---	---	29.58%	---
3403	TN	Gallatin	4	---	---	29.05%	---
3407	TN	Kingston	1	-18.40%	116.06%	12.85%	---
3407	TN	Kingston	2	-11.54%	149.70%	12.18%	---
3407	TN	Kingston	3	-17.37%	124.01%	11.90%	---
3407	TN	Kingston	4	-15.34%	94.61%	12.77%	---
3407	TN	Kingston	5	-15.44%	126.95%	17.08%	---
3407	TN	Kingston	6	-10.09%	166.60%	14.55%	---
3407	TN	Kingston	7	-13.41%	169.60%	14.26%	---
3407	TN	Kingston	8	-16.25%	185.71%	22.54%	---
3407	TN	Kingston	9	-18.46%	141.20%	22.27%	---
54304	VA	Birchwood Power Facility	001	-8.42%	135.49%	26.62%	---
3797	VA	Chesterfield Power Station	4	-48.00%	332.31%	116.15%	---
3797	VA	Chesterfield Power Station	6	-37.53%	174.23%	58.90%	---
7213	VA	Clover Power Station	1	-12.06%	18.48%	6.32%	---
7213	VA	Clover Power Station	2	-17.31%	21.38%	13.10%	---

10377	VA	Cogentrix-Hopewell	BLR01 A	---	---	---	-88.09%
10377	VA	Cogentrix-Hopewell	BLR01 B	---	---	---	-88.38%
10377	VA	Cogentrix-Hopewell	BLR01 C	---	---	---	-88.24%
10377	VA	Cogentrix-Hopewell	BLR02 A	---	---	---	-88.15%
10377	VA	Cogentrix-Hopewell	BLR02 B	---	---	---	-88.18%
10377	VA	Cogentrix-Hopewell	BLR02 C	---	---	---	-87.89%
10071	VA	Cogentrix-Portsmouth	BLR01 A	---	---	---	-82.66%
10071	VA	Cogentrix-Portsmouth	BLR01 B	---	---	---	-81.93%
10071	VA	Cogentrix-Portsmouth	BLR01 C	---	---	---	-81.91%
10071	VA	Cogentrix-Portsmouth	BLR02 A	---	---	---	-81.92%
10071	VA	Cogentrix-Portsmouth	BLR02 B	---	---	---	-81.28%
10071	VA	Cogentrix-Portsmouth	BLR02 C	---	---	---	-81.24%
52007	VA	Mecklenburg Power Station	1	---	---	---	-77.70%
52007	VA	Mecklenburg Power Station	2	---	---	---	-78.76%
54081	VA	Spruance Genco, LLC	BLR01 A	-25.03%	30.60%	14.88%	---
54081	VA	Spruance Genco, LLC	BLR01 B	-25.17%	28.54%	14.81%	---
54081	VA	Spruance Genco, LLC	BLR02 A	-26.83%	20.49%	19.58%	---
54081	VA	Spruance Genco, LLC	BLR02 B	-26.78%	23.28%	19.32%	---
54081	VA	Spruance Genco, LLC	BLR03 A	-41.01%	16.11%	10.79%	---
54081	VA	Spruance Genco, LLC	BLR03 B	-40.91%	16.51%	11.09%	---
54081	VA	Spruance Genco, LLC	BLR04 A	-37.10%	10.73%	4.38%	---
54081	VA	Spruance Genco, LLC	BLR04 B	-36.78%	10.28%	4.76%	---
56808	VA	Virginia City Hybrid Energy Center	1	-30.00%	---	---	---
3943	WV	Fort Martin Power Station	1	---	---	---	-84.66%
3943	WV	Fort Martin Power Station	2	---	---	---	-82.59%
3944	WV	Harrison Power Station	1	-66.79%	394.01%	207.73%	---

3944	WV	Harrison Power Station	2	-5.43%	358.91%	211.48%	---
3944	WV	Harrison Power Station	3	-6.00%	367.93%	226.60%	---
3935	WV	John E Amos	1	-28.19%	79.50%	69.72%	---
3935	WV	John E Amos	2	-35.45%	113.78%	61.54%	---
3935	WV	John E Amos	3	---	109.59%	21.30%	---
56671	WV	Longview Power	001	-2.71%	---	---	---
3948	WV	Mitchell (WV)	1	---	17.77%	17.77%	---
3948	WV	Mitchell (WV)	2	---	94.98%	3.32%	---
3954	WV	Mount Storm Power Station	1	-29.79%	59.37%	49.54%	---
3954	WV	Mount Storm Power Station	2	-39.95%	68.87%	67.22%	---
3954	WV	Mount Storm Power Station	3	-10.71%	16.41%	11.85%	---
6264	WV	Mountaineer (1301)	1	-28.53%	81.40%	46.25%	---
6004	WV	Pleasants Power Station	1	-71.80%	265.74%	251.78%	---
6004	WV	Pleasants Power Station	2	-69.13%	489.49%	227.95%	---

Bibliography

Advanced Resources International, Inc. (2013), EIA/ARI World Shale Gas and Shale Oil Resource Assessment.

Air Resources Laboratory (2013), HYPLIT4 User's Guide, U.S. National Oceanic and Atmospheric Administration.

Allen, D. J., K. E. Pickering, R. W. Pinder, B. H. Henderson, K. W. Appel, and A. Prados (2012), Impact of lightning-NO on eastern United States photochemistry during the summer of 2006 as determined using the CMAQ model, *Atmospheric Chemistry and Physics*, *12*, 1737-1758, doi:10.5194/acp-12-1737-2012.

Allen, D. T., V. M. Torres, J. Thomas, D. W. Sullivan, M. Harrison, A. Hendler, S. C. Herndon, C. E. Kolb, M. P. Fraser, A. D. Hill, B. K. Lamb, J. Miskimins, R. F. Sawyer, and J. H. Seinfeld (2013), Measurements of methane emissions at natural gas production sites in the United States, *Proceedings of the National Academy of Sciences of the United States of America*, *110*(44), 17768-17773, doi:10.1073/pnas.1304880110.

Allen, D. T., D. W. Sullivan, D. Zavala-Araiza, A. P. Pacsi, M. Harrison, K. Keen, M. P. Fraser, A. D. Hill, B. K. Lamb, R. F. Sawyer, and J. H. Seinfeld (2014), Methane Emissions from Process Equipment at Natural Gas Production Sites in the United States: Liquid Unloadings, *Environmental Science & Technology*, doi:10.1021/es504016r

Alvarez, R. A., S. W. Pacala, J. J. Winebrake, W. L. Chameides, and S. P. Hamburg (2012) Greater focus needed on methane leakage from natural gas infrastructure, *Proceedings of the National Academy of Sciences of the United States of America*, *109*(17), 6435–6440, doi:10.1073/pnas.1202407109.

Anderson, D.C., C.P. Loughner, G. Diskin, A. Weinheimer, T.P. Canty, R.J. Salawitch, H.M. Worden, A. Fried, T. Mikoviny, A. Wisthaler, and R.R. Dickerson (2014), Measured and modeled CO and NOy in DISCOVER-AQ: An evaluation of emissions and chemistry over the eastern US., *Atmos. Environ.*, *96*, 78-87. doi:10.1016/j.atmosenv.2014.07.004

Annual Survey of Manufacturers (2016), ASM Table, United States Census Bureau, https://www.census.gov/programs-surveys/asm/data/tables.html (Accessed on May 17, 2016)

Appel, K. W., G. A. Pouliot, H. Simon, G. Sarwar, H. O. T. Pye, S. L., Napelenok, F. Akhtar, and S. J. Roselle (2013), Evaluation of dust and trace metal estimates from the Community Multiscale Air Quality (CMAQ) model version 5.0, *Geosci. Model Dev.*, *6*, 883-899, doi:10.5194/gmd-6-883-2013

Archer, D (2011), *Global Warming: Understanding the Forecast*, Second Edition, Wiley, Hoboken, NJ.

Atwood, S. A., J. S. Reid, S. M. Kreidenweis, L. E. Yu, S. V. Salinas, B. N. Chew, and R. Balasubramanian (2013), Analysis of source regions for smoke events in Singapore for the 2009 El Nino burning season, Atmospheric Environment, *78*, 219-230, doi: 10.1016/j.atmosenv.2013.04.047

Auch, T. (2014), Hydrocarbon Industrial Complex Map in Detail, FracTracker Alliance, https://www.fractracker.org/2014/01/us-hydrocarbon-map/ (Accessed on May 3, 2015)

Aydin, M., K. R. Verhulst, E. S. Saltzman, M. O. Battle, S. A. Montzka, D. R. Blake, Q. Tang, and M. J. Prather (2011), Recent decreases in fossil-fuel emissions of ethane and methane derived from firn air, *Nature*, *476*(7359), 198–201, doi:10.1038/nature10352.

Bash, J. O., K. R. Baker, and M. R. Beaver (2015), Evaluation of improved land use and canopy representation in BEIS v3.61 with biogenic VOC measurements in California, *Geosci. Model Dev. Disc.*, *8*, 8117–8154.

Belay, Acefaw, Maryland Department of the Environment, personal communication, acefaw.belay@maryland.gov.

Bey, I., D. J. Jacob, R. M. Yantosca, J. A. Logan, B. D. Field, A. M. Fiore, Q. B. Li, H. G. Y. Liu, L. J. Mickley, and M. G. Schultz (2001), Global modeling of tropospheric chemistry with assimilated meteorology: Model description and evaluation, *J. Geophys. Res.*, *106*(D19), 23,073–23,095. doi:10.1029/2001JD000807

Blake, N. J., and D. R. Blake (2003), Tropospheric Chemistry and Composition | VOCs: Overview, *Encyclopedia of Atmospheric Sciences*, 2438-2446, doi:10.1016/B0-12-227090-8/00422-X.

Brown, S. G., A. Frankel, and H. R. Hafner (2007), Source apportionment of VOCs in the Los Angeles area using positive matrix factorization, *Atmospheric Environment*, *41*(2), 227-237, doi: 10.1016/j.atmosenv.2006.08.021.

Brown, S. G ., S. Eberly. P. Pentti, and G. A. Norris (2015) Methods for estimating uncertainty in PMF solutions: Examples with ambient air and water quality data and guidance on reporting PMF results, *Science of The Total Environment*, *518-519*, 626-635, doi:10.1016/j.scitotenv.2015.01.022

Bullin, K. A. and P. F. Krouskop (2009), Compositional variety complicates plans for processing US shale gas, *Oil & Gas Journal*, *107(*10), 50–57.

Burley, J. D., A. Bytnerowicz, J. D. Ray, S. Schilling, and E. B. Allen (2014), Surface ozone in Joshua Tree National Park, *Atmospheric Environment*, *87*, 95-107, doi: 10.1016/j.atmosenv.2013.12.043

Buzcu-Guven, B. and M. P. Fraser (2008), Comparison of VOC emissions inventory data with source apportionment results for Houston, TX, *Atmospheric Environment*, *42*(20), 5032-5043, doi: 10.1016/j.atmosenv.2008.02.025

Canty, T. P., L. Hembeck, T. P. Vinciguerra, D. C. Anderson, D. L. Goldberg, S.F., Carpenter, D. J. Allen, C. P. Loughner, R. J. Salawitch, and R. R. Dickerson (2015), Ozone and NOx chemistry in the eastern US: Evaluation of CMAQ/CB05 with satellite (OMI) data, *Atmos. Chem. Phys.*, *15*, 10965-10982, http://dx.doi.org/10.5194/acp-15-10965-2015

Carlton, A. G., P. V. Bhave, S. L. Napelenok, E. D. Edney, G. Sarwar, R. W. Pinder, G. A. Pouliot, and M. Houyoux (2010), Model representation of secondary organic aerosol in CMAQv4.7, *Environ. Sci. Technol.*, *44*(22), 8553–8560. doi:10.1021/es100636q

Carter, W. P. L. (1994), Development of Ozone Reactivity Scales for Volatile Organic Compounds, *Journal of the Air and Waste Management Association*, *44*, 881-899.

Carter, W. P. L. (2010), "Updated Maximum Incremental Reactivity Scale and Hydrocarbon Bin Reactivities for Regulatory Applications," California Air Resources Board Contract 07-339.

Carter, W. P. L. (2012), "Development of revised SAPRC aromatic mechanism," California Air Resources Board Contract 07-730 and 08-326.

Caulton, D. R., P. B. Shepson, R. L. Santoro, J. P. Sparks, R. W. Howarth, A. R. Ingraffea, M. O. L. Cambaliza, C. Sweeney, A. Karion, K. J. Davis, B. H. Stirm, S. A. Montzka, and B. R. Miller (2014), Toward a better understanding and quantification of methane emissions from shale gas development, *Proceedings of the National Academy of Sciences of the United States of America*, *111*(17), 6237-6242, doi:10.1073/pnas.1316546111.

Chen, L.-W. A., B. G. Doddridge, R. R. Dickerson, J. C. Chow, R. C. Henry (2002), Origins of fine aerosol mass in the Baltimore–Washington corridor: implications from observation, factor analysis, and ensemble air parcel back trajectories, *Atmospheric Environment*, *36*, 4541-4554, doi:10.1016/S1352-2310(02)00399-0.

Choi, Y. and S. H. Ehrman (2004), Investigation of sources of volatile organic carbon in the Baltimore area using highly time-resolved measurements, *Atmospheric Environment*, *38*, 775-791, doi: 10.1016/j.atmosenv.2003.10.004.

Choi, Y. (2004), A study of ground-level ozone over the Baltimore/Washington ozone nonattainment area, doctoral dissertation, University of Maryland, College Park, MD.

Cleveland, C. J., editor-in-chief (2004), Natural Gas Transportation and Storage, *Encyclopedia of Energy*, Elsevier Science & Technology.

CMAQ (2015), CMAQ version 5.0.2 (April 2014 release) Technical Documentation, http://www.airqualitymodeling.org/cmaqwiki/index.php?title=CMAQ_version_5.0.2_%28April_2014_release%29_Technical_Documentation (accessed December 11, 2015).

Conder, M. W. and K. A. Lawlor (2014), Production Characteristics Of Liquids-Rich Resource Plays Challenge Facility Design, *The American Oil and Gas Reporter*.

Crawford, J. H., R. R. Dickerson, *and* J. Hains (2014), DISCOVER-AQ observations and early results, *Environ. Manage.*, 8–15.

Crippa, P. and S. C. Pryor (2013), Spatial and temporal scales of new particle formation events in eastern North America, *Atmospheric Environment*, *75*, 257-264, doi:10.1016/j.atmosenv.2013.04.051.

Crutzen, P. J. (1974), Photochemical reactions initiated by and influencing ozone in unpolluted tropospheric air, *Tellus*, *26*(1-2), 47-57.

deGouw, J. A., D. D. Parrish, G. J. Frost, and M. Trainer (2014), Reduced emissions of CO_2, NOx, and SO_2 from U.S. power plants owing to switch from coal to natural gas with combined cycle technology, *Earth's Future*, *2*, 75–82, doi:10.1002/2013EF000196.

Dolwick, P., D. Kang, K. Baker, S. Phillips, N. Possiel, H. Simon, J. Kelly, C. Misenis, and B. Timin (2014), Initial evaluation of 2011 CMAQ and CAMx simulations during the DISCOVER-AQ period in the mid-Atlantic. Presentation. 13th Annual CMAS Conference, https://www.cmascenter.org/conference/2014/slides/pat_dolwick_three-dimensional_evaluation_2014.pptx (accessed on December 16, 2015).

Draxler, R. R. (1999), HYSPLIT4 user's guide. NOAA Tech. Memo. ERL ARL-230, NOAA Air Resources Laboratory, Silver Spring, MD.

Duncan, B. N., Y. Yoshida, J. R. Olsen, S. Sillman, R. V. Martin, L. Lamsal, Y. Hu, K. E. Pickering, D. J. Allen, C. Retscher, and J. H. Crawford (2010), Application of OMI Observations to a Space-Based Indicator of NOx and VOC Controls on Surface Ozone Formation, *Atmos. Env. 44*, 2213-2223, doi:10.1016/j.atmosenv.2010.03.010

Eubanks, L. P., C. H. Middlecamp, C. E. Heltzel, and S. W. Keller (2006), *Chemistry in Context: Applying Chemistry to Society*, Sixth Edition, McGraw-Hill, New York, NY.

ExxonMobil (2014), The Outlook for Energy: A View to 2040.

Foley, K. M., S. J. Roselle, K. W. Appel, P. V. Bhave, J. E. Pleim, T. L. Otte, R. Mathur, G. Sarwar, J. O. Young, R. C. Gilliam, C. G. Nolte, J. T. Kelly, A. B. Gilliland, and J. O. Bash (2010), Incremental testing of the Community Multiscale Air Quality (CMAQ) modeling system version 4.7, *Geosci. Model. Dev.*, 3, 205-226.

Foster, J. (2013), Can shale gale save the naphtha crackers?, Platts, http://www.platts.com/IM.Platts.Content/InsightAnalysis/IndustrySolutionPapers/ShaleGasReport13.pdp, last accessed on March 12, 2015.

FracTracker Alliance (2014), US Oil and Gas Wells (February 2014), http://www.fractracker.org/downloads/us-oil-and-gas-wells-february-2014/ (Accessed on November 13, 2014)

Fujita, E. M. (2001), Hydrocarbon source apportionment for the 1996 Paso del Norte Ozone Study, *Science of The Total Environment*, *276*(1-3), 171-184, doi: 10.1016/S0048-9697(01)00778-1.

Gilman, J.B., B. M. Lerner, W. C. Kuster, and J. A. de Gouw (2013), Source signature of volatile organic compounds from oil and natural gas operations in Northeastern Colorado. *Environ. Sci. Technol.*, *47*, 1297e1305. http://dx.doi.org/10.1021/es304119a.

Goldberg, D.L., C.P. Loughner, M. Tzortziou, J.W. Stehr, K.E. Pickering, L.T. Marufu, and R.R. Dickerson (2014), Higher surface ozone concentrations over the Chesapeake Bay than over the adjacent land: Observations and models from the DISCOVER-AQ and CBODAQ campaigns, *Atmospheric Environment*, *84*, 9-19, doi:10.1016/j.atmosenv.2013.11.00

Goldberg, D. L., T. P. Vinciguerra, D. C. Anderson, L. Hembeck, T. P. Canty, S. H. Ehrman, D.K. Martins, R.M. Stauffer, A. M. Thompson, R. J. Salawitch, and R.R. Dickerson, (2016), CAMx ozone source attribution in the eastern United

States using guidance from observations during DISCOVER-AQ Maryland. *Geophys. Res. Lett. 43*, doi:10.1002/2015GL067332.

Guenther, A. B., X. Jiang, C. L. Heald, T. Sakulyanontvittaya, T. Duhl, L. K. Emmons, and X. Wang (2012), The Model of Emissions of Gases and Aerosols from Nature version 2.1 (MEGAN2.1): an extended and updated framework for modeling biogenic emissions, *Geoscientific Model Development*, *5*, 1471–1492, doi:10.5194/gmd-5-1471-2012.

Haagensmit, A. J., C. E. Bradley, and M. M. Fox (1953), Ozone Formation in Photochemical Oxidation of Organic Substances. *Industrial and Engineering Chemistry*, *45*(9), 2086-2089.

Hahnenberger, M. and K. Nicoll (2012), Meteorological characteristics of dust storm events in the eastern Great Basin of Utah, U.S.A, *Atmospheric Environment*, *60*, 601-612, doi: 10.1016/j.atmosenv.2012.06.029.

Hains, J. C., B. F. Taubman, A. M. Thompson, J. W. Stehr, L. T. Marufu, B. Doddridge, and R. R. Dickerson (2008), Origins of chemical pollution derived from Mid-Atlantic aircraft profiles using a clustering technique, *Atmospheric Environment*, *42*(8), 1727-1741, doi:10.1016/j.atmosenv.2007.11.052.

Hallquist, M., J. Wenger, U. Baltensperger, Y. Rudich, D. Simpson, M. Claeys, J. Dommen, N. M. Donahue, C. George, A. H. Goldstein, J. F. Hamilton, H. Herrmann, T. Hoffmann, Y. Iinuma, M. Jang, M. E. Jenkin, J. L. Jimenez, A. Kiendler-Scharr, W. Maenhaut, G. McFiggans, T. F. Mentel, A. Monod, A. S. H. Prevot, J. H. Seinfeld, J. D. Surratt, R. Szmigielski, and J. Wildt, (2009) The formation, properties and impact of secondary organic aerosol: current and emerging issues, Atmos. Chem. Phys., 9, 5155-5236.Henry, R. C. (2003), Multivariate receptor modeling by N-dimensional edge detection, *Chemometrics and Intelligent Laboratory Systems*, *65*(2), 179-189, doi: 10.1016/S0169-7439(02)00108-9.

He, H., L. Hembeck, K. M. Hosley, T. P. Canty, R. J. Salawitch, and R. R. Dickerson (2013a), High ozone concentrations on hot days: The role of electric power demand and NOx emissions, *Geophysical Research Letters*, *40*(19), 5291-5294, doi: 10.1002/grl.50967.

He, H., J. W. Stehr, J. C. Hains, D. J. Krask, B. G. Doddridge, K. Y. Vinnikov, T. P. Canty, K. M. Hosley, R. J. Salawitch, H. M. Worden, and R. R. Dickerson (2013b), Trends in emissions and concentrations of air pollutants in the lower troposphere in the Baltimore/Washington airshed from 1997 to 2011, *Atmospheric Chemistry and Physics*, *13*(15), 7859-7874, doi:10.5194/acp-13-7859-2013 .

He, H., C. P. Loughner, J. W. Stehr, H. L. Arkinson, L. C. Brent, M. B. Follette-Cook, M. A. Tzortziou, K. E. Pickering, A. M. Thompson, D. K. Martins, G. S. Diskin, B. E. Anderson, J. H. Crawford, A. J. Weinheimer, P. Lee, J. C. Hains, and R. R. Dickerson (2014), An elevated reservoir of air pollutants over the Mid-Atlantic States during the 2011 DISCOVER-AQ campaign: Airborne measurements and numerical simulations, *Atmospheric Environment*, *85*, 18-30, doi:10.1016/j.atmosenv.2013.11.039.

Healey, B., and K. Pergande (2014), Breaking Down Quad-O Regulations, Compliance Needs, *Pipeline & Gas Journal*, *241*(6), 90-94.

Hopke, P. K. (2003), A Guide to Positive Matrix Factorization, Department of Chemistry, Clarkson University, Potsdam, NY.

Hopke, P. K. (2016), Review of receptor modeling methods for source apportionment, *Journal of Air & Waste Management Association*, *66*(3), 237-259, doi: 10.1080/10962247.2016.1140693.

Howarth, R. W., R. Santoro, and A. Ingraffea (2011), Methane and the greenhouse-gas footprint of natural gas from shale formations, *Climatic Change*, *106*(4), 679–690, doi:10.1007/s10584-011-0061-5

The Institute for the Environment (2012), SMOKE v3.1 User's Manual, The University of North Carolina at Chapel Hill.

Intergovernmental Panel on Climate Change (2001), IPCC third assessment report (AR3). Working Group 1, The Physical Science Basis.

Intergovernmental Panel on Climate Change (2007), IPCC fourth assessment report (AR4). Working Group 1, The Physical Science Basis.

Intergovernmental Panel on Climate Change (2013), IPCC fifth assessment report (AR5). Working Group 1, The Physical Science Basis.

Jaars, K., J. P. Beukes, P. G. van Zyl, A. D. Venter, M. Josipovic, J. J. Pienaar, V. Vakkari, H. Aaltonen, H. Laakso, M. Kulmala, P. Tiitta, A. Guenther, H. Hellén, L. Laakso, and H. Hakola (2014), Ambient aromatic hydrocarbon measurements at Welgegund, South Africa, Atmospheric Chemistry and Physics, *14*, 7075-7089, doi: 10.5194/acp-14-7075-2014.

Kang, M., C. M. Kanno, M. C. Reid, X. Zhang, D. L. Mauzerall, M. A. Celia, Y. Chen, and T. C. Onstott (2014), Direct measurements of methane emissions from abandoned oil and gas wells in Pennsylvania, *Proceedings of the National Academy of Sciences of the United States of America*, doi:10.1073/pnas.1408315111.

Karamchandani, P., J. Johnson, G. Yarwood, and E. Knipping (2014), Implementation and application of sub-grid-scale plume treatment in the latest version of EPA's third-generation air quality model, CMAQ 5.01, *Journal of the Air & Waste Management Association*, *64*(4), 453-467, doi:10.1080/10962247.2013.855152

Karion, A., C. Sweeney, G. Petron, G. Frost, R. M. Hardesty, J. Kofler, B. R. Miller, T. Newberger, S. Wolter, R. Banta, A. Brewer, E. Dlugokencky, P. Lang, S. A. Montzka, R. Schnell, P. Tans, M. Trainer, R. Zamora, and S. Conley (2013), Methane emissions estimate from airborne measurements over a western United States natural gas field, *Geophysical Research Letters*, *40*(16), 4393–4397, doi:10.1002/grl.50811.

Kear, T., D. Eisinger, D. Niemeier, and M. Brady (2008), US vehicle emissions: Creating a common currency to avoid model comparison problems, *Transportation Research Part D*, *13*(3), 168-176, doi: 10.1016/j.trd.2008.01.004.

Kemball-Cook, S., A. Bar-Ilan, J. Grant, L. Parker, J. Jung, W. Santamaria, J. Mathews, and G. Yarwood (2010), Ozone Impacts of Natural Gas Development in the Haynesville Shale, *Environmental Science & Technology*, *44*, 9357-9363, doi:10.1021/es1021137.

Kirchgessner, D., R. Lott, R. Cowgill, M. Harrison, and T. Shires (1997), Estimate of methane emissions from the US natural gas industry, *Chemosphere*, *35*(6), 1365–1390, doi: 10.1016/S0045-6535(97)00236-1.

Kleinman, L. I., P. H. Daum, Y.-N. Lee, L. J. Nunnermacker, S. R. Springston , J. Weinstein-Lloyd, and J. Rudolph (2005), A comparative study of ozone production in five U.S. metropolitan areas, *Journal of Geophysical Research*, *110*, D02301, doi: 10.1029/2004JD005096.

Leuchner, M. and B. Rappenglück (2010), VOC source–receptor relationships in Houston during TexAQS-II, *Atmospheric Environment*, *44*(33), 4056-4067, doi: 10.1016/j.atmosenv.2009.02.029.

Liao, D., Y. Duan, E. A. Whitsel, Z. J. Zheng, G. Heiss, V. M. Chinchilli, and H. M. Lin (2004), Association of higher levels of ambient criteria pollutants with impaired cardiac autonomic control: A population-based study. *American Journal of Epidemiology*, *159*, 768–777. doi: 10.1093/aje/kwh109.

Loughner, C. P., D. J. Allen, K. E. Pickering, Y. X. Shou, D. L. Zhang, and R. R. Dickerson (2011), Impact of fair-weather cumulus clouds and the Chesapeake Bay breeze on pollutant transport and transformations lifetimes, *Atmos. Environ.*, *45*, 4060-4072, doi:10.1016/j.atmosenv.2011.04.003

Maryland Department of the Environment (2011), State of Maryland 8-Hour Ozone Reasonably Available Control Technology (RACT) State Implementation Plan.

Maryland Department of the Environment (2012), Implementation, Maintenance, and Enforcement of the 0.075 ppm 8-hour Ozone National Ambient Air Quality Standard State Implementation Plan, SIP Number 12-12, http://www.mde.state.md.us/programs/Air/AirQualityPlanning/Documents/Ozone_ISIP_2012.pdf (Accessed on April 21, 2016).

Maryland Department of the Environment (2015), Proposed Action on Regulations – 26.19.01 Oil and Gas Exploration and Production, *Maryland Register*, *42*(1), 94-116.

Maryland Department of Transportation (2013), Consolidated Transportation Program: 2013 State Report on Transportation, FY 2013-2018.

Maryland General Assembly (2015), Senate Bill 409, Department of Legislative Services, http://mgaleg.maryland.gov/2014RS/fnotes/bil_0009/sb0409.pdf (Accessed on April 27, 2016)

McBean, E. A., and F. A. Rovers (1998), *Statistical Procedures for Analysis of Environmental Monitoring Data and Risk Assessment*, Prentice Hall, Upper Saddle River, N. J.

Mid-Atlantic Regional Air Management Association (2016a), 2007 Regional Emissions Inventory Version 3, http://www.marama.org/technical-center/emissions-inventory/2007-emissions-and-projections/version-3-2007-emissions-inventory (Accessed on April 25, 2016).

Mid-Atlantic Regional Air Management Association (2016b), MARAMA Future Year Inventories - Version 3, http://www.marama.org/technical-center/emissions-inventory/2007-emissions-and-projections/future-year-inventory-version-3 (Accessed on April 25, 2016).

Mid-Atlantic Regional Air Management Association (2016c), ERTAC EGU Forecasting Tool Documentation, http://www.marama.org/2013-ertac-egu-forecasting-tool-documentation (Accessed on April 27, 2016).
Mid-Atlantic Regional Air Management Association (2016d), 2011 /2018 /2028 Alpha2 - Regional Emissions Inventory, http://www.marama.org/technical-center/emissions-inventory/2011-inventory-and-projections (Accessed on May 15, 2016).
Miller, M.S., S. K. Friedlander, and G. M. Hidy (1972), A chemical element balance for the Pasadena aerosol, *Journal of Colloid and Interface Science*, *39*, 165–176, doi: 10.1016/0021-9797(72)90152-X.
Morino, Y., T. Ohara, Y. Yokouchi, and A. Ooki (2011), Comprehensive source apportionment of volatile organic compounds using observational data, two receptor models, and an emission inventory in Tokyo metropolitan area, *Journal of Geophysical Research*, *116*, D02311, doi:10.1029/2010JD014762.
New York State Department of Environmental Conservation (2015), The Final Supplemental Generic Environmental Impact Statement on the Oil, Gas and Solution Mining Regulatory Program, http://www.dec.ny.gov/docs/materials_minerals_pdf/findingstatehvhf62015.pdf
Nolte, C. G., K. W. Appel, J. T. Kelly, P. V. Bhave, K. M. Fahey, J. L. Collett Jr., L. Zhang, and J. O. Young (2015), Evaluation of the Community Multiscale Air Quality (CMAQ) model v5.0 against size-resolved measurements of inorganic particle composition across sites in North America, *Geosci. Model Dev.*, *8*, 2877-2892. doi:10.5194/gmd-8-2877-2015
Norris, G., R. Duvall, and S. Brown (2014), EPA Positive Matrix Factorization (PMF) 5.0 Fundamentals & User Guide, EPA/600/R-14/108, Office of Research and Development, U.S. EPA, Washington, DC.
Ohio Oil and Gas Association (2016), Ohio Oil & Gas Activity, http://www.ooga.org/?page=OilAndGasActivity (Accessed on May 10, 2016).
Ohio River Valley Water Sanitation Commission, River Facts/Conditions, http://www.orsanco.org/factcondition (accessed on January 15, 2016).
Ozone Transport Commission (2015), Comparison of CSAPR Allowance Prices to Cost of Operating SCR controls. Final Draft. OTC Stationary and Area Source Committee, Largest Contributors Workgroup. http://www.otcair.org/upload/Documents/Reports/Draft%20Final%20Allowance%20v%20SCR%20operating%20costs%2004-15-15.pdf (accessed on June 15, 2016).
Paatero, P., S. Eberly, S. Brown, and G. A. Norris (2014) Methods for estimating uncertainty in factor analytic solutions, *Atmospheric Measurement Techniques*, *7*, 781-797, doi:10.5194/amt-7-781-2014.
Pace Global (2010) NiSource Gas Transmission and Storage Presentation to WVONGA Spring Meeting. Referenced in: Weisman, C. (2013) The US Shale Oil & Gas Revolution, Groundwater & Environmental Services, Inc., http://www.atlantapipeliners.com/wp-content/uploads/2012/09/2013_03_11-The-US-Shale-Oil-and-Gas-Revolution.pdf, last accessed on March 12, 2015.

Parrish, D. D., A. Stohl, C. Forster, E. L. Atlas, D. R. Blake, P. D. Goldan, W. C. Kuster, and J. A. de Gouw (2007), Effects of mixing on evolution of hydrocarbon ratios in the troposphere, *J. Geophys. Res.*, *112*, D10S34, doi:10.1029/2006JD007583.

Peischl, J., T. B. Ryerson, J. Brioude, K. C. Aikin, A. E. Andrews, E. Atlas, D. Blake, B. C. Daube, J.A. de Gouw, E. Dlugokencky, G.J. Frost, D.R. Gentner, J.B. Gilman, A.H. Goldstein, R. A. Harley, J. S. Holloway, J. Kofler, W. C. Kuster, P.M. Lang, P. C. Novelli, G. W. Santoni, M. Trainer, S. C. Wofsy, and D. D. Parrish (2013), Quantifying sources of methane using light alkanes in the Los Angeles basin, California, *Journal of Geophysical Research-Atmospheres*, *118*(10), 4974–4990, doi:10.1002/jgrd.50413.

Peischl, J., T. B. Ryerson, K. C. Aikin, J. A. de Gouw, J. B. Gilman, J. S. Holloway, B. M. Lerner, R. Nadkarni, J. A. Neuman, J. B. Nowak, M. Trainer, C. Warneke, and D. D. Parrish (2015), Quantifying atmospheric methane emissions from the Haynesville, Fayetteville, and Northeastern Marcellus shale gas production regions, *J. Geophys. Res. Atmos.*, *120*, 2119–2139, doi:10.1002/2014JD022697.

Pekney, N. J., G. Veloski, J. Tamilia, E. Rupp, and A. Wetzel (2014), Measurement of atmospheric pollutants associated with oil and natural gas exploration and production activity in Pennsylvania's Allegheny National Forest, *Journal of the Air & Waste Management Association*, *64*(9), 1062-1072, doi:10.1080/10962247.2014.897270.

Pennsylvania Department of Environmental Protection (2014), PA DEP Oil & Gas Reporting Website: Production Reports by County, https://www.paoilandgasreporting.state.pa.us/publicreports/Modules/Production/ProductionByCounty.aspx, last accessed on September 24, 2014.

Pennsylvania Department of the Environment (2016a), Wells Drilled by County, http://www.depreportingservices.state.pa.us/ReportServer/Pages/ReportViewer.aspx?/Oil_Gas/Wells_Drilled_By_County, (Accessed on May 10, 2016).

Pennsylvania Department of the Environment (2016b), Air Emissions Data from Natural Gas Operations, http://www.dep.pa.gov/Business/Air/BAQ/BusinessTopics/Emission/Pages/Marcellus-Inventory.aspx (Accessed on May 10, 2016).

Petron, G., G. Frost, B. R. Miller, A. I. Hirsch, S. A. Montzka, A. Karion, M. Trainer, C. Sweeney, A. E. Andrews, L. Miller, J. Kofler, A. Bar-Ilan, E. J. Dlugokencky, L. Patrick, C. T. Moore, Jr., T. B. Ryerson, C. Siso, W. Kolodzey, P. M. Lang, T. Conway, P. Novelli, K. Masarie, B. Hall, D. Guenther, D. Kitzis, J. Miller, D. Welsh, D. Wolfe, W. Neff, and P. Tans (2012), Hydrocarbon emissions characterization in the Colorado Front Range: A pilot study, *Journal of Geophysical Research-Atmospheres*, *117*, doi:10.1029/2011JD016360.

Pope, C. A., III and D. W. Dockery (2006), Health effects of fine particulate air pollution: Lines that connect, *Journal of Air & Waste Management Association*, *6*, 709-742, doi:10.1080/10473289.2006.10464485

Rasulov, B., K. Hüve, I. Bichele, A. Laisk, and Ü. Niinemets (2010), Temperature response of isoprene emission in vivo reflects a combined effect of substrate

limitations and isoprene synthase activity: a kinetic analysis. *Plant Physiology*, *154*, 1558–1570.
Ren, Xinrong, National Oceanic and Atmospheric Administration, personal communication, xinrong.ren@noaa.gov.
Rinsland, C. P., R. Zander, C. B. Farmer, R. H. Norton, and J. M. Russell (1987), Concentrations of ethane (C_2H_6) in the lower stratosphere and upper troposphere and acetylene (C_2H_2) in the upper troposphere deduced from atmospheric trace molecule spectroscopy/Spacelab 3 spectra, *Journal of Geophysical Research-Atmospheres*, *92*(D10), 11951–11964, doi:10.1029/JD092iD10p11951.
Riuttanen, L., M. Hulkkonen, M. Dal Maso, H. Junninen, and M. Kulmala (2013), Trajectory analysis of atmospheric transport of fine particles, SO2, NOx and O3 to the SMEAR II station in Finland in 1996–2008, Atmospheric Chemistry and Physics, *13*, 2153-2164, doi: 10.5194/acp-13-2153-2013
Ross, P. (2013), Fracking Off California's Coast 'Far More Common Than Anyone Realized,' *International Business Times*.
Roy, A. A., P. J. Adams, and A. L. Robinson (2014), Air pollutant emissions from the development, production, and processing of Marcellus Shale natural gas, *Journal Of The Air & Waste Management Association*, *64*(1), 19–37.
Roy, A. and Y. Choi (2015), Potential impact of changing the coal-natural gas split in power plants: an emissions inventory perspective, *Atmospheric Environment*, *102*, 413-415.
Ryan, W. F., B. G. Doddridge, R. R. Dickerson, R. M. Morales, K. A. Hallock, P. T. Roberts, D. L. Blumenthal, J. A. Anderson, and K. L. Civerolo (1998), Pollutant transport during a regional O3 episode in the mid-Atlantic states, *Journal of the Air & Waste Management Association*, *48*(9), 786-797.
Rudolph, J., R. Koppmann, and C. Plass-Dulmer (1996), The budgets of ethane and tetrachroloethane: Is there evidence for an impact of reactions with chlorine atoms in the troposphere?, *Atmospheric Environment*, *30*(10-11), 1887–1894, doi:10.1016/1352-2310(95)00385-1.
Sakulyanontvittaya, T., G. Yarwood, R. Morris, C. Loomis, and Z. Adelman (2012), Final Technical Memorandum No. 9: Biogenic Emissions, ENVIRON.
Sandoval, F. J., O. Marroquín de la R., L. J. Jaimes; L. Zúñiga L., O. González, and F. Guzmán Lopéz-Figueroa (2001), Effect of hydrocarbons and nitrogen oxides on ozone formation in smog chambers exposed to solar irradiance of Mexico city, *Atmósfera*, 14(1), 17-27.
Sarwar, G., H. Simon, P. Bhave, and G. Yarwood (2012), Examining the impact of heterogeneous nitryl chloride production on air quality across the United States, *Atmos. Chem. Phys.*, *12*, 6455-6473, doi:10.5194/acp-12-6455-2012
SAS Institute Inc. (2013), JMP® 11 Basic Analysis.
Schneising, O., J. P. Burrows, R. R. Dickerson, M. Buchwitz, M. Reuter, and H. Bovensmann Remote sensing of fugitive methane emissions from oil and gas production in North American tight geologic formations, *Earth's Future*, 2014.Simpson, I. J., M. P. S. Andersen, S. Meinardi, L. Bruhwiler, N. J. Blake, D. Helmig, F. S. Rowland, and D. R. Blake (2012), Long-term decline

of global atmospheric ethane concentrations and implications for methane, *Nature*, *488*, 490-494, doi:10.1038/nature11342.

Schuetzle, D., D. Cronn, A. L. Crittenden, and R. J. Charlson (1975) Molecular composition of secondary aerosols and its possible origin, *Environ. Sci. Technol.*, *9*, 838, doi:10.1021/es60107a007

Seinfeld, J. H. and S. N. Pandis (2006), *Atmospheric Chemistry and Physics: From Air Pollution to Climate Change*. Second Edition. John Wiley & Sons.

Sillman, S., J. A. Logan, and S. C. Wofsy (1990), The Sensitivity of Ozone to Nitrogen Oxides and Hydrocarbons in Regional Ozone Episodes, *Journal of Geophysical Research*, *95*(D2), 1837-1851, doi: 10.1029/JD095iD02p01837.

Sillman, S. (1999), The relation between ozone, NOx and hydrocarbons in urban and polluted rural environments, *Atmospheric Environment*, *33*(12), 1821-1845, doi: 10.1016/S1352-2310(98)00345-8.

Skamarock, W. C. and J. B. Klemp (2008), A time-split nonhydrostatic atmospheric model for weather research and forecasting application, *Journal of Computational Physics*, 227(7), 3465-3485.

Smith, J.B. and D. Tirpak (1989), The Potential Effects Of Global Climate Change On The United States, United States Environmental Protection Agency, EPA-230-05-89-050.

SMOKE (2012), SMOKE v3.1 User's Manual, The Institute for the Environment - The University of North Carolina at Chapel Hill, https://www.cmascenter.org/smoke/documentation/3.1/manual_smokev31.pdf (accessed on December 11, 2015).

Song, Y., W. Dai, M. Shao, Y. Liu, S.H. Lu, W. Kuster, and P. Goldan (2008), Comparison of receptor models for source apportionment of volatile organic compounds in Beijing, China. *Environmental Pollution*, *156*, 174–83, doi:10.1016/jenvpol.2007.12.014

Sonoma Technology, Inc. (2011), Session 4: VOCs and Air Toxics. http://www.ladco.org/reports/workshops/2011/data_validation/presentations/session_4_VOC_and_toxics2011.pdf (accessed on April 13, 2016)

Stein, A. F., R. R. Draxler, G. D. Rolph, B. J. B. Stunder, M. D. Cohen, and F. Ngan (2015), NOAA's HYSPLIT atmospheric transport and dispersion modeling system, *Bulletin of the American Meteorological Society*, *96*, 2059-2077, doi:0.1175/BAMS-D-14-00110.1

Taubman, B. F., L. T. Marufu, C. A. Piety, B. G. Doddridge, J. W. Stehr, and R. R. Dickerson (2004), Airborne characterization of the chemical, optical, and meteorological properties, and origins of a combined ozone/ haze episode over the eastern U.S., *Journal of the Atmospheric Sciences*, *61*(14), 1781 - 1793.

Taubman, B. F., J. C. Hains, A. M. Thompson, L. T. Marufu, B. G. Doddridge, J. W. Stehr, C. A. Piety and R. R. Dickerson (2006), Aircraft vertical profiles of trace gas and aerosol pollution over the mid-Atlantic United States: Statistics and meteorological cluster analysis, *Journal of Geophysical Research-Atmospheres*, *111*(D10), doi:10.1029/2005JD006196.

Thielmann, A., Prévôt, A. S. H., F. C. Grüebler, and J. Staehlin (2001), Empirical ozone isopleths as a tool to identify ozone production regimes, *Geophysical Research Letters*, *28*(12), 2369-2372, doi: 10.1029/2000GL012787.

Travis, K. R., D. J. Jacob, J. A. Fisher, P. S. Kim, E. A. Marais, L. Zhu, K. Yu, C. C. Miller, R. M. Yantosca, M. P. Sulprizio, A. M. Thompson, P, O, Wennberg, J. D. Crounse, J. M. St. Clair, R. C. Cohen, J. L. Laugher, J. E. Dibb, S. R. Hall, K. Ullmann, G. M. Wolfe, I. B. Pollack, J. Peischl, J. A. Neuman, and X. Zhou (2016), NO_x emissions, isoprene oxidation pathways, vertical mixing, and implications for surface ozone in the Southeast United States, *Atmos. Chem. Phys. Discuss.*, doi:10.5194/acp-2016-110 (in review)

U.S. Department of Energy (2014), Alternative Fuels Data Center: Data Downloads, http://www.afdc.energy.gov/data_download, last accessed on September 24, 2014.

U.S. Department of Transportation (2016), Average Age of Automobiles and Trucks in Operation in the United States. Bureau of Transportation Statistics, http://www.rita.dot.gov/bts/sites/rita.dot.gov.bts/files/publications/national_transportation_statistics/html/table_01_26.html (Accessed on April 21, 2016).

U.S. Energy Information Administration (2012), Annual Energy Outlook 2012 Early Release Overview.

U.S. Energy Information Agency (2013), Maps: Exploration, Resources, Reserves, and Production, http://www.eia.gov/pub/oil_gas/natural_gas/analysis_publications/maps/maps.htm (Accessed on October 14, 2013).

U.S. Energy Information Administration (2014a), Annual Energy Outlook 2014.

U.S. Energy Information Administration (2014b), Shale Gas Production, http://www.eia.gov/dnav/ng/ng_prod_shalegas_s1_a.htm, last accessed on September 24, 2014.

U.S. Energy Information Administration (2014c), U.S. Natural Gas Gross Withdrawals and Production, http://www.eia.gov/dnav/ng/ng_prod_sum_dcu_NUS_a.htm, last accessed on September 24, 2014.

U.S. Energy Information Administration (2014d), Natural Gas Weekly Update, http://www.eia.gov/naturalgas/weekly/, last accessed on September 24, 2014.

U.S. Energy Information Administration (2014e), Underground Natural Gas Storage Capacity, http://www.eia.gov/dnav/ng/ng_stor_cap_dcu_SMD_a.htm, last accessed on December 22, 2014.

U.S. Energy Information Administration (2014f), Natural Gas Consumption by End Use, http://www.eia.gov/dnav/ng/NG_CONS_SUM_DCU_SMD_A.htm, last accessed on September 24, 2014.

U.S. Energy Information Administration (2015a), Propane Explained: Use of Propane, http://www.eia.gov/energyexplained/index.cfm?page=propane_use, last accessed on January 7, 2015.

U.S. Energy Information Administration (2015b), 4-Week Avg East Coast (PADD 1) Refiner, Blender, and Gas Plant Net Production of Propane and Propylene, http://www.eia.gov/dnav/pet/hist/LeafHandler.ashx?n=PET&s=WPRNPP12&f=4, last accessed on March 12, 2015.

U.S. Energy Information Administration (2015c), East Coast (PADD 1) Gas Plant Production of Propane and Propylene, http://www.eia.gov/dnav/pet/hist/LeafHandler.ashx?n=PET&s=MPRFPP11&f=M, last accessed on March 12, 2015.

U.S. Energy Information Administration (2015d), East Coast (PADD 1) Refinery Net Production of Propane and Propylene, http://www.eia.gov/dnav/pet/hist/LeafHandler.ashx?n=PET&s=MPRRX_R10_1&f=M, last accessed on March 12, 2015.

U.S. Energy Information Administration (2016a), Natural Gas Weekly Update. http://www.eia.gov/naturalgas/weekly/ (Accessed on May 3, 2016).

U.S. Energy Information Administration (2016b), Monthly Energy Review January 2016. DOE/EIA-0035(2016/1), http://www.eia.gov/totalenergy/data/monthly/pdf/mer.pdf (accessed February 18, 2016).

U.S. Energy Information Administration (2016c), Underground Natural Gas Storage by All Operators, https://www.eia.gov/dnav/ng/ng_stor_sum_dcu_SWV_a.htm (accessed June 29, 2016).

U.S. Environmental Protection Agency (1989), User's Manual for OZIPM-4 (Ozone Isopleth Plotting with Optional Mechanisms) Volume 1, EPA-450/4-89-009a.

U.S. Environmental Protection Agency (2003a), Air Pollution Control Technology Fact Sheet, Selective Catalytic Reduction (SCR), EPA-452/F-03-032, http://www3.epa.gov/ttn/catc/dir1/fscr.pdf (accessed December 8, 2015).

U.S. Environmental Protection Agency (2003b), Air Pollution Control Technology Fact Sheet, Selective Non-Catalytic Reduction (SNCR), EPA-452/F-03-031, http://www3.epa.gov/ttn/catc/dir1/fsncr.pdf (accessed December 8, 2015).

U.S. Environmental Protection Agency (2008a), National Emission Standards for Hazardous Air Pollutants for Source Categories: Gasoline Distribution Bulk Terminals, Bulk Plants, and Pipeline Facilities; and Gasoline Dispensing Facilities; Final Rule, *Federal Register*, *73*(7), 1916-1953.

U.S. Environmental Protection Agency (2008b), National Ambient Air Quality Standards for Ozone; Final Rule, *Federal Register* 73(60):16436-16514.

U.S. Environmental Protection Agency (2009), The NOx Budget Trading Program: 2008 Emission, Compliance, and Market Analyses, https://www.epa.gov/sites/production/files/2015-08/documents/nbp_2008_ecm_analyses.pdf (Accessed on April 27, 2016).

U.S. Environmental Protection Agency (2012), Oil and Natural Gas Sector: New Source Performance Standards and National Emission Standards for Hazardous Air Pollutants Reviews; Final Rule, *Federal Register*, *77*(159), 49490-49600.

U.S. Environmental Protection Agency (2014a), Photochemical Assessment Monitoring Stations (PAMS), http://www.epa.gov/ttnamti1/pamsmain.html (Accessed on September 24, 2014).

U.S. Environmental Protection Agency (2014b), Air Emissions, http://www.epa.gov/cleanenergy/energy-and-you/affect/air-emissions.html, (Accessed on September 24, 2014).
U.S. Environmental Protection Agency (2014c), Control of Air Pollution from Motor Vehicles: Tier 3 Motor Vehicle Emission and Fuel Standards Final Rule – Regulatory Impact Analysis, EPA-420-R-14-005.
U.S. Environmental Protection Agency (2014d), Air Markets Program Data, http://ampd.epa.gov/ampd/ (Accessed on July 16, 2014).
U.S. Environmental Protection Agency (2014e), Technical Support Document (TSD), Preparation of Emissions Inventories for the Version 6.0, 2011 Emissions Modeling Platform, http://www3.epa.gov/ttn/chief/emch/2011v6/outreach/2011v6_2018base_EmisMod_TSD_26feb2014.pdf (accessed on December 16, 2015).
U.S. Environmental Protection Agency (2014f), Meteorological Model Performance for Annual 2011 WRF v3.4 Simulation, https://www3.epa.gov/scram001/reports/MET_TSD_2011_final_11-26-14.pdf (accessed on March 24, 2016).
U.S. Environmental Protection Agency (2014g), 2011ed_v6_11f_state_sector_totals, ftp://ftp.epa.gov/EmisInventory/2011v6/v1platform/reports/2011_emissions/2011ed_v6_11f_state_sector_totals.xlsx (accessed on December 16, 2015).
U.S. Environmental Protection Agency (2014h), Technical Support Document (TSD), Preparation of Emissions Inventories for the Version 6.1, 2011 Emissions Modeling Platform, http://www3.epa.gov/ttn/chief/emch/2011v6/2011v6.1_2018_2025_base_EmisMod_TSD_nov2014_v6.pdf (accessed on December 16, 2015).
U.S. Environmental Protection Agency (2014i), EPA Sets Tier 3 Motor Vehicle Emission and Fuel Standards, EPA-420-F-14-00, https://www3.epa.gov/otaq/documents/tier3/420f14009.pdf (Accessed on May 15, 2016).
U.S. Environmental Protection Agency (2015a), Criteria Air Pollutants, https://www.epa.gov/sites/production/files/2015-10/documents/ace3_criteria_air_pollutants.pdf (Accessed on April 27, 2016)
U.S. Environmental Protection Agency (2015b), National Emissions Inventory (NEI) Air Pollutant Emissions Trends Data, http://www.epa.gov/ttnchie1/trends/ (Accessed on January 11, 2015).
U.S. Environmental Protection Agency (2015c), National Ambient Air Quality Standards for Ozone; Final Rule, *Federal Register*, *80*(206), 65292- 65468.
U.S. Environmental Protection Agency (2015d), Cross-State Air Pollution Rule (CSAPR), http://www3.epa.gov/crossstaterule/ (accessed on December 8, 2015).
U.S. Environmental Protection Agency (2015e), The 2011 National Emissions Inventory, http://www3.epa.gov/ttnchie1/net/2011inventory.html (accessed on December 8, 2015).
U.S. Environmental Protection Agency (2015f), Technical Support Document (TSD) for the Cross-State Air Pollution Rule for the 2008 Ozone NAA, EPA-HQ-OAR-2015-0500, http://www.epa.gov/sites/production/files/2015-

11/documents/egu_nox_mitigation_strategies_tsd_0.pdf (accessed February 18, 2016).
U.S. Environmental Protection Agency, (2015g), EPA Base Case v.5.14 Using IPM Incremental Documentation, http://www.epa.gov/sites/production/files/2015-08/documents/epa_base_case_v514_incremental_documentation.pdf (accessed February 18, 2016).
U.S. Environmental Protection Agency, (2015h), Emissions Monitoring, Clean Air Markets, http://www2.epa.gov/airmarkets/emissions-monitoring (accessed on December 16, 2015).
U.S. Environmental Protection Agency (2016a), Ozone: Regional Trends in Ozone Levels, https://www3.epa.gov/airtrends/ozone.html (Accessed on May 12, 2016).
U.S. Environmental Protection Agency (2016b), Particulate Matter: Regional Trends in Particulate Matter Levels, https://www3.epa.gov/airtrends/pm.html (Accessed on May 12, 2016).
U.S. Environmental Protection Agency (2016c), NAAQS Table, https://www.epa.gov/criteria-air-pollutants/naaqs-table (Accessed on April 26, 2016).
U.S. Environmental Protection Agency (2016d), SIP Status and Information, https://www3.epa.gov/airquality/urbanair/sipstatus/ (Accessed on May 10, 2016).
U.S. Environmental Protection Agency (2016e), Health Effects of Ozone Pollution, https://www.epa.gov/ozone-pollution/health-effects-ozone-pollution (Accessed on April 22, 2016).
U.S. Environmental Protection Agency (2016f), Particulate Matter (PM): Health, https://www3.epa.gov/airquality/particlepollution/health.html (Accessed on April 22, 2016).
U.S. Environmental Protection Agency (2016g), Urban Air Toxic Pollutants, https://www.epa.gov/urban-air-toxics/urban-air-toxic-pollutants (Accessed on April 22, 2016).
U.S. Environmental Protection Agency (2016h), Milestones in Mobile Source Air Pollution Control and Regulations, https://www3.epa.gov/otaq/consumer/milestones.htm (Accessed on April 21, 2016).
U.S. Environmental Protection Agency, (2016i), Cross-State Air Pollution Rule (CSAPR): Frequently Asked Questions, http://www3.epa.gov/crossstaterule/faqs.html (accessed March 1, 2016).
U.S. Environmental Protection Agency (2016j), Oil and Natural Gas Sector: Emission Standards for New, Reconstructed, and Modified Sources, FRL-9944-75-OAR, https://www3.epa.gov/airquality/oilandgas/may2016/nsps-finalrule.pdf (Accessed on May 14, 2016).
U.S. Environmental Protection Agency (2016k), https://www.epa.gov/benmap/how-benmap-ce-estimates-health-and-economic-effects-air-pollution (Accessed on May 11, 2016).

U.S. Geological Survey (2014), Hydraulic Fracturing, http://energy.usgs.gov/OilGas/UnconventionalOilGas/HydraulicFracturing.aspx, last accessed on September 24, 2014.

U.S. National Oceanic and Atmospheric Administration (2016), ESRL/GMD FTP Data Finder, Earth System Research Laboratory, http://www.esrl.noaa.gov/gmd/dv/data/index.php (Accessed on May 10, 2016).

Vinciguerra, T., S. Yao, J. Dadzie, A. Chittams, T. Deskins, S. Ehrman, and R. R. Dickerson (2015), Regional air quality impacts of hydraulic fracturing and shale natural gas activity: Evidence from ambient VOC observations, *Atmospheric Environment*, *110*, 144–150, doi:10.1016/j.atmosenv.2015.03.056.

Virginia Department of Mines Minerals and Energy (2016), Division of Gas and Oil Data Information System, https://www.dmme.virginia.gov/dgoINQUIRY/frmMain.aspx?ctl=2 (Accessed on May 10, 2016).

Warneke, C., F. Geiger, P. M. Edwards, W. Dube, G. Pétron, J. Kofler, A. Zahn, S. S. Brown, M. Graus, J. B. Gilman, B. Lerner, J. Peischl, T. B. Ryerson, J. A. de Gouw, and J. M. Roberts (2014), Volatile organic compound emissions from the oil and natural gas industry in the Uintah Basin, Utah: oil and gas well pad emissions compared to ambient air composition, *Atmospheric Chemistry and Physics*, *14*, 10977-10988, doi:10.5194/acp-14-10977-2014.

Watson, J., J. C. Chow, and E. M. Fujita (2001) Review of volatile organic compound source apportionment by chemical mass balance, *Atmospheric Environment*, *35*(9), 1567-1584, doi: 10.1016/S1352-2310(00)00461-1.

Wayland, R. (2014), Draft Modeling Guidance for Demonstrating Attainment of Air Quality Goals for Ozone, PM2.5, and Regional Haze, Memorandum, http://www3.epa.gov/scram001/guidance/guide/Draft_O3-PM-RH_Modeling_Guidance-2014.pdf (accessed on December 16, 2015).

Weber, R. J., A. P. Sullivan, R. E. Peltier, A. Russell, B. Yan, M. Zheng, J. de Gouw, C. Warneke, C. Brock, J. S. Holloway, E. L. Atlas, and E. Edgerton (2007), A study of secondary organic aerosol formation in the anthropogenic-influenced southeastern United States, *Journal of Geophysical Research - Atmospheres*, *112*(D13302), doi:10.1029/2007jd008408

West Virginia Department of Environmental Protection (2016), Gas Well Search, https://apps.dep.wv.gov/oog/wellsearch_new.cfm (Accessed on May 10, 2016).

Wheeling, Christopher, Maryland Department of the Environment, personal communication, christopher.wheeling@maryland.gov.

Whitten, G. Z., G. Heo, Y. Kimura, E. McDonald-Buller, D. Allen, W. P. L. Carter, and G. Yarwood (2010), A new condensed toluene mechanism for Carbon Bond: CB05-TU, *Atmos. Environ.*, *44*, 5346–5355.

World Health Organization (2005), WHO Air quality guidelines for particulate matter, ozone, nitrogen dioxide and sulfur dioxide, Global update 2005, Summary of risk assessment,

http://apps.who.int/iris/bitstream/10665/69477/1/WHO_SDE_PHE_OEH_06.02_eng.pdf (Accessed on April 22, 2016).

Yarwood, G., S. Rao, M. Yocke, and G. Whitten (2005), Updates to the Carbon Bond Chemical Mechanism: CB05. Final Report to the US EPA, RT-0400675, http://www.camx.com/publ/pdfs/CB05_Final_Report_120805.pdf (accessed on December 16, 2015).

Yuan, B., M. Shao, J. de Gouw, D. D. Parrish, S. Lu, M. Wang, L. Zeng, Q. Zhang, Y. Song, J. Zhang, and M. Hu (2012), Volatile organic compounds (VOCs) in urban air: How chemistry affects the interpretation of positive matrix factorization (PMF) analysis, *Journal of Geophysical Research*, *117*, D24302, doi:10.1029/2012JD018236.

Publications

Vinciguerra, T., S. Yao, J. Dadzie, A. Chittams, T. Deskins, S. Ehrman, and R. R. Dickerson (2015), Regional air quality impacts of hydraulic fracturing and shale natural gas activity: Evidence from ambient VOC observations, *Atmospheric Environment, 110*, 144-150, doi:10.1016/j.atmosenv.2015.03.056

Goldberg, D. L., **T. P. Vinciguerra**, D. C. Anderson, L. Hembeck, T. P. Canty, S. H. Ehrman, D. K. Martins, R. M. Stauffer, A. M. Thompson, R. J. Salawitch, and R.R. Dickerson, (2016), CAMx ozone source attribution in the eastern United States using guidance from observations during DISCOVER-AQ Maryland. *Geophys. Res. Lett. 43*, 2249-2258, doi:10.1002/2015GL067332.

Goldberg, D. L., K. M. Hosley, **T. P. Vinciguerra**, C. P. Loughner, T. P. Canty, R. J. Salawitch, and R. R. Dickerson (2015), Evidence for an increase in the ozone photochemical lifetime in the eastern United States using a regional air quality model, *J. Geophys. Res. Atmos., 120*, 12778–12793, doi:10.1002/2015JD023930

Canty, T. P., L. Hembeck, **T. P. Vinciguerra**, D. C. Anderson, D. L. Goldberg, S.F., Carpenter, D. J. Allen, C. P. Loughner, R. J. Salawitch, and R. R. Dickerson (2015), Ozone and NOx chemistry in the eastern US: Evaluation of CMAQ/CB05 with satellite (OMI) data, *Atmos. Chem. Phys.*, *15*, 10965-10982, doi:10.5194/acp-15-10965-2015

Vinciguerra, T., E. Bull, T. Canty, H. He, E. Zalewsky, M. Woodman, G. Aburn, S. Ehrman, and R. R. Dickerson (2016), Expected ozone benefits from electricity generating unit NOx reductions in the Eastern United States, *J. Air & Waste Management Assoc.*, (in review, submitted April 22, 2016).

Satam, C., **T. Vinciguerra**, S. Ehrman, T. Canty, and R. R. Dickerson, Ammonia emissions control and changing air quality in the Mid-Atlantic region of the United States, *J. Air & Waste Management Assoc.*, (submitting Summer 2016)

Presentations

Regional Influences of Marcellus Shale Natural Gas Activity: Back-trajectory Analysis of Baltimore/ Washington Ethane Concentrations (Poster, 2015 AGU Fall Meeting, San Francisco, CA, December 14, 2015)

Expected ozone benefits from EGU NOx reductions (Presentation, 14th Annual CMAS Conference, Chapel Hill, NC, October 6, 2015)

Regional Air Quality Impacts of Hydraulic Fracturing and Natural Gas Activity: Evidence from Ambient VOC Observations (Poster, 2014 AGU Fall Meeting, San Francisco, CA, December 15, 2014)

Potential Regional Air Quality Impacts of Hydraulic Fracturing Activity (Poster, 13th Annual CMAS Conference, Chapel Hill, NC, October 28, 2014)

Improved air quality by reducing ammonia emissions from chicken manure (Poster, ACS 43rd Middle Atlantic Regional Meeting, Baltimore, MD, May 31, 2012)